

Stellingen behorende bij het proefschrift  
**Modelling of Cooled-ceiling Air-conditioning Systems**  
van **Jianlei Niu**

1. Besides turbulence modelling, numerical discretization schemes, and iteration solution convergence, further simplification of a real physical situation that is to be modelled is also necessary, justification of these simplifications is no less important in achieving good simulation results.
2. The applications of turbulence models are associated with the availability of computing facilities. The k- $\epsilon$  model is compatible with today's computing power; no doubt, more sophisticated models will gain their places and less simplifications will be required as the computer power is constantly increasing.
3. Direct solution of transient N-S equations is already performed at the transit flow regime to study flow instability. In the near future, direct solution of transient N-S equations may be applied for engineering purposes.
4. Analogy is a common method in scientific research by which many of the new concepts are conceived and great breakthroughs in scientific history are made this way. However, it is important to know that the new concepts or ideas so created proved, for the most part, to be wrong and had to be discarded.
5. In building practice, architects would pursue variation and diversities in their design. This practice makes our man-made world very beautiful or ugly. However, building service engineers are constantly challenged with the limited time to finish the design and the consciousness to cope with any energy and environmental consequences. As a result, the practising of system optimization is much hindered. Simulation studies on project bases are carried-out usually in simplified forms. The next-generation of complicated-simulation-based design tools with human-like interfaces may help design engineers to design more energy efficient buildings with good indoor environment quality.
6. The developed countries have undergone the cycle of industrialization, environment deterioration, and environment protection; at present, global environment protection has become an important issue in international politics; the developing countries have the possibility to pursue development in parallel with environment protection.
7. In the architectural practices in China, the selection of building location and orientation is usually based on opinions of the professional *Master Feng-Shui* ('Feng Shui' literally means wind and water in the Chinese language). Master Feng-Shui must be an aged man with a long and white beard. The consulting opinions are usually delivered in mystical and superstitious terms. In such a way, while the master demonstrates his superiority in the area, the technical know-how is never released. Similarly, most of today's commercial

computer codes are not provided with source code.

8. The booming economy in the Asian Pacific region has greatly improved the living standards of its inhabitants, which include the cool comfort standard. As a result, the continental, tropical and subtropical countries in this region are becoming the major markets of air-conditioning products. In China, more than one million unit airconditioners were sold in 1993.

9. Elimination of mechanical cooling in buildings was a concept expressed in several papers in a recent international conference CLIMA 2000; in fact, passive cooling has been a practice for thousands of years. In the traditional family houses in the rural area of central China, the roofed entrance to the yard serves as a parlour with free convective-cooling using wind effect.

10. In the temperate climate, the requirement of mechanical cooling is largely due to the increased occupant density and electrical appliances in the working place. However, if taking these features into account at the design stage of a building, it is still possible to eliminate mechanical cooling by proper design of building envelopes and other components such as solar shading and window openings.

11. The comfort standard is never the same when we talk about mechanical cooling and natural cooling; generally speaking, passive systems always have risks of overheating. Therefore, the magnitude of the overheating risks associated with a natural or passive cooling scheme should always be estimated, along with its energy saving.

12. The current higher priority on energy efficiency in building practice in the Netherlands can be seen by the small window sizes of some castle-like new apartment buildings.

**TR diss  
2393**

**Modelling of Cooled-  
Ceiling Air-Conditioning Systems**  
- Influences on Indoor Environment and Energy Consumption

**Jianlei Niu**

CIP-DATA KONINKLIJKE BIBLIOTHEEK, DEN-HAAG

Niu, Jianlei

Modelling of cool-ceiling air-conditioning systems :  
influences on indoor environment and energy consumption /  
Jianlei Niu. - Delft: Delft University of Technology ,  
Faculty of Mechanical Engineering and Marine Technology.  
- Ill.

Thesis Technische Universiteit Delft. - With ref. - With  
summary in Dutch.

ISBN 90-370-0105-X

Subject headings: Air-conditioning systems / energy  
estimation / computational fluid dynamics.

Copyright ©1994,                      Faculteit der Werktuigbouwkunde en Maritieme Techniek,  
Technische Universiteit Delft.

Alle rechten voorbehouden. Niets uit dit rapport mag op enigerlei wijze worden  
verveelvoudigd of openbaar gemaakt zonder schriftelijke toestemming van de auteur.

All rights reserved. No part of this book may be reproduced by any means, or transmitted  
without the written permission of the authors.

Gebruik of toepassing van de gegevens, methoden en/of resultaten enz., die in dit rapport  
voorkomen, geschiedt geheel op eigen risico. De Technische Universiteit Delft, Faculteit  
der Werktuigbouwkunde en Maritieme Techniek, aanvaardt geen enkele aansprakelijkheid  
voor schade, welke uit gebruik of toepassing mocht voortvloeien.

Any use or application of data, methods and/or results etc., occurring in this report will be  
at user's own risk. The Delft University of Technology, Faculty of Mechanical Engineering  
and Marine Technology, accepts no liability for damages suffered from the use or  
application.

# **Modelling of Cooled-Ceiling Air-Conditioning Systems**

**- Influences on Indoor Environment and Energy Consumption**

**PROEFSCHRIFT**

ter verkrijging van de graad van doctor  
aan de Technische Universiteit Delft,  
op gezag van de Rector Magnificus Prof. ir. K.F. Wakker,  
in het openbaar te verdedigen ten overstaan van een commissie,  
door het College van Dekanen aangewezen,  
op dinsdag 14 juni 1994 te 16:00 uur  
door

Jianlei NIU

Master of Science in Mechanical Engineering

geboren te Changyuan, China

Dit proefschrift is goedgekeurd door  
de promotor: Prof. ir. H. van der Ree  
en  
de toegevoegd promotor: Dr. ir. J. van der Kooi

to Xiu-hong and Shuang-yuan  
to my parents

## SUMMARY

The contents presented in this thesis consist of four principal parts: 1). the critical review of turbulence CFD(Computational Fluid Dynamics) techniques and their application in building air flow study, and the experimental evaluation of the widely-used  $k-\epsilon$  turbulence model for in-room air flow situations; 2). the development of a thermodynamic mathematical model for cooled-ceiling air-conditioning systems, and the enhancement of an existing computer code ACCURACY to fulfil the numerical simulation task, and the experimental validation of the convective parameters involved in the models; 3). the combined use of building dynamic simulation and CFD technique for the investigation of thermal comfort and ventilation effectiveness performance of three typical air-conditioning systems, i.e., the conventional displacement ventilation system, the air-panel type cooled-ceiling(ACC) system, and the water-panel type cooled-ceiling(CC) system; 4). the use of the dynamic model coupled with air-handling-unit(AHU) and primary equipment models to simulate the annual energy consumption of CC systems and all-air systems and to estimate thermal performances of some passive cooling schemes, especially the evaporative free-cooling scheme.

The review of the state-of-the-art of turbulence modelling shows that, despite all its inherent inadequacies in modelling certain important features of turbulence flow such as the non-isotropy of buoyancy-driven turbulence in comparison with some other more rigorous models, such as the Reynolds-stress turbulence model or Large-Eddy-Simulation(LES) model, the  $k-\epsilon$  turbulence model still remains the most-widely used 'engineering model'. In the present research, two practical effects of using  $k-\epsilon$  model are specifically investigated, i.e., the boundary air flow effect and the turbulence kinetic energy effect. These investigations are performed by both macro- and micro-scale comparisons between simulation and measurements. Smoke is used for air flow visualization to see the macro-scale air flow patterns, while anemometry measurements are done to diagnose local turbulent flow quantities. Generally speaking, prediction of wall surface convective heat transfer using the standard  $k-\epsilon$  turbulence model in conjunction with logarithmic wall functions tends to be uniquely grid-dependent in the near wall region. It was found that large first-grid distance under-predicts wall surface convective heat flow, and *vice versa*. The dimensionless first-grid distance  $y^+$  has long been used as a criterion to locate the spacing of the first near-wall grid line, and it is established that, for fully-developed forced-convection boundary layers, the value of  $y^+$  should be in the range of 40 to 130. The present research finds out that this criterion gives too low surface convective heat predictions if used for buoyancy-driven, or commonly named as natural-convection, boundary flows. Therefore, a new criterion is recommended for locating discretization grids in a buoyancy-driven boundary layer, i.e.,  $y^+ = 9.2$  for situations of *Rayleigh Number*  $Ra=10^9$ , which is typical of room air flows. Based on our research, it is also alternatively



recommended that experimentally or otherwise available surface convective heat transfer coefficients be used. Once the convective heat flow can be calculated in reasonable accuracy using these empirical approaches, the other predicted mean flow parameters such as air velocity and air temperature seems to be reasonable, the predicted turbulent kinetic energy  $k$  tends to be about one order higher than measured in the most regions in a room. The practical indication is that the predicted draft risks in terms of Percentage Dissatisfied(PD) tend to be 5~10% higher than those found in the measurements. The Lam and Bremhorst low-Reynolds number model is found demanding extremely fine grid-spacing in the near-wall region to achieve convergence and good prediction accuracy.

The dynamic simulation program for cooled-ceiling system modelling is based on an established method, i.e., room energy balance method. However, different from the ordinary air-conditioning cooling-load calculation or energy analysis procedure, the main characteristics of the present modelling strategy is to take into account the direct radiant effects on thermal comfort and heat storage dynamics of the ceiling-panels present in a room space in the overall heat balance matrix. Therefore, cooled-ceiling panels as a system component is modelled interactively in the cooling-load calculation procedure. To be able to estimate thermal performances of some passive building cooling schemes, the thermal comfort index PMV(predicted mean vote) weighted temperature over-exceeding hours(PWH) are integrated into the simulation procedure. The simulation procedure is fulfilled by enhancing an existing home-made computer program ACCURACY. The program can predict not only the required cooling-load (or heat extraction rate) but also the chilled-water temperatures at different ceiling-panel areas. Some convective parameters, such as the ceiling-panel surface convective heat transfer coefficients and the convective air-exchanges through ceiling-openings, contained in the models are experimentally measured in a test room, and their sensitivities are also investigated. It is found that the thermodynamic responses in a room with cooled-ceiling installations to step-up heating and step-down cooling can be well predicted by the enhanced program. The possibility of using CFD simulation to generate correlations about the internal convective air-exchanges are found to be feasible, but expensive and inaccurate.

The CFD technique and building dynamic simulation technique are combined to investigate the thermal comfort and ventilation effectiveness performance of three typical HVAC systems, namely, the conventional displacement ventilation system, the air-panel type cooled-ceiling(ACC) system, and the water-panel type cooled-ceiling system. The thermal dynamic simulation serves to generate boundary conditions required for the CFD simulation. By such an approach, we try to represent the influences of thermal load types, especially the radiant effect. Based upon the CFD technique which was first experimentally evaluated, some practical conclusions are drawn from the three-dimensional simulation results. It is concluded that CC system combined with displacement ventilation reduces the vertical temperature stratification in the occupied zone in a room, especially at cooling loads higher than 50 W/m<sup>2</sup> floor area, while still maintaining a ventilation effectiveness of higher than one. The ACC system tends to present a performance that is close to a mixed ventilation system in terms of ventilation effectiveness. The simulation results also indicate that the performance of an ACC system can be much improved if the air diffuser is located near the floor level.

Extensive simulations are performed to compare the annual energy consumptions

of the water-panel cooled-ceiling system and the conventional all-air systems. This is done by coupling the cooling-load calculation with models for air-handling-unit(AHU) and models for primary equipments such as boilers, chillers, cooling-towers and air fans. It is found that two characteristics of the CC system play the key role in determining the annual running cost of the system. The radiant effect tends to reduce the heat storage capacity of building envelopes on one hand but raise the acceptable room air temperature on the other hand. The second effect enhances the heat removal capacities of any supplied air volume. The reduced supply air volume with a CC system means reduced fan energy but also reduces free-cooling possibilities using outdoor air. The overall effect is that, in the temperate Dutch climate, the annual energy consumption of a CC system is close to that of a variable-air-volume all-air system. The simulation results also indicate that the benefits of heat recovery in both systems are substantial.

Some unique energy-saving measures with a CC system are estimated based on these simulation results. It is found that by system integration such as extra proper piping between ceiling-panels and heating/cooling coils in the AHU, much external heating and cooling can be saved with a CC system. Also, several possibilities using cooling tower for evaporative free cooling are simulated. The first possibility is to use evaporative cooling to reduce the running time of the compressor chiller system. The second possibility is to use relatively larger-size cooling tower and larger areas of ceiling-panels to eliminate the use of the compression chilled-water system. The simulation results indicate the possible energy savings with the former one at different ceiling panel areas, and the seasonal thermal performances with the later one. While some other possibilities may exist, the present simulation results demonstrate the capabilities of the enhanced simulation program in assisting us to estimate their performances.

## SAMENVATTING

De inhoud van dit proefschrift bestaat uit vier hoofddelen: 1) een kritisch overzicht van turbulente CFD (Computational Fluid Dynamics) technieken en de toepassing hiervan in luchtstromingsonderzoek voor gebouwen, tezamen met de experimentele evaluatie van het algemeen toegepaste k- $\epsilon$  turbulentiemodel voor luchtstromingssituaties binnenskamers; 2) de ontwikkeling van een dynamisch simulatiemodel voor koelplafondsystemen en de uitbreiding van een bestaand computermodel ACCURACY om numerieke simulatie mogelijk te maken, met daarnaast de experimentele validatie van de convectieve parameters toegepast in het model; 3) het gecombineerde gebruik van de dynamische warmtesimulatie van een gebouw en CFD technieken voor het onderzoek van thermisch comfort en ventilatie-effectiviteit van drie specifieke luchtbehandelingssystemen n.l. het verdringings-ventilatie systeem, het type koelplafond met lucht-panelen (ACC) en het type koelplafond met water-panelen (CC); 4) de toepassing van het dynamisch simulatiemodel gekoppeld met luchtbehandelingseenheid (AHU) en primaire-energiemodellen voor het berekenen van het jaarlijkse energiegebruik van koelplafondsystemen en "all-air"systemen en daarnaast het vaststellen van de thermische prestaties van enkele passieve koelsystemen met in het bijzonder het systeem met verdampingskoeling.

Het overzicht van de huidige stand van zaken met betrekking tot turbulentie-modellering geeft aan dat het k- $\epsilon$  turbulentiemodel nog steeds het meest toegepaste praktische model blijft, ondanks al de inherente onvolledigheden in modellering van belangrijke onderdelen van turbulente stroming zoals het niet-isotrope karakter van door opstijgen van warme lucht veroorzaakte turbulentie in vergelijking met enkele andere meer gedetailleerde modellen, zoals het Reynolds-stress turbulentiemodel en het Large-Eddy-Simulatie (LES) model. In het hier beschreven onderzoek zijn twee praktische effecten bij toepassing van het k- $\epsilon$  model speciaal onderzocht n.l. het verloop van de luchtstroming en en van de turbulente kinetische energie bij vaste begrenzingen. Deze onderzoeken zijn verricht door vergelijken van simulatie en metingen zowel op macro- als op micro-schaal. De luchtstromingspatronen op macro-schaal zijn zichtbaar gemaakt door middel van rook, terwijl anemometer-metingen zijn uitgevoerd om de plaatselijke turbulente stromingsgegevens te bepalen. In het algemeen blijkt de berekende convectieve warmteoverdracht aan het wandoppervlak door toepassing van het standaard k- $\epsilon$  turbulentiemodel in samenhang met logaritmische wandfuncties sterk afhankelijk te zijn van de roosterverdeling in het gebied dicht bij de wand. Gevonden is dat bij een te grote eerste roosterafstand de warmteoverdracht aan de wand te laag berekend wordt en omgekeerd. De dimensieloze eerste roosterafstand  $y^+$  is lange tijd gebruikt als een criterium om de afstand tot de eerste roosterlijn vast te stellen en het is algemeen geaccepteerd dat de waarde van  $y^+$  moet liggen tussen 40 en 130. Het hierbeschreven onderzoek geeft aan dat dit criterium te lage waarden voor de warmteoverdracht oplevert, wanneer het gebruikt wordt voor door temperatuurverschil

veroorzaakte stroming, ook wel aangeduid met vrije convectie stroming. Daarom wordt een nieuw criterium aanbevolen voor de afstand tot de eerste roosterlijn bij een vrije convectie grenslaag n.l.  $y^+ = 9,2$  voor situaties met Rayleighgetal  $Ra = 10^9$ , hetgeen gebruikelijk is voor luchtstroming in vertrekken. Op basis van ons onderzoek wordt als alternatieve mogelijkheid aanbevolen experimenteel bepaalde of op andere wijze beschikbare convectieve warmteoverdrachtscoëfficiënten toe te passen. Wanneer eenmaal de convectieve warmtestroom met redelijke nauwkeurigheid is berekend door gebruik te maken van deze empirische benaderingen, blijken andere stromingsparameters zoals gemiddelde luchtsnelheid en luchttemperatuur redelijk overeen te stemmen; de berekende turbulente kinetische energie  $k$  blijkt ongeveer een factor 10 hoger dan gemeten in het vertrek. Het praktische gevolg hiervan is dat de berekende kans op tochtklachten uitgedrukt in percentage ontevreden (PD) 5 à 10 % hoger blijkt te zijn dan dat afgeleid uit de metingen. Het Lam en Bremhorst lage-Reynolds-model blijkt een extreem fijne roosterverdeling te vergen nabij de wandbegrenzing om convergentie en een goede nauwkeurigheid te verkrijgen.

Het dynamische simulatieprogramma voor modellering van het koelplafond is gebaseerd op een alom bekende methode n.l. op die voor de warmtebalans van het vertrek. Echter verschillend van gebruikelijke koellastberekening of energie-analyse-procedure voor air-conditioning is het meest karakteristieke van de hier gebruikte modellering de methode om het directe stralingseffect op thermisch comfort en de dynamische warmteopslag van de plafondpanelen in rekening te brengen in de algemene warmtebalans-matrix. Daarom is het koelplafond als systeemcomponent inter-actief gemodelleerd in de koellastberekenings procedure. Om de thermische opbrengst van enkele passieve koelsystemen te kunnen beoordelen is een met thermische comfort index (PMV) gewogen temperatuuroverschrijdingsmethode (PWH) ingebouwd in het simulatieproces. Het simulatieproces is uitgevoerd door een eerder ontwikkeld computerprogramma ACCURACY uit te breiden. Het programma kan niet alleen de benodigde koellast (of door de koeler opgenomen warmtestroom) berekenen maar ook de koelwatertemperatuur van de verschillende koelpanelen. Bepaalde convectieve parameters zoals de convectieve warmteoverdrachtscoëfficiënt aan het oppervlak van de koelpanelen of de convectieve lucht-uitwisseling door de openingen in het plafond, die in het model zijn opgenomen, zijn experimenteel bepaald in een klimaatkamer. De gevoeligheid van deze parameters op het eindresultaat is eveneens onderzocht. Gebleken is dat de thermische respons van een vertrek met een koelplafondsysteem op een stapvormige verwarming of koeling goed wordt weergegeven door het uitgebreide programma. De mogelijkheid om CFD berekeningen toe te passen om correlaties af te leiden voor de luchtuitwisseling door het plafond blijken uitvoerbaar te zijn maar kostbaar en onnauwkeurig.

De CFD techniek en de techniek voor het berekenen van het thermische gedrag van gebouwen zijn gecombineerd om het thermisch comfort en ventilatie-effectiviteit van drie speciale klimaatsystemen te onderzoeken n.l. het verdringingsventilatie-systeem, het koelplafondsysteem met lucht-panelen (ACC) en het koelplafondsysteem met waterpanelen. De thermische-gebouw-simulatie dient om de grenscondities op te leveren nodig voor de CFD simulatie. Op deze manier is getracht de invloed van het type thermische belasting na te gaan op de koellast, speciaal het stralings en convectie aandeel. Uit de driedimensionale berekeningsresultaten, die gebaseerd zijn op de experimenteel geëvalueerde

CFD techniek, zijn enkele praktische conclusies getrokken. Geconcludeerd is dat het koelplafondsysteem (CC) in combinatie met verdringingsventilatie de verticale temperatuurstratificatie in de leefzone van een vertrek vermindert, speciaal bij een koellast hoger dan  $50 \text{ W/m}^2$  vloeroppervlak, terwijl een ventilatie-effectiviteit hoger dan één gehandhaafd blijft. Het ACC systeem blijkt wat betreft ventilatie-effectiviteit een gedrag te vertonen dat vergelijkbaar is met een mengend-ventilatiesystemen. De berekeningsresultaten geven aan dat het gedrag aanzienlijk verbeterd kan worden wanneer de luchttoevoer op vloerniveau plaats vindt.

Uitgebreide berekeningen zijn verricht om de jaarlijkse energieconsumptie van een watergekoeld koelplafond te vergelijken met die van een conventioneel "all-air"-systeem. Dit is gedaan door de koellastberekening te koppelen met modellen voor de luchtbehandelingseenheid (AHU) en modellen voor de primaire apparaten, zoals verwarmingsketels, koelers, koeltorens en ventilatoren. Gebleken is dat twee karakteristieke eigenschappen van het koelplafondsysteem de hoofdrol spelen bij de bepaling van de jaarlijkse bedrijfskosten van het systeem. Door het stralingseffect wordt de warmteopslagcapaciteit van de omwandelingen gereduceerd en het gereduceerde luchtdebiet brengt een gereduceerde ventilatorenergie met zich mee maar vermindert ook de mogelijkheid om vrije koeling te gebruiken door toevoer van buitenlucht. Het totale effect is dat voor het nederlandse klimaat het jaarlijkse energiegebruik van een koelplafondsysteem praktisch gelijk is aan dat van een variabel-debiet-luchtsysteem. De berekeningsresultaten geven verder aan dat het voordeel van warmteterugwinning voor beide systemen aanzienlijk is.

Enkele speciale energiebesparingsmaatregelen voor een koelplafondsysteem zijn onderzocht, gebaseerd op simulatieresultaten. Gevonden is dat door systeemintegratie zoals aanleg van extra leidingen tussen koelpanelen en verwarming/koelspiralen in de luchtbehandelingskast veel verwarming en koeling kan worden bespaard bij een koelplafondsysteem. Daarnaast zijn verschillende mogelijkheden onderzocht om een koeltoren toe te passen voor vrije verdampingskoeling. De eerste mogelijkheid is om verdampingskoeling te gebruiken om de draaitijd van de compressorkoelmachine te verminderen. De tweede mogelijkheid is om door een relatief grote koeltoren en een groter oppervlak aan koelplafond te gebruiken het gebruik van de compressorkoelmachine te elimineren. De berekeningsresultaten geven de mogelijke energiebesparing aan vergeleken met het eerste systeem voor verschillende oppervlakten aan koelplafond en de thermische comfortsituaties voor het laatste systeem. De vermelde berekeningsresultaten demonstreren de mogelijkheid van het uitgebreide simulatieprogramma om ook voor andere mogelijkheden de energiebesparing te bepalen.

# Contents

SUMMARY .....	vii
SAMENVATTING .....	x
<b>Chapter 1 Introduction .....</b>	<b>1</b>
1.1 Background .....	1
1.2 Statement of the Problem .....	2
1.3 Objectives and Scope .....	3
1.4 Outline of the Thesis .....	4
<b>Chapter 2. Numerical Simulation of Indoor Air Flows .....</b>	<b>7</b>
2.1 INTRODUCTION .....	7
2.2 MATHEMATICAL PRESENTATION OF THE AIR FLOW .....	9
2.2.1 Conservation Laws .....	9
2.2.2 Turbulence Modelling .....	10
2.3 k- $\epsilon$ TURBULENCE MODELS .....	12
2.3.1 The Standard k- $\epsilon$ Model .....	13
2.3.2 Boundary Conditions .....	16
2.3.3 Low-Reynolds Number Models .....	17
2.4 COMPUTING THE FLOW FIELD - NUMERICAL TECHNIQUES .....	18
2.4.1 Finite Volume/Difference Methods .....	19
2.4.2 Finite Element Methods .....	20
2.5 VALIDATION AND APPLICATIONS OF CFD FOR BUILDING AIR FLOW INVESTIGATIONS .....	20
2.6 CONCLUSIONS .....	23
<b>Chapter 3       Validation of k-<math>\epsilon</math> Turbulence Models for Natural Convection Flow                   in an Enclosed Room .....</b>	<b>25</b>
3.1. INTRODUCTION .....	25
3.2. EXPERIMENTAL INSTRUMENTATION .....	26
3.3. MEASUREMENT RESULTS .....	27
3.3.1. Flow Pattern Observation .....	27

3.3.2. Temperature Distribution .....	28
3.3.3. Convective Heat Transfer .....	30
3.3.4. Details of Boundary Flow .....	31
3.4. EVALUATION OF $k$ - $\epsilon$ MODEL PERFORMANCES .....	35
3.4.1. Buoyancy Effects and Flow Instability .....	35
3.4.2. Under-relaxation Devices and Convergence .....	36
3.4.3. Standard $k$ - $\epsilon$ Turbulence Model .....	39
3.4.4. Lam & Bremhorst Low Reynolds Number Turbulence Model .....	41
3.5. CONCLUSIONS .....	44
<b>Chapter 4 Dynamic Simulation of Building Thermal Processes .....</b>	<b>47</b>
4.1 INTRODUCTION - Thermal Processes in and around a Building .....	47
4.2 MATHEMATICAL MODELLING OF THE THERMAL PROCESSES .....	51
4.2.1 Modelling Strategy .....	51
4.2.2 Thermal Balance of Wall(opaque) Surfaces .....	52
4.2.3 Thermal Balance of Window(transparent) Surfaces .....	59
4.2.4 Thermal Balance of Zonal(room) Volume Air .....	62
4.2.5 Thermal Balance of Cooled-ceiling Panels .....	64
4.3 CRITERION FOR LONG TERM THERMAL COMFORT ESTIMATION .....	67
4.3.1 Mean Radiant Temperature .....	67
4.3.2 Thermal Comfort and Thermal Sensation - Predicted Mean Vote(PMV) .....	68
4.3.3 Long Term Estimation Criterion of Thermal Comfort .....	70
4.3.4 Operative Temperature Control .....	71
4.4 SOLUTION ALGORITHM .....	72
4.5 ENHANCEMENT OF THE COMPUTER PROGRAM ACCURACY .....	74
4.6 CONCLUSIONS .....	76
<b>Chapter 5 Experimental Validation of the Enhanced Cooling Load Program ACCURACY for Cooled- ceiling Systems .....</b>	<b>79</b>
5.1. INTRODUCTION .....	79
5.2. EXPERIMENTAL SET-UP AND INSTRUMENTATION .....	80
5.3. EXPERIMENTAL RESULTS .....	83
5.3.1. Panel Surface Convective Heat Transfer .....	83
5.3.2. Air Exchanges between Cavity and Room .....	84
5.3.3. Thermal Responses of the Room .....	86
5.4. SIMULATION OF THE THERMAL DYNAMIC RESPONSES .....	90
5.5. CFD PREDICTION OF THE AIR EXCHANGE .....	91
5.6 CONCLUSIONS .....	94
<b>Chapter 6 Thermal Comfort and Indoor Contaminant Distributions with Cooled-ceiling Systems .....</b>	<b>95</b>
6.1 INTRODUCTION .....	95
6.2 THERMAL COMFORT INDICES .....	95
6.3 VENTILATION EFFECTIVENESS .....	97

6.4 MEASUREMENTS WITH AIR-PANEL COOLED CEILING SYSTEM .	98
6.5 EVALUATION OF CFD SIMULATION FOR COOLED CEILING SYSTEMS .....	105
6.6 NUMERICAL SIMULATION OF THREE COOLING SYSTEMS ....	108
6.6.1 Dynamic Simulation of the Thermal Processes .....	109
6.6.2 CFD Simulation of Thermal Comfort and Contaminant Distributions .....	110
6.6.3 Discussions of the Simulation Results .....	116
6.7 CONCLUSIONS .....	116
<b>Chapter 7 Annual Energy Analysis: Cooled-Ceiling System     versus All-Air Systems .....</b>	<b>119</b>
7.1 INTRODUCTION .....	119
7.2 METHODOLOGY .....	121
7.3 MODELLING AIR HANDLING UNITS .....	121
7.4 PRIMARY ENERGY EQUIPMENTS MODELS .....	122
7.5 SIMULATION CONSIDERATIONS .....	124
7.6 SIMULATION RESULTS .....	125
7.6.1 Required Heat Extraction Rates .....	125
7.6.2 Annual Energy Cost .....	129
7.6.3 Benefit of Heat Recovery .....	135
7.6.4 Using Outdoor Air for Free-cooling in CC systems .....	137
7.6.6 Combination of Cooled-ceiling with Cooling Tower for Free-cooling .....	138
7.6.7 CFC-free Evaporative Cooling Using Cooled-ceiling .....	141
7.7 CONCLUSIONS .....	144
<b>Chapter 8 Concluding Remarks and Recommendations .....</b>	<b>145</b>
8.1 Turbulence Modelling and Application .....	145
8.2 Building Thermal Dynamic Simulation Coupled with Cooled-ceiling Modelling .....	146
8.3 Combination of CFD and Building Dynamic Simulation .....	146
8.4 Some Practical Conclusions .....	147
8.5 Remarks about CC Systems and Recommendations for Future Research	148
<b>References .....</b>	<b>151</b>
<b>Appendix A .....</b>	<b>163</b>
<b>Nomenclature .....</b>	<b>167</b>
<b>Acknowledgements .....</b>	<b>173</b>
<b>Curriculum Vitae .....</b>	<b>175</b>





## CHAPTER 1

# INTRODUCTION

### 1.1 BACKGROUND

The need to stay comfort in an oppressive climate no doubt has existed since the dawn of mankind. This need caused our distant ancestors to devise many schemes to stay warm or cool when necessary. In its broader sense, building a house is one of these schemes. Probably, keeping warm by using fire came to existence earlier than architectural practices, and nevertheless it has long been a traditional way to keep houses warm. The cooling schemes of the ancients are, for the most part, unknown to us. However, various ancient 'passive' schemes to stay cool can be still seen today in some monument buildings. In the famous Summer Palace in Beijing, which used to be one of the many royal parks, in a hot summer day when the air temperature is as high as 35°C, people can still feel comfortably cool sitting in the long pavement parlour and enjoying the beauty of the glittering Qunming Lake. In the west-Asian area, it is still a common practice to pour water onto the ground on the windward side of a camp located in a hot dry dessert to get some cool breeze. Anyhow, it is due to the increased availability of fossil fuels - coals, gases and oil, and electricity that the modern practice of heating and cooling took their shapes. Radiators coupled with district heating system or domestic gas boilers are virtually keeping most houses warm in the developed countries(Steimle 1983). In some developing countries such as in China, while coal-stoves, and some other more traditional heating technologies such as flue-gas warmed beds and floors are still widely used for heating especially in rural areas, the network of district heating is extending rapidly. For cool comfort, more and more air conditioning systems are being installed in offices, hotels and homes. In fact, in today's market in China, unit air-conditioners rank among the top 'best-sellers'. Today, about 30% of global primary energy consumptions are attributed to building heating and cooling(Davis 1983).

The energy crisis which occurred in early 1970's caused dramatic changes in energy policies in the developed countries. In practice, various energy conservation measures were adopted in various energy consumption sectors. As a result, together with many other factors, world oil demand dropped by 20% in the early 1980's(Strub 1983).

Though the crisis was over, energy conservation in buildings remains to be an important issue, but not only on the economy basis, but also on the global environment protection basis. The global warming phenomenon due to the green house effect of carbon dioxide CO<sub>2</sub> and the ozone layer depletion effect of the currently used refrigerants CFCs(Chlorofluorocarbons) become two very important environmental factors in determining energy conservation measures in building sector. On the other hand, the stringent energy conservation measures imposed on building design and operation practices include the air-tight building design to reduce energy losses caused by air infiltrations. Together with the increased use of some new building materials, this contributes to the so called sick building syndrome(SBS) prevalent in certain buildings. And furthermore, in the modern society, a large portion of people spend most of their time indoors. Therefore, in the last decades, indoor air quality(IAQ) in residences, offices and other indoor non-industrial environments has been an issue of increasing concern. Therefore, concerns over both the global environment and indoor environment have made building sector become into an interdisciplinary engineering and social branch.

These concerns, on one hand, have brought about many new building elements and systems, such as the passive systems proposed by Paassen(1988, 1993) and controllable natural vents(Knoll 1993) and cooled-ceiling systems(Mertz 1992, Wilkins 1992), and on the other hand, have stimulated many research activities concerning building thermal behaviour and its optimum control(Lute and Paassen 1990, 1993) and indoor air quality study. As a result, building practice has very much advanced, not only as an art but also as a science. One prominent progress in building research is the application of computer simulation technique for building thermal behaviour studies, building service components and system performance study, as well as for indoor air flow investigation purposes. In order to estimate various novel energy-saving building design concepts and their integral effects, computer models are playing increasingly important roles. This is, of course, attributed to the massive availability of computers. Already, such models are being used by architects even though they are not always reliable and sometimes can yield large discrepancies(Strub 1983)

## 1.2 STATEMENT OF THE PROBLEM

Since the principal purpose of heating and cooling is to maintain an comfortably-acceptable indoor temperature, air humidity and air flow velocity, it is obvious that the indoor air flow characteristics should be fully understood and quantitatively mastered by design engineers. Unfortunately, this is not the case in practice. In general, indoor air flows are characterized by mixed-convection flows, i.e., buoyancy effect due to density differences caused by temperature variation usually plays a competitive role with the forced flow imposed by a supplied air jet. This gives difficulty to design engineers in estimating the velocity and air temperature distributions in a room, as well as their comfort effects in the design stage. Experimental correlations about the diffusion and decay of supplied air jets are usually obtained from laboratory tests; much uncertainties arise when they are extrapolatedly applied to some practical situations to design a ventilation system. Full scale tests are expensive, and time and labour consuming, and sometimes impossible regarding the size

of the individual building space. If necessary, tests have to be performed on geometrically reduced-scale models to estimate the performance of a design. However, because of the conflicting requirement between Reynolds number( $Re$ ) similarity and Archimedes number( $Ar$ ) similarity, an undistorted similitude scaled-down model is not possible for rooms with internal heat sources(Zhang, et al 1989). Therefore, a success of a design very much relies upon the experiences of a designer, and yet troublesome post-construction remedies can not always be avoided.

Since late 1970's, the numerical simulation technique of turbulent flows has been very much advanced, which may be attributed to the rapid development of computation capacity and the availability of several engineering turbulence models. Soon CFD technique found its use also in building air flow studies. The roles of numerical simulation of air flows are still expanding, while the technique itself needs to be improved and perfected through establishment of better hypothesis and refined experimental validations.

Ideally, a cooling or heating system is to maintain an thermally comfortable indoor environment at minimum energy costs. This requires understanding the thermal dynamic behaviours of the building components both individually and as a whole, and the operational dynamics of the heating and cooling systems. The last few years have witnessed great advancement in the mathematical modelling technique of building thermal dynamics and system performances, and especially the related computer simulation tools. It is virtually possible to simulate the heat transfer and energy transport processes involved in buildings in rather vigorous detail. Now it is also widely acknowledged that building energy concern should be involved in the early architectural design stage. For this purpose, some kind of easy-to-use computer tools based on complicated mathematical modelling technique will be very useful so that the building energy estimation can be reasonably approached at the early design stage. This trends can be better perceived in the recent international conference Building Simulation'93. However, this trans-disciplinary information exchange is by no means an easy task. Still, within the research community, some duplication of effort exists as each country or research institute develops its own simulation tools, on one hand, to maintain a presence in the field, and on the other hand, to cater for its particular needs. The later factor reflects the difficulties in working-out some generic computer simulation systems that can rigorously cater for any particular details of interest. This may be also due to the large variations in building and its service system design.

Although indoor air flow is an essential part of all the thermal processes involved in the whole building thermal dynamics. The simulation technique of the indoor air flow and whole building dynamics were developed somewhat independently. The tendency to combine the two has been shown in some recent works(Chen 1988, Holmes 1990). However, there remains the problem of the too much computing time required for the CFD part.

### **1.3 OBJECTIVES AND SCOPE OF THE PRESENT RESEARCH**

Therefore, the study of building simulation models constitutes the topic of the work presented in this book. This work is conceived in view of, on one hand, the need and

usefulness of computer simulation tools for researchers and building design engineers, and on the other hand, the fact that current models are not always reliable and their experimental validation was and remains an essential part of model perfection and application. In particular, the present study tries to address two specific issues. One is what a design engineer can benefit from CFD simulation, given the limit of the present state-of-the-art of turbulence modelling. The second is how a room installed with cooled-ceiling systems can be modelled in such rigorous way so that some practical issues such as thermal comfort and energy performances can be investigated numerically.

Therefore, the first part of the present research involves the brief survey of the engineering turbulence models available. Then, the most widely used  $k-\epsilon$  turbulence models are tested against the measurements in a real sized climate room. This work is intended to use  $k-\epsilon$  turbulence models to give more accurate predictions of room air flows in terms of flow pattern and convective heat transfer, by optimizing the grid-node locations in the numerical schemes and combining some experimentally-obtained surface convective heat transfer coefficients. For this purpose, the widely-used and commercially available computer code PHOENICS is used. The CFD code will be used to calculate some practical indices such as PD(Percentage Dissatisfied) due to draft, vertical temperature stratification, as well as ventilation effectiveness that are associated with different air-conditioning systems. These ultimate indices will be compared with detailed anemometry measurements.

The validated program will be further used for indoor comfort studies for several practical situations. The program is also used for the simulation of flows in a room with cold ceiling systems. These simulation will demonstrate how far the CFD technique can go in assisting us to estimate thermal comfort and ventilation effectiveness problems.

The second part of the present research deals with building thermal dynamic simulation and HVAC system energy and performance simulation. The principle of the technique is reviewed and its miscellaneous applications are also briefly reviewed. Most part of this work is spend on the construction of a computer program that allows energy and thermal comfort estimations for both air system and hydronic(water) cooling systems. In particular, the cooled-ceiling systems that are currently applied widely in the European countries are built into the model in detail. The cooled-ceiling systems studied will include both the air-panel type and water-panel type. Then great effort is put on the validation of the program against the dynamic measurements in a climate room with cooled ceiling systems. The work will be aimed ultimately at simulation of annual energy consumption of different air-conditioning systems, as well as thermal performances of some passive cooling schemes. The cooling schemes studied include the combination of the evaporative cooling schemes with the water-type cooled-ceiling techniques.

#### 1.4 OUTLINE OF THE THESIS

The works mentioned above are presented in the thesis as follows: Chapter 2 presents the review of the state-of-art of CFD(Computational Fluid Dynamics) and its application in indoor climate engineering. For those who are familiar with the CFD area and only interested in the new contributions of the present research, Chapter 2 may be skipped. Chapter 3 presents the experimental evaluation the  $k-\epsilon$  turbulence models done by the

present author. These results will highlight some specific problems associated with the turbulence models and will give some new recommendations to properly apply the models for indoor air flow simulation purposes. Chapter 4 gives a brief review of building thermal dynamic energy analysis methods, the purpose is to show how the traditional methods can be integrated with new models for cooled-ceiling panels. In Chapter 4, one essential differences between an all-air system and a cooled-ceiling system, i.e. the radiant effects will be addressed in the mathematical models. This will lay down a foundation for the study of some practical aspects of the systems. Chapter 5 presents measurements of the convective parameters involved in the model, as well as the validation of the enhanced program ACCURACY against the dynamic measurements in the room with cooled ceilings. After these tool construction and validation work, Chapter 6 and Chapter 7 present the application of these tools for the numerical simulation to address practical issues. Chapter 6 tries to demonstrate how the CFD simulation can be combined with building dynamic simulation to give a more thorough understanding of the indoor climate of three typical air-conditioning systems, i.e., the conventional displacement ventilation system, the water-panel type cooled-ceiling coupled with displacement ventilation system, and the air-panel type cooled-ceiling system. Chapter 7 presents the year round simulation of energy consumption of cooled-ceiling systems versus all-air systems. Various potentials of energy savings are also simulated in the chapter, which demonstrates the powers of the present simulation program. The last chapter, Chapter 8 gives an overall conclusion drawn from the present work, and suggestions for future researches are also given in the chapter.



## CHAPTER 2

# NUMERICAL SIMULATION OF INDOOR AIR FLOWS

### 2.1. INTRODUCTION

Indoor air flow has great influence on human thermal comfort, energy consumption for heating or/and cooling, as well as on indoor contaminants distribution and their removal. Anyone can feel the velocity of the air movement, and therefore the direct influence of velocity on the human comfort is thus obvious. This influence was investigated in certain administered subjects tests, as reported by McIntyre(1979), Jones et al.(1986) and Fanger et al(1986). Researches by Fanger et al(1988) have shown that turbulence intensity of the air flow also has great influence on the sensation of draft - a sensation of cooling. Further, not only the average temperature but also the air temperature difference around the human body have influence on the thermal comfort(Oleson et al. 1979 and ISO7730, 1984). The temperature stratification also has influence on the energy efficiency of a ventilation system(Chen and Kooi, 1990). The air flow pattern also determines how the indoor contaminants such as the odorous substances produced by occupants will be distributed in the occupied space and therefore the indoor air quality can be greatly influenced by differences in flow patterns(Chen 1988, Chen, Kooi and Meyers 1988). Therefore, understanding of the indoor air flow is an important factor for the design and maintaining of a comfortable, healthy and energy efficient indoor climate.

The indoor air flow may be caused by one or several combinations of the following sources. In most rooms, the external wall or window surface will be cooler in winter and warmer in summer than other indoor surfaces, the adjacent air will be either heated or cooled. Moreover, the air adjacent to the occupants and other internal heat sources is always heated. When the air is heated or cooled, its density changes, i.e., it becomes lighter or heavier, and therefore it tends to float upward or sink downward due to buoyancy effect. We usually call this kind of flow natural convection, or more strictly buoyancy driven flows. Such flows are also originated from a heating radiator or cooling panels. In most cases, this buoyancy effect tends to create a vertical temperature difference in a room; hot air floats above near the ceiling level while cold air sticks to the floor.



Indoor air flow is also caused by air infiltration through openings on building envelopes, and traditionally this provided the necessary air required by indoor human occupants. This flow itself may be caused by two sources - the wind pressure around the building and the stack effect due to indoor and outdoor air temperature differences. Since the energy crisis occurred in 1970's, one of the energy conservation measures imposed on buildings is the air-tight building design to reduce energy losses caused by air infiltration. Obviously, this flow very much depends on building types. For naturally-ventilated buildings, this flow is an important factor that decide the performances of the building.

In an air-conditioned or mechanically ventilated room, an air jet is introduced into the room. Depending on the supplied air temperature, the jet may behave differently. Again, the buoyancy effect plays an important role in this case. Also, a well known phenomenon in fluid flow, the so called Coanda effect, plays an important part, i.e., a jet tends to attach to the adjacent wall. Therefore, the overall flow in rooms is a kind of mixed convection flow.

These characteristics make the air flow in a room rather complicated. In practice, it is desired that the air temperature be uniform in the occupied zone, and that the air velocity at a reasonable level for thermal comfort. For a better indoor air quality, it is also desirable that the air flows in such a way that the contaminants from various indoor sources(including human beings) go to the exhaust directly without recirculation. For a better energy efficiency, it will be ideal that the air leaving the room has maximum temperature in cooling situations and minimum temperature in heating situation. Unfortunately, these requirements may conflict with each other. For example, the positive vertical temperature stratification may be favourable for contaminants removal and for a better energy efficiency for cooling systems, but it may also cause thermal discomfort if the vertical temperature difference is too large between the feet and the head. Therefore, a good design has to be a compromise among these requirements. In order to optimise design and to ensure a healthy interior, increasing attention is being focused on building air flow behaviour and mixing characteristics.

In many instances it is difficult to consider in detail the pattern of air flow or the influence of air movement on thermal and pollutant transport. In the past, numerical techniques for building air flow analysis have tended to concentrate on the calculation of mass flow rates through defined openings and on the direction of flow into and out of zones due to wind-pressure or stack effect. These methods provide information on interzonal air flow patterns and they may also be used to predict air exchange rates.

However, these methods ignore air flow behaviour within individual zones, since this is assumed to be instantaneously and perfectly mixed. Often if more detail is required, ventilation effectiveness measurements may be made using tracer gas techniques. This approach is used to determine the degree to which fresh air is circulated and mixed within the occupied zone. Alternatively, anemometry measurements may be made, either within the building or within a suitably constructed scale model. However, for mixed convection cases, full similarity may be difficult to realize at scaled-down models. At the design stage of air distribution systems, the few empirical correlations about the decay of a free or attached jet are usually applied to size and locate air inlets and determine the supplied air temperature and flow-rate. However, if the application situation differs from that in which

a correlation is derived, as often encountered in practice, the risk is great that the designed system may ill-function in operation.

Recently, increasing interest has been shown in the use of computational fluid dynamics(CFD) to predict the pattern of air flow in buildings(Nielson 1989). Potentially, these techniques offer substantial benefits in the design and evaluation of both energy efficient and air quality efficient ventilation installations. However, as in many other areas of building physics, the successful implementation of these methods is substantially complicated by the individuality of building design and construction and almost limitless variations in building use combined with the flow characteristics mentioned above.

As a consequence, the validity and range of applicability of CFD codes for building air flow analysis is far from certain. The objective of this chapter is to outline recent developments in building air flow analysis and to focus on some of the difficulties associated with this complex field of study. Considerable developments in the area of CFD are currently taking place, both in relation to turbulence model modifications and in relation to refinements in calculation techniques. Rather than present an in-depth study of these developments, this chapter concentrates on the specific aspects in relation to air flow in buildings.

## 2.2. MATHEMATICAL PRESENTATION OF AIR FLOW

### 2.2.1. Conservation Laws

Air movement occurs as a consequence of pressure differences between adjacent air masses which are sustained by naturally and/or mechanically derived forces. This movement is governed by the conservation laws for mass, momentum, thermal energy and species concentration. These conservation equations are introduced in this section, although no attempt has been made to present a full derivation. The intention is to illustrate the necessity of each parameter and to show how they combine to describe the total flow field. For incompressible flows, these conservation laws can be expressed in tensor notation as

Mass conservation: continuity equation

$$\frac{\partial u_i}{\partial x_i} = 0 \quad (2.1)$$

Momentum conservation: Navier-Stokes equations

$$\frac{\partial u_i}{\partial t} + u_j \frac{\partial u_i}{\partial x_j} = - \frac{1}{\rho_0} \frac{\partial p}{\partial x_j} + \nu \frac{\partial^2 u_i}{\partial x_j \partial x_j} + g_i \frac{\rho - \rho_0}{\rho_0} \quad (2.2)$$

Thermal energy/species concentration conservation

$$\frac{\partial \Phi}{\partial t} + u_i \frac{\partial \Phi}{\partial x_i} = \lambda \frac{\partial^2 \Phi}{\partial x_i \partial x_i} + S_\Phi \quad (2.3)$$

where  $u_i$  is the instantaneous velocity component in the direction  $x_i$ ,  $p$  is the modified instantaneous static pressure, i.e.,  $p = p_s - \rho_0 g_i x_i$ , where  $p_s$  is the static pressure; and  $\Phi$  is a scalar quantity which may stand for either temperature  $T$  or species concentration  $C$ .  $S_\Phi$  is a volumetric source term expressing, for example, heat generation due to chemical reactions.  $\nu$  and  $\lambda$  are the molecular(kinematic) viscosity and diffusivity (of  $\Phi$ ) respectively. Use has been made in the above equations of the Boussinesq approximation so that the influence of variable density appears only in the buoyancy term on the right hand side of Eq.(2) involving the reference density  $\rho_0$  and the gravitational acceleration in the direction  $x_i$ . Together with an equation relating the local density  $\rho$  to the local values of  $T$  and  $c$ , e.g.,  $(\rho - \rho_0)/\rho_0 = \beta (T_0 - T)$ , Eqs.(2.1) to (2.3) form a closed set equations; and in principle they describe all the details of the turbulent motion. But unfortunately, these equations cannot at present be solved directly for turbulent flows of practical relevance, though efforts being made in this direction. This difficulty may attribute to the complex nature of turbulence in theory and the available computation capacity restrictions in practice.

Therefore, in the following section, a statistical approach, which was first suggested by Osborne Reynolds and which forms the basis of turbulence modelling, will be introduced.

### 2.2.2. Turbulence modelling

The starting point of this statistical approach is to separate the instantaneous values of the velocity  $u_i$ , the pressure  $p$  and the scalar quantity  $\Phi$  into mean and fluctuating quantities

$$u_i = \bar{u}_i + u_i' , \quad p = \bar{p} + p' , \quad \Phi = \bar{\Phi} + \Phi' \quad (2.4)$$

where the mean quantities are defined as

$$\bar{u}_i = \frac{1}{\Delta t} \int_t^{t+\Delta t} u_i d\tau , \quad \bar{p} = \frac{1}{\Delta t} \int_t^{t+\Delta t} p d\tau , \quad \bar{\Phi} = \frac{1}{\Delta t} \int_t^{t+\Delta t} \Phi d\tau \quad (2.5)$$

where  $\Delta t$  is the averaging time. For brevity, the overbars indicating the mean values will be dropped from now on. Introducing Eqs.(2.4) into Eqs.(2.1) to (2.3) and subsequently averaging the equations again in the same way yields the following equations:

$$\frac{\partial u_i}{\partial x_i} = 0 \quad (2.6)$$

$$\frac{\partial u_i}{\partial t} + u_j \frac{\partial u_i}{\partial x_j} = -\frac{1}{\rho_0} \frac{\partial p}{\partial x_i} + \frac{\partial}{\partial x_j} \left( \nu \frac{\partial u_i}{\partial x_j} - \overline{u_i u_j'} \right) + g_i \frac{\rho - \rho_0}{\rho_0} \quad (2.7)$$

$$\frac{\partial \Phi}{\partial t} + u_i \frac{\partial \Phi}{\partial x_i} = \frac{\partial}{\partial x_i} \left( \lambda \frac{\partial \Phi}{\partial x_i} - \overline{u_i \Phi'} \right) + S_\Phi \quad (2.8)$$

where,  $u_i' u_j'$  and  $u_i' \Phi'$  are turbulent correlations and they are defined similarly as those defined by Eq.(2.5) as follows

$$\overline{u_i u_j'} = \frac{1}{\Delta t} \int_t^{t+\Delta t} u_i' u_j' d\tau, \quad \overline{u_i \Phi'} = \frac{1}{\Delta t} \int_t^{t+\Delta t} u_i' \Phi' d\tau$$

Equations (2.6), (2.7) and (2.8) are known as Reynolds average equations and can be solved for the mean values of velocity, pressure and temperature or concentration only when the turbulence correlations  $u_i' u_j'$  and  $u_i' \Phi'$  can be determined in some way (for brevity, the overbars will be dropped from now on in this context). For this purpose of equation closure, different turbulence models are introduced, which approximate the correlations  $u_i' u_j'$  and  $u_i' \Phi'$  either in terms of the mean-flow quantities or by introducing the transport equations for the correlations.

Most turbulence models today are still based upon the oldest proposal for modelling the turbulent or Reynolds stresses -  $\rho u_i' u_j'$ , which is the eddy-viscosity concept proposed by Boussinesq(1887). This concept assumes that, in analogy to the viscous stresses in laminar flows, the turbulent stresses are proportional to the mean velocity gradients. For general flow situations, this concept may be expressed as

$$-\overline{u_i u_j'} = \nu_\tau \left( \frac{\partial u_i}{\partial x_j} + \frac{\partial u_j}{\partial x_i} \right) - \frac{2}{3} k \delta_{ij} \quad (2.9)$$

where  $\nu_\tau$  is the turbulent or eddy viscosity which, in contrast to the molecular viscosity  $\nu$ , is not a fluid property but depends strongly on the state of turbulence;  $k$  is the turbulent kinetic energy of the fluctuating motion:

$$k = \frac{1}{2}(\overline{u_1'^2} + \overline{u_2'^2} + \overline{u_3'^2}) \quad (2.10)$$

and  $\delta_{ij}$  is the so called Kronecker delta in tensor notation ( $\delta_{ij} = 1$  for  $i = j$  and  $\delta_{ij} = 0$  for  $i \neq j$ ).

In direct analogy, the turbulent heat or mass transport is assumed to be related to the gradient of the average transported quantity,

$$-\overline{u_i \Phi'} = \Gamma \frac{\partial \Phi}{\partial x_i} \quad (2.11)$$

where  $\Gamma$  is the turbulent diffusivity of heat or mass and is closely related to  $\nu_\tau$ :

$$\Gamma = \frac{\nu_\tau}{\sigma_\tau} \quad (2.12)$$

$\sigma_\tau$  is called the turbulent Prandtl number for heat transfer and Schmidt number for mass transfer and assumed to be a constant.

Also turbulence models were developed which do not make use of the turbulent viscosity/diffusivity concept but introduce differential transport equations for the turbulent momentum and heat / mass fluxes  $u'_i u'_j$  and  $u'_i \Phi'$ , such as the Reynolds-stress-equation model(Chou,1945). The model will not be fully described here, however, it should be noted that this model is potentially superior to the eddy-viscosity concept based models.

A completely different turbulence-modelling approach should be mentioned here which aims to simulate the time-dependent Eqs.(2.1) to (2.3). Based on the hypothesis that the turbulent motion is the motion of a highly disordered array of eddies of widely different sizes and that the small-scale eddies are less problem dependent, the small-turbulence is represented by relatively simple models. Therefore, only large-scale motion is solved for through the time-dependent equations(Deardorf, 1969). Even though, numerical solution of the modelling equations still requires high computer capacity(Lafeber, 1987). This model is considered to be useful as an aid for developing and testing the conventional type turbulent models that calculate the Reynolds stresses and heat or mass fluxes. More descriptions of the LES model can be found in literature, such as by Deardorf(1973), and Nieuwstadt and Brost(1986).

At present, the turbulence models that have given practical contributions in engineering are those based upon Boussinesq's eddy-viscosity concept. For numerical simulation of indoor airflows, the k- $\epsilon$  turbulence model is most-widely used. Therefore, these models will be explained below.

### 2.3 k- $\epsilon$ TURBULENCE MODELS

### 2.3.1 The Standard k-ε Turbulence Model

If the velocity fluctuations in turbulence are to be characterized by one scale, the physically meaningful scale is  $\sqrt{k}$ , where  $k$  is the kinetic energy of the turbulent motion per unit mass defined by Eq.(2.10).  $\sqrt{k}$  is also easily related to quantities of practical interest. In room air flows, the turbulent intensity  $I$  has direct influence on human comfort, which is related to  $k$  by

$$I = \frac{\sqrt{2k}}{V} \quad (2.13)$$

where  $V$  is the magnitude of the time-mean air velocity in the room.

In the turbulence flows,  $\sqrt{k}$  is a velocity scale for the large-scale turbulent motion. In k-ε turbulence models, this velocity scale is used for the eddy viscosity calculation

$$\nu_\tau = C_\mu \sqrt{k} l \quad (2.14)$$

where  $C_\mu$  is an empirical constant;  $l$  is the so called 'mixing length' of turbulent motion, which is proposed by Prandtl in analogy to the molecular 'free paths'. In k-ε turbulence models,  $l$  is related to  $k$  and another turbulent quantity  $\epsilon$  by

$$l = k^{3/2} / \epsilon \quad (2.15)$$

where,  $\epsilon$  is the turbulence energy dissipation rate, and is defined as

$$\epsilon = \nu \overline{\frac{\partial u_i}{\partial x_j} \frac{\partial u_i}{\partial x_j}} \quad (2.16)$$

Further, two transport equations about  $k$  and  $\epsilon$  are introduced, which will be solved together with the basic transport equations. For this reason, k-ε turbulence model is classified as a two-equation turbulence model as distinct from other zero-equation or one-equation turbulence models. The  $k$  and  $\epsilon$  equations can be derived in exact form from the Navier-Stokes equation (2.2) and the Reynolds time-mean equation (2.7). Through mathematical manipulation, the  $k$  equations reads

$$\begin{aligned} \frac{\partial k}{\partial t} + u_j \frac{\partial k}{\partial x_j} &= u_i \frac{\partial}{\partial x_j} \overline{v \left( \frac{\partial u_i}{\partial x_j} + \frac{\partial u_j}{\partial x_i} \right)} \\ &- \frac{1}{2} \frac{\partial}{\partial x_j} \overline{u_i u_i u_j} + P_k + G_B - \frac{1}{\rho_0} u_i \frac{\partial p'}{\partial x_i} \end{aligned} \quad (2.17)$$

where

$$P_k = -\overline{u_i u_j} \frac{\partial u_i}{\partial x_j}, \quad G_B = \overline{\rho' u_i} g_i / \rho_0 \quad (2.18)$$

However, the right hand terms contain new unknown correlations. To obtain a closed set of equations, model assumptions have to be made. In analogy, the first term is split into a viscous diffusion part and a viscous dissipation part

$$\overline{u_i' \frac{\partial}{\partial x_j} v \left( \frac{\partial u_i'}{\partial x_j} + \frac{\partial u_j'}{\partial x_i} \right)} = \frac{\partial}{\partial x_j} \left( v \frac{\partial k}{\partial x_j} \right) - \epsilon \quad (2.19)$$

The second term is modelled according to

$$\frac{1}{2} \frac{\partial \overline{u_i' u_i' u_j'}}{\partial x_j} = \frac{\partial}{\partial x_j} \left( \frac{v_\tau}{\sigma_k} \frac{\partial k}{\partial x_j} \right) \quad (2.20)$$

where  $\sigma_k$  is the turbulent Prandtl number for  $k$ . The Reynolds stress  $-u_i' u_j'$  in the third term is modelled according to Eq.(2.9). Under the Boussinesq approximation density fluctuation is approximated by temperature fluctuation, and therefore  $\rho' u_i'$  in the fourth term is modelled according to

$$\overline{\rho' u_i'} = -\rho_0 \beta \overline{u_i' T'} = \rho_0 \beta \frac{v_\tau}{\sigma_T} \frac{\partial T}{\partial x_i} \quad (2.21)$$

This approximation is rather arbitrary, and is considered not taking into account the non-isotropic effect of buoyancy on turbulence production. The effect of this approximation on indoor air flow situations deserve special investigations.

The fifth term is much smaller and therefore can be neglected.

Through mathematical manipulation, the transport equation for  $\epsilon$  is obtained as

$$\begin{aligned} \frac{\partial \epsilon}{\partial t} + u_j \frac{\partial \epsilon}{\partial x_j} &= -\frac{\partial}{\partial x_k} \left( v u_k' \frac{\partial u_i'}{\partial x_j} \frac{\partial u_i'}{\partial x_j} + 2 \frac{v}{\rho_0} \frac{\partial u_k'}{\partial x_i} \frac{\partial \rho'}{\partial x_j} - v \frac{\partial \epsilon}{\partial x_k} \right) \\ &- 2v \frac{\partial u_i'}{\partial x_k} \frac{\partial u_i'}{\partial x_j} \frac{\partial u_k'}{\partial x_j} - 2v^2 \frac{\partial^2 u_i'}{\partial x_k \partial x_j} \frac{\partial^2 u_i'}{\partial x_k \partial x_j} + 2 \frac{v}{\rho_0} \frac{\partial u_i'}{\partial x_j} \frac{\partial \rho'}{\partial x_j} \\ &- 2v \frac{\partial u_i'}{\partial x_k} \left( \frac{\partial u_i'}{\partial x_j} \frac{\partial u_k'}{\partial x_j} + \frac{\partial u_j'}{\partial x_i} \frac{\partial u_j'}{\partial x_k} \right) - 2v u_k' \frac{\partial u_i'}{\partial x_j} \frac{\partial^2 u_i}{\partial x_j \partial x_k} \end{aligned} \quad (2.22)$$

This equation is an exact deduction from the N-S equations. However, the right hand terms contain new unknown correlations, and again for equation closure purposes, these correlation terms are mathematically modelled by associating them with the mean flow quantities.

The first term consists of three contributions: turbulent diffusion, pressure diffusion and molecular diffusion. The pressure diffusion is neglected and the remaining part is modelled analogously as

$$-\frac{\partial}{\partial x_k} \left( v u_k' \frac{\partial u_i'}{\partial x_j} \frac{\partial u_i'}{\partial x_j} - v \frac{\partial \epsilon}{\partial x_k} \right) = \frac{\partial}{\partial x_j} \left( v + \frac{v_\tau}{\sigma_\epsilon} \right) \frac{\partial \epsilon}{\partial x_j} \quad (2.23)$$

where  $\sigma_\epsilon$  is the turbulent Prandtl number for  $\epsilon$ . The sum of the second and third terms is modelled as

$$-2v \frac{\partial u_i'}{\partial x_k} \frac{\partial u_i'}{\partial x_j} \frac{\partial u_k'}{\partial x_j} - 2v^2 \frac{\partial^2 u_i'}{\partial x_k \partial x_j} \frac{\partial^2 u_i'}{\partial x_k \partial x_j} = (C_{\epsilon 1} P_k - C_{\epsilon 2} \epsilon) \frac{\epsilon}{k} \quad (2.24)$$

where  $C_{\epsilon 1}$  and  $C_{\epsilon 2}$  are empirical constants in the model. The fourth term is modelled as

$$2 \frac{v}{\rho_0} \frac{\partial u_i'}{\partial x_j} \frac{\partial \rho'}{\partial x_j} g_i = C_{\epsilon 3} C_{\epsilon 3} G_B \frac{\epsilon}{k} \quad (2.25)$$

where  $C_{\epsilon 3}$  is an empirical constant. The fifth and sixth terms are much smaller and thus are neglected for fully turbulent flows.

After these modelling, the equations (2.6) - (2.8), (2.17) and (2.22) form a closed set of partial differential equations. In summary, all the equations in  $k-\epsilon$  turbulence models can be represented in the general form

$$\frac{\partial(\rho\Phi)}{\partial \tau} + \text{Div}(\rho U \Phi - \Gamma_{\Phi, \text{eff}} \text{grad} \Phi) = S_\Phi \quad (2.26)$$

where  $U$  is the velocity vector, The corresponding coefficients and constants for the individual equations are presented in Table (2.1). The values of the empirical constants are those recommended by Launder and Spalding(1974).



Table 2.1 Terms, Coefficients and Constants in Eq.(2.26)

Equation	$\Phi$	$\Gamma_{\Phi,eff}$	$S_{\Phi}$
Continuity	1	0	0
Momentum	$u_i$	$\mu_{eff}$	$-\partial p/\partial x_i - \rho\beta/C_p g_i\theta$
	$k$	$\mu_{eff}/\sigma_k$	$P_k - \rho\varepsilon + G_B$
	$\varepsilon$	$\mu_{eff}/\sigma_\varepsilon$	$\varepsilon(C_1P_k - C_2\varepsilon)/k + C_3G_B \varepsilon/k$
Enthalpy	H	$\mu_{eff}/\sigma_H$	$S_H$
Concentration	C	$\mu_{eff}/\sigma_C$	$S_C$

$P_k = \mu_t (\partial u_i/\partial x_j + \partial u_j/\partial x_i) \partial u_i/\partial x_j$   
 $G_B = \beta/C_p g_i \mu_t/\sigma_{H,t} \partial\theta/\partial x_i$   
 $\theta = H - H_0$   
 $\mu_{eff} = \mu_t + \mu$   
 $\mu_t = C_\mu \rho k^2/\varepsilon$   
 $C_1=1.44, C_2=1.92, C_3=1.44, C_\mu=0.09, \sigma_k=1.0, \sigma_\varepsilon=1.3, \sigma_H=0.9, \sigma_C=1.0$

### 2.3.2. Boundary Conditions

In principle, the k-ε model described above is valid only in the flow region where turbulent transport is dominating. Therefore, special boundary conditions need to be specified to describe the flow close to the wall. For this purpose, the logarithmic law wall functions are used.

The logarithmic wall functions were initially developed for forced convection boundary layers. The flow close to the wall is considered as consisting of a purely viscous sub-layer, a fully turbulent outer layer, and a buffer-layer in-between. The velocity and temperature profiles in a forced convection boundary layer, with zero pressure gradient, are approximated by the logarithmic wall functions

$$u^* = \frac{1}{0.41} \ln(9y^*) \tag{2.27}$$

$$T^* = 2.195 \ln(y^*) + 13.2Pr - 5.66 \tag{2.28}$$

for  $y^* > 15$ , with

$$y^* = y u_\tau^*/\nu, \quad u^* = u/u_\tau, \quad T^* = (T_w - T)/T_\tau$$

$$u_\tau = \sqrt{\nu(\partial u/\partial y)_w}, \quad T_\tau = -\frac{\nu}{P_r u_\tau} \left(\frac{\partial T}{\partial y}\right)_w \tag{2.29}$$

The boundary conditions for k and ε are obtained by simplifying the differential

equation for  $k$  in Eq.(2.16) in the boundary layer and applying Prandtl's mixing length hypothesis

$$v_t = (0.41y)^2 \frac{\partial u}{\partial y} \quad (2.30)$$

in the boundary layer. The wall functions for  $k$  and  $\epsilon$  are thus found to be

$$\frac{k}{u_\tau^2} = \frac{1}{\sqrt{C_u}} \quad (2.31)$$

$$\frac{v\epsilon}{u_\tau^4} = \frac{1}{0.41y^*} \quad (2.32)$$

for  $y^* > 11.5$ .

### 2.3.3. Low-Reynolds-number $k$ - $\epsilon$ Model

#### 2.3.3.1. Basic Equations

As mentioned in the last section, the standard  $k$ - $\epsilon$  turbulence model only holds in the region where turbulent-transport is overwhelming, i.e, the turbulence based Reynolds-number,  $Re_t = k^2 / (v\epsilon)$ , is large. However, flows close to a fixed wall are much determined by the molecular viscous effect. To adapt the  $k$ - $\epsilon$  concept to boundary flows, a number of modifications have been made to the standard  $k$ - $\epsilon$  model, and therefore a number of so called low-Reynolds number models are developed. In these low-Reynolds number models, several functions are introduced into the  $k$ - $\epsilon$  equations:

$$u \frac{\partial k}{\partial x} + v \frac{\partial k}{\partial y} = \frac{\partial}{\partial x} \left( v + \frac{v_t}{\sigma_k} \right) \frac{\partial k}{\partial x} + P_k - \epsilon + D \quad (2.33)$$

$$u \frac{\partial \epsilon}{\partial x} + v \frac{\partial \epsilon}{\partial y} = \frac{\partial}{\partial x} \left( v + \frac{v_t}{\sigma_\epsilon} \right) \frac{\partial \epsilon}{\partial x} + (C_{\epsilon_1} f_1 P_k - C_{\epsilon_2} f_2 \epsilon) \epsilon / k + E \quad (2.34)$$

There are different forms of functions for  $f_1$ ,  $f_2$ ,  $f_\mu$ ,  $D$  and  $E$  in different low Reynolds number models (Patel *et al* 1985). It is reported by Henkes *et al* (1989) that, among the low Reynolds number turbulence models, the Lam & Bremhorst model (LB model) and the Jones and Launder model (JL model) gave better predictions of convective heat transfer for the turbulent natural convection in an enclosed cavity, although about 20% errors exist.

Therefore, the LB model is chosen for the present investigations, and to improve the prediction accuracy of convective heat transfer, different boundary conditions will be tested. The above functions in the LB model are:

$$f_{\mu} = (1 - \exp(-0.0165 Re_k))^2 (1 + 20.5/Re_e)$$

$$f_1 = 1 + (0.05/f_{\mu})^3$$

$$f_2 = 1 - \exp(-Re_e^2)$$

$$D = E = 0$$

where,  $Re_k$  and  $Re_e$  are local turbulence Reynolds numbers:

$$Re_k = k^{1/2} y / \nu_p, \quad Re_e = k^2 / \nu \epsilon$$

where  $y$  is the distance from the solid wall.

### 2.3.3.2. Boundary Conditions

In principle, for low Reynolds number  $k$ - $\epsilon$  models, no wall functions are required for boundary conditions. However, boundary conditions for  $k$  and  $\epsilon$  must be specified in one form or another. For the Lam & Bremhorst model, there are at least four different forms of wall boundary specification (Henkes 1990). The following two approaches were reported by Chen, Moser and Huber (1990).

1). boundary specification I

$$k_w = 0, \quad \epsilon_p = 2 \nu_1 k_p / y_p^2 \quad (2.35)$$

i.e., the turbulence kinetic energy at the wall surface is assumed to be zero while the energy dissipation rate at the first grid is associated with  $k_p$  by the second equation .

2). boundary specification II

The logarithmic law wall function is still used. However, different from the standard  $k$ - $\epsilon$  model, the grid lines can be and should be located in the viscous sub-layer.

In principle, boundary condition specification I requires that at least the first grid line be located in the viscous sub-layer. It can be expected that finer grids are needed in the low Reynolds number turbulence model than in the standard  $k$ - $\epsilon$  model. For boundary specification II, the proper location of the first grid-line remains a question.

## 2.4. COMPUTING THE FLOW FIELD - NUMERICAL TECHNIQUES

Obviously the simultaneous solution of the many equations needed to describe the fully turbulent, convective flow field in the form of 3-dimensional partial differential flow equations, can be expected to require considerable computational effort. Despite any possible simplifications, analytical solution of the transport equations is impossible and, therefore, numerical techniques must be applied. The purpose of this section is to outline

some of these techniques.

Basically, numerical techniques used in air flow analysis include both finite difference and finite element methods. Whichever technique is applied, it is essential to discretise the space into control volumes or elements and, then, to use the discretisation equations to represent the physics of flow within each of the elements. In the case of finite volume methods, the flow condition within each of the control volumes is represented by a single value. In the case of finite element techniques, the flow condition is represented by such a functional relationship that the value of the flow parameter is continuously variable through out the discretised element. In both cases all parameters must be given initial arbitrary values from which the iteration process can commence. Iteration is a structured process in which the initial values of each flow parameter are adjusted until the flow equations balance. The process of reaching a successful balance point is known as convergence.

#### **2.4.1. Finite Volume/Difference Methods**

Solving the flow equations is complicated by the fact that the various flow fields are interdependent and that none of them are initially defined. Further complications arise because the velocity components in each of the three directions are present in both the continuity and momentum equations. A method for overcoming these problems is described by Patankar(1980) using a finite difference/volume technique known as the Semi-Implicit Method for Pressure Linked Equations(SIMPLE). This method has subsequently formed the basis of many flow simulation computer codes. The technique involves progressively improving upon an assumed pressure field, using a pressure correction formula, until the resultant component velocity values satisfy the continuity and the momentum equations. This procedure is essentially a sequential approach. An initial pressure distribution is assumed and this is substituted into the momentum equations to evaluate an initial velocity distribution. A pressure correction term is then applied and the consequent new pressure distribution and velocity distributions are valued. Other transport equations which influence the flow field(i.e., temperature field, turbulence etc.) are similarly solved. This iteration process is continued until the continuity equation is satisfied.

For discretisation of the transport equations, staggered grids are used so that velocity components are located at the faces of each control volume. For the discretisation of the convection terms, the up-wind differencing scheme is usually employed to reflect the nature that convection is an asymmetric phenomenon(Patankar 1988). A problem with the sequential SIMPLE procedure to solve the flow equations is the weak coupling between the momentum and buoyancy forces. Changes in the temperature field during an iteration step are transferred to the momentum equations at the start of the following iteration. As a consequence, when the natural convection is dominating, the convergence may become very slow. While the procedure is still widely used in most of the computer codes, new developments are being made both in the differencing schemes and solving algorithms. These new developments are expected either to reduce the so called false-diffusion errors introduced in the discretisation process(Patankar 1988) or to speed up the convergence process(Thompson et al 1988, Vanka et al 1987). One break-through in

reducing the computing time lies in the possibilities of using multitask capabilities of actual and future generations of supercomputers. This will require new algorithms. Efforts have been made by Nobile et al(1989) to solve N-S equations using FORTRAN structured multiprogramming. It is concluded that, for massive parallel architectures, it is not clear how much of old algorithms can be efficiently utilized.

After all, under-relaxation devices are necessary to prevent the iteration from being divergent. Obviously, the values adopted for the relaxation factors for the solved variables have decisive influence on the quickness of convergence. If heavy under-relaxations are used, convergence may become too slow. On the other hand, inadequate under-relaxation may present divergence. Convergence is checked by two criterions: The change in field values between two successive iterations becomes very small and the residuals of the discretised conservation equations are decreasing(Patankar, 1980). While divergence can be easily judged if the residuals are increasing, convergence should be judged with caution. Especially with natural convection in an enclosed space, there will be no reference value to judge if the magnitude of the residuals is small enough. In this case, extra iterations may be necessary to avoid premature termination of the iteration process.

#### **2.4.2. Finite Element Methods**

The particular advantage of finite element methods is in its being able to apply an irregular grid which can be selectively refined and chosen to match the boundaries of the domain. Methods also tend to employ direct simultaneous solution of the continuity equation, the momentum equation and the remaining dependent variables rather than adopting a sequential approach to achieve more rapid convergence. However, difficulties exist in progressing from a 2-dimensional network to a three dimensional system. Examples of the application of the finite element approach for the analysis of three dimensional turbulent air flow are described by Matsumoto et al(1985,1987) and Keresteciolu(1989). This approach is also being developed by Baker(1990) for use as a potential ASHRAE code.

It has generally been found that convergence depends more on the starting conditions when using finite element methods than using finite difference techniques. However an advantage of the finite element method is that once appropriate initial conditions have been found, the process of convergence tends to be faster. Current developments in numerical analysis are focusing on combining the convergence reliability of the finite difference approach with the convergence pace of the finite element methods. Such an attempt is described by Lonsdale(1988).

### **2.5. VALIDATION AND APPLICATIONS OF CFD FOR BUILDING AIR FLOW INVESTIGATIONS**

A number of examples of the validation or evaluation of air flow simulation code may be found in the literature. Generally, measurement methods are, in addition, being used in conjunction with numerical methods as a technique to fine tune or adjust the so called 'empirical' model parameters. Measurements for validation purposes tend to be difficult to control in full size buildings and hence much is being done on scale models or test

chambers. Smoke is widely used as a qualitative measure of air flow and the flow patterns obtained have been used as comparison against the numerical solutions. Kooi and Chen(1986) give examples of the use of measurement result for the fine tuning of wall functions applied to CHAMPION and PHOENICS code. To avoid the underestimated convective heat transfer from the solid wall when the logarithmic wall functions are used, Chen, Meyers and Kooi(1989) used measured convective heat transfer coefficient for 3-dimensional k- $\epsilon$  model prediction of displacement ventilation system. Despite measurement difficulties of low velocities and heat fluxes, generally good comparisons between measurement and calculation have been achieved. The paper highlighted the importance of correct boundary heat transfer simulations.

Murakami et al(1987,1988,1989) compared turbulence modelling results with measurements in a 1/6th test chamber for various configurations of ventilation, internal room obstructions and contaminant sources. In each case a tandem type, parallel hot wire anemometer was used to determine the vector components of turbulent flow. Also flow visualisation of flow across any section was made possible by using a laser light sheet combined with magnesium carbonate powder. Good correspondence between calculation and measurement was observed.

Awbi and Nemri(1989) compare numerical prediction with experimental data for a two dimensional isothermal and non-isothermal flow regime and use the results as a guide for more complex simulation regimes. Comparisons between calculation and measurement were based on the use of a test chamber of 4.2m square section and a height of 2.8m. Calculations were found to correlate well with measurement away from the boundaries but discrepancies close to the boundary of the chamber were associated with the inability of the k- $\epsilon$  model to represent flow at low Reynolds number. Under non isothermal conditions, agreement between predicted and measured flow and temperature profiles was found to be close for most practical purposes.

When k- $\epsilon$  turbulence model is used, the predicted average temperature and air flow patterns are generally in reasonable agreement with measurements. Specific problems arise in the near solid-wall regions. At present, k- $\epsilon$  turbulence model is used in conjunction with the logarithmic wall functions. Some researchers have done certain special investigations of the wall functions. Renz & Terhaag(1990) compared the k- $\epsilon$  model simulation with measurements in a room ventilated by a air jet from a convector. It was found that, best simulation results were achieved when the first grid nodes are located in the region where  $40 < y^+ < 130$  and that the simulated velocity and turbulent intensity are 25% lower and the simulated air temperatures are 5% lower than those found in their measurements. The boundary flow was dominated by the ventilation air jet in this case. However, it has been shown in section 2.3.2, the log-law wall functions are derived from fully developed turbulent isothermal boundary layer flows. In room air flows, it is possible that flows are in the transit regime. And also, buoyancy force plays a competitive role with the forced convection. Therefore, the logarithmic law may, in principle, not apply for the buoyancy driven boundary flows, such as the natural convective boundary flow along the windows or along a heating radiator. However, few evaluations are available about the k- $\epsilon$  simulation of natural convective boundary flows occurring in room air flow situations. In fact, Ozoe et al(1985) found out that  $y^+ > 11.5$  presented wrong

prediction of the heat transfer for natural convection in water, and therefore suggested that  $y^+ < 11.5$  should be used to locate the first grids. Henkes et al.(1989) used very fine grids within the boundary layer in their simulation of turbulent natural convection of air in a cavity, and higher-biased heat transfer was found. Therefore, it may be concluded that, if natural convection is present in a room, boundary condition treatment is still a possible source of errors of simulation results of k- $\epsilon$  model. On the other hand, the low-Reynolds-number k- $\epsilon$  model is recommended by Chen, Moser and Huber(1990) for room air flow simulations. Its validity is yet subject to further investigation for typical in-room air flow situations.

Other turbulence models that have been evaluated for in-room air flow simulation purposes are the algebraic Reynolds-stress model(ASM)(Renz and Terhaag, 1990) and the large eddy simulation(LES) turbulence model(Tsutsumi, 1990). It is shown that ASM predicts a better velocity distribution than the standard k- $\epsilon$  model with log-law wall functions. The only LES application is the simulation of the natural convection through dual-openings in a 2-dimensional air cavity. At present, the applicability of these models is still limited since too much computer-time is required for practical purposes.

Therefore, most applications are k- $\epsilon$  model simulations. The application of CFD to building air flow as part of the design process is relatively new(Nielson, 1989). A few examples are illustrated in this section to give an indication of the scope of applications of CFD techniques.

Broyd et al(1983) give examples of the use of a 2-dimensional CFD code(CAFE) in the assessment of safety and air quality in industrial buildings. A further example of clean room design using this code is also described by Broyd, Deaves and Oldfields(1983) in which computational results are supported by full scale measurements. Altmayer et al.(1983) performed 'numerical experiments' instead of real-size experiments to obtain experimental convective heat transfer correlations for several typical room flow configurations. Markatos(1983) gives an example of the use of 3-dimensional PHOENICS in the analysis of air flow and heat transport in a television studio. The purpose of the study was to determine an optimum ventilation configuration for acceptable flow velocities and temperatures within the occupied zone of the studio. In a series of papers, Chen and Kooi(1988), Chen(1988) and Chen, Meyers and Kooi(1989) described the analysis of 3-dimensional flow in an office type room with cooling using CFD analysis combined with experimental verification. The purpose of the investigation was to evaluate the performance of various heating/cooling and ventilation systems in relation to both energy requirements and comfort conditions. In further studies, by Kooi and Chen(1989) and Chen, Hoonstra and Kooi(1990), the performance of displacement ventilation systems are evaluated in relation to air quality and energy use. Later, Chen, Suter, and Moser(1990) incorporated the olf and decipol concept, which are developed by Fanger et al.(1989) to quantify the emission source and distributions of indoor air odorous contaminants, into the computer code PHOENICS to numerically evaluate the performances of various ventilation systems. Chen, Kooi and Meyers(1988) also developed the methodology of combining indoor air flow simulation with cooling load calculation and system energy estimations. Since the long computer hours needed to solve the flow equations, full coupling is not used. Instead, air flow patterns calculated at several typical load situations are used data

files, which were subsequently used to calculate local room air temperature differences. The local air temperatures are used in the cooling load program ACCURACY (which will be described in Chapter 4).

In a recent development, Haghghat et al (1989) have reported on a numerical study investigating natural convection and air flow patterns within a partitioned enclosure subjected to turbulent flow. Thus an attempt has been made to combine multi-zone air flow with air movement within individual zones. In a recent paper, Niu and Kooi (1992) have used numerical simulation to study the natural ventilation through window openings caused by stack effect. Therefore this is an attempt to combine natural ventilation study with indoor air movement investigations. Efforts have been made by Holmes et al. (1990) to fully couple CFD and building envelope thermal analysis to analyze the transient flow behaviours in the perimeter zone of an office space. It is reported that, with 2-D calculations, 99.5% of the computation time is spent on the CFD part. The simulated results gave practical indications for optimal thermostat location, as well as the system dynamic controller time constant selections. Since the heat transfer at enclosure surfaces are critical for the coupling, experimental correlations about the convective heat transfer coefficients were used. This reflects the inadequacy of CFD in treating boundary flows for practical purposes in room flows. This issue will be further investigated in our research.

## 2.6. CONCLUSIONS

1. The air flow in a room is characterized by turbulent, mixed convective flows. It is also influenced by limitless building factors.
2. The mathematical modelling of turbulence flows contains empirical parameters, their performance for building flow investigation is far from fully validated.
3. The k- $\epsilon$  turbulence model has been widely used in indoor air flow simulations. The applications can be classified into three categories: 1). for thermal comfort, and ventilation effectiveness analysis; 2). for dynamic building energy or HVAC system control analysis via coupled or semi-coupled simultaneous simulation of the transient thermal behaviour of building envelopes and indoor air flows; and 3). for performance of 'numerical experiments' in place of real-size experiments to obtain empirical correlations that could be used for heat and mass transfer calculations.
4. The k- $\epsilon$  turbulence model can generally give reasonable predictions. However, the low Reynolds number effect in the region next to a wall needs to be handled with extra-caution. For forced boundary air flow, it can be approximated by optimizing the first grid location  $40 < y^+ < 130$ . For natural convective boundary layer, the influences of grid location has not yet been evaluated for room flow situations.
5. Review of the various applications of CFD in building air flow investigations shows great potentials of CFD in assisting new system estimation and design, and therefore, evaluation of the standard k- $\epsilon$  model as well as some new developments would be necessary and significant.





## CHAPTER 3

# VALIDATION OF $k$ - $\epsilon$ TURBULENCE MODELS FOR NATURAL CONVECTION FLOWS

### 3.1. INTRODUCTION

As has been mentioned in Chapter 2, mathematical modelling of turbulence involves quite a few empirical parameters. Here, the term "empirical" means that the values of these parameters were determined just because they predicted a better correspondence when a model was originally evaluated against experimental results. Therefore, there are a few concerns about the reliability of the standard  $k$ - $\epsilon$  turbulence model prediction of room air flows.

First, the standard  $k$ - $\epsilon$  turbulence model was developed for fully developed turbulent flows, and therefore, a certain kind of wall functions have to be used to account for the viscosity effect in the near wall region. Nevertheless, using the values recommended by Launder and Spalding(1974) for the empirical constants, and including the logarithmic law wall function in the near wall region, reasonable mean field values can generally be predicted. However, it is reported by many researchers that the convective heat transfer is rather uncertainly predicted. This issue has following significant practical indications. First, the convective heat transfer from window and wall surfaces couples the room air flow with the heat conduction through window or walls, and therefore, is decisive in determining the prediction accuracies; secondly, the turbulent intensity has great influence on human comfort, therefore good prediction of turbulent kinetic energy has direct influence on the comfort estimation.

Secondly, the overall turbulence level is relatively low in air conditioned rooms, and may not be characterized by fully developed turbulent flows. Rather, some large time and large size scale oscillating flow may be expected, due to the complicated interactions of buoyancy effects and Coanda effects. Therefore,  $k$ - $\epsilon$  model simulation of air flows at low Reynolds number or low Rayleigh number conditions needs to be further investigated.

Moreover, in building spaces, negative vertical temperature gradients may exist, e.g., when the floor of the room is heated by direct solar radiation or floor heating element,

or the ceiling of a room is cooled by cooling panels or a cold air jet is supplied in the near ceiling level. More often is the case when a heating radiator is located below a cold window in winter. In flow dynamics, it is well known that fluctuating flow will be initiated by buoyancy effects when negative vertical temperature gradients exist (Tennekes and Lumley, 1978). Therefore, such a kind of temperature stratification is called unstable temperature stratification. Henkes (1990) has numerically solved the unsteady N-S equations directly for the 2-dimensional natural convection flow in a cavity at the near critical Rayleigh number conditions. It was found that, when unstable temperature stratification exists, transit from steady state laminar flow to unsteady, oscillating flow occurs at much lower Rayleigh numbers. It was also analyzed that the oscillation frequency due to buoyancy contributions to the overall turbulence is lower than those caused by other instability mechanisms, such as the hydraulic jump and the Tollmien/Schlichting instabilities. However, it is almost impossible to obtain any quantitative practical parameters such as the average surface convective heat transfer coefficients at higher Rayleigh numbers as the oscillation frequency increases. In comparison, the Reynolds average equations are attempted to obtain a statistical mean solution of the fluctuating flows. In the  $k$ - $\epsilon$  turbulence models, the fluctuating velocities caused by various instability mechanisms is characterised by the overall quantity - turbulent kinetic energy  $k$ , while the velocity fluctuation caused by buoyant convection is modelled as buoyant production term  $G_b$  in Eqs.(2.20) and (2.25), and often neglected for stable temperature stratification situations. By this way, the buoyancy effects are modelled isotropically. It is reported that such a model technique is robust and the  $k$ - $\epsilon$  model itself seldom leads to convergence problems. Recently, it is reported that the buoyant effects are modelled non-isotropically, by introducing the non-isotropic algebra Reynolds stress model (ASM) corrections into the Reynolds stress tensor in the  $k$ - $\epsilon$  model in a linear uncoupled manner (Davidson 1990). However, numerical convergence problems arose when the  $G_b$  was modelled similarly. Therefore, for unstable temperature stratification situations, special investigations are needed about the  $k$ - $\epsilon$  turbulence model performances.

To address these problems, a special experimental configuration was constructed in an enclosed, real-sized climate room to simulate a typical natural convection flow encountered in room situation - a cold window surface with a heating radiator below. Therefore, negative vertical temperature gradients will be generated in the flow field. Numerical simulation results of different turbulence models will be compared with the measurements in respect to flow patterns, temperature distribution, as well as the local velocity and turbulent kinetic energies, so that their performances can be estimated. Beside the standard  $k$ - $\epsilon$  turbulence model, the Lam and Bremhorst (LB) low Reynolds turbulence model will also be investigated.

### 3.2. EXPERIMENTAL SET-UP AND INSTRUMENTATION

The measurements were done for the natural convection in a real-size, enclosed room. The configuration of the room is shown in Fig.3.1a). Three plate radiators are located at the end wall of the room, with the upper two cooled and the lower one heated. A plank wood of 250mm in width is located horizontally between the heating and cooling plates to simulate a window sill.

The surface temperature of the heating plate,  $T_{H1}$ , can be maintained at a certain

temperature in the range of 25°C to 60°C, and that of the cooling plate,  $T_c$ , 10°C to 20°C, while the room average temperatures,  $T_r$ , are balanced at about 25°C. The other enclosure surface temperatures are actively regulated so that near-adiabatic conditions are maintained. The temperature differences,  $\Delta T_H = T_H - T_r$  and  $\Delta T_c = T_r - T_c$ , will determine the eventual flow patterns. Natural convection can be described by two dimensionless parameters, the *Grashof number* ( $Gr$ ) and Prandtl number ( $Pr$ ). In the present study,  $Gr = 10^8 - 10^9$ , which is typical in real rooms and is just above the critical transit *Grashof number*. The heating plate was heated by an electric heater in the circulating flow circuit, the supply power of which are measured by a watt-meter, while the cooling plates are cooled by the glycol/water mixture from an chiller, as shown in Figure 3.1b).

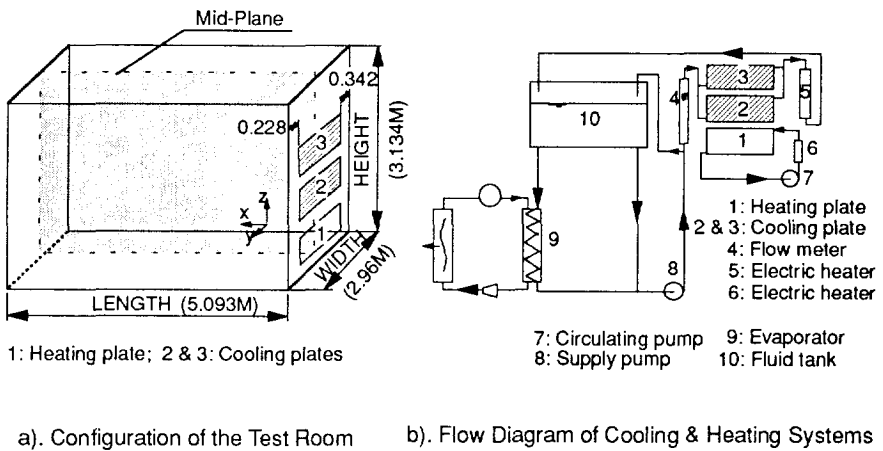


Figure 3.1 Schematic for the test room

The middle vertical plane (illustrated in Fig. 3.1a) of the room was lit by a planar-light source. The air flow in the middle plane was visualised through the movement of smokes, generated by a smoke machine. A video-camera was used to take pictures of the motion.

A number of thermocouples are attached to all of the internal enclosure surfaces, and with six thermal-couples on each of the heating and cooling surfaces, to measure the surface temperature. Also in the middle vertical plane of the room, 20 thermal couples are located to measure the air temperature.

### 3.3. MEASUREMENT RESULTS

#### 3.3.1. Flow Pattern Observation

Since the air flow velocities are rather low in most part of a room at normal situations,

detailed measurements are difficult by using the conventional type anemometers, as reported by many researchers. Alternatively, flow visualisation technique is widely used to obtain qualitative indications of the air flow pattern in a whole domain. In our test, a perforated tube is located vertically close to the end wall. Smoke generated by a smoke-machine is introduced into the room air through the small holes on the tube. The air movement is made visible through the motion of the smoke. Ideally, the smoke particles generated should be as fine as possible so that they may have a velocity as close as possible to the local air, though this is less important for qualitative purposes. The motion pictures were taken by a video-camera and recorded on a video-tape. The movement can be further observed by slow or fast replay of the video-tape.

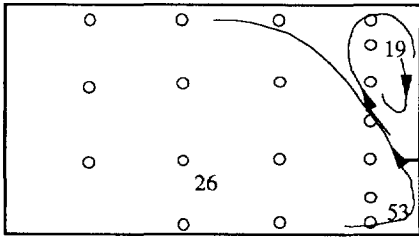
Shown in Fig. 3.2 are drawings of the visualised flow patterns at several different temperature conditions. As expected, an upward-flow and an downward-flow were initiated by the heating and cooling plates, respectively. The two streams meet at certain height, subsequently change their direction and a converged outward-flow is formed at the meeting point. The converged-flow turns into a horizontal flow 'jet', enhanced by the horizontally-placed window-sill. This jet is further biased upward or downward, depending on the relative temperature differences. In most part of the room, no clear movement of the smoke could be seen - the smokes appear stagnant, which indicates that the velocities are very low in these region, especially in the lower region of the room. For thermal comfort in reality in the heating season, this is desirable. No wonder that a radiator located below the window has become a common practice of heating.

By closer observation of the video-replay, the converged-flow appears to be constantly fluctuating. The flow angle tilts up and down rather frequently. It is interesting to notice that the window-sill has great influence on the stability of the flow pattern. Without the window sill, it was found that the meeting point of the hot and cold streams fluctuates up and down and the direction of the converged flow oscillates more frequently, and that the smoke diffuses more rapidly. The sill blocks the direct impingement of the two streams and enhances the horizontal inertial movement, and the mixing of the two streams is delayed.

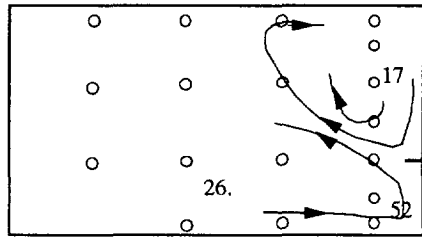
### 3.3.2. Temperature Distribution

The air temperatures were measured by copper-constantan thermal couples. To avoid the influence of radiation, small cylinders of aluminium foil were used as shades for each of the thermal couples. These thermal couples were located in the mid-plane, along four vertical lines.

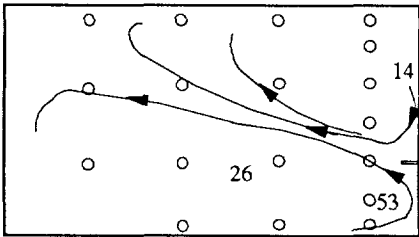
The measured temperature distributions in Case 3 are plotted in Fig.3.2e. It can be seen that the temperatures are rather uniform. Greater temperature differences exist closer to the plates. It should be noticed that the air temperature is higher in the lower region and lower in the upper region, especially closer to the plates, i.e., negative vertical temperature gradients exist. This kind of temperature distribution is considered unstable due to buoyancy effect. Therefore, it is expected that flow fluctuations may



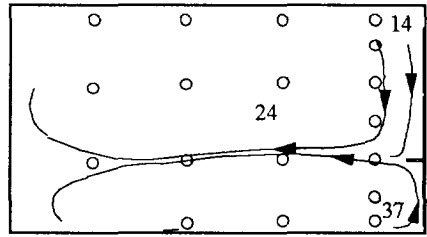
a). Case 1



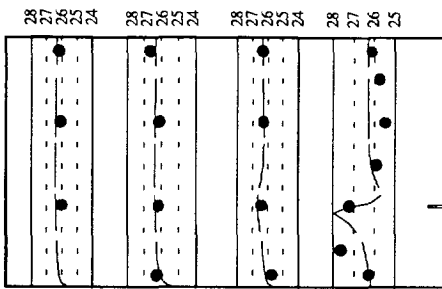
b). Case 2



c). Case 3

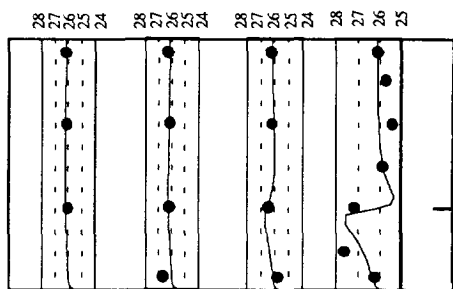


d). Case 4



● Measured — Simulated(Standard k-ε)

e).



● Measured — Simulated(LB Model)

f).

Figure 3.2 Visualized flow patterns and measured, as well as simulated temperature profiles in the mid-plane

(both sub-figures e. and f. are the measured room air temperature profiles of Case 3, with the simulated results by the standard k-ε model and the LB low Reynolds number model respectively)

simultaneously be caused by the buoyant convection. This may explain the observed oscillation of the converged flows.

### 3.3.3. Convective Heat Transfer

In the past, convective heat transfer correlations for isolated vertical or horizontal plates placed in an isothermal environment were used for heat transfer calculation in rooms. Due to the interactive nature of air flow in an enclosed space, these correlations are literally not applicable. In a recent paper (Khalifa and Marshall, 1990), experiments on convection heat transfer in enclosures are reviewed. It is generally concluded that it is difficult to obtain universal convective heat transfer correlations due to the variety of room configurations. Altmayer *et al* (1983) used 'numerical experiments' and investigated several combinations of heating and cooling enclosure sub-surfaces. Of particular interest to the author, is the correlation about the natural convection heat transfer along a vertical hot plate in an isothermal environment

$$Nu = 0.13 \cdot (Gr \cdot Pr)^{0.33} \quad (3.1)$$

Altmayer's result has shown that the correlation is also valid for the 'most hot' subsurface when the adjacent subsurface temperatures are close to the air temperature. In our experiment, one purpose is to obtain the convective heat transfer from the cooling and heating plates. Eq.(3.1) will be used as a reference for the measurements of convection heat transfer in the climate room.

The overall heat supply to the heating plate is taken to be equal to the power supplied to the electric heater,  $Q_H$  plus the mechanical energy contribution from the circulation pump. With the surface temperatures measured, the radiant heat exchanges were obtained by calculation, taking into account the multi-reflectance between the enclosure surfaces. Here, the method used will be briefly explained. All the enclosure surfaces are treated as grey surfaces. First, the term radiosity  $J$  is defined as the total radiation which leaves a surface per unit time and per unit area, and the term irradiation  $G$  is defined as the total radiation incident upon a surface per unit time and per unit area. The radiosity is the sum of the energy emitted and the energy reflected:

$$J = \epsilon W_b + (1 - \epsilon)G \quad (3.2)$$

where  $\epsilon$  is the emittance of an opaque surface and  $W_b = \sigma T^4$ . The net energy lost by a surface is the difference between the radiosity and the irradiation:

$$q/A = J - G = \epsilon W_b + (1 - \epsilon)G - G \quad (3.3)$$

Substituting for  $G$  in terms of  $J$  from Eq (3.2):

$$q = \frac{(W_b - J)A}{(1 - \epsilon)/\epsilon} \quad (3.4)$$

Consider an enclosure of  $n$  isothermal surfaces with areas of  $A_1, A_2, \dots, A_n$ , emittances of  $\epsilon_1,$

$\epsilon_2, \dots, \epsilon_n$  respectively. The angle factor or view factor between two surfaces  $i$  and  $j$  is  $F_{i,j}$ . The irradiation of surface  $i$  is the sum of the radiation incident upon it coming from all  $n$  surfaces, i.e.,

$$G_i A_i = \sum_{j=1}^n F_{j-i} J_j A_j = \sum_{j=1}^n F_{i-j} J_j A_i \quad (3.5)$$

or

$$G_j = \sum_{i=1}^n F_{i-j} J_i$$

Substituting in Eq. (3.3) yields the following simultaneous equations when each of the  $n$  surfaces is considered:

$$J_i = \epsilon_i W_{b_i} + (1 - \epsilon_i) \sum_{j=1}^n F_{i-j} J_j, \quad (i=1, 2, \dots, n) \quad (3.6)$$

Eq. (3.6) is solved for the unknown  $J$ 's. Then the net radiant energy lost by each surface is determined from Eq.(3.4) as:

$$q_i = \frac{(W_{b_i} - J_i) A_i}{(1 - \epsilon_i)/\epsilon_i} \quad (3.7)$$

The convective heat flow from the plate is obtained by subtracting the radiant part from the overall supply. The convection heat transfer coefficient  $h$  is calculated from the equation  $h=Q/A \cdot \Delta T_H$ , where  $A$  is the surface area of the plate and  $\Delta T_H$  is the temperature difference between the surface concerned and the room air average. Shown in Fig.3.3 is the convection heat transfer coefficient  $h$  measured for different temperature conditions. Also plotted in the chart, is the curve of correlation Eq.(3.1). The measured values of  $h$  are slightly higher than those from the correlation.

### 3.3.4. Details of Boundary Flow

A DISA(Jørgensen 1985) anemometer was used to measure the local velocities close to the heating plate. The anemometer was first calibrated in a small scale wind-tunnel at five different ambient air temperatures(Fig.3.4). It can be seen that the ambient air temperature has remarkable influence on the velocity-voltage correlations. Therefore, another thermocouple was used to measure the air temperatures simultaneously so that the influence of the temperatures could be corrected through interpolation among the calibration curves.

The measurements were done at two height positions, 375mm and 750mm from the floor respectively, for the heating plate. The corresponding Grashof numbers are  $1.5 \times 10^8$  and  $8.6 \times 10^8$ , respectively. During the measurements, a digital oscilloscope was used to monitor the instantaneous velocity fluctuations. A high speed datalog was used to take data at the speed of 250 points per second for a period of 20 seconds and the data for



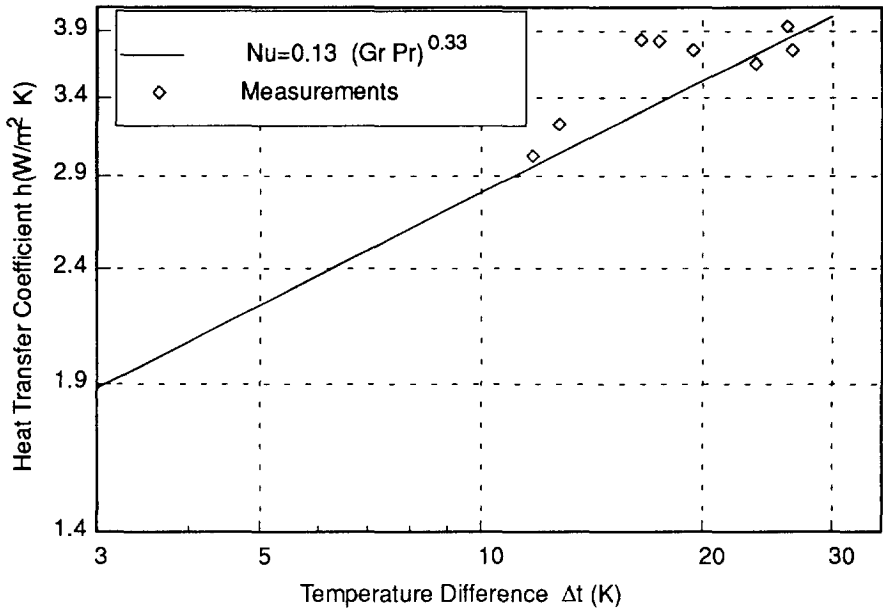


Fig.3.3 Measured convective heat transfer coefficients

each measured position were stored in the hard-disc of a PC. An example of the monitored velocity fluctuations is shown in Fig.3.5, measured at the height corresponding with  $Gr \cdot Pr = 8.6 \times 10^8$  and 20 mm away from the surface. Compared with measurements in the occupied zone of ventilated spaces (Thorshauge 1982), the velocity fluctuation frequency is much higher. Since sampling speed was rather low in the reported paper (about 5 times per second), the real fluctuation frequency might not have been detected. However, if compared with other engineering turbulent flows, such as turbulent flows in pipes or flows in an air-cooled food-storage room (Wang, 1991), the fluctuation frequency is much lower.

Mean velocities as well as the turbulent kinetic energies were worked out afterwards. First, the instant voltage is converted into velocity  $u_i$  according to the calibration at different temperatures. Then the average velocity  $\bar{u}$  is calculated as:

$$\bar{u} = \frac{1}{N} \sum_{i=1}^N u_i \quad (3.8)$$

where  $N$  is the number of the sampling points. The velocity fluctuation  $u'_i$  is then

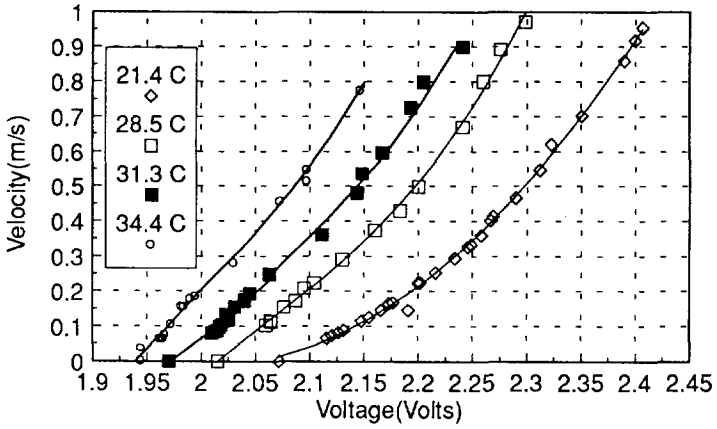


Fig. 3.4 Calibration curves of the DISA anemometer at different ambient air temperatures

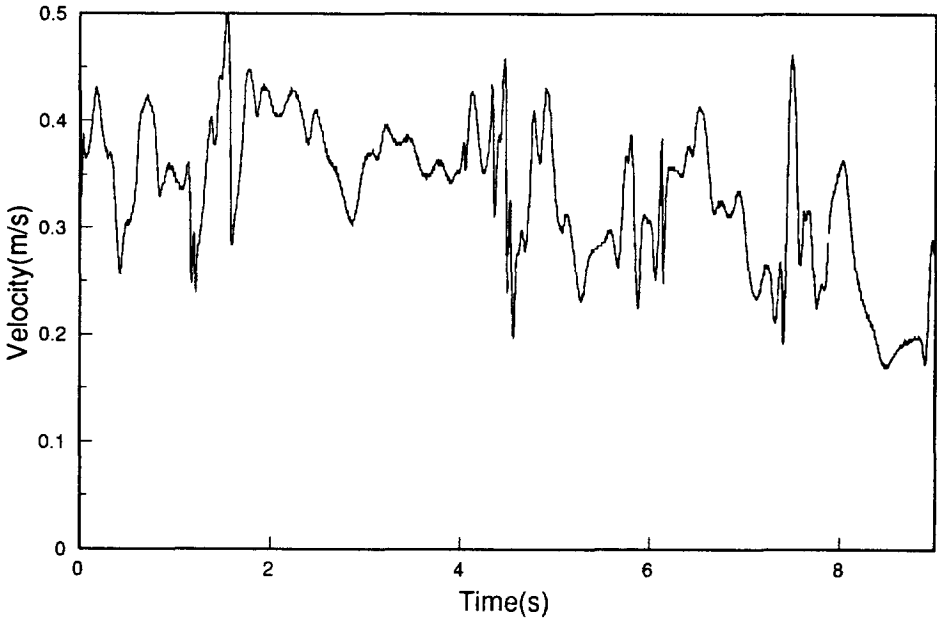


Fig. 3.5 Velocity fluctuations at one of the measurement points

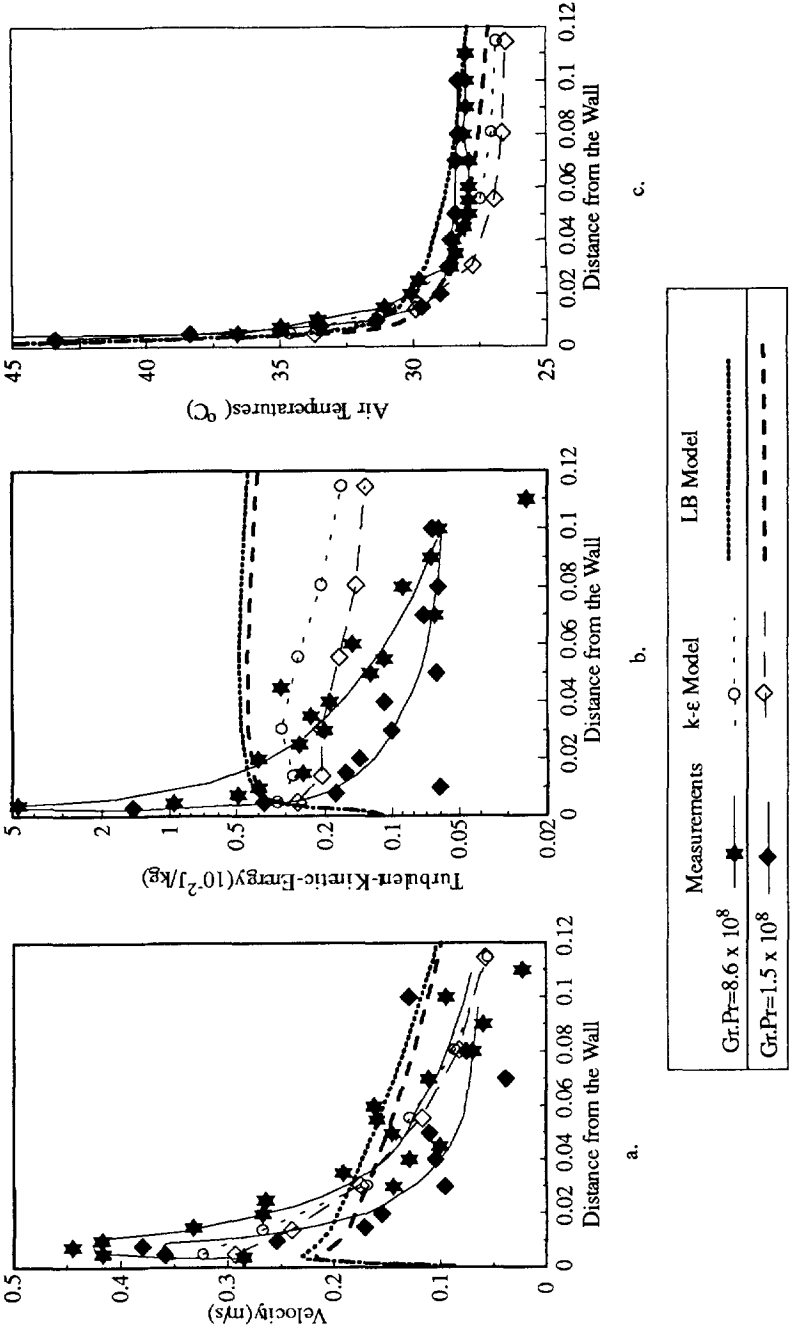


Figure 3.6 Measured and simulated velocity, turbulent kinetic energy, as well as temperature profiles of the boundary layer flow

calculated as  $u_i' = u_i - \bar{u}$ . The turbulent kinetic energy is calculated as

$$k = \frac{1}{2} \overline{u_i u_i'} = \frac{1}{2} \frac{\sum_{i=1}^N u_i u_i'}{N} \quad (3.9)$$

The average velocities and turbulent kinetic energies are plotted against the distance from the wall surface in Fig. 3.6. The data are scattered around due to random errors in measurements, but the velocity profile can still be seen. The velocity profile agrees with Hammond's analysis(1982) that a plane wall jet consists of three layers: the outer turbulent layer, the inner turbulent layer and the viscous sub-layer. The position where the maximum velocity lies is considered to be the boundary between the outer and inner turbulent layers. The thickness of a buoyancy-driven turbulent boundary layer is defined as the distance of the maximum velocity position from the wall. This distance is less than 10mm in our measurements. Compared with the scale of the room, this size is very small.

### 3.4. EVALUATION OF k-ε TURBULENCE MODEL PERFORMANCES

The computer program PHOENICS is used for the present calculations. The underlying numerical scheme is as follows. The differential equations of momentum and enthalpy are discretized by finite-volume method. The 'staggered grid' was introduced in the program PHOENICS, and for the convection term, the up-wind scheme was used. The continuity equation is taken into account by solving the pressure-correction equation. The overall solution procedure is an iteration process, which is similar to the procedure SIMPLE, which stands for Semi-Implicit Method for Pressure-Linked Equations.

#### 3.4.1. Flow Instability and Buoyancy Effects

As was described in Section 3.3.1, large scale flow oscillation was observed in the visualised flow. Since turbulence itself is a kind of instability, here it is necessary to explain various instability factors involved in fluid flows. Generally, flow instabilities are related to the interaction of viscous terms and nonlinear terms in the equations of motion. This interaction is very complex: the mathematics of nonlinear partial differential equations has not been developed to a point where general solutions can be given. In a certain sense, turbulence theory suffers from the absence of sufficiently powerful mathematical methods. Nevertheless, first, it is analytically known that, at large Reynolds numbers, turbulence arises from instabilities caused by shear stresses. Secondly, if unfavourable temperature stratification exists in a flow field, flow instability will also occur. The most-widely known instability phenomenon is the Bernard cell formed in a fluid layer between two horizontal plates, with the upper plate cooled and lower plated heated. The third type of instability occurs after a hydraulic jump, which refers as the phenomenon that a thin horizontal layer of fluid at high-speed(with a free surface) almost discontinuously 'jumps' to a thicker low-speed horizontal layer. The flow after the jump becomes unstable and the free-coming jump energy is dissipated via an unsteady oscillating wave pattern.

In room air flow situations, all these instabilities can be present simultaneously, therefore, a wide spectrum turbulence flow may be present. As far as the numerical solution

is concerned, buoyancy driven flow simulation may present convergence problems. Therefore, preliminary simulations were conducted to investigate the convergence problems.

The simulations are conducted for the standard k- $\epsilon$  turbulence model in the 2-dimensional mid-plane, the measured wall temperatures are used as imposed boundary conditions. Indeed, for the cases without the sill, convergent solutions were hard to achieve. Looking at the intermediate graphics output of the predicted velocity vector field, it appears that the flow around the meeting point fluctuates against the iteration numbers, which seems to correspond to the flow fluctuations observed in the visualised flows. After all, a converged solution is found, which is reasonable when compared with the corresponding visualised flow pattern. Special investigations were made by neglecting or including the buoyant production term  $G_B$  in the k and  $\epsilon$  equations. It was found that it has no influence either on convergence or predicted results of the numerical simulation.

Therefore, the k- $\epsilon$  turbulence model appears to be a 'robust' one in modelling the flow fluctuations caused by various instability mechanisms. It tends to give convergence solutions through delicate manipulation of the under-relaxation devices. In the following section, the experiences of specifying the under-relaxation factors will be presented.

### 3.4.2 Influence of under-relaxation devices on numerical convergence

As already described in Section 2.4 about numerical techniques, due to the iteration solution procedures, under-relaxation devices have to be used to obtain a converged solution. In the current finite-volume method program PHOENICS, two basic under-relaxation devices are available: the relaxation factors and the false-time steps (Rosten and Spalding 1987). For the pressure-correction equations, an under-relaxation factor of  $\alpha$  is used, i.e., the pressure iteration is underrelaxed via

$$p = \alpha p_{new} + (1 - \alpha) p_{old} \quad (3.11)$$

and the other variables will be underrelaxed through the adoption of the false-time step (Patankar 1980). In this approach, even for solving a steady state problem, the transient terms in the transport equations still remain. When the iteration eventually reaches convergence, the transient terms will become null. Therefore, the value of the discretised (false)time step  $\Delta t_f$  is a numerical device to improve convergence speed of the iteration. It is recommended that for velocity components  $u_i$ ,  $\Delta t_f$  should be equal to the value of

$$\Delta t_{f, u_i} = 5 \frac{\Delta x_i}{u_{i, max}} \quad (3.12)$$

where,  $\Delta x_i$  is the grid-spacing in  $x_i$  direction, and  $u_{i, max}$  is the estimated maximum velocity component in the same direction. The false-time step  $\Delta t_f$  for variable k and  $\epsilon$  can adopt different values, depending on specific flow characteristics. When simulating buoyancy-driven flows, the temperature will also have influence on the convergence of momentum equations, via the source term in Equation(2.26). What false-time-step values should be adopted for temperature or enthalpy to ensure full convergence for simulation remains a question (Niu 1990, Niu and Visser 1991).

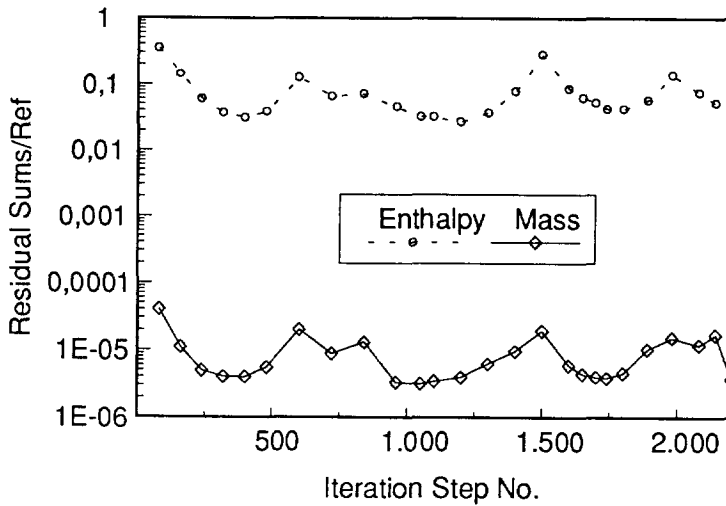
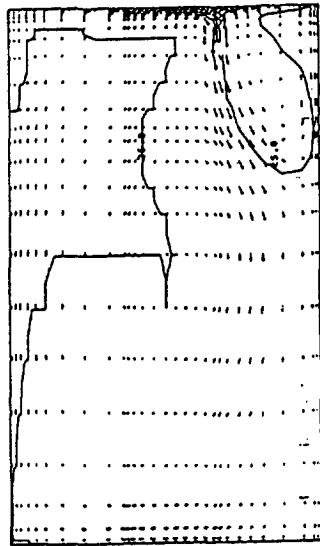
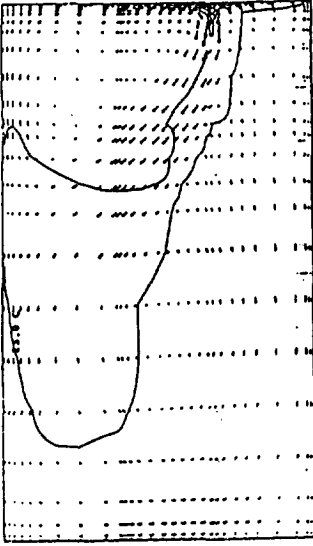


Fig. 3.7 Periodical changing of the residuals of the discretized equations as iteration proceeds

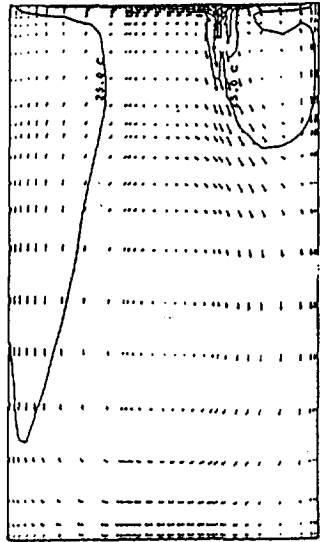
Therefore, special simulations are conducted to test the influences of these under-relaxation devices on the whole convergence process. It is generally found that convergence can not always be reached with arbitrary under-relaxation devices. When larger values for the  $\Delta t_i$ 's are used, divergence occurs. At one case, when heavy under-relaxation is used for  $k$ ,  $\epsilon$  and temperature (the  $\Delta t_i$ 's are about one order lower than those for the velocity component), the iteration seems to go to convergence in the first 400 steps. However, as the iteration continues, the iteration presents a oscillating character. As the iteration proceeds, the residuals of the discretized equations changes periodically, instead of steadily decreases. The changes of the residuals of the continuity equation and enthalpy equations versus the iteration steps (sweep number) are plotted in Figure 3.7 (The residuals are summation at all nodal points, and are divided by a reference value). It can be seen that minimums occur at every 500 to 700 iteration steps. The corresponding air flow patterns at the minimums of the residuals are presented in Figure 3.8. It is interesting to see that the flow varies alternatively between two patterns, i.e., the upward-tilting and the downward-tilting. Eventually, by selecting a value of the false-time steps for the  $k$ ,  $\epsilon$  of the same order as for the velocity components, and a ten times higher value of  $\Delta t_i$  for enthalpy, converged results are achieved. This reflects the state-of-the-art of combatting divergence in CFD calculations. It requires caution to judge convergence. In addition to the two basic criterions recommended by Patankar (1980), i.e., the consistent residual decreasing and the ultimate unchanging of the solved-for variables, some other quantities, such as the total



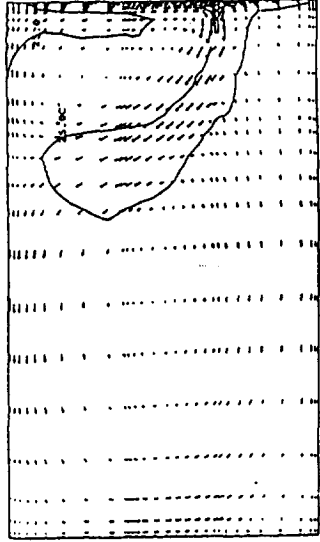
a). at 400 sweeps



b). at 1,100 sweeps



c). at 1,700 sweeps



d). at 2,200 sweeps

Figure 3.8 Periodical changing of the simulated air flow patterns as the iteration proceeds

mass and energy balance through the domain boundary, and net mass flow through a specific cross section in the calculation domain, should be also used to check if convergence is reached. In later simulations, these criterions are used, and all the simulation results are considered numerically converged.

The following sections will focus on prediction accuracies of using different models at different grid-spacing. For this purpose, in all the simulation cases, the measured enclosure surface temperatures of Case 3 (indicated in Figure 3.3c) are used for the thermal boundary conditions, so that the experimental result from the measurements can be used directly to validate the simulation results. The average surface temperature of the heating and cooling plates are 52.6°C and 14.5°C, respectively, and the ceiling and wall temperature 25.6°C, floor temperature 24.5°C. Details of these simulations are described as below.

### 3.4.3 Evaluation of the Standard k-ε Turbulence Model

With the standard k-ε turbulence model in the program PHOENICS, the logarithmic wall functions are used (Rosten and Spalding 1987). In the program, the skin friction factor is first calculated from the formula

$$S = \left[ \frac{0.435}{\ln(1.01 + 9Re S^{0.5})} \right]^2 \quad (3.13)$$

where  $Re = uv/y_p$ ,  $y_p$  is the distance of the first grid node from the wall.

To calculate the convective heat transfer from the solid wall, the Stanton number  $St$  is calculated from

$$St = \frac{S}{Pr_t (1.0 + P S^{0.5})} \quad (3.14)$$

where

$$P = 9.0 \times (Pr_t/Pr_l - 1.0) (Pr_t/Pr_l)^{0.25}$$

and  $Pr_l$  and  $Pr_t$  are the laminar and turbulent Prandtl numbers respectively.

For the k and ε equations, the boundary conditions are fixed by the following two formulas

$$k_p = \tau_s / (\rho C_p^{0.5}) \quad (3.15)$$

and

$$\epsilon_p = \frac{(\tau_s / \rho)^{1.5}}{0.41 y_p} \quad (3.16)$$

where  $\tau_s$  is the skin shear stress.

First, six simulation cases are conducted to examine the sensitivity of the



simulation results to the distance of the first grid line(Niu and Kooi 1992). In these cases, the simulation is conducted only in the 2-dimensional X-Z vertical plane and the grid coarseness has been determined in such a way that, close to the enclosure surface, the node distribution is denser than in the central domain. The only difference among these cases is the distances of the first grid-line from the plates. In these cases, the distances of the first grid-nodes are 0.625mm, 1.25mm, 2.5mm, 5mm, 9mm and 20mm, respectively. It is found that this first distance has a remarkable influence on the simulation results, in respect of the simulated flow patterns, temperature distributions and especially the predicted convection heat transfer coefficients. The resulting dimensionless distance  $y^+$  of the first grid-line is calculated for each case, and it is found that the  $y^+$  value varies, along the heating plate, from 5.0 to 7.4, 8.1 to 10.3, 10.2 to 13.0, and 14.2 to 16.8 in each of the simulation cases. The predicted heat transfer coefficients in each case are plotted against the maximum dimensionless distance  $y^+_{max}$  in Fig.3.9. It can be seen that a smaller  $y^+$  value over-estimates the  $h$  value, and vice versa. In other words, the predicted  $h$  is rather sensitive to the  $y^+$  value. By interpolation, it can be expected that the predicted  $h$  value would be closer to the measured value if such grid-spacing is used that  $y^+_{max}$  is around the value of 9.2. Therefore, if the  $y^+_{max}$  is used as a criterion to locate the first grid lines, the optimum value is  $y^+_{max,opt}=9.2$ . This requirement is different from that for forced convection boundary layers. Much finer grids should be used next to the wall for natural convection, and also the optimum value range is much smaller.

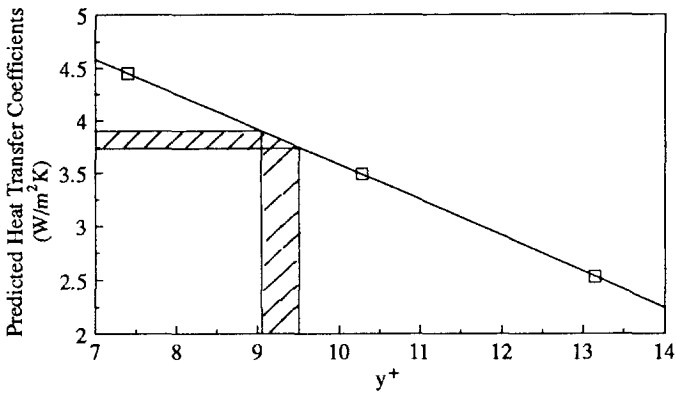


Fig. 3.9 Dependence of the simulated  $h$  on the first grid dimensionless distance

Then, a three dimensional simulation is conducted. The grid number used is  $NX \times NY \times NZ = 25 \times 22 \times 30$ . The graphics results of the simulation are shown in Fig. 3.10.

The simulated velocity vectors in the middle plane(Figure 3.10a) can be compared with the visualised flow pattern(Fig.3.2c). In terms of the angles of the converged 'jet' and the relative sizes of the two recirculation zones, the simulated flow pattern is reasonable. Also, both measured and simulated temperature profiles along the four vertical lines in the mid-plane are plotted in Fig. 3.2e. It can be seen that the agreement is good farther away from the plates, while larger discrepancy exists closer to the plates.

Some local values (close to the heating plate) of the predicted velocity, turbulent kinetic energy, as well as temperatures are plotted in Figure 3.6 for comparison with the anemometry measurements. The mean velocity and temperature agreement is reasonable, while greater discrepancies exist for turbulent kinetic energies. The predicted convection heat transfer is very close to the measurements, and the nominal transfer coefficient, calculated from the temperature difference of the heating plate surface and the room-air average, is  $3.59 \text{ W/m}^2 \text{ K}$ , which is slightly lower than the measured value (about  $3.7 \text{ W/m}^2 \text{ K}$ ). In comparison with the measured velocity profile of the boundary flow (Fig.3.6a), the grid cells of the first line are located just within the inner boundary layer. Post-check shows that the  $y^+$  values of the grid line next to the heating plate are in the range of 8.1 and 10.0. This agrees with the 2-dimensional analysis above.

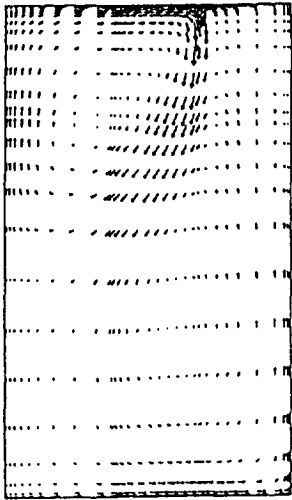
#### **3.4.4 Lam & Bremhorst(LB) Low Reynolds Number Turbulence Model**

Some subroutines are added to the standard PHOENICS computer code to calculate the modified functions indicated in Eqs. (2.33) and (2.34), and to use the boundary conditions for  $k$  and  $\epsilon$  specified by Eq. (2.35). In comparison with the standard  $k$ - $\epsilon$  turbulence model, only the source terms for  $k$  and  $\epsilon$  equations are modified. Correspondingly, some FORTRAN statements are inserted in the subroutine GROUND.F(Rosten and Spalding, 1987) for the implementation of the model modifications in the computer code PHOENICS. Both boundary conditions described in Section. 2.3.3.2, i.e., the logarithmic wall functions and the  $k$ - $\epsilon$  correlations specified in (2.35), are tested for the Lam & Bremhorst low Reynolds number  $k$ - $\epsilon$  turbulence model.

1. With boundary conditions for  $k$  and  $\epsilon$  as described in Eq.(2.35), different grid-fineness in the boundary layer close to the wall are tested. It was found that, only with the finest grid tested, a converged solution was achieved. However, the predicted heat flow from the heating plate is 300% of the measurement. In comparison with the visualised flow pattern(Fig.3.2c), the size of the upper recirculation zone of the air flow is much over-predicted(Figure 3.10d), while that of the lower recirculation zone is under-predicted.

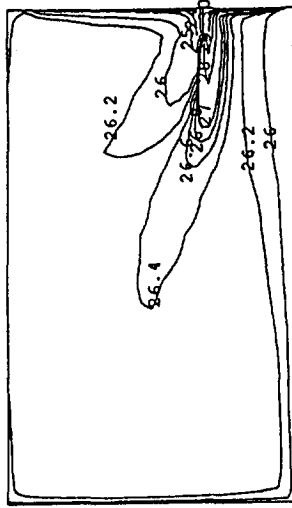
In comparison with the standard  $k$ - $\epsilon$  model prediction(Figure 3.10a), the predicted temperature variations of the room air(Figure 3.10e) are larger. Also the predicted  $k$ (Figure 3.10f) is about 10 times higher. In summary, this prediction is far from reliable. Since almost 10 grid lines were already located within the 10 mm range near wall region, no further refining of grids was tested.

2. The logarithmic wall functions are still used with the low Reynolds number model. The same grid fineness is tested. It was found that, no converged solution can be found with coarse grids in the near wall region. During the iteration process, the predicted heat flow oscillates in a certain range around the level that is close to the measurements. The

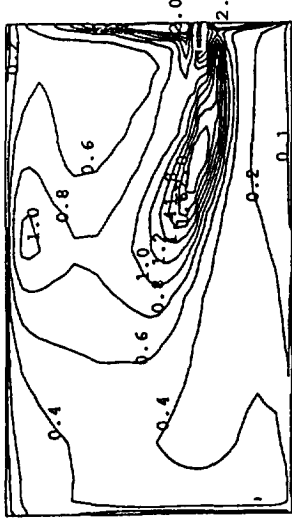


a

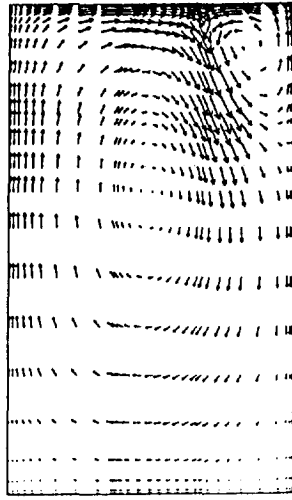
— : 0.50 m/s.



b

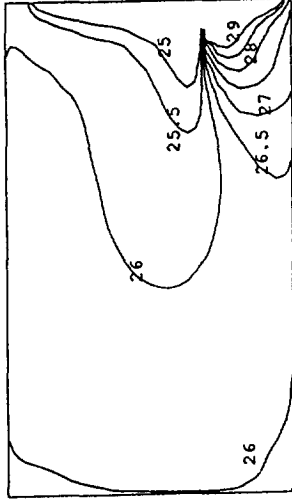


c

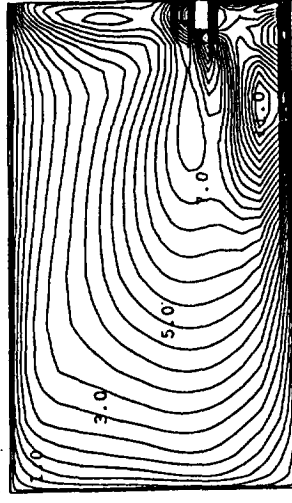


d

— : 0.40 m/s.



e



f

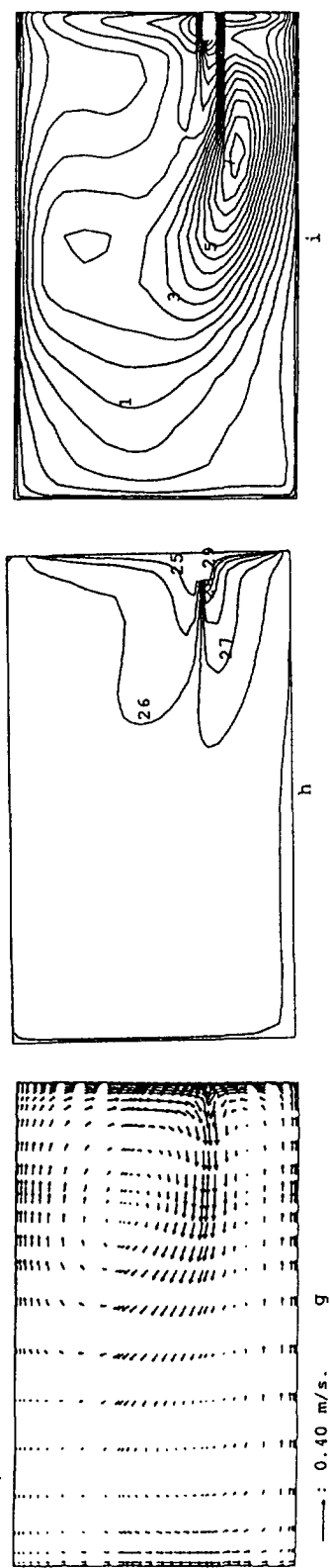


Figure 3.10 Simulated flow fields by different turbulence models  
**a, b, and c:** by standard  $k-\epsilon$  turbulence model + logarithmic law wall functions; **d, e, and f:** by LB low-Reynolds number turbulence model + wall boundary condition of Eq.(2.35); **g, h, and i:** by LB low-Reynolds number turbulence model + logarithmic law wall functions

predicted  $k$  tends to be zero in most region, except in the region close to the heating and cooling surfaces and in the region where the two streams meet. Again, a converged solution is achieved only with the finest grids tested. In this case, the comparison with measurements is encouraging. The simulated flow pattern is reasonable (Figure 3.10g). The simulated temperature contours(isotherms) of room air (Figure 3.10h) are similar with the standard  $k$ - $\epsilon$  simulation (Figure 3.10b). What is important is that the predicted heat flow is within the error range of the measurements.

On the other hand, the agreements of local velocities and turbulent kinetic energies with measurements of the near wall region are no better than those from the standard  $k$ - $\epsilon$  model (Fig.3.6 a and b), though the temperature agreement looks better in the plotting (Fig.3.2f and Fig3.6c). The low Reynolds number model tends to predict higher  $k$  values - about 3 times of the standard  $k$ - $\epsilon$  model predictions (Figure 3.10i). But both models fail to predict the peak values of  $k$  close to the plate, which were found in the measurement (Fig.3.6b).

### 3.5. CONCLUSIONS AND DISCUSSIONS

#### 1). Applicability of the standard $k$ - $\epsilon$ Turbulence Model

The standard  $k$ - $\epsilon$  turbulence model appears to be a 'robust' model, in the sense of its being able to give numerically converged solutions, even for the flow at low turbulence level and with unstable temperature stratifications. It is found that the influence on simulation results of the buoyant production term  $G_b$  in the  $k$  and  $\epsilon$  equations is negligible. The predicted flow pattern as well as the temperature distribution can be in reasonable agreement with experimental investigations. However, it is found that the prediction results, especially the convection heat transfer next to the wall is very dependent on the dimensionless distance  $y^*$  of the first grid, when the built-in wall functions are used. The optimum  $y^*_{max}$  found to be around the value 9.2. It must be noted that this optimum  $y^*$  is different for forced convection and natural convection situations.

In air conditioned rooms, unfortunately, forced convection and natural convection play compatible roles in the air flow, heat transfer, as well as the mass transfer processes. Therefore, careful attention should be paid to the grid optimisation in simulation. The convection nature along the individual enclosure surfaces should be analyzed in advance, and different grid sizes are used for the different surfaces. It is suggested that empirical convection heat transfer data be used when available, which can lead to more reliable results, especially when the flow parameter and air contaminant distributions in the occupied zone are of interest of the simulation.

#### 2). Application of low Reynolds No. $k$ - $\epsilon$ Models

In principle, the low Reynolds No. model can eliminate the first-grid-dependent characteristics of the standard  $k$ - $\epsilon$  model, as long as the grids are fine enough within the boundary layer. In fact, it was found in the present study that, when less than 8 grid cells are located in the boundary layer, no converged results could be obtained. It seems that the Lam & Bremhorst model only works when extremely fine grids are located in the near wall region. Also, the logarithmic wall functions should be used, purely on empirical basis. In

comparison with the equivalent standard  $k$ - $\epsilon$  model simulation, about 2 or 3 times CPU time will be required on a SUN work-station.

3). It is essential that explanation of the numerical simulation results be based on the converged ones. However, due to the iteration nature of the solution procedure, and heavy under-relaxation devices used, premature numerical results may be erroneously considered as converged. Therefore, different values of the false-time-steps are tested to ensure good convergence with reasonably-large iteration numbers. It is found that, for the buoyancy-driven air flow case, about same order of false-time-step values should be used for  $u$ ,  $k$ ,  $\epsilon$ , and enthalpy(or temperature). At later stage of the iteration, large-false-time steps for  $k$ ,  $\epsilon$ , and enthalpy may speed-up the convergence. Ultimately, the convergence should be judged on the basis of overall mass and heat balances, as well as the mass and heat balances at specific locations, in addition to the consistent equation-residual decreasing.



## CHAPTER 4

# DYNAMIC SIMULATION OF BUILDING THERMAL PROCESSES

### 4.1 INTRODUCTION - Thermal Processes in and around a Building

The principal purpose of a house is to provide a thermally comfort environment under various hostile climates for its occupants. A building undergoes several thermal processes to achieve this purpose, as illustrated in Figure 4.1. Before introducing any mathematical descriptions or modelling, it is necessary to briefly explain the various processes involved. Specifically, the dynamic interaction between a cooled-ceiling(CC) system and the building served by the system will be highlighted.

First, *transient conduction heat transfer* occurs within the building envelopes. The diurnal outdoor air temperature change and the daily solar radiation change impose an external transient boundary condition, not to mention the vagaries of weather. Also, the internal heat generated by occupants, as well as the electrical/electronic appliances and other facilities tends to be casual or intermittent. Due to these transient features, not only the heat conductance, but also the heat capacity of the building envelopes will have decisive influences on the thermal and energy performances of a building. At present, insulation materials are used for energy conservation. It is generally found that the order of the insulation among a multi-layer wall is very important on the energy effects. Therefore, the overall conduction heat transfer, which describes the insulation index at steady heat transfer state of a wall, is far from adequate to indicate the real thermal performances of a particular wall. Alternatively, indices for transient behaviours will be required.

Radiative energy exchanges occur both inside and outside a building. The radiative energy may be classified into *short wave* and *long wave* radiations. Solar radiation consists of mainly short wave radiation and mostly constitutes a significant portion of the total cooling load. The radiation from building surfaces is long wave radiation. A building receives long wave radiation also from ground surfaces, ambient buildings and sky radiation. Generally, an external building surface may be higher or lower than the ambient air temperature resulting from the overall heat balances. During the day it may be higher



since the solar radiation is dominating; during the night, it may be lower if the long wave emission to the sky is dominating. Obviously, precise account of the mechanism require reliable solar data and weather data, especially cloud data. Solar radiation also enters the building space directly through window fenestration, and subsequently absorbed through multiple reflection by the internal wall surfaces. Part of the energy is conducted into the wall and the other part is convected into the indoor air. Also, heat generated by various internal heat sources may be released in radiation and convection simultaneously. Also, energy is redistributed among the internal surfaces through long wave radiations. Only the heat convected into the indoor air forms the *cooling load* for an air system. This means that the *heat gains from various sources* will be converted into the cooling load at a later stage and may be attenuated due to the storage in the building envelopes or other internal thermal masses, such as heavy furniture(see illustrations in Figure 4.4).

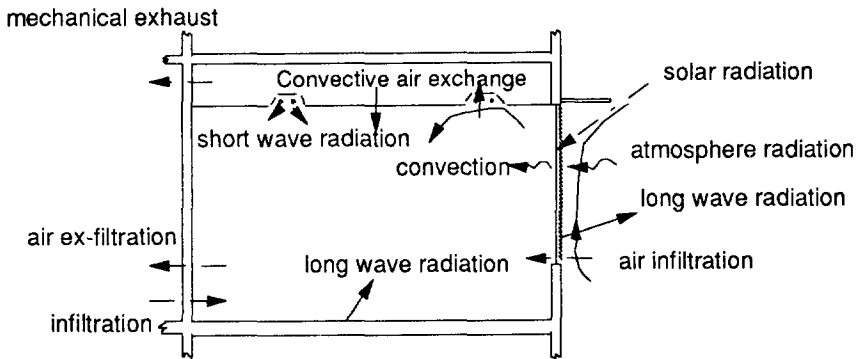


Figure 4.1 Thermal processes in and around a building

*Convective heat transfer* occurs between a heated or cooled surface and its adjacent air. Convective heat transfer occurs both inside and outside a building and may occur in natural convection and/or forced convection forms. The internal convection characteristics are already briefly mentioned in the Section 2.1, Chapter 2. Typically, for external building surfaces, *forced convection* occurs, the intensity of which depends on the wind velocity and direction.

In relation with the convective heat transfer, *fluid flow* occurs in and around a building. From the point of view of air exchanges, the air flow takes its path in the form of infiltration, or in the form of inter-zonal or zone-coupled flows. Infiltration is the

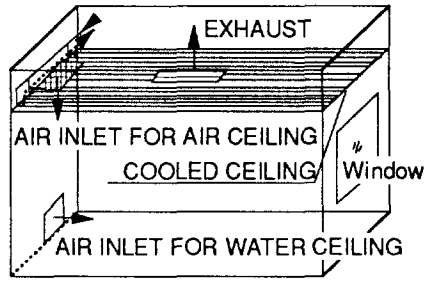


Figure 4.2 Construction of cooled-ceiling panels in a room

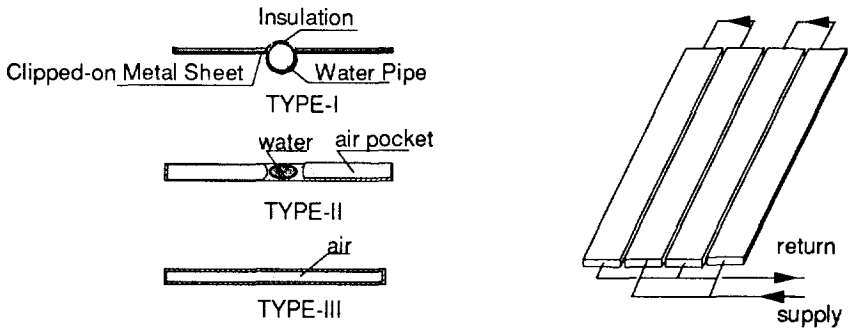


Figure 4.3 Different types of ceiling panels and their arrangement in a room

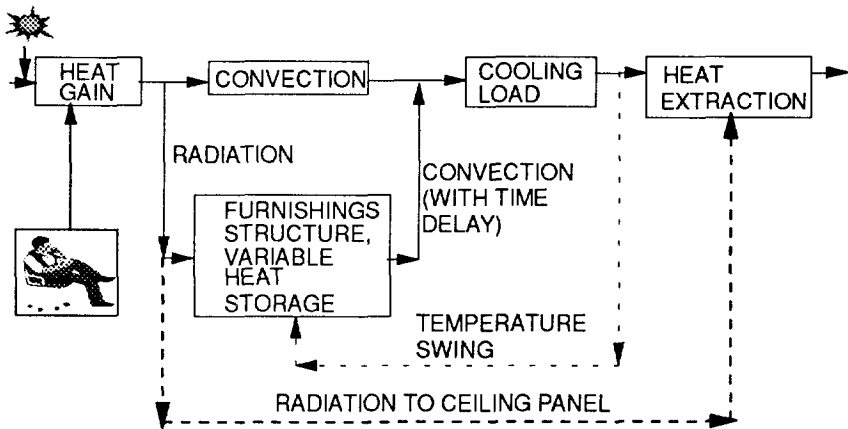


Figure 4.4 Illustrations of new cooling-load dynamics with CC systems

name given to the leakage of air from outside and can be considered as comprising two components: the unwanted, and sometimes unavoidable movement of air through distributed leakage paths such as the small cracks around windows and doors, through the fabric itself and at material junctions; and the ingress of air through intentional openings (windows, vents etc), often referred to as *natural ventilation*. Inter-zonal flow, like infiltration, is caused by pressure variations and by buoyancy forces caused by density variations due to the temperature difference between the coupled zonal volumes of air. The random occurrences such as window and door openings, which are dependent upon the occupants' behaviour, and changes in the prevailing wind conditions or the intermittent use of mechanical ventilation will have some effect on infiltration, natural ventilation and inter-zonal air flow.

In many buildings the effects of heat gain from lighting installations, occupants and miscellaneous equipment can be considerable. This heat is released into the indoor environment in convective and radiant form. The convective heat is convected directly into the air, and the radiant portion is apportioned among the internal surfaces according to some angular distribution strategy, and so has a relationship with the room configuration and thermal capacity and will be usually lagged.

*HVAC* system has become an inseparable part of a modern building. For instance, the presence of a heating radiator below a window is a common practice. The radiator releases its heat both convectively and radiantly. Currently, cooled ceiling (CC) technique is getting popular in many European countries and has found its use in many office buildings as an air-conditioning alternative (Mertz 1992; Wilkins 1992). A cooled ceiling can have many variations, and shown in Figure 4.3 is the horizontal plate type which will be the focus of the present research. In this type of design, specially made cooling panels are installed as part of a false or lowered ceiling, through which cold water flows and extracts heat from the room (Figure 4.2). Two types of ceiling constructions in a room exist: one type is totally closed and the other with gaps open between ceiling panels. For the first type of construction insulation is applied on the top of the cooling panels. The latter usually has no insulation on top, and the open gaps will allow natural convection to occur between the room air and cavity air above the ceiling. Some manufacturers also produce ceiling panels that function as air ducts, through which ventilation air is preheated by internal room heat before entering the room through air diffusers. Various ventilation systems can be combined with the water ceiling system to provide the required outside air and latent cooling. Usually separate heat devices are located conventionally underneath the windows. In some cases the ceiling panels are also used for heating purposes. The cooled ceiling system imposes certain unique characteristics. A portion of radiant heat will be absorbed by the chilled panels and directly converted into cooling load without the delay and attenuation that usually occur in a conventional air conditioning system, as illustrated in Figure 4.4. On the other hand, the existence of the cooled panel surface will lower the radiant temperature in a room. Therefore, it is clear that, with a cooled-ceiling system, the building component thermal behaviour becomes directly coupled with HVAC equipment component. This will call for special cooling load calculation methods. The direct absorption of radiation by the ceiling-panel will be counted as required cooling load. The radiant temperature should be taken into account for the indoor *design temperature* in addition to the room air temperature.

In the present research, a new methodology is developed, which is to combine the

thermal dynamic modelling of building elements and the ceiling panels with each other and to integrate the thermal comfort indices in the calculation procedure. Generally speaking, different modelling strategies can be adopted, depending on the purpose of analysis and computation capacities available. For instance, the CFD techniques reviewed in Chapter 2 can be viewed as the detailed theoretical modelling of the internal flow processes, the purpose of which is to investigate the distributed indoor thermal comfort and contaminants at different air supply, or indoor heating or cooling configurations. Such a modelling approach alone requires large computer capacity, apart from being integrated with the building system modelling. Therefore, in this chapter, a somewhat different modelling approach will be introduced. This approach is already built in a computer-code ACCURACY(Chen 1988). Here in this Chapter, the involved modelling technique is only introduced in outlines. The purpose is to indicate how models for ceiling-panels are integrated with the established method so that the unique characteristics of cooled-ceiling systems can be fully addressed by rigorous numerical simulation techniques.

## 4.2 MATHEMATICAL MODELLING OF BUILDING THERMAL PROCESSES

### 4.2.1 Modelling Strategy

The practice of building energy analysis started with the heating load calculation for equipments (such as radiators, boilers, pumps as well as pipelines) sizing. The calculation usually adopts the steady state calculation approach. A constant outdoor design temperature is determined based on the statistical weather data, and this temperature is used as the outdoor temperature for the heat conduction heat loss through external walls and air infiltration. Infiltration is obtained also from empirical basis of building types and climate. Internal heat gains, as well as the solar insolation are considered only as favourable factors and not quantitatively taken into account. Therefore, the whole approach can be considered as *empirical steady state modelling* of building thermal performances.

The early stage of cooling load calculation also adopted a similar approach. A so-called sol-air temperature is derived as an equivalent outside design temperature. The sol-air temperature takes solar radiation into account in the calculation of heat gains through exterior walls and windows. However, since late 1960s, to address the transient thermal behaviours described above, several cooling load calculation methods have been developed. These methods are described in the *ASHRAE Handbook - Fundamentals*. These methods are: The Total Equivalent Temperature Differential Method(TETD), the Transfer Function Method(TFM), and the CLTD/CLF Method. These methods distinguish the space heat gain from the space cooling load, so that the effect of time delay due to heat storage is included. These methods involve hour-by-hour load calculations. TETD was a computer-based method used prior to the introduction of CLTD/CLF values. CLTD/CLF tabular data are customized data generated by the TFM for specific projects or types of buildings. Here, it should be noted that the established CLTD/CLF tabular data will not be applicable to cooled-ceiling systems since building-dynamics is expected to be drastically different due to the presence of cooled ceiling-panels.

The concept of Transfer Function Method was first introduced for the calculation of the transient heat conduction through walls(Mitalas 1968, Mitalas and Arsenneault 1970, Muncey 1981). Analogously, the concept of Room Transfer Functions, also called Room

Response Factors(Mitalas and Stephenson 1967), were introduced to convert the space heat gain into the space air cooling load. The derivation of the Room Response Factors involves the calculation of the overall room energy balance calculations. At present, the so called room energy balance method is considered to be the fundamental method for building load calculation and energy analysis, as well as for HVAC system control simulation purposes.

This modelling strategy is to divide the building into some basic elements, the number of which should be large enough to represent physical reality and meanwhile small enough to be economically solvable on available computing facilities, and apply the basic transient heat and mass transfer principles to the elements to obtain mathematical descriptions. The second step is to integrate these elementary equations to form a numerically solvable simultaneous equations. Usually, the equations are linearised so that linear algebra algorithms can be applied. The present modelling approach will divide a building into following elements:

- zones, a zone contains a volume of air, which may exchange with that in the adjacent zone and exchange heat with its enclosures through convection;
- wall(opaque) surfaces, on the one side, the surface exchange heat through conduction, on the other side, through radiant and convective heat exchanges; it may absorb and reflect long wave radiation, and usually only emit long wave radiations;
- window(transparent) surfaces, in addition to the features as for wall surfaces, a window surface may transmit short wave radiation;

If the integrated modelling includes the HVAC components as well as the control loops, the same principle applies. The main difference is that, if the control loop is simulated, small time-steps must be used.

Our modelling of cooled ceiling system will be based on this method. To integrate the ceiling-panel with other building elements, ceiling-panels will be treated as one of the opaque surfaces. The following sections will give detailed of the modelling.

#### 4.2.2 Energy Balance Equation of Wall(opaque) Surfaces

The thermal balance of an internal wall surface  $i$  can be described as

$$q_{s,i} + q_{ir,i} + q_{t,i} = q_{c,i} + \sum_{k=1}^N q_{r,i-k} \quad (4.1)$$

where,

$q_{s,i}$  is the solar radiation through window(s) that is apportioned to the surface;  
 $q_{ir,i}$  is the radiant heat from *internal heat sources*, e.g., lighting, cooking facilities or other electrical appliances, occupants;

$q_{t,i}$  is the transmission heat from wall internals, which will be calculated through the wall transfer function method;

$q_{c,i}$  is the convective heat from the surface into the air volume;

$q_{r,i-k}$  is the radiative heat exchanges with other internal surfaces due to long wave radiation. All these terms are illustrated in Figure 4.5.

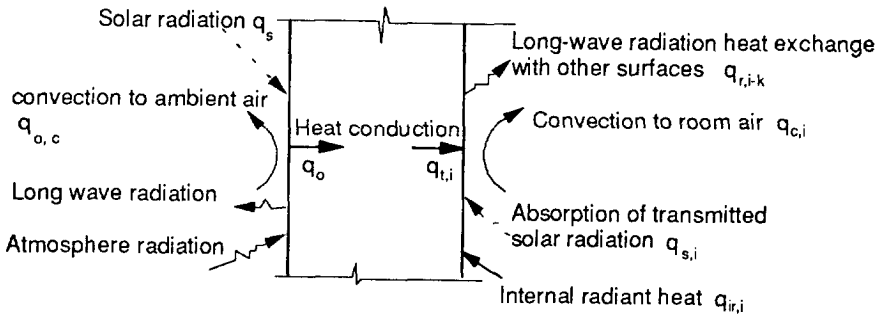


Figure 4.5 Energy balance of inside and outside wall surfaces

#### 4.2.2.1 Insolation calculation

Solar radiation enters the building space through the transparent part of a building envelope. This heat usually comprise an considerable part of the cooling load. For the present calculation, the transmission, reflection and absorption process of the solar radiation through a window with double glass and venetian blinds and extra shading devices will be mathematically modelled in detail(Oegema 1970, Chen 1988). The calculation will give the following indices of a multi-layer window(Figure 4.6):

For the direct solar radiation, the overall transmission coefficient  $T^o$ , and the overall absorption coefficients for the individual layers  $A^o_j$ , ( $j=1,2,3$ );

For diffuse solar radiation from the sky and the reflection from the ground, the overall transmission coefficient  $t^o$ , and  $t^o_p$ , the overall absorption coefficients of the individual layers  $a^o_{j,i}$  and  $a^o_{j,i}(j=1,2,3)$ .

The shading effect calculation(Sun 1968) gives the shading factors of various combinations of overhang and side fins for the direct solar radiation, diffuse solar radiation, and ground reflection  $S_D$ ,  $S_s$  and  $S_f$ .

Obviously, reliable solar radiation data will be required. For hour-by-hour simulations, this will require the hourly solar position and the cloud cover(CC) data. This will be done by using the ASHRAE method. For each hour, the direct solar radiation  $I_{DC}$  that strikes upon a tilted surface, the diffuse radiation on a horizontal surface and vertical surface  $I_{dHC}$  and  $I_{dvs}$ , and the diffuse reflected radiation from the ground on a vertical surface

$I_{def}$  are calculated.

With these calculations, the total solar radiation  $Q_s$  that enters the building space is

$$Q_s = S_D I_{Dc} T^0 + S_i I_{def} t_i^0 + S_f I_{def} t_f^0 \quad (4.2)$$

Since the use of venetian blinds has become a common practice, and therefore the transmission can be treated as 'diffuse' within the building space, the  $Q_s$  is apportioned among the internal surfaces according to their areas. By this approach, the  $q_{i,i}$ 's in Eqs. (4.1) will be obtained.

#### 4.2.2.2 Radiant heat from internal heat sources

Internal heat sources include occupants, electrical appliances, lighting installations, etc.. In modern offices, this internal heat sources are increasing. Therefore, a better treatment is required to accurately assess their cooling load contributions. One approach uses the weighting factor to convert the total heat gain into cooling load. For the present requirement, the splitting of the heat generated into radiant and convective part is essential. To the author's knowledge, a special project is carried on by one ASHRAE committee, the target of which is to give a specification about the split of the heat generated by various office equipments. Once these data are available, the next step is to apportion these radiant energy among the internal surfaces according to the geometry configurations of the heat source in a room. In most case,  $q_{i,i}$  can be reasonably approximated according to the area ratios of the surface.

#### 4.2.2.3 Transient heat conduction through walls (including floor and ceiling and heat exchange of outside surfaces)

The calculation of  $q_i$  involves the transient heat conduction process through a wall(Fig.4.2). According to the Fourier's law, the governing equation of one-dimensional unsteady state heat conduction in a homogeneous wall is

$$\frac{\partial T}{\partial t} = a \frac{\partial^2 T}{\partial x^2} \quad (4.3)$$

where,  $a = \lambda/(\rho C_p)$ , is the thermal diffusivity of the material. The equation can be numerically solved by finite-difference method. To be easily integrated into the whole model, in the present modelling, the other approach, the Z-transfer function method(Mitalas and Arsenault, 1970) will be introduced. Given the properties of the wall material, a series of so called Z-transfer factors can be worked out for a multi-layer wall. Then the conduction heat flux on both sides of a wall are related to the past values and the present and past surface temperatures by

$$q_{o_n} = \sum_{j=0}^N ZD_j T_{o_{n-j}} - \sum_{j=0}^N ZI_j T_{M_{n-j}} - \sum_{j=1}^N ZB_j q_{o_{n-j}} \quad (4.4)$$

$$q_{M_n} = \sum_{j=0}^N ZI_j T_{o_{n-j}} - \sum_{j=0}^N ZA_j T_{M_{n-j}} - \sum_{j=1}^N ZB_j q_{M_{n-j}} \quad (4.5)$$

where,  $ZD_j$ ,  $ZI_j$ ,  $ZA_j$  and  $ZB_j$  are the Z-transfer factors;  $N$  is the number of terms of the Z-transfer factors;  $n$  represents the current time step;  $T_o$ ,  $T_M$ ,  $q_o$  and  $q_M$  are the outside and inside surface temperatures and conduction heat fluxes respectively. These two equations reflect the thermal storage capacity of a wall by incorporating the past temperatures and heat fluxes into the calculation.

In the equations,  $T_{o,n}$ ,  $T_{M,n}$ ,  $q_{o,n}$  and  $q_{M,n}$  are the current values, and are to be solved for. For equation closure, the energy balance equation for the outside surface of the wall must be introduced(Figure 4.5). This balance can be expressed as

$$q_s + q_{o,ex} = q_{o,rc} + q_o \quad (4.6)$$

where,  $q_s$  is solar radiation absorbed by the outside surface,  $q_{o,ex}$  is extra heat flux pressed on and absorbed by the outside surface,  $q_{o,rc}$  is the combined radiative and convective heat transfer from the outside surface to the ambient air and atmosphere,  $q_o$  is the heat conduction flux at the outside surface into the wall, as expressed in Eq.(4.5).

With solar radiation known, the absorbed solar radiation can be calculated by

$$q_s = a_{od} I_{DC} + a_{od} (I_{dcs} + I_{def}) \quad (4.7)$$

where,  $a_{od}$  and  $a_{od}$  are the absorptivities of the outside surface for direct and diffuse radiation respectively,  $I_{DC}$  is the direct solar radiation that strikes upon a normal surface, and  $I_{dcs}$  and  $I_{def}$  are respectively the diffuse radiation and reflected radiation from the ground on the surface considered. For the roof of a building,  $I_{def}$  is null. The combined radiative and convective heat loss can be expressed as(Kimura, 1977)

$$q_{o,rc} = \alpha_o (T_o - T_a) + q_z \quad (4.8)$$

where,  $T_o$  is the outside surface temperature,  $\alpha_o$  is the combined surface heat exchange coefficient, which accounts for the exchange by atmospheric radiation, earth radiation, wall surface radiation and the convection between the outside wall surface and the ambient air,  $\alpha_o = \alpha_{o,c} + \alpha_{o,r}$ ; and  $\alpha_{o,r}$  is defined as the radiative heat transfer coefficient between the outside wall surface and the hypothetical black hemispherical surface surrounding the wall, i.e.,

and  $q_z$  in Eq.(4.8) is expressed as



$$\alpha_{o,r} = \frac{\epsilon_o \sigma T_o^4 - \sigma T_a^4}{T_o - T_a} \quad (4.9)$$

$$q_z = \sigma T_a^4 [1 - \phi_a (1 - a_c K_c) Br] - \phi_a a_c K_c \sigma T_e^4 - \phi_c \epsilon_c \sigma T_e^4 \quad (4.10)$$

where,  $T_a$  is the ambient air temperature,  $\phi_a$  is the view factor of the sky from the outside surface,  $a_c$  is the cloud cover ratio,  $K_c$  is cloud reduction factor dependent upon the height of cloud as given by Kimura(1977),  $Br$  is the emissivity of atmosphere, meaning the ratio of radiation from the atmosphere to the radiation from a black hemisphere whose temperature is equal to the ambient air temperature and dependent on the water vapour content in the atmosphere,  $\phi_c$  is the view factor of the ground from the outside surface,  $\epsilon_o$  and  $\epsilon_c$  are respectively the emissivity of the wall surface and ground, and  $T_e$  is the ground surface temperature.

Concerning the calculation of  $q_{o,r}$ , the most uncertain value in Eq.(4.8) could be the convective heat transfer coefficient on the outside surface  $\alpha_{o,c}$ . It is considered that the principal factors governing the convective heat transfer coefficient are wind speed and direction in relation to the geometry of the surface. Since the air flow along the outside surface of buildings may possibly be quite different from the natural wind speed, Ito *et al*(1972) adopted field experiment method to determine the convective heat transfer coefficient. From these experiments, an algorithm for computer calculation of  $\alpha_{o,c}$  is obtained. In this algorithm, wind direction relative to the wall surface concerned is first calculated, and according to the relative direction angle, the surface is classified as being windward or leeward. Then the air velocity near the surface is calculated according to:

$$\begin{aligned} u &= 0.25U && \text{(for } U \geq 2 \text{ m/s)} && \text{if the surface is windward;} \\ u &= 0.5 && \text{(for } U \leq 2 \text{ m/s)} && \\ \\ u &= 0.3 + 0.05U && && \text{if the surface is leeward.} \end{aligned}$$

Once the wind velocity near the surface is determined, the convective heat exchange coefficient  $\alpha_{o,c}$  is calculated from(Kimura 1977)

$$\alpha_{o,c} = 3.5 + 5.6u \quad (4.11)$$

#### 4.2.2.4 Internal between-surface radiant heat exchanges

The long wave radiant heat exchange between the enclosed surfaces in a building space can be treated as radiative exchange within a diffuse-grey enclosure. A somewhat different viewpoint from what is used in Chapter 3, which has been set forth by Gebhart(Siegel and Howell, 1981), will be briefly presented here. The special utility in this formulation is that it yields coefficients that provide the fraction of energy emitted by a surface that is *absorbed* at another surface after reaching the absorbing surface by all possible paths. These

values, once obtained, can be used repeatedly for a fixed room configurations, this is especially useful for the hour-by-hour annual simulation purposes.

Same as in Chapter 3, an enclosure having  $N$  diffuse-grey surfaces is considered. For a typical surface  $A_k$  the net energy loss is the emission from the surface minus the energy that is absorbed by the surface from all incident sources. The emitted energy is  $A_k \epsilon_k \sigma T_k^4$ . Let  $\psi_{jk}$  be the fraction of the emission from surface  $A_j$  that reaches  $A_k$  and is absorbed. This includes all the paths for reaching  $A_k$ ; that is, the direct path, paths by means of one reflection, and the paths by means of multiple reflections. Thus  $A_j \epsilon_j \sigma T_j^4 \psi_{jk}$  is the amount of energy emitted by  $A_j$  that is absorbed by  $A_k$ . A heat balance on  $A_k$  then gives

$$\begin{aligned} Q_k &= A_k \epsilon_k \sigma T_k^4 - \sum_{j=1}^N A_j \epsilon_j \sigma T_j^4 \psi_{jk} \\ &= \sum_{j=1}^N A_k \epsilon_k \sigma T_k^4 \psi_{kj} - \sum_{j=1}^N A_j \epsilon_j \sigma T_j^4 \psi_{jk} \\ &= \sum_{j=1}^N A_k \psi_{kj} \sigma (\epsilon_k T_k^4 - \epsilon_j T_j^4) \end{aligned} \quad (4.12)$$

Here, the equation  $A_k \psi_{kj} = A_j \psi_{jk}$  has been used. The  $\psi_{jk}$  would generally not be zero since even for a plane or convex surface some of the emission from a surface will be returned to itself by reflection from other surfaces. Eq. (4.10) can be written for each surface; this will relate each of the  $Q$ 's to the surface temperatures in the enclosure. The  $\psi$  factors must now be found.

The quantity  $\psi_{jk}$  is the fraction of energy emitted by  $A_j$  that reaches  $A_k$  and is absorbed. The total emitted energy from  $A_j$  is  $A_j \epsilon_j \sigma T_j^4$ . The portion travelling by a direct path to  $A_k$  and then absorbed is  $A_j \epsilon_j \sigma T_j^4 F_{j-k} \epsilon_k$ , where for a grey surface  $\epsilon$  is equal to the absorptivity. All other radiation from  $A_j$  arriving at  $A_k$  will first undergo one reflection, the emission from  $A_j$  that arrives at a typical surface  $A_n$  and is then reflected is  $A_j \epsilon_j \sigma T_j^4 F_{j-n} \rho_n$ . The fraction  $\psi_{nk}$  then reaches  $A_k$  and is absorbed. then all the energy absorbed at  $A_k$  originating by emission from  $A_j$  is

$$A_j \epsilon_j \sigma T_j^4 F_{j-k} \epsilon_k + \sum_{i=1}^N A_j \epsilon_j \sigma T_j^4 F_{j-n} \rho_n \psi_{nk} \quad (4.13)$$

Dividing this energy by the total emission from  $A_j$  gives the fraction

$$\psi_{jk} = F_{j-k} \epsilon_k + \sum_{n=1}^N F_{j-n} \rho_n \psi_{nk} \quad (4.14)$$

By letting  $j$  take on all values from 1 to  $N$ , A set of equations is obtained and can be solved simultaneously for  $\psi_{nk}$  ( $n=1,2,\dots, N$ ), and the  $k$  index can correspond to any of the surfaces in the enclosure.

To include Eq.(4.12) into Eq.(4.1), and eventually to construct a set of linear equations, it is desirable to express the rate of radiant heat transfer from one surface to the other in the linear form

$$Q_{j \rightarrow k} = \alpha_{r,j \rightarrow k} (T_j - T_k) A_i \quad (4.15)$$

where  $\alpha_{r,j \rightarrow k}$  is defined as radiative heat exchange coefficient from surface  $i$  to surface  $k$ . According to the definition of  $\psi_{j \rightarrow k}$ , we have

$$Q_{j \rightarrow k} = A_j \psi_{jk} \sigma (\epsilon_j T_j^4 - \epsilon_k T_k^4) \quad (4.16)$$

Thus,

$$\begin{aligned} \alpha_{r,j \rightarrow k} &= \psi_{jk} \sigma \frac{\epsilon_j T_j^4 - \epsilon_k T_k^4}{T_j - T_k} \\ &= \psi_{jk} \sigma \theta \end{aligned} \quad (4.17)$$

where,

$$\theta = \frac{\epsilon_j T_j^4 - \epsilon_k T_k^4}{T_j - T_k} \quad (4.18)$$

When  $\epsilon_j \approx \epsilon_k$ , and the difference between  $T_j$  and  $T_k$  is not too large ( $0.7 \leq T_j/T_k \leq 1.4$ ),  $\theta$  can be simplified as

$$\theta = 4\epsilon_j \left[ \frac{T_j + T_k}{2} \right]^3 \quad (4.19)$$

which indicates that if the average temperature of the room does not change very much, the radiative heat transfer coefficients will be nearly constant. Taking the advantage of this fact can very much simplify the whole solution algorithm. For instance, the  $\alpha_{r,j \rightarrow k}$  calculated by Eq.(4.18) using the temperatures of the previous time step can be used for the current time step calculation. Therefore in most cases, iterative calculation for a more accurate  $\alpha_{r,j \rightarrow k}$  becomes unnecessary.

#### 4.2.2.5 Convective heat transfer on an inside surface

This process is most uncertainly described in building thermal simulations. As already described in section 3.3.3, in the past, correlation about the natural convection heat transfer along the isolated vertical or horizontal plate are used. However, in room situations, air

flows originating from various sources interact with each other, so that more complicated flows are formed in a room. This may create two difficulties: 1).the correlations do not apply, 2). temperature differences are created in the room so that, for different surfaces, different temperature differences should be used. In the previous research, Chen and Kooi(1990) have tried several methods to overcome the later difficulties. However, the empirical film convective heat transfer coefficients were still used for the calculation of  $q_{c,i}$  in Equation (4.1).

In the present research, the CFD prediction of the air convection are expected to be improved with grid-optimization, as recommended in Chapter 3. However, fully coupling the CFD calculation with the building energy estimation is not realistic because of the too long computation time required for the CFD part. Therefore, for the internal surface convective heat exchange calculation, the approach described by Chen and Kooi(1990) will still be adopted. After all, the  $q_{c,i}$  in Eq. (4.1) will be substituted by

$$q_{c,i} = \alpha_{c,i}(T_i - (T_r + \Delta T_{r,i})) \quad (4.20)$$

where,  $T_i$  is the inside surface temperature;  $T_{r,i}$  is the average room air temperature, and  $\Delta T_r$  is the temperature difference of the air volume adjacent to the wall from the average room air temperature;  $\alpha_{c,i}$  is the film convective heat transfer coefficient, for the natural convection along a vertical surface, or a hot surface facing upward or a cold surface facing downward, i.e.

$$\alpha_{c,i} = 1.52 (\Delta t)^{0.33} \quad (4.21a)$$

will be used; for other surfaces whereby the forced convection is negligible, the following equation recommended by ASHRAE(1989) will be used

$$\alpha_{c,i} = 0.6(\Delta T/d)^{1/5} \quad (4.21)$$

where  $d$  is the characteristic dimension of the flow, and is equal to panel width in this case.

Many other empirical formulations can be found in the literature (Jocab 1949, Wong 1977, Alamdari and Hammond 1983). As already said, though efforts have been made to make the formulations more universal, errors will exist when applied to various room situations. Some sensitivity analysis was done previously by Jansen(1984), and it was tested that, when the values of  $\alpha_c$  used ranges between 3 to 5, the simulation results were reasonable in rooms where forced convection is weak.

#### 4.2.3 Thermal Balance of Multi-Layer Window

The energy process through a window involves the absorption, reflection and transmission of solar radiation, in addition to the conduction and surface convective heat transfer that are involved for other surfaces. Detailed calculation method of the overall absorption, reflection and transmission coefficients for a multi-layer window has been developed by Oegema(1970). The usage of the coefficients have been illustrated in section 4.2.2.1. In this section, the mathematical modelling for the overall energy balance for a window will be

described.

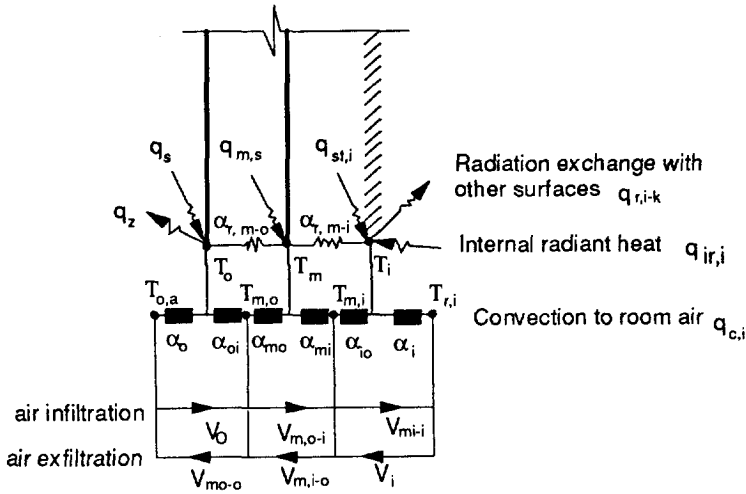


Figure 4.6 Energy balances of a multi-layer window(double-glazing with venetian blinds)

A double glazing window with venetian blinds as illustrated in Figure 4.6 is considered here. The window consists of three layers: the inside and outside window panes and the venetian blind, which can be located either inside or outside, or between the two layers of glass. For the mathematical modelling, the venetian blinds and the glass are treated in the same method: both of the thermal resistances due to conduction and the thermal storage capacity are neglected. As a consequence, a quasi-steady state heat balance will be maintained among the layers.

Similar to the energy balance equation for an internal wall surface, the heat balance equation on the inside layer of the window as shown in Fig. 4.3 can be expressed as

$$q_{st,i} + q_{m,i} + q_{ir,i} + q_{t,i} = \sum_{k=1}^N q_{r,i-k} + q_{c,i} \tag{4.22}$$

where  $q_{st,i}$  is the solar radiation absorbed by the inside window layer. It is determined from the formula

$$q_{st,i} = S_D a_{iD} I_{Dc} + S_s a_{is} I_{dcs} + S_f a_{if} I_{def} \tag{4.23}$$

where  $I_{Dc}$ ,  $I_{dcs}$ , and  $I_{def}$  are direct, diffuse and ground reflection components of solar radiation that strike upon the outside surface respectively,  $S_D$ ,  $S_s$ , and  $S_f$  are the shade ratios of the

window for  $I_{Dc}$ ,  $I_{dcs}$ , and  $I_{dcf}$  respectively,  $a_{D}$ ,  $a_{i}$  and  $a_{f}$  are the absorptivity of the inside layer for the direct, sky diffuse and ground reflection of solar radiation  $I_{Dc}$ ,  $I_{dcs}$ , and  $I_{dcf}$  respectively; and

$$q_{m,i} = \alpha_{io}(T_{mi} - T_i) + \alpha_{r,m-i}(T_m - T_i) \quad (4.24)$$

where,  $\alpha_{io}$  and  $\alpha_{r,m-i}$  are the convective heat transfer coefficient of the inner window pane into the air layer, and the long wave radiative heat transfer coefficient between the inner layer and middle layer respectively.  $\alpha_{r,m-i}$  is determined according to Eq.(4.16), using  $T_i$  and  $T_m$ .  $T_{mi}$  is the temperature of the air pocket between the inside layer and the middle layer. The other terms in Eq.(4.22) are similar to those in Eq.(4.1).

Very similar to the heat transfer on the outside surface of a wall, the heat balance equation on the outside layer of the window can be expressed as

$$q_s + q_{o,ex} = q_{o,c} + q_o \quad (4.25)$$

Beside the similar terms as those in Eq.(4.6) for the energy balance of outside surface of a wall, the rest term  $q_r$  can be rewritten as follows:

$$q_s = S_D a_{oD} I_{Dc} + S_s a_{os} I_{dcs} + S_I a_{of} I_{dcf} \quad (4.26)$$

where  $a_{oD}$ ,  $a_{os}$  and  $a_{of}$  are the absorptivity of the outside layer for  $I_{Dc}$ ,  $I_{dcs}$ , and  $I_{dcf}$  respectively; the term  $q_o$  is the sum of the convective heat, released to the air between outside layer and middle layer, and the radiant heat transferred to the middle layer, i.e.,

$$q_o = \alpha_{oi}(T_o - T_{mo}) + \alpha_{r,m-o}(T_o - T_m) \quad (4.27)$$

where  $\alpha_{oi}$  is the inside surface convective heat transfer coefficient of the outside layer,  $T_{mo}$  is the air temperature between the outside layer and the middle layer,  $T_m$  is the middle layer temperature, and  $\alpha_{r,m-o}$  is the radiative heat exchange coefficient between the outside layer and the middle layer.

To eliminate the unknown intermediary layer temperatures, the energy balance equation for these layers are introduced. For the middle window layer, the energy balance equation is:

$$q_{ms} = q_{mo} + q_{mi}$$

i.e.,

$$\begin{aligned} q_{ms} = & \alpha_{mo}(T_m - T_{mo}) + \alpha_{r,m-o}(T_m - T_o) \\ & + \alpha_{mi}(T_m - T_{mi}) + \alpha_{r,m-i}(T_m - T_i) \end{aligned} \quad (4.28)$$

where  $\alpha_{mo}$  and  $\alpha_{mi}$  are the convective heat transfer on the outside and inside surfaces of the middle layer. For the air layer between the middle layer and outside layer, the heat

balance equation is

$$\begin{aligned} \alpha_o(T_o - T_{mo'}) + \alpha_{mo}(T_m - T_{mo'}) + V_o C_p \rho T_a + V_{m,i-o} C_p \rho T_{mi} \\ = (V_{mo-o} + V_{m,o-i}) C_p \rho T_{mo} \end{aligned} \quad (4.29)$$

where  $V_o$  and  $V_{mo-o}$  are the infiltration and ex-filtration rate per unit surface area of the outside air layer, for a single layer window, this will be the room air infiltration and ex-filtration rate;  $V_{m,o-i}$  and  $V_{m,i-o}$  are the air infiltration and ex-filtration between the outside and inside air layers, and for mass conservation  $V_o + V_{m,i-o} = V_{mo-o} + V_{m,o-i}$ . Similarly for the air layer between the middle layer and the inside layer, the energy balance equation can be written as

$$\begin{aligned} \alpha_{mi}(T_m - T_{mi'}) + \alpha_{io}(T_i - T_{mi'}) + V_i C_p \rho (T_r + \Delta T_{r,i}) + V_{m,o-i} C_p \rho T_{mo} \\ = V_{mi-i} C_p \rho T_{mi} + V_{m,i-o} C_p \rho T_{mi} \end{aligned} \quad (4.30)$$

where  $V_i$  and  $V_{mi-i}$  are the air exchange rate per unit area between the room and the air layer, and  $V_i + V_{m,o-i} = V_{mi-i} + V_{m,i-o}$ .

Through algebraic manipulation of Eq.(4.22) - (4.24) and Eqs. (4.27) - (4.30), the unknown temperatures  $T_o$ ,  $T_{m'o}$ ,  $T_m$ ,  $T_{mi}$  can be expressed in explicit forms. Substitute the  $T_{mi}$  and  $T_m$  in Eq.(4.22) with the explicit expressions, then Eq.(4.22) will only involve other internal surface temperatures and the indoor air temperatures.

#### 4.2.4 Zonal(Room) Volume Air Energy Balance

A zone is a volume of air which is enclosed by certain solid partitions(which are described as surfaces in this context). The energy balance equation for a volume of air is

$$V_R \rho C_p \frac{dT}{dt} = Q_{ic} + \sum_{i=1}^N Q_{c,i} + Q_{ext} + Q_{inf} - Q_{exf} \quad (4.31)$$

where,  $Q_{ic}$  is the direct convective heat from internal heat sources, including those from occupants;

$Q_{c,i}$  is the convective heat from individual wall surfaces;

$Q_{ext}$  is the heat extraction by mechanical ventilation,  $Q_{ext} = v \rho C_p (T_{ext} - T_{sup})$ , where  $v$  is the mechanical ventilation rate ( $m^3/s$ ), and  $T_{ext}$  and  $T_{sup}$  are the supplied and exhaust temperatures respectively;

$Q_{inf}$  is the heat from air infiltration, which includes those from adjacent zones;  $Q_{exf}$  is the heat loss due to air exfiltration, which includes those to the adjacent zones.

Among these terms, the air infiltration rate is the most uncertain factor. This value varies with building types(air tightness), inhabitants behaviours(the closing and opening of window and doors), and also subject to the vagaries of weather. In the last decade, the IEA has coordinated the research project on the infiltration and ventilation through buildings. Measurements method as well as the mathematical modelling approaches are discussed in a series of AIVC(Air Infiltration and Ventilation Centre) publications(Liddament and

Carolyn 1982, Liddament 1986, Charlesworth 1988, Basset 1990, and Wilson and Walker 1993 ). It is possible to calculate the air infiltration rate for a certain type of building at certain weather conditions. For the present modelling, empirical values will be used for the external infiltration.

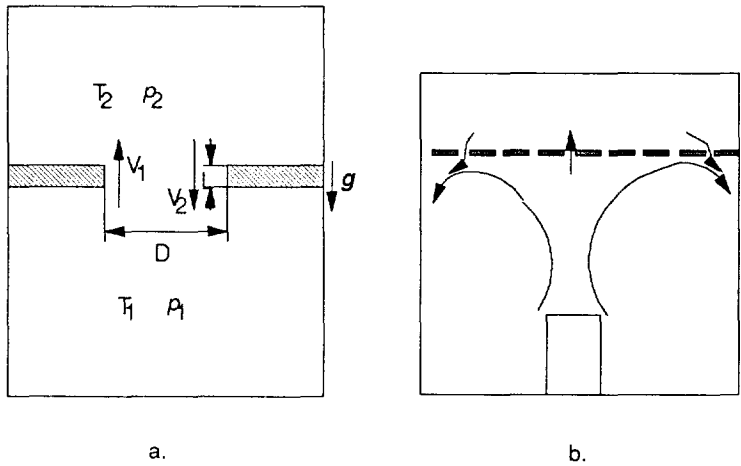


Figure 4.7 Air exchange through horizontal openings: a. simplification for Eq.(4.32); b. in room situation with multi-ceiling openings

Particular significant to the cooled ceiling system, is the air exchange between the cavity above the ceiling panels and the occupied room below. Let us first have a look at the physical situation(Figure 4.7b). The building space is divided into two vertical parts by the cooled ceiling panels or other ceiling panels(such as acoustic panels). Normally, gaps exist between these panels. It can be expected that various heat sources are present in the room, so that normally the room air temperature will be higher than that in the cavity above. This is especially true if the air above the ceiling is cooled by the cooling ceiling panels. As a consequence, a vertical temperature difference may be present. Due to the buoyancy effect, an oscillating air exchange will occur. The practical indication is that the effectiveness of the cooling capacity of the upside of the cooling panels may be determined by the air exchange. On the other side, during the night when the room is not occupied, the room air temperature may be lower than that in the cavity due to night ventilation or conduction heat loss through external windows or walls. Therefore, a stable vertical temperature stratification may exist during the night. In summary, this exchange rate may be unstable, and in the long time transient.

Relevant studies can be found in the literature about the air flow through large openings. Various studies about this kind of flows are reviewed in a recent paper(Allard



and Utsumi, 1992). Several investigations have been done on the air flow through horizontal openings. The unstable condition that the fluid above the opening has a greater density than the fluid below was first studied by Brown(1962), but a few researchers have made a consistent contribution towards solving it. In a recent paper Epstein(1988) discusses the buoyancy exchange flow through small openings in horizontal partitions(Figure 4.7a). He presents an experimental study using brine above the partition and fresh water below the partition and identifies four different regimes as the aspect ratio of the opening is increased. At very small L/D Taylor instability leads to the intrusion of each fluid into the other one and an oscillatory exchange is observed; A Bernoulli flow is subsequently found as the L/D increases, which is somewhat a stable flow; for higher values of L/D a turbulent diffusion regime appears; also a combination of Bernoulli flow and turbulent diffusion takes place. It is found that the maximum exchange flows occur for aspect ratios around unity and they correspond to the limit of the Bernoulli flow regime. Each regime can be defined by a particular flow equation but an empirical formulation of the flow through the whole range of aspect ratios  $0.01 \leq L/D \leq 20$  and  $0.025 < \Delta\rho/\rho < 0.17$  has also been proposed(Epstein 1988):

$$\frac{m'}{(D^5 g \Delta\rho/\rho)^{1/2}} = \frac{0.055[1 + 400(L/D)^3]^{1/6}}{[1 + 0.0527(1 + 400(L/D)^3)^{1/2}(L/D)^6 + 117(L/D)^2]^{3/4}}^{1/3} \quad (4.32)$$

Therefore this study gives a good description of the flow processes but remains limited to purely natural convection effects and the results are difficult to extend to more general configurations.

For a room with a cooled ceiling, multi-openings(slots) exist and also the room flow may be characterised by mixed convection. The air intrusion may be also influenced by the presence of hot plumes originated from internal heat sources and boundary flows. Therefore, special investigations will be done both by experimental approaches and numerical approaches. In the experiments, tracer gas technique will be used to obtain empirical exchange values, as will be seen in Chapter 5; one the other hand, using the CFD approach, a thorough field flow analysis will be carried out(Chapter 6). After all these study, empirical values for the air exchange at typical conditions will be used for long term dynamic simulations.

#### 4.2.5 Energy Balance for Cooled Ceiling Panels

Different construction types of the ceiling panels are available, as shown in Figure 4.3. They are pipes clipped on with metal sheet(Type I), extruded aluminum water panels(Type II), or plate-type air duct(Type III). As will be explained later, the mathematical modelling is basically the same. Let us first consider the extruded aluminum plate(water panel) type(Type II). It can be considered as a plate water-air exchangers. Normally, two panels form a loop for the cooled water(Fig.4.3). A single panel can be further divided into a series of smaller elements successively along the flow path. For each element, one

dimensional heat conduction heat transfer analysis may be used(Figure 4.8). First consider the energy balance of the metal shell. The shell is no more than 3 millimetres thick. Taking into account the high conductivity of the metal and the large time step usually used for energy simulation purposes, the shell may be treated as a single node. For the side facing the room:

$$\alpha_w(T_{p,r} - T_w) = (\delta \rho C)_m \frac{dT_{p,r}}{d\tau} \quad (4.33)$$

$$+ \alpha_{c,p}((T_r + \Delta T_r) - T_{p,r}) + \sum_{j=1}^{N_r} \alpha_{p,j}(T_j - T_{p,r}) + q_s + q_{ir}$$

where,  $(\delta\rho C)_m$  is the heat capacity of the metal shell;  $T_{p,r}$  is the shell temperature facing the room;  $N_r$  is the total number of room surfaces;  $T_w$  is the average water temperature, and  $\alpha_w$  is the forced convective heat transfer coefficient in the channel, which can be calculated according to the formula recommended by ASHRAE(1989) for turbulent flow inside tubes

$$\alpha_w D / \lambda_w = 0.023 (GD / \mu_w C_{p,w} / \lambda_w)^{0.4} \quad (4.33a)$$

where  $\mu_w$  is the viscosity of water;  $D$  is the hydraulic diameter

$$D = 4 \frac{\text{Cross-sectional area for flow}}{\text{Total wetted perimeter}}$$

Similarly, for the side facing the cavity above, the energy balance equation for the shell is:

$$\alpha_w(T_{p,c} - T_w) = (\delta \rho C)_m \frac{dT_{p,c}}{d\tau} \quad (4.34)$$

$$+ \alpha_c(T_c - T_{p,c}) + \sum_{j=N_r+1}^{N_c} \alpha_{p,j}(T_j - T_{p,c}) + q_s + q_{ir}$$

where,  $T_{p,c}$  is the panel surface temperature facing the cavity, and  $N_c$  is the total number of enclosure surfaces including the cavity enclosures.

For the water layer, the heat balance is:

where,  $T_{w,i}$ ,  $T_{w,o}$  and  $T_w$  are the inlet, outlet and average temperature of water, and  $T_w = T_{w,o}$  can be taken as a good approximation if the element is small enough;  $G$  is the water flow

$$\alpha_w(T_{p,r} - T_w) + \alpha_w(T_{p,c} - T_w) = \frac{GC_{p,w}}{\Delta A}(T_{w,o} - T_{w,i}) + (\delta \rho C_p)_w \frac{dT_w}{dt} \quad (4.35)$$

rate(kg/s);  $\delta_w$  is the thickness of the water layer;  $\rho_w$  and  $C_{p,w}$  are water density and specific heat.

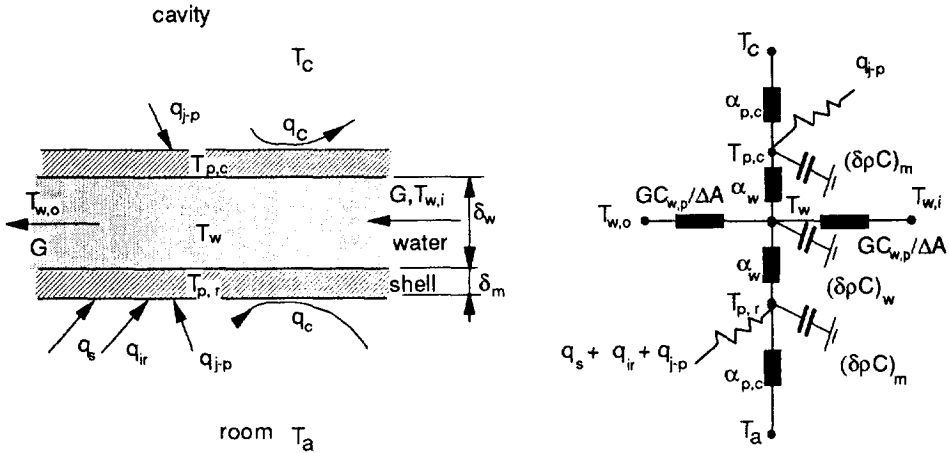


Figure 4.8 Heat balances of ceiling panel and its mathematical modelling

It was tested by a few researchers (Morant and Strengart 1985, Aiulfi et al 1985) that for energy simulation purposes, a single element model for a heating radiator is accurate enough while for control dynamic analysis multi-element model is necessary. Therefore, for the present modelling, the whole water panels will be treated as one element. To take into account the temperature variation along the water flow path, which generally takes the logarithmic form, it is assumed that the rising of the chilled water through the panel can be approximated by a linear form,

$$T_w = (1 - a_i)T_{w,o} + a_i T_{w,i} \quad (4.36)$$

where  $a_i$  is an empirical constant,  $a_i = 2/9$  is a good approximation for the temperature difference  $T_{w,o} - T_{w,i} = 10 \text{ K}$ .

The influences of fin-effectiveness of different panel types can be further considered by modifying the internal convective heat transfer coefficient  $\alpha_w$ . In such a way, different panel types can be treated in a universal way.

Also, substitute all the quantities concerning water layer with those concerning air

layer, Eq.(4.33) until Eq.(4.36) can be applied to air panels. After the air flows through the panel, its temperature is raised from  $T_{s,i}$  to  $T_{s,o}$ . The air subsequently enters the room, may further extract room heat according to:

$$Q_{\text{ext}} = v \rho C_p (T_{\text{ext}} - T_{s,o}) \quad (4.37)$$

where,  $T_{\text{ext}}$  is the exhaust air temperature,  $v$  is the ventilation rate.

### 4.3 CRITERIA FOR LONG TERM THERMAL COMFORT ESTIMATION

A number of quantitative indices have been developed in the last two decades, which describe the satisfactory degree by which an occupant feels about a thermal environment. The thermal sensation of human beings is, as a matter of fact, the interactive effect of the human body with its environment, the very feeling of comfort will depend on both the thermal environmental factors and the human factors. Therefore, in this section, the thermal quantities that characterise a thermal environment will be briefly explained, and then the thermal comfort indices that combine the environment and human factors will be introduced, and finally, the thermal comfort index will be used for the long term(annual) analysis of energy consumption that is required to maintain a environment at the desired comfort level. This work is trying to integrate the latest development in the research about human thermal comfort with the energy analysis.

#### 4.3.1 Mean Radiant Temperature

The thermal environment may be characterized by convective and radiant environment. The convective environment are described by the air temperature, humidity and air flow velocity, which are somewhat straight-forward quantities and can be directly measured. Here only the indices that describe the radiant environment will be explained in detail.

Consider a room that is enclosed by  $N$  surfaces which have areas  $A_1, A_2, \dots, A_N$ , temperatures  $T_1, T_2, \dots, T_N$ , and emissivities  $\epsilon_1, \epsilon_2, \dots, \epsilon_N$ . The long wave radiation from the surfaces will enact a radiant field within the room. As was explained in section 3.3.3 of Chapter 3, for each surface, the gross radiant energy leaving a surface is referred to as radiosity  $J_k$ . Imagine a person sitting or standing in the room somewhere, and the view factor of the person from the surfaces are  $F_{1,p}, F_{2,p}, \dots, F_{N,p}$ . The radiant energy that strikes upon the person is

$$\sum_{k=1}^N J_k F_{k-p} \quad (4.38)$$

To quantify this radiant energy in a single term, the *mean radiant temperature*  $t_{mr}$  is usually used. It is the uniform temperature of an imaginary enclosure in which radiant heat transfer from the human body equals the radiant heat transfer in the actual non-uniform enclosure. By definition, we have

$$T_{mr}^4 = \frac{1}{\sigma} \sum_{k=1}^N J_k F_{k-p} \quad (4.39)$$

where  $\sigma$  is the Boltzman constant. As most building materials have a high emittance  $\epsilon$ , the radiosity of all the surfaces can be very close to the black-body emissions at the surface temperature. Then the following equation is a good approximation:

$$T_{mr}^4 = \sum_{k=1}^N T_k^4 F_{k-p} \quad (4.40)$$

As the sum of the view factors is unity, Equation(4.40) means that the fourth power of mean radiant temperature equals the surrounding surface temperature of the fourth power, weighted by the respective view factors. If relatively small temperature differences exist between the surfaces of the enclosure, Eq.(4.40) can be simplified to a linear form:

$$t_{mr} = \sum_{k=1}^N t_k F_{k-p} \quad (4.41)$$

Eq. (4.41) always gives a slightly lower mean radiant temperature than Eq.(4.40), but in many cases the difference is small. The view factors normally depends on the position and orientation of the person and can be calculated according to Fanger's(1970) graphical chart. The so-calculated mean radiant temperature will be integrated into the comfort model described below. In such a way the radiant effect of the presence of cooled-ceiling panels will be counted precisely.

#### 4.3.2 Thermal Comfort and Thermal Sensation of Human Body - The Predicted Mean Vote

A person's thermal response to a given set of environmental conditions is strongly influenced by clothing and activity level. In a moderate environment man's thermoregulatory system will automatically try to modify the skin temperature and the sweat secretion to maintain heat balance. Man is in thermal balance when the internal heat production in the body is equal to the loss of heat to the environment. However, heat balance alone is not sufficient to establish thermal comfort. In the wide range of environmental conditions, where heat balance can be obtained, only a narrow range provides thermal comfort. Using the basic energy balance equations for human body, Fanger(1982) deducted a single equation that relates the environment parameter and human factors to calculate the balanced body skin temperatures for normal indoor clothing level and with low or moderate activity levels. These The equation is expanded to obtain a thermal sensation index - the Predicted Mean Vote(PMV). The PMV is an index that predicts the mean value of the votes of a large group of persons on the following 7-point scale:

+3	hot
+2	warm
+1	slightly warm
0	neutral
-1	slightly cool
-2	cool
-3	cold

The PMV is given by the equation:

$$\begin{aligned}
 \text{PMV} = & (0.030e^{-0.036M} + 0.028)[(M - W) - 3.05 \times 10^{-3}[5733 - 6.99(M - W) - P_a] \\
 & - 0.42 \times [(M - W) - 58.15] - 1.7 \times 10^{-5}M(5867 - P_a) \\
 & - 0.001M(34 - t_a) - 3.96 \times 10^{-8}f_d \times ((t_d + 273)^4 - (t_{mr} + 273)^4) \\
 & - f_d h_c(t_d - t_a)]
 \end{aligned} \quad (4.42)$$

where

$$\begin{aligned}
 t_d = & 35.7 - 0.028(M - W) - I_d[3.96 \\
 & \times 10^{-8}f_d \times ((t_d + 273)^4 - (t_{mr} + 273)^4) + f_d h_c(t_d - t_a)]
 \end{aligned} \quad (4.43)$$

and

$$h_c = \begin{cases} 2.38(t_d - t_a)^{0.25} & \text{for } 2.38(t_d - t_a)^{0.25} > 12.1\sqrt{V_a} \\ 12.1\sqrt{V_a} & \text{for } 2.38(t_d - t_a)^{0.25} < 12.1\sqrt{V_a} \end{cases} \quad (4.44)$$

$$f_d = \begin{cases} 1.00 + 1.290I_d & \text{for } I_d \leq 0.078 \text{ m}^2 \cdot \text{C/W} \\ 1.05 + 0.645I_d & \text{for } I_d > 0.078 \text{ m}^2 \cdot \text{C/W} \end{cases} \quad (4.45)$$

where  $M$  is the metabolic rate, in watts per square metre of body surface area;  $W$  is the external work, in watts per square metre, which equals to zero for most activities;  $I_{cl}$  is the thermal resistance of clothing, in  $m^2 \cdot ^\circ C/W$ ;  $f_{cl}$  is the ratio of man's surface area while clothed, to man's surface area while nude;  $t_a$  is the air temperature,  $^\circ C$ ;  $t_{mr}$  is the mean radiant temperature,  $^\circ C$ ;  $V_a$  is the relative air velocity, m/s;  $P_a$  is the partial water vapour pressure, in pascals;  $h_c$  is the convective heat transfer coefficient,  $W/m^2 \cdot ^\circ C$ ;  $t_{cl}$  is the surface temperature of clothing,  $^\circ C$ . It should be noted that the coefficients in the above equations only apply with the units described here.

From Eq.(4.42) the PMV can be calculated for different combinations of metabolic rate, clothing, air temperature, mean radiant temperature, air velocity and air humidity, the equations for  $t_{cl}$  and  $h_{cl}$  may be solved by iteration.

### 4.3.3 Long Term Estimation of Thermal Comfort

As illustrated by the Eqs.(4.42) to (4.45), the activity level has great influence on the comfort air temperature. This feature should be used for energy conservation for comfort control. For example, in the morning when man goes to work, he may undergo a high level of activity such as cycling, walking or car-driving, therefore he may subsequently feel too warm when he enters his office. In that case, a relatively lower indoor air temperature may be desired in the beginning hour of the day. This may imply that, in the heating season, the thermostat may be set at a lower value for the night temperature set-back of the room so that heat loss is much reduced; and that, in the cooling season, the room temperature can also be regulated to a lower temperature by night ventilation or mechanical cooling to store cooling energy in the building thermal mass, so that mechanical cooling during the day peak-demand period can be reduced. Another important factor that influences the thermal sensation of human body is the length of exposure time to a thermal environment. Studies by Rohles and Nevins(1971) and Rohles(1973) on 1600 college-age student revealed the statistical correlation of comfort level, length and other factors. This may add another dimension of energy saving by allowing temperature swing in a certain range through system-control.

The impact of temperature swing on energy saving is accomplished by a dynamic process, and therefore has to be investigated by dynamic modelling of the process. The purpose of this section is to introduce a thermal comfort criterion that can be used for long term thermal environment estimations. Integrating the criterion with the annual energy estimation will allow us to investigate the energy impact of temperature swings.

A weighting factor(WF) was reported by Brouwers and Linden(1989), which is based upon the PMV index described above. The weighting factor is related to the PMV by the formula

$$WF = 0.47 + 0.22 \times |PMV| + 1.30 \times PMV^2 + 0.97 \times |PMV|^3 - 0.39 \times PMV^4 \quad (4.46)$$

If  $|PMV| > 0.5$  occurs during the period  $\Delta\tau$ , the PMV weighted time is calculated as  $WF \times \Delta\tau$ . Summation of the PMV weighted time of all the period will give a total PMV weighted time. Since only the periods at which the  $|PMV|$  exceeds the value 0.5 are counted, this total time is called PMV Weighted Exceeding Hours(PWH)

(overschrijdingsweeguren in Dutch). The authors subsequently recommend that the maximum PWH allowed in a year is 150 hours respectively for the over-exceeding and under-exceeding. This may be considered as an estimation criterion of thermal environment for long term analysis. The deficiency of the criterion PWH < 150 may be that it does not specify how the 150 weighted hours are distributed against time within the year. For an ideal system, the over-exceeding hours would be evenly distributed in the summer period (cooling season), while the under-exceeding hours may be distributed not only in the winter period (heating season) but also in the summer season to use the cooling storage capacity of the room thermal mass. In this respect, the 150 weighted under-exceeding hours allowed for a year may be too strict.

#### 4.3.4 Operative Temperature Control

The comfort range of thermal comfort is normally considered as  $-0.5 < PMV < 0.5$ . Therefore, the target of a climate system is to maintain the PMV within the comfort shreshold. However, the value of PMV is not directly detected and therefore is not directly regulated. Rather it is the air temperature that is used as the controlled variable. In practice, the temperature sensor may be located in the return air duct, or mounted on the wall. In the later case, the sensor may detect a temperature also influenced by radiant effect. In rooms with cooled ceiling installations, it is significant to count for the radiant effect to select the setting point for the control system.

The *operative temperature*  $t_o$  is normally used for this purpose.  $t_o$  is the uniform temperature of a radiantly black enclosure in which an occupant would exchange the same amount of heat by radiation plus convection as in the non-uniform environment. In most practical cases where the relative air velocity is small ( $< 0.2$  m/s), or where the difference between mean radiant temperature and air temperature is small ( $< 4$  °C), the operative temperature can be calculated with sufficient approximation as the mean value of air and mean radiant temperature. For higher precision the following formula may be used:

$$t_o = a_a t_a + (1 - a_a) t_{mr} \tag{4.47}$$

where,  $t_a$  and  $t_{mr}$  are respectively the room air temperature and mean radiant temperature; the value of  $a_a$  can be found from the values below as a function of the relative air velocity  $V_a$  (m/s).

$V_a$	<0.2	0.2 - 0.6	0.6 - 1.0
$a_a$	0.5	0.6	0.7

At the relative humidity of 50%, air velocity  $V_a$  of 0.15 m/s, clothing level  $I_a$  of 0.7, and metabolism  $M$  of 70 W/m<sup>2</sup>, the correspondence between the PMV and  $t_o$  is as below, which are calculated from Eqs.(4.42):



PMV	-0.5	0	0.5	0.8
$t_o$ (°C)	22.0	23.9	25.6	26.8

For the present simulation, the target of control is to maintain  $t_o$  at the desired value, for example, at 23.9°C at the conditions mentioned above. In this way the PMV of comfort level is automatically satisfied. In comparison with air-temperature-control, Eq.(4.47) will be added as a supplementary equation in the simulation, as will be described in the following section.

#### 4.4 SOLUTION ALGORITHMS

In general, the energy balance equations described in section 4.2 are coupled with each other. Simultaneous solution of the equation set will give a quantitative description of the overall thermal processes of a building space. In fact, the equations described in section 4.2.2 are already discretized forms of original partial differential equations, though the partial differential terms remains for the temperature variation against time. Therefore, the solution of the equations are numerical in nature. Here, the overall solution algorithm will be explained.

For the discretization of the time differential terms, the implicit, backward finite difference scheme is used. That is to say:

$$\frac{dT}{d\tau} \approx \frac{T(n) - T(n-1)}{\Delta\tau} \quad (4.48)$$

where  $T(n)$  and  $T(n-1)$  are the temperatures of the present and last time step respectively.

For the linearized convective and radiative heat transfer terms, the temperatures of the current time steps are always used. As was already mentioned when each of the equations are introduced, the unknown temperatures of the current time step of other than the internal surfaces can be substituted by the combinations of the internal surface temperatures of current time step through mathematical manipulations. Consequently, the energy balance equations of the internal surface including window surface, wall surface and the cooling panel surface, and the zone-air energy balance equation will form a closed set of simultaneous linear equations. The prominent feature of the equation set is that the coefficient matrix is diagonal-element dominating, which ensures that the direct solution of the equation set will have good precision. Given the temperatures of the past, the present internal surface temperatures of the current time step will be first obtained. Then other temperatures of interest such as the required inlet water temperature can be calculated according to the relevant equations. Subsequently, comfort indices of the building space can be calculated.

Such a numerical procedure will be able to simulate various physical realities of a building system. How does the room temperature change against time under natural conditions, e.g., at night when the system is off? How much energy is required to maintain the room operative temperature at the desired comfort level? How does the room

temperature swing against time if the throttling range of the equipment is exceeded? These are three basic processes that a building will undergo in normal circumstances. Therefore, being able to simulate these processes will be enable us to investigate the thermal comfort and energy consumptions of a building system and the influencing parameters, such as building material, operation strategy, and night cooling effect, to name a few.

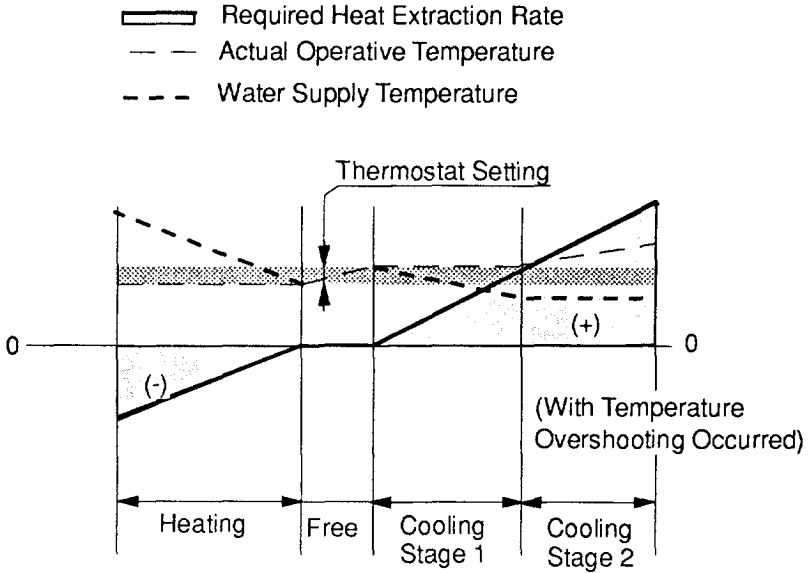


Figure 4.9 Illustration of CC system control strategies modelled by the program

For a cooled ceiling system, the required ceiling-panel surface temperature  $T_{pr}$  is solved for together with other internal surface temperatures. Then according to Eq.(4.33), the required average water temperature  $T_w$  will be determined. Further, the required inlet water temperature  $T_{w,i}$  can be calculated from Eq.(4.35) and Eq.(4.36). If this required temperature is too low, for example, the required temperature is beyond the reach of chiller capacity, or the temperature is lower than the minimum temperature that is allowed in order to avoid surface condensation,  $T_{w,i}$  will be set to the minimum value allowed. Then the equation set will be solved for again for the same time step, with the known inlet water temperature. The corresponding room air temperature will be solved so that the temperature swing is also predicted. Such a simulation will give the prediction of possible temperature exceeding that may occur with a system that has specified capacities.

For a room with ceiling systems, the whole control strategy can be illustrated in Figure 4.9. The cooling stage 2 may occur due to the capacity limits of primary equipments, such as the minimum chilled water temperature available with mechanical cooling, or the minimum wet-bulb temperature available with evaporative cooling. Such cases will be presented in more detail in Chapter 7.

#### 4.5 ENHANCEMENT OF THE COMPUTER PROGRAM ACCURACY

The implementation of the mathematical modelling has to be done on computers. A FORTRAN 77 program ACCURACY, originally developed by Chen and Kooi(1988), is modified and enhanced to be able to integrate several new features. The main features added are:

- model for cooled ceilings;
- model for the calculation of mean radiant temperatures;
- model for long term thermal comfort estimation;
- simulation of operative temperature control strategies;
- multi-zone air exchange through openings.

The original construction principle of the program ACCURACY(acronym name for A Cooling-load Code Using Room Air Current)was detailed in the report(Chen 1987). Here, mainly the modified features will be introduced.

The methodology of combining the CFD calculation of multi-zone air exchange with the overall thermal dynamic modelling is developed, as an enhancement to the original capability of ACCURACY's using CFD to calculate the local temperature differences  $\Delta T_{r,i}$ . As already mentioned, for a given room configuration, the air exchange rate between the cavity above the ceiling and the room will depends on the overall heat gain in the room. As an approximation, the air exchange and eventually can be empirically related to the air temperature differences of the cavity and the room. This empirical relation will be obtained through 3-dimensional calculation of the detailed flow in the whole domain, including the cavity. The calculation will be carried out for several typical situations. Then from these calculations, a correlation form

$$m' = f(T_r - T_c) \quad (4.49)$$

can be obtained. Unlike formula (4.31), this correlation is more specifically related to the particular room configuration and all other significant practical factors, such as location of the internal heat source and thermal boundary convection flows.

In principle, iterations between the energy balance equation set and Eq.(4.49) will be necessary. The overall flow chart of the program ACCURACY is shown in Figure 4.10. The iterations are carried out in the following way:

(1). Use the equation set to calculate the inside surface temperatures  $t_i$  and the average zone temperature  $t_r$  and  $t_c$ , which are based on the guessed or last-time-step local temperature difference  $\Delta t_{r,i}$ 's, cavity and room air temperature difference  $\Delta t_{r,c}$ , and surface convective heat transfer coefficients  $\alpha_{c,i}$ 's;

(2). Use one of the five methods described by Chen (1988) to calculate  $t_i$  and  $\Delta t_{r,i}$ s, use the new temperature differences  $t_i - (t_i + \Delta t_{r,i})$  to update  $\alpha_{c,i}$ , and use  $t_c$  and  $t_r$  to calculate the air exchange rate  $m$  according to Eq.(4.49);

(3). Iteration between step (1) and (2) are necessary until

$$\max |(\Delta t_{r,i})_{\text{iteration no. } j} - (\Delta t_{r,i})_{\text{iteration no. } j-1}| \leq \delta$$

where  $\delta$  is a small value; or  
alternatively or simultaneously until

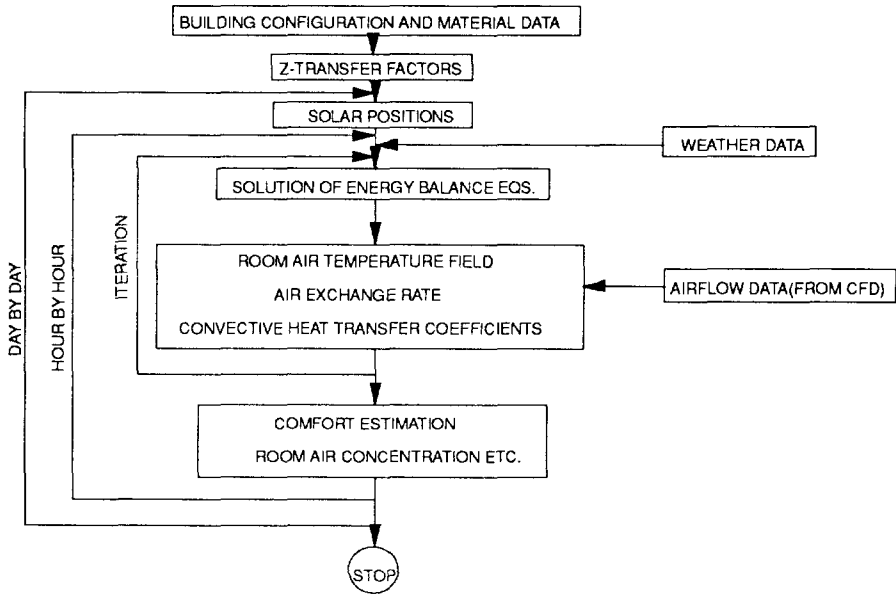


Figure 4.10 Flow Diagram of the enhanced program ACCURACY

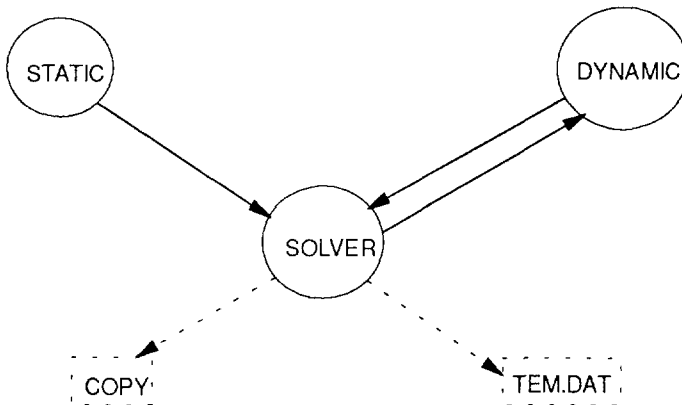


Figure 4.11 Structures of the program ACCURACY

(COPY is the tabular form output, TEM.DAT are the output data for graphics presentations)

$$\max |(t_r - t_c)_{\text{present}} - (t_r - t_c)_{\text{last iteration}}| \leq \delta_1$$

where  $\delta_1$  is another small value;

(4). Calculate thermal comfort indices, concentration distributions, etc.

The basic structure of the original version of ACCURACY is still used. It is constructed as a general purpose program that can be easily adapted for a solution of various particular problems. As a general rule, the common core of such a program must be a highly efficient and constantly maintained item of software with which a user can communicate only in carefully controlled ways. At the same time, the program must provide a subroutine in which a program user can implement his own models or modifications to the models that are provided in the common core. Such a program will allow other building simulators to perform his own task very efficiently. The program has been constructed to meet these requirements.

The user-friendly program consists of three modules, as shown in Figure 4.11: (1) STATIC, which provides problem-defining data, such as room configurations, wall and window materials, etc, and performing some fundamental computations such as calculation of the wall Z-transfer functions; (2) SOLVER, which is the central equation solver, and (3) DYNAMIC, which is attached to the main part of the program, SOLVER, assisting the latter to complete a particular simulation tasks. All variables in the program are equipped with default values that are set in BLOCK DATA. New values can be specified by calling the standard subroutines provided, instead of by modifying them. The input parameters defined in STATIC can be updated in DYNAMIC if required. For example, if the slat angle of venetian blinds changes at different times of a day, or the draper of a window is put on use during the night, then the window materials should be updated in the DYNAMIC. The DYNAMIC also offers the possibility of printing out some especially interesting part of the calculation results. This enables a building simulator of a special process to provide computer code to interact with SOLVER during its operations.

The main part of the program, SOLVER, contains approximately 8000 FORTRAN statements. It is equipped with all the equations described in section 4.4. The SOLVER first receives the static input data from STATIC, and then performing all the jobs hour by hour. If necessary, SOLVER will visit DYNAMIC to update the input data that are provided in STATIC, but dynamic in nature. What needs to be updated is up to the user in the light of properly modelling the practical processes.

#### 4.6 CONCLUSIONS

The various thermal and flow processes that occur in and around a building are briefly described in this chapter. The principle of the dynamic simulation of building thermal behaviours are explained, and the mathematical models of each process are presented. In particular, mathematical modelling of cooled ceiling panels are integrated together with the building element modelling equations. Methods of combining zone-air exchange calculation with the dynamic simulation of multi-building spaces are developed and presented in this chapter. Thermal comfort index PMV and the long term estimation criterion PWH are introduced into the dynamic building thermal behaviour analysis program. The parameters that are subject to experimental validations are indicated, such as the air exchange rate between the cavity and room airs.

To realise these modelling purposes, the computer program **ACCURACY** is enhanced, and briefly described. The program has been constructed as a user-friendly and general purpose program for building cooling and heating load calculation, annual energy estimation and overall building thermal-dynamic behaviour analysis.



## CHAPTER 5

# EXPERIMENTAL VALIDATION OF THE ENHANCED PROGRAM ACCURACY

### 5.1 INTRODUCTION

In the last chapter, the mathematical models for cooled-ceiling panels coupled with building components are introduced. Here, we will examine the most common sources of prediction inaccuracy - the uncertainties in modelling the convection processes. The quantities involved will be the air infiltration and exfiltration rates, air exchange between adjacent air spaces, and surface convective heat transfer as well as local air temperature differences that may exist in a building space.

Specifically, we will look more closely at the surface convective heat transfer from the ceiling panels and air exchanges between the cavity and the room that are encountered in a room with cooled ceiling systems. The cooled ceiling panels are located horizontally as parts of ceilings. Some manufacturers provide the ceiling panels with insulation above, and the others do not. For the Type-II and Type-III panels, as illustrated in Figure 4.3 in Chapter 4, no insulation will be used. Both sides can absorb heat through convection and radiation. Consequently, the cooling capacity of a unit area of panel is enhanced. However, it is well known that a cooled horizontal surface facing upward has much weaker convection than facing downward. Furthermore, the effect of the upper side cooling is brought down by the air exchange between the room and cavity. As far as the modelling is concerned, proper modelling of the convective heat transfer and the air exchange is obviously very decisive in the calculation accuracy of cooling load and required chilled water temperature.

Therefore, the cooled ceiling systems are installed in our climate room. The convective processes are experimentally investigated. The results about the convective heat transfer is to estimate the correlations available from literature. The tracer gas measurements will serve to identify the magnitude of the air exchange rate, and then to estimate the possibilities of CFD simulation. Finally, the step-up heating and step-down cooling processes are observed, and the results are used to check the simulations by the program ACCURACY. In this chapter, these investigations will be described.



## 5.2 EXPERIMENTAL SET UP AND INSTRUMENTATION

Shown in Figure 5.1 is the construction of the test room, which has a thick heavy concrete floor and roof of 175 mm thick and medium-light sidewalls of expanded concrete of 80 mm thick. All the outside surfaces are insulated with slabs of polystyrene foams of 80 mm thick. Between the concrete slab and the insulation layer are 50 mm thick air cavities, in which the air temperatures can be regulated independently by some electric heaters. In fact, the whole test room is located in a large hall, in which air temperatures are maintained at about 19°C.

Eight ceiling panels of water type(Type-II) and air type(Type-III) are installed respectively in the room, and each type constitutes 30% of the total ceiling area. The rest part are light fittings and a kind of fibre-board ceiling materials. Between two adjacent panels, a gap of 5-mm wide exists. These gaps altogether give about 5% openings in the whole ceiling area.

The water ceiling panels are supplied with chilled water/glycol mixtures, with a constant flow rate and temperature. The flow rate is measured by a rotator flowmeter, which is calibrated on site by direct weighing method. The chiller systems is illustrated in Figure 5.2. The temperature in the tank can be maintained at any values ranging from 5 to 50°C by on-off control of the compressor and the heater. The heat extraction of the fluid can be directly obtained by the measured flow rate and the inlet-outlet temperature differences. The fluid temperature difference over the ceiling panels is measured by a three-pair joint thermopile to increase the measurement precision. Thermal couples are also located in the supply pipe and return pipe so that the instantaneous inside fluid temperature can be estimated. Five thermocouples are attached on the panel surfaces along the flow route of the fluid, so that the mean panel surface temperature can be calculated.

The air panels are connected to an air handling system, conditioned air is supplied into the ceiling panels and then lead to the air diffuser mounted horizontally in flush with the ceiling and near the rear wall. Similarly, the air temperature difference over the ceiling panels is measured by a three-pair joint thermopile, which enables us to calculate the heat absorbed by the air panels. Five thermocouple are attached along the air flow path on the panel surfaces to measure the panel surface temperatures. The exhaust duct, which is a kind of flexible aluminum hose, is connected to the light-fittings, so that it is the air immediate below the panel and trapped in the light-fittings that is extracted. In practice, the exhaust is sometimes just simply located at the wall above the panel, and it is the immediate air from the cavity that is extracted. In the test, two thermocouples are located in the exhaust duct close to the light-fittings, and close to the exit at the wall respectively. Since the aluminium ducts run along and, in fact, in contact with the cool panels, the air in the duct may lose its heat to the ceiling panel before it reaches the exit. The measurements will identify the quantity of this heat.

20 thermocouple are located in the mid-plane of the room to measure room air temperatures, and 4 thermocouples in the mid-plane of the cavity to measure the cavity air temperatures. Each wall surface has 2 attached thermocouples to monitor the surface temperature. Floor and the ceiling respectively have 4 attached thermocouples.

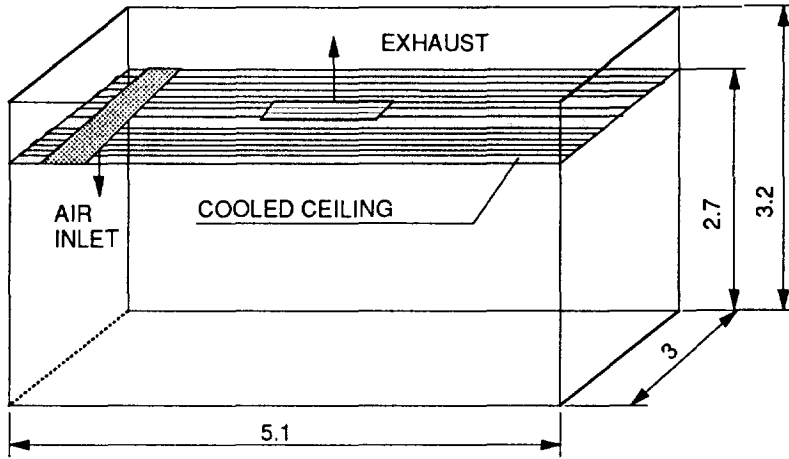


Figure 5.1 Configuration of the test room

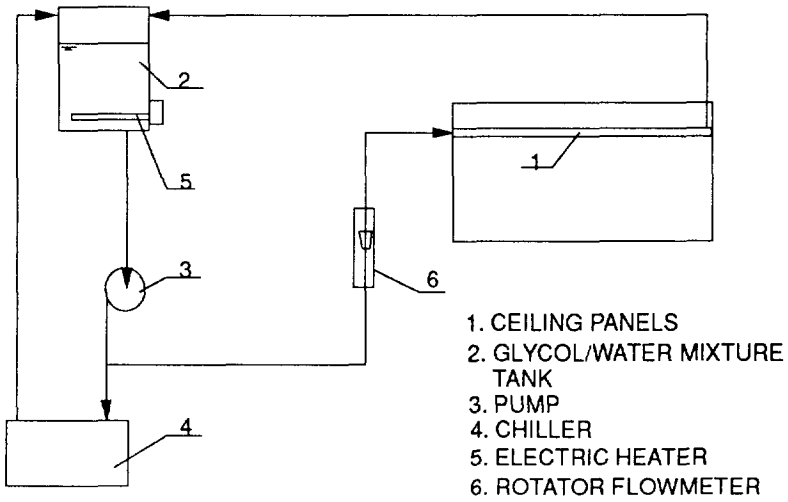


Figure 5.2 Schematic for the cooling system for water-ceiling panels

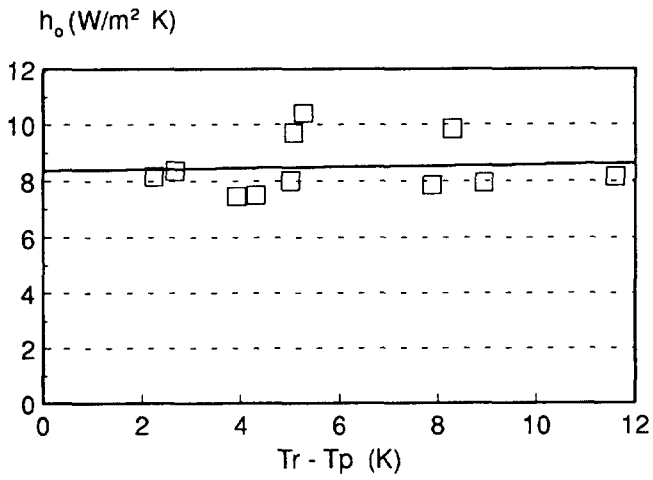


Figure 5.3 Measured surface total heat transfer coefficients

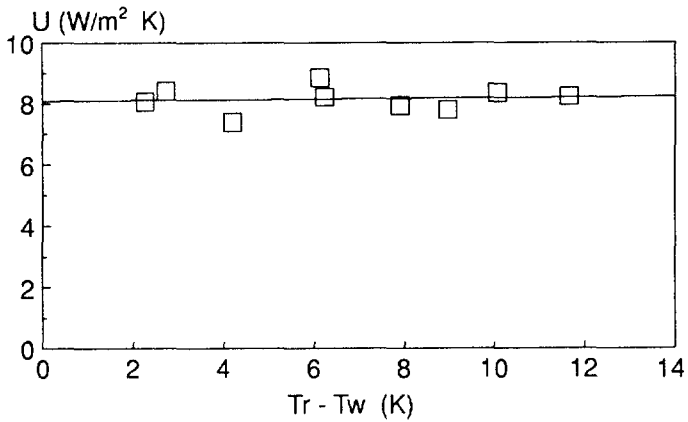


Figure 5.4 Measured overall heat transfer coefficients of the water panels

Internal heat is generated by ordinary electric lamps. The lamps are mounted in wooden boxes with holes for air convection. As a result, most of the heat goes into the air by convection, while the rest by radiation in long wave form by surface radiation of the boxes.

### 5.3 EXPERIMENTAL RESULTS

#### 5.3.1 Surface Convective Heat Transfer of Ceiling Panels

This measurement is done for water ceiling-panels. At nine steady state conditions of different water/glycol supply temperatures, the panel surface temperature and room air temperatures are measured. The heat extraction is calculated according to the liquid inlet and outlet temperature differences and the fluid flow rate. The flow rate has been adjusted to such a quantity that the temperature rise of the fluid through the panels is about 1°C. With the heat extraction by the cool ceiling panels measured, the overall nominal surface heat transfer coefficient, which takes into account both convective and radiative heat transfer effects, are calculated by the formula

$$h_o = \frac{GC_p \Delta T_w}{A_p (T_r - T_p)} \tag{5.1}$$

where, G is the water flow rate, C<sub>p</sub> is the specific heat of water, ΔT<sub>w</sub> is the water inlet and outlet temperature difference, A<sub>p</sub> is the total surface area(including the upper side) of the cooled panels, and T<sub>r</sub> and T<sub>p</sub> are the average room-air and panel surface temperatures respectively. The h<sub>o</sub> values are plotted against the temperature differences in Figure 5.3. The values of h<sub>o</sub> are found to be around 8 W/m<sup>2</sup> K. According to Equation (4.17) to (4.19), it can be expected that the equivalent radiant heat transfer coefficient will change very little within normal variation ranges of room wall surface temperatures. Moreover, a small portion of the internal heat from the lamp-box is in radiant form and is directly absorbed by the panels, independent of the temperature differences. Therefore, the temperature-dependence is mainly attributed to the convective transfer coefficient, which in present cases varies around the value of 3.0 W/m<sup>2</sup> K.

These convective heat transfer coefficients are compared with those calculated according to the equations recommended by ASHRAE, which are already described in Chapter 4 , respectively as Eq.(4.21a) for the cooling surfaces facing downward, and Eq.(4.21) for horizontal cooling surfaces facing upward. In the value range of Δt between 2 - 12°C, the convective heat transfer coefficients may range from 1.0 to 3.0 W/m<sup>2</sup> K for the upper side and from 2 to 3.5 W/m<sup>2</sup> K for the lower side, according to Equations (4.21a) and (4.21). The overall convective heat calculated accordingly is about 10% lower that from the measurements.

Similarly, the overall effective heat transmission coefficient U is calculated according to the formula

$$U = \frac{GC_p(T_{w,o} - T_{w,i})}{A_p(T_r - T_w)} \quad (5.2)$$

where,  $T_r$  is the average room air temperature; and  $T_w$  is the average temperature of the water/glycol mixture flowing inside the panel. The  $U$  values thus calculated are plotted against the temperature difference  $T_r - T_w$  in Figure 5.4. It can be seen that the  $U$  values are very close to the  $h_o$  values, which indicates that the Type-II water panel illustrated in Figure 4.3 has a very high fin-effectiveness and therefore low heat resistance and that the convective resistance from the panel shell to the fluid is also negligible. Therefore, the  $U$  value obtained in the present experiment using glycol/water mixture should apply for water. The main heat resistance is the outside convective and radiative resistance.

Also the measured  $U$ -values are in agreement with the values that are usually used in engineering for determination of the cooled ceiling areas and temperatures. From the practical point of view, this measurement indicates the maximum cooling capacities that this kind of cold ceiling panel may offer. Assuming 80% of the ceiling is installed with cooling panels with water temperature of 18°C, the cooling capacity will reach  $2 \times 8 \times (24 - 18) \times 80\% = 77$  watts/m<sup>2</sup> floor area. With additional cooling capacities of ventilation air, the cooling capacity can easily reach 100 watts/m<sup>2</sup> floor area. However, the remaining question is if the comfort in such a room can be guaranteed. This task is left to the simulation in Chapter 5.

For air panels, no specific measurements are conducted. Since the air panel has a relatively regular-shape cross-section, its internal convective heat transfer coefficients can be easily calculated according to Eq.(4.33 a and b). The surface convective heat transfer coefficients should be the same as for water-panels.

### 5.3.2 Determination of Air Exchange Between Cavity and Room Spaces

The principle of the measurements is detailed in the Appendix A. In the test, the tracer gas used is sulphur hex-fluoride(SF<sub>6</sub>), which has a density six times of the air at atmospheric pressure. The advantage of this gas is that it can be easily detected at very low concentrations, e.g., several micro-grams/m<sup>3</sup> by using an on-line infra-red multi-gas analyzer. Therefore, the density difference will have little influence on the air movement when it is well-mixed with the air at such low concentrations.

To realise a good initial well-mixed condition of the tracer gas in the room below, two approaches that enhance the mixing process are combined. Ten supply hoses are located uniformly in the room to charge a sufficient amount of tracer gas into the room in a matter of several seconds. Simultaneously, an air fan located in the room was switched on for a few seconds to intensify the mixing. However, the fan will have interference on the natural convection. Therefore, it is essential that the fan, on one hand, is powerful enough to make the air fully mixed in a matter of several seconds while, and on the other hand, not disturb or cause much air exchange through the ceiling gaps within this mixing process. Different fan mixing speeds were tested. It was

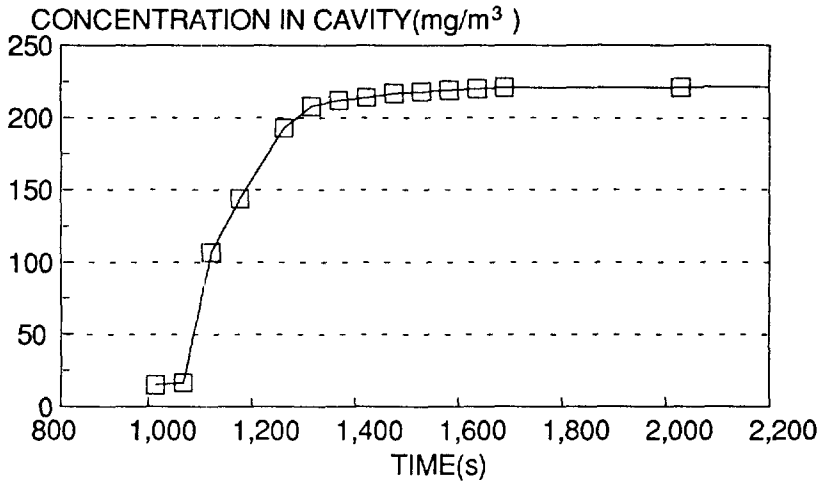


Figure 5.5 Monitored concentration increase of SF6 in the cavity  
(water-ceiling 30%, cooling load 20W/m<sup>2</sup>)

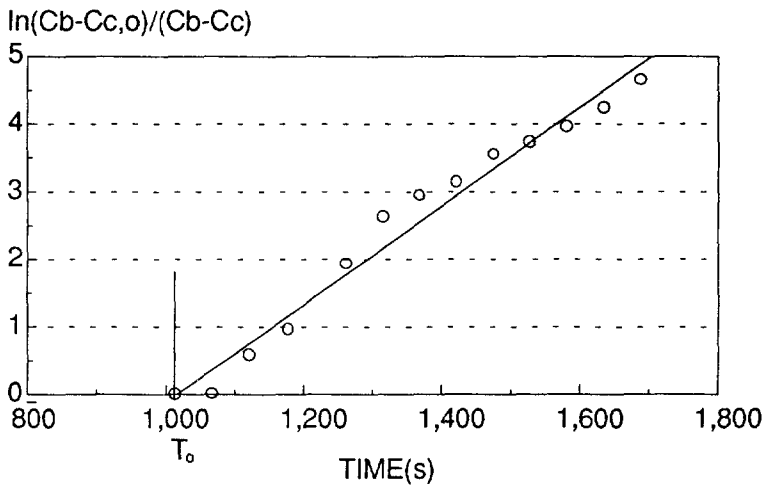


Figure 5.6 Logarithmic plotting of the measured dimensionless concentration  
in the cavity

found, by monitoring the concentrations at different locations in the room, that low fan speed worked very well, probably because the tracer gas is already purged into the room at diversified positions. Since the air enters the cavity from the room through the gaps scattered all over the ceiling, the average concentration might be close to the nominal instantaneous 'fully mixed concentration', even if the concentration in the room is not 100% uniform. Therefore, very short time fan mixing at low speed was used at the beginning of the measurements.

The monitored SF<sub>6</sub> concentration in the cavity, which is the on-line diagnosis of the mixed samples from four locations, is shown in Figure 5.5. Due to the preliminary test, some background concentration exists in the room: the initial concentration  $C_{c,0}$  in the cavity is about 17 mg/m<sup>3</sup>. It takes about 5 or 6 minutes to reach the equilibrium state. The equilibrium concentration is about 225 mg/m<sup>3</sup>.

Some measurement errors are taken into consideration in the later data processing. In the later stage of the concentration increasing, the measured  $C_c$  will be very close to the final equilibrium concentration  $C_b$ . Consequently, any error in the measured value of  $C_c$  at this stage will create large errors in the calculation of the logarithmic value of the dimensionless concentration  $\ln(C_b - C_{c,0})/(C_b - C_c)$ . Therefore, in the plotting of logarithm of the dimensionless concentration against time, only the measurements in the early stages - the first seven minutes - are used for regression analysis. The plotting shows a good straight line (Figure 5.6). The slope of the line  $k$  is  $1/120 \text{ s}^{-1}$ . Then according to Equation (A.8), the air exchange rate  $v/V_R$  will be  $k(V_c/V_R)/(1+V_c/V_R) = 4.8 \text{ ach (or 1/hour)}$ .

This amount is considerably high, and its effect certainly should not be overlooked. The difficult point is that this quantity is always related to the specific geometries. For example, for office buildings at night, the thermal load in the room are absent or becomes inactive. Meanwhile, the night cooling effect through window or ventilation may make the room have a lower temperature than the cavity. In that case, a stable temperature stratification may exist. Therefore little convection between the cavity and the room will occur even if with sufficient opening areas. Obviously, a variable  $v/V_R$  will be necessary for the program to simulate this dynamic behavior. The opening area ratio is certainly an very important factor. In fact, a lot of work has been done related to the ordinary lowered ceiling openings. One special issue that has been investigated is the minimum opening area ratio required to allow effective air convection so that heat can be stored in the ceiling concrete slabs (Peutz & Associés 1986, 1988). The intention of the present measurement is just to identify the significance of the issue regarding cool ceiling installations. To make the program ACCURACY be able to handle large range variations, CFD simulation will be used. The measurements mentioned above will serve to validate the feasibility of using CFD approaches to estimate the value of  $v/V_R$ .

### 5.3.3 Thermal Dynamic Responses of the Room

Equilibrium steady state of the room was first achieved by closing the door for two days, without any internal heat sources. Theoretically, a uniform temperature should be obtained since the whole envelope of the room is insulated externally. However, small temperature differences still exist between the cavity air and the room air (Figure 5.7 a). This indicates that the heat loss through the insulated envelopes still needs to be taken into account. A step-up heating is realised by switching on three lamp-bulb boxes of 150 watts. After 48

hours, the cooled ceiling is suddenly switched on respectively with water or air which has a controlled constant inlet temperature and flow rate. During these three processes, all the surface temperatures inside the room, ceiling panel surface temperatures, air temperatures in the mid-plane of the room and cavity, as well as the inlet and outlet temperatures of the water or air are measured and recorded in a data file. Some of the measured data are plotted in Figure 5.7 and Figure 5.8. For comparison purposes, different temperatures are plotted in one chart. The respective temperatures are averages of a number of thermocouples at several points.

Let us first analyze the step-up heating processes. If we look at Figure 5.7 a and Figure 5.8 a closely, we can see that the room air temperature is higher than the cavity air temperature during the heating up process, although the initial room air temperature is lower than the initial cavity air temperature. This demonstrates the barrier effect of the ceilings, probably due to both convective and radiative effect. The floor surface temperature is much lower than the room air and wall surface temperatures, which demonstrates the heat storage effect of heavy envelope materials(Figure 5.8 c). In the other test when the floor was covered with planks of wood, with an air cavity in between, the floor surface (wooden board surface) temperature has much quicker response(Figure 5.8b) to the step-up heating, which indicates that, in practice, the thermal storage capabilities of heavy concrete floors will be very much hindered by the presence of any similar light floor decoration materials.

For the air-cooled ceiling panel system, we tried to achieve a step-down cooling by suddenly switching on the air fans. Before switching-on the air fan, the cooling coil in the air handling unit was cooled in advance with the air fan off, but the air duct remains at a higher temperature. For this reason, the air was heated-up by the duct before reaching the air panels, and therefore a real step-down cooling is difficult to achieve. After about 4 hours, the supplied air temperature into the air panels reaches the set point - about 14°C (Figure 5.7b). The average air panel surface temperature is about 2 K lower the average room air temperature. This indicates the capability of air panels, i.e., the air panel will also absorb heat by radiation. The heat extraction by the ventilation air is illustrated in Figure 5.7 e. The total heat extraction is calculated using the temperature difference between the air into the panel and the temperature in the exhaust duct close to the light fittings(see Figure 5.9), i.e.,

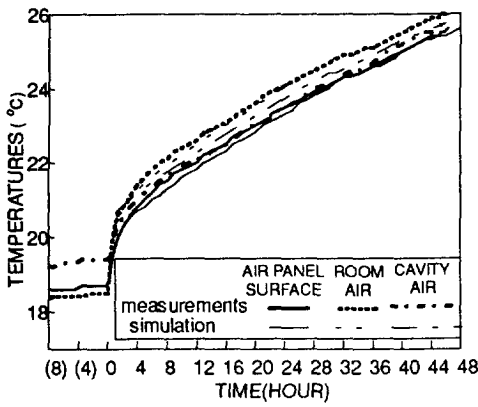
$$Q_{\text{ext}} = v\rho C_p(T_e - T_{s,i}) \quad (5.6)$$

Plotted in the same figure(Figure 5.7 e), is the heat extraction over the air panels. This amount of heat is calculated from the temperature differences between the air into the panel and the air leaving the panel at the air diffuser(Figure 5.9), i.e.,

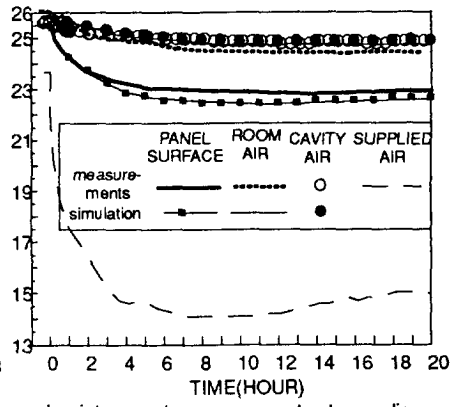
$$Q_p = v\rho C_p(T_{s,o} - T_{s,i}) \quad (5.7)$$

As shown in Figure 7.7e, the total heat extraction is about 50 watts higher than the panel heat extraction. However, since the exhaust air is cooled down by the air panels in

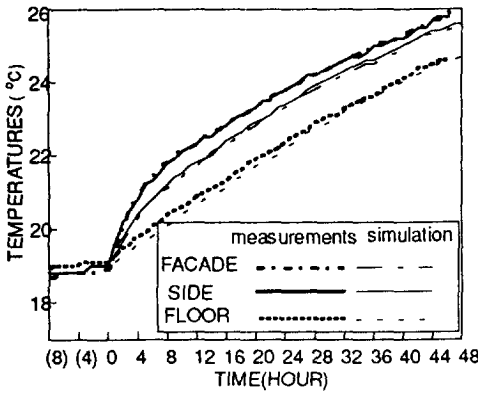




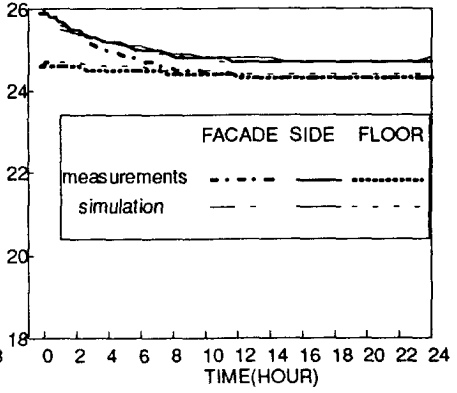
a. air temperature responses to step-heating



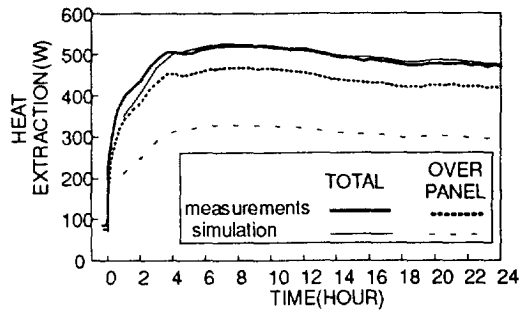
b. air temperature responses to step cooling



c. wall temperature responses to step heating

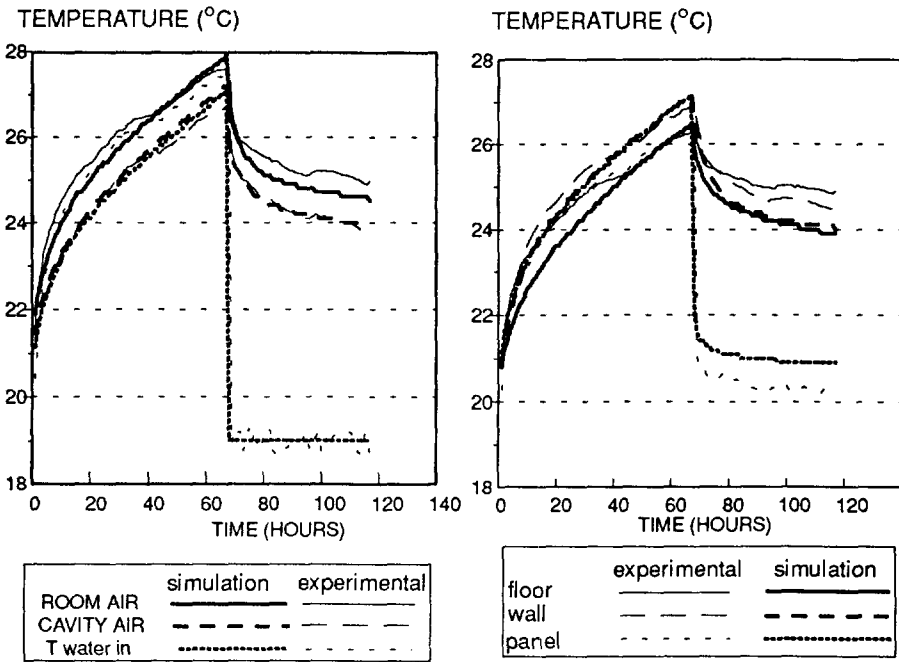


d. wall temperature responses to step cooling



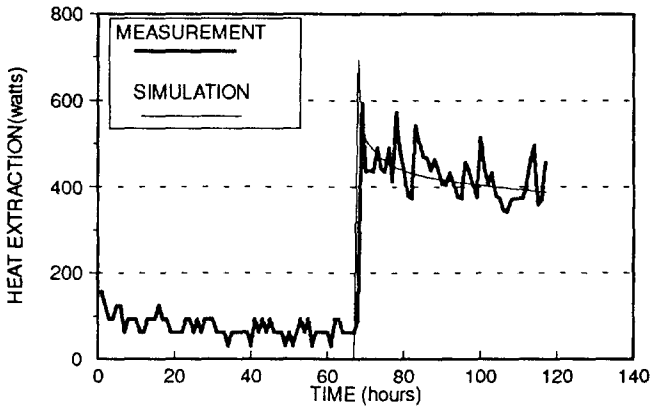
e. heat extraction by the ventilation air

Figure 5.7 Comparisons of experimental and simulated thermal dynamic responses of a room with air-ceiling system (air supply rate = 2.5 ach)



a. volume air temperatures

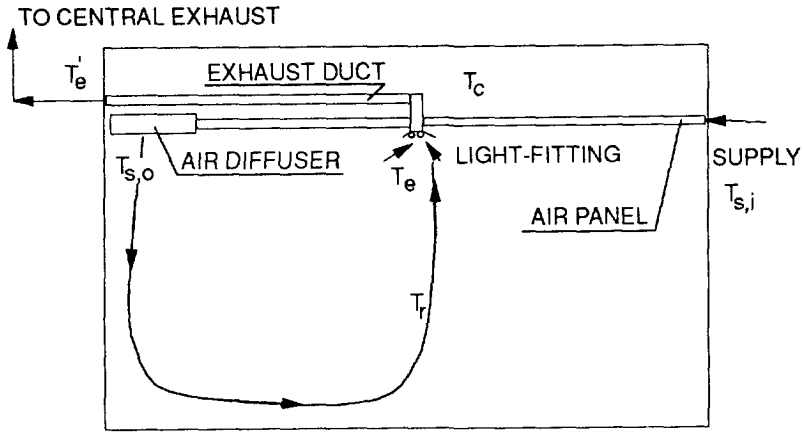
b. inside surface temperatures



c. heat extraction by cooled water

Figure 5.8 Comparison of experimental and simulated thermal dynamic responses of the room with water-ceiling system

the exhaust duct between the light-fittings and the main exit on the rear wall, the air temperature leaving the air exit on the rear wall  $T_e'$  became lower than  $T_e$ . Therefore, the actual total heat extraction of the test case was lower, and in fact, it was almost equal to the heat absorptions by the panel. In practice, this means lowered heat extraction effectiveness of the cooling system. It seems that the exhaust duct should be insulated in practice.



$$T_{s,i} < T_{s,o} < T_r < T_e, \text{ but } T_e' < T_e$$

Figure 5.9 Flow route of the ventilation air in a room with air-ceiling panels

For the water system, no air is supplied in the test. The step-down cooling effect is rather drastic. When the valve is open, the chilled water/glycol flows through the panels with a temperature of 19°C (Figure 5.8 a), and undergoes a temperature rise of nearly 1 K. Consequently the average panel surface is only about 1.2 K higher than the supplied water temperature(Figure 5.8 b). The supplied water temperature fluctuation is due to the on-off control of the compressors, and correspondingly the heat extraction by the ceiling panels also has some fluctuations(Figure 5.8 c). However, this fluctuation does not cause any considerable fluctuations of the panel surface temperature, and nor of the room air temperature.

#### 5.4 SIMULATION OF THE THERMAL RESPONSES BY ACCURACY

Using the measured temperatures as the initial condition and the supplied air or water temperature and the monitored outdoor temperature as input boundary conditions, the air and all inside surface temperatures and the heat extraction are calculated by the program ACCURACY. Since the air temperature is not a real step-down one, the measured data at each hour have been used, whereas the supplied water temperature is taken as constant

19°C, excluding the fluctuations. The simulation results are plotted in the corresponding charts for the measurements (Figure 7 and Figure 8). It can be seen that the overall agreement between measurements and simulation are reasonable.

In the simulation, constant convective heat transfer coefficients are used. It is assumed that  $\alpha_c = 3.5 \text{ W/m}^2 \text{ K}$  for all the wall surfaces, and  $\alpha_c = 4.5 \text{ W/m}^2 \text{ K}$  for the cooled panel surface facing the room and  $\alpha_c = 3.5 \text{ W/m}^2 \text{ K}$  for the cooled panel surface facing the cavity. Also a constant value for  $v_{r,c}$  is used for the whole simulation period. Different values of  $v_{r,c}$  are tested and indeed the air-exchange rate has rather large influence on the simulated energy as well as the air temperatures. Lower values over-predict the temperature difference between the room and cavity, and vice versa. The results plotted in Fig.5.7 and 5.8 are obtained at the value  $v_{r,c} = 10 \text{ ach}$ , which is higher the value 4.8 ach, found in the tracer gas measurements. Closer look at the plotting, especially in Figure 6.8 a, indicates that the room air temperature is under-predicted and the cavity air temperature is over-predicted by the present simulation. The overall simulation of the heat extraction by the water panels corresponds very well with the measurements, disregarding the frequent fluctuations.

It is worthwhile to have a special look at Figure 5.7e, in which the heat extractions of air-panel are compared. The total heat extraction by ventilation air is in good agreement, by assuming that the air is extracted from the room space via the light-fittings, and that the heat loss through the exhaust duct is distributed into the cavity air convectively. But the heat extraction over the panel is very much under-predicted, i.e., the temperature of the ventilation air entering the room is under-predicted. This should be attributed to the heat losses by the exhaust air duct to the ceiling panels in the test room. Probably, a larger portion of this heat should go to the ceiling panels(Figure 5.9). Moreover, the vertical temperature gradient that exists in the room is not taken into account in the present simulation. These two factors certainly will improve the agreement if taken into account. However, no efforts were made to adjust these parameters in the simulation to make the agreement perfect because the program is devoted to insulated exhaust-duct situations.

This comparison validates the feasibility of the program ACCURACY for the simulation of the thermal behaviours for rooms with cooled ceiling systems. Especially the energy extraction can be simulated at rather high precision for both the air-ceiling and water ceiling systems. Some discrepancies may be attributed to the specific situations in the climate room. The measured parameters concerning convection, such as the surface convective heat transfer coefficients and the air exchanges, can be used in the simulation program. As already mentioned in Chapter 4, local temperatures will be calculated through special air flow simulation, and this method is tested previously by Chen and Kooi(1988). Therefore, the next section explores the possibility of using CFD approach to predict the air exchanges through the ceiling gaps.

## 5.5 CFD PREDICTION OF THE INTER-ZONAL AIR EXCHANGES

The comparison between the simulation of ACCURACY and measurements indicates that reasonable simulation of the thermal dynamic behaviour can be achieved with reliable data about the surface convective heat transfer and the inter-zonal air exchange.

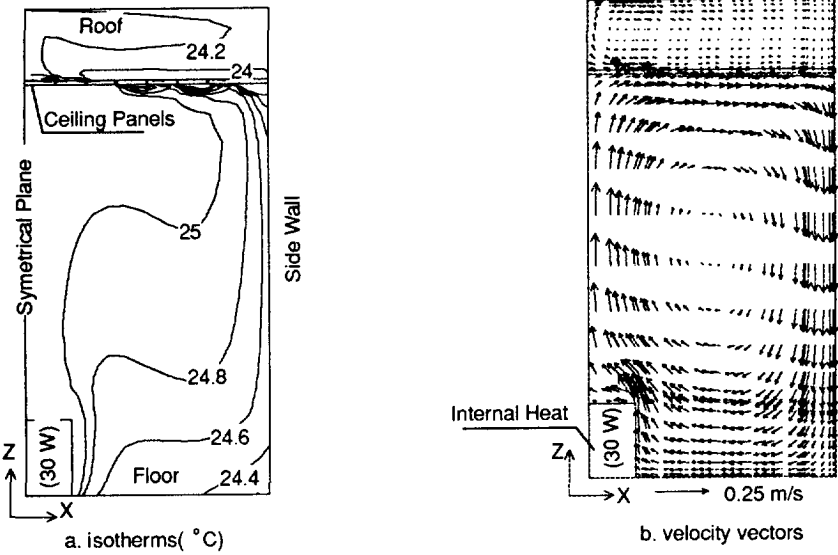


Figure 5.10 Simulated temperature distribution and air flow pattern in the room and cavity (The surface temperature of the ceiling panels is 20.4 °C, and wall surface temperature is 25.2 °C in the room, and 24 °C in the cavity)

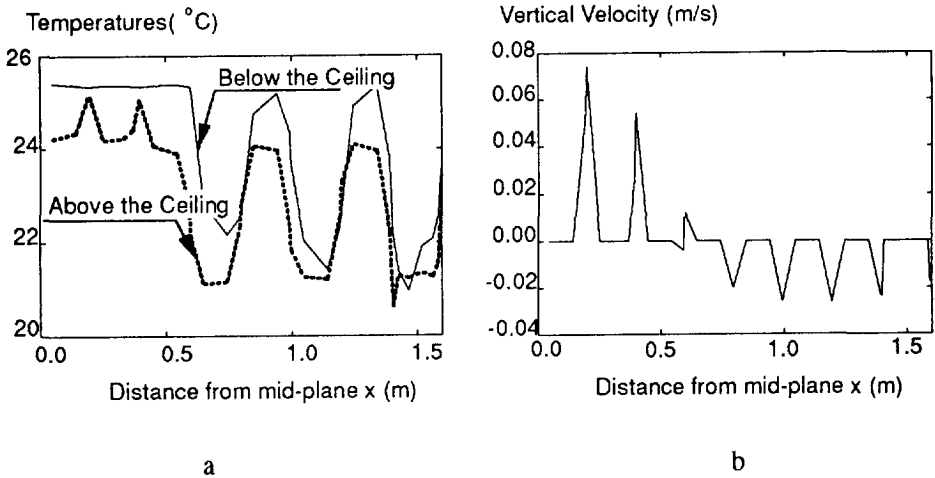


Figure 5.11 Plotting of the simulated air temperatures immediately below and above the ceiling (subfigure a) and air velocities through the gaps (subfigure b)

In the simulation mentioned above, these data are obtained through experimental measurements.

However, the air exchange rate is influenced by many factors in reality, such as the different area ratios of gaps to panels and panels to total ceiling area, location of the ceiling panels in relation to the internal heat sources. The data obtained in the measurements may not be directly used for simulation of different situations. To enable the program to cater for various possibilities, more data about the inter-zonal air exchange will be required to obtain a general purpose correlation.

Therefore, we resort to the CFD approaches to calculate the inter-zonal air exchanges. As already described in Chapter 2, the CFD still remains to be an art rather than science. Looking into the physical process of the convection, heat sources are located below a cooling surface. This is typical of an unstable flow situation. Consequently, the air flow through the gaps may be in a haphazard oscillating way. It will be time- and expertise-demanding to fully understand this phenomenon alone. Therefore, for our practical purposes, we resort to the statistical approach. The  $k-\epsilon$  turbulence model will be used. While any possible oscillating behaviors can not be really revealed by this model, the mean flow field will be obtained.

As a test case, the wall surface temperatures and the internal convection heat source measured at one steady state are used as the boundary conditions of the CFD calculation. The room geometry is simplified into 2-dimension case. Using the standard  $k-\epsilon$  turbulence model that is built into the computer program PHOENICS, the air flow and temperature distributions in the room and cavity are calculated simultaneously. A good converged solution is obtained. The results are presented in graphical form in Figure 5.10. The simulated average room air temperature and cavity air temperature are in good agreement with the measurements. Particularly, the vertical air velocities and air temperatures close to the ceiling surfaces are plotted against the width of the room(Fig.5.11). With this velocity distribution, the circulated flow rate through the gaps can be easily calculated. In this simulation, the flow rate is  $8 \text{ m}^3/\text{hr}$  per meter length, and 1.85 ach in terms of the air change rate of the room volume air, which is lower than the value 4.8 ach identified by tracer gas technique. Since only two nodal-points are located in the ceiling gaps, the grid-spacing might be not fine enough to account for the sharp air temperature gradients around the ceiling panels. To improve the simulation accuracy, grid-refinement will be necessary. Since the gaps are no more than several millimeters thick, more computing time will be required. After all, it could be expected that the agreement can be much improved by 3-dimensional simulation with grid-refinement around the gaps.

The advantage of the CFD simulation lies in its flexibility in simulating various possibilities. For a specific case, correlations between the air exchange rate and the room-cavity air temperature difference can be obtained using the CFD results. Then this correlation can be used in the program ACCURACY. Therefore, a special subroutine is provided in the program ACCURACY. A series of CFD simulations can be performed for a specific room configuration, the correlations can then be built into the subroutine. Then the program will search for the proper correlations as required, e.g., when the internal heat sources are absent during the night and the room temperature becomes lower than the cavity temperature, smaller  $V_{r,c}$  value will be used at that moment. Therefore, instead building a universal correlation into the program(which is virtually impossible), we build

a structure in the program, which makes the program to be able to cater for various possibilities.

## **5.6 CONCLUSIONS**

1. The validation of the enhanced simulation program ACCURACY shows that it can give a good prediction of the thermal dynamic behaviour and cooling load of a room with cooled ceiling systems. This validates the feasibility of the fundamental modelling techniques as well as the numerical algorithms.

2. Parameters concerning the surface convection and inter-zonal air-exchange processes are highlighted in this validation. The parametrical study indicates the importance of the proper calculation of the inter-zonal air-exchanges for the cooled-ceiling-system cooling load calculation purpose.

3. The CFD approach of establishing the correlation between the air exchange rate and the room-cavity air exchange is tested and found to be feasible, although errors can be expected. This approach will enable the program ACCURACY to simulate different ceiling panel constructions with changeable thermal conditions.

## CHAPTER 6

# THERMAL COMFORT AND INDOOR CONTAMINANT DISTRIBUTIONS WITH COOLED CEILING SYSTEMS

### 6.1 INTRODUCTION

In the previous chapters, mathematical modelling techniques of the air flow and building thermal performance simulation are introduced and experimentally evaluated. Now it is time to apply these modelling techniques to investigate the engineering problems. As the title implies, this chapter will deal with the issue of thermal comfort and ventilation effectiveness. Particularly, the purpose is to evaluate the performances of cooled-ceiling systems in comparison with mixed ventilation systems or displacement ventilation systems.

This chapter will first give a brief review of the thermal comfort and ventilation performance indices that are developed and accepted in HVAC practices in recent years, since they are fundamental for system comparisons. Also different ventilation systems such as mixed ventilation and displacement ventilation will be discussed, in parallel with ventilation effectiveness. Then this chapter will present the air flow, thermal comfort and contaminant distribution measurements in our test room with the air-ceiling systems. The measurements are used to validate CFD simulation of the same system. As the main contents of this chapter, the combined use of CFD and thermal process simulation will be presented.

### 6.2 THERMAL COMFORT INDICES

The thermal sensation index PMV is already mentioned in Chapter 4. In fact, in cooling load calculation or energy estimate procedures, it is underlined that a homogeneous thermal comfort exists in the room space. However, this uniformity very much depends on the system installation, such as the locations of the heating or cooling elements and air supply location, as well as the operation conditions. Therefore it is necessary to investigate the distributions of the air flow velocity, temperatures as well as the turbulence in the occupied zone of a room, so that the local discomfort could be avoided by proper design of the system and operation parameters. Many experimental



investigations on the draft effect, which is the undesired local cooling of the human body by air movement, have been done in the last two decades (Jones *et al.* 1986; Fanger and Christensen 1986; MacIntyre 1979). A mathematical model is developed to quantify the draft risk by Fanger *et al.* 1988). In this model, the percentage dissatisfied people due to draft, PD(%), is calculated from

$$PD = (34 - T_a)(V - 0.05)^{0.62}(3.14 + 0.37V \cdot I) \quad (6.1)$$

for  $V < 0.05$  m/s insert  $V = 0.05$  m/s, and for  $PD > 100$  let  $PD = 100$ , where  $T_a$  is the local air temperature(°C),  $V$  is the mean velocity(m/s), and  $I$  is the turbulence intensity(%), which is the velocity fluctuation over the mean velocity. The turbulent intensity can be calculated from

$$I = \frac{100(2k)^{0.5}}{V} \quad (6.2)$$

where,  $k$  is the turbulent kinetic energy(J/kg) of the air flow.

The  $T_a$ ,  $V$  and  $k$  can be obtained from measurements or air flow simulation, and therefore, the PD distribution can be calculated. Equation(6.1) is the regression for the sense of draft at the head level. It is noted that when the equation is used to estimate the draft risks at the foot/ankle level, the calculated PD will be 5% higher than the real value. Therefore, the draft risk at foot/ankle level should be corrected with the formula

$$PD_{foot} = PD(Eq.6.1) - 5 \% \quad (6.1a)$$

In most cases in buildings, the air temperature normally increases with height above the floor. If the gradient is sufficiently large, local warm discomfort can occur at the head, and/or cold discomfort can occur at the feet, although the body as a whole is thermally 'neutral'. The few experimental investigations that have been conducted to examine the influence of the vertical temperature difference on human comfort, are reviewed in ASHRAE handbook(1989). It was found that people are more sensitive to the positive temperature difference - higher above and lower below, and less sensitive to the negative vertical temperature differences. In the research conducted by Olesen *et al.*(1979), seated subjects in their preferred average temperatures were subjected to the vertical temperature differences of different magnitude. It was found that, when the temperature difference is larger than 3°C between head(1.1 m above the floor) and ankles(0.1 m above the floor), the percentage dissatisfied people increases drastically. In the ISO standard(1984), it is recommended that this vertical temperature difference be less than 3°C.

In the present study, Eq.(6.1) will be used to evaluate the draft risks. Since this PD index does not take into account the influence of the temperature stratification, the overall thermal comfort will also be analyzed from the temperature stratifications.

### 6.3 VENTILATION EFFECTIVENESS

Besides the comfort requirements, indoor air quality is another important aspect of indoor environment. Many research results have shown that indoor air quality has very much influence on the productivity and the health of human inhabitants. In the modern society, more and more people are spending their time indoors. Therefore, indoor air qualities in residences, offices and other nonindustrial indoor environments have become an issue of increasing concern. Many investigations show that indoor pollutants are normally at higher concentrations than their outdoor counterparts(ASHRAE 1985). While efforts are being made to identify and to eliminate the indoor contaminant sources whenever possible, ventilation is usually considered to be the engineering solution to improve indoor air quality. Outdoor air is introduced into the room, conditioned or in its ambient state through natural or mechanical ways, to remove the contaminant and odorous substances from the indoor environment. On the other hand, ventilation may cost energy in several ways. First, in a mechanical ventilation system, an air fan consumes electricity in its operation. Secondly, except in the free-cooling seasons during which the temperature of the outdoor air is appropriate for building cooling without any conditioning, energy will be required for the conditioning of the outdoor air, or alternatively energy losses will occur in the heating season when cold air is introduced into the room while hot air is driven out of the room. While heat recovery devices can be installed to reduce this energy loss, it is not always cost-effective. Therefore, the potential of energy saving in ventilation comprises the reduction of the amount of air supplied and the simultaneous adoption of the best strategies for supplying this quantity of air to achieve the maximum ventilation performance in the occupied zone. After last few years study on ventilation performances, quite a few indices are developed to quantify the ventilation effectiveness of various ventilation systems(Skarret and Mathisen 1981; Sandberg 1982). Here, one definition of the ventilation effectiveness is introduced(EC, 1992). The ventilation effectiveness  $\epsilon_v$  is defined as the relation between the pollutant concentration in the exhaust( $C_e$ ) and in the breathing zone( $C_i$ ) according to the formula

$$\epsilon_v = \frac{C_e}{C_i} \quad (6.3)$$

According to this definition, a good ventilation system will have a ventilation effectiveness greater than one while a poor ventilation system will have a ventilation effectiveness less than one.

In practice, there are so-called mixed-ventilation and displacement ventilation systems. The idea of mixed-ventilation is to make the supplied air well mixed in the space so that indoor contaminants are diluted in the breathing zone of the occupants. This idea is often realized by locating the air inlet and exhaust near the ceiling. The idea of displacement ventilation is to make the fresh air reach the occupants directly while the pollutants are carefully swept away, i.e., a condition of "plug flow" is created in a room. This idea is often realized by locating the air inlet near the floor and the exhaust near the ceiling. The ventilation effectiveness is about one for mixed-ventilation

systems and greater than one for displacement ventilation systems. The ventilation effectiveness becomes less than one if "short circuit" occurs in the air flow path, i.e., if supplied air goes to the exhaust directly without carrying away any pollutants. Therefore, the  $\epsilon$ , defined by Eq.(6.3) is generally an effective index to quantify the performances of various ventilation systems.

In recent years, displacement ventilation got popular due to its relatively high ventilation effectiveness (Skarret 1989), especially in Scandinavia countries. However, this system has its capacity limit due to thermal comfort requirement, as was found in many previous experimental investigations (Sandberg and Blomqvist 1989). When the supplied air temperature is too low, as required at higher cooling loads, a too large temperature gradient in the vertical direction will be created and this causes complaints of discomfort. Therefore, it is still significant to find alternative air-conditioning systems that have both high cooling capacity and high ventilation effectiveness.

Currently, various cooled ceiling techniques are emerging in the European market, which provides an air-conditioning alternative (Mertz 1992; Wilkins and Kosonen 1992). Still, this chapter will consider the horizontal type. The horizontal plate type design may be combined with various ventilation systems. Especially, the ceiling panels can function as air ducts, through which cold ventilation air is preheated before entering the room through an air diffuser. The cooled ceiling system will impose some unique characteristics in a room. With water ceiling system, air is supplied mainly for ventilation purposes. With ceiling air system, ventilation air can be supplied at lower temperatures, so that a smaller volume of air supply will be required. These characteristics have influence not only on the indoor thermal comfort and air quality but also on the whole system configuration and energy consumption.

In this chapter, the thermal comfort, such as risks of draft, vertical temperature stratification, and ventilation effectiveness and odour distributions in a room will be investigated. This will be done by performing numerical simulation of three representative cases. However, measurements are conducted first to provide information about the cooling capacities of the cooled ceiling panels. Also, the measured field values of temperature, tracer gas distribution and local velocities will serve to evaluate the validity of CFD simulations.

#### **6.4 MEASUREMENTS WITH AIR-PANEL COOLED-CEILING SYSTEM**

The experimental system and instrumentation is already described in Chapter 5. The main operation parameters for the measurements are given in Table 6.1. The ventilation rate is about 2.4 ach, or 1.77 l/s per m<sup>2</sup> floor area, which is typical of practical values in European design (Christopher, 1992).

The cooled air is supplied at 14.7°C and is heated up to 22.3°C within the ceiling panel, which is close to the air temperature at the height of 1.2 meters above the floor, and about 1.5°C lower than the room air temperature near the ceiling, but half degree higher than the floor temperature.

Table 6.1 Measurements conditions of the air ceiling systems

Cooled Panel Area	Ventilation Rate	Air Temperatures			Heat Extraction Rate	
		T <sub>s,i</sub>	T <sub>s,o</sub>	Text	(watts)	W/m <sup>2</sup>
(%)	(ach)	(°C)	(°C)	(°C)	(watts)	W/m <sup>2</sup>
30	2.4	14.7	22.3	23.7	295	20

Again, the air temperatures in the mid-plane of the room are measured and plotted against the height above the floor(Figure 6.1). It seems that the vertical temperature gradients are rather small. The temperature difference  $\Delta T_{0.1-1.1}$  is about 1.5 °C. Even though, the vertical temperature gradients shows its effect by the fact that the ventilation air through the panel is heated to a higher temperature than that in the occupied zone.

The air flow is visualised using smoke(Figure 6.2). It appears that the air leaving the air diffusers goes to the floor and subsequently spreads and penetrates into the whole floor areas. Then the air goes up in a very slow and unclear motion. Later recirculation of this air flow could not be seen in the visualisation as the smokes are dispersed uniformly in the room.

Using a Brüel & Kjær thermal-comfort meter, the air velocities and temperatures are measured in the region below the air diffuser at two height levels, respectively 0.10 m and 1.1 meters above the floor, and subsequently the turbulent quantities and draft risks are calculated. These results are presented in Figure 6.3a and b, and Figure 6.4a and b. For the velocity measurements, the results are not so consistent due to measurements errors at low velocity. Also manual positioning of the probes during measurements might have added some disturbances to the steady state, and thus adding some random errors. Especially, the flow direction changes very much below the air diffusers, which may give some extra errors - lower biased readings might have been obtained when the probe and flow direction meet at certain angles. Moreover, given the large size of the probe, errors will also be introduced due to large velocity gradients and temperature gradients in this region. Nevertheless, the results still indicate that the supplied air jet is accelerated due to buoyancy effect. The air velocity leaving the outlet is about 0.06 m/s, and reaches about 0.1 m/s near the floor. This acceleration is unfavourable from the point of view of avoiding draft near the floor.

The turbulent kinetic energies range around the order of  $10^4$  J/kg (Figure 6.3a and Figure 6.4a), and the corresponding turbulent intensity  $I$  ranges from 30% to 60%(Figure 6.3b and Figure 6.4b). These values are in close agreement with those found by other researchers in air-conditioned building spaces[Hanzawa *et al.* 1987]. The air temperatures measured simultaneously with the velocities are rather uniform in the two horizontal planes, while there exists an average difference of about 1.5 K between the two planes(Figure 6.3a and Figure 6.4a).

Based on these measurements, draft risks are estimated in terms of PD quantified by Eq.(6.1). The results are also illustrated in Figure 6.3a and Figure 6.4a. It

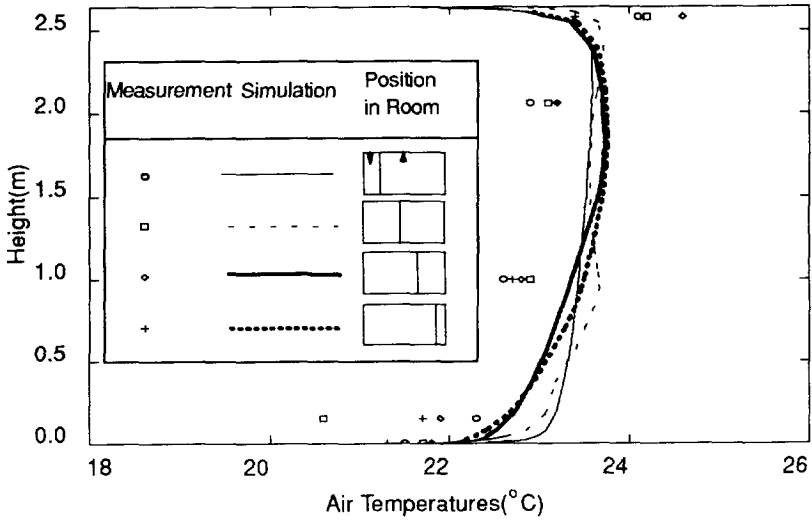


Figure 6.1 Measured and simulated vertical temperature variations in the test room

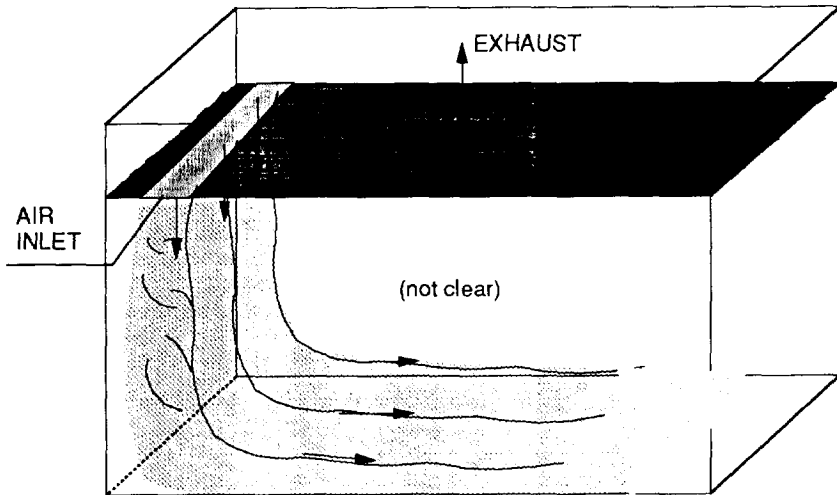
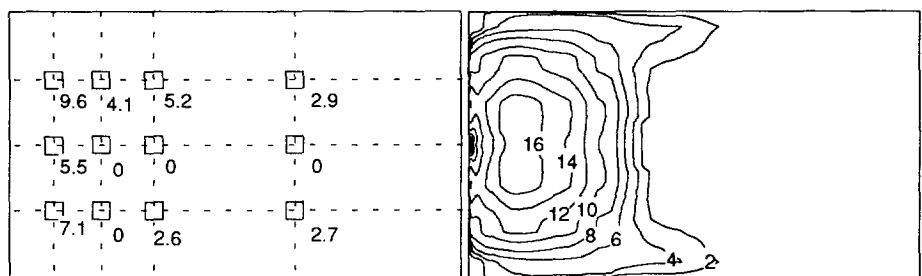
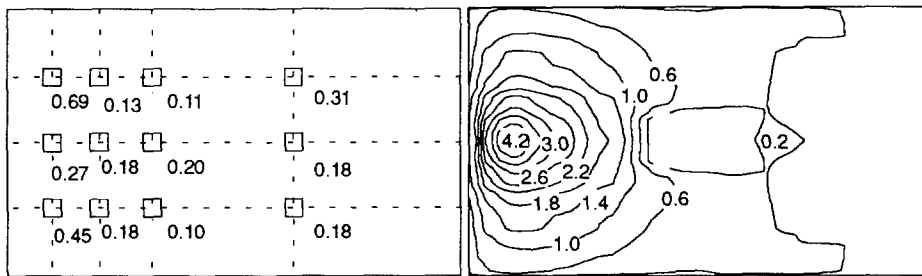
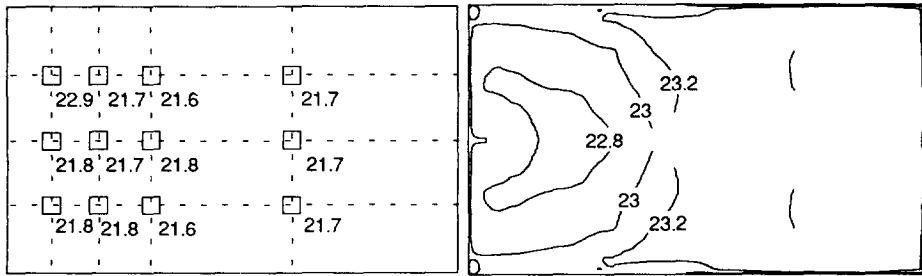
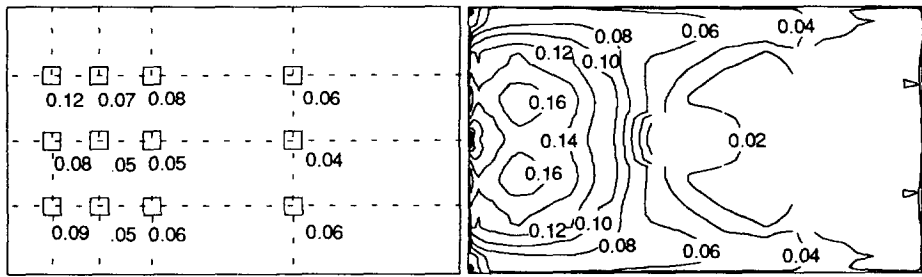


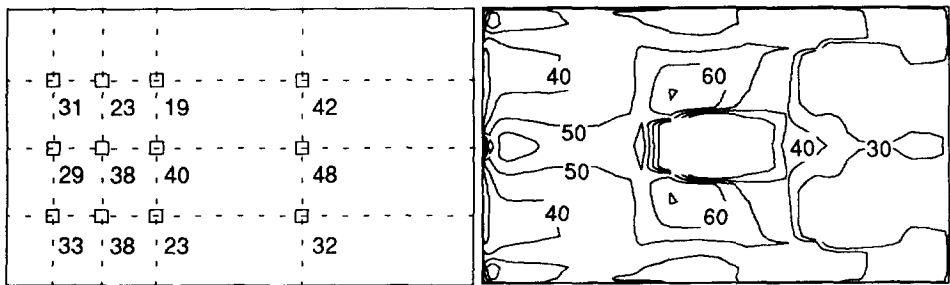
Figure 6.2 Visualized flow of the supplied air by smoke



MEASUREMENTS

SIMULATION

Figure 6.3a Measured and simulated air flow distribution and draft risks(PD) in the horizontal plane of 10 cm above the floor



turbulence intensity(in %)

MEASUREMENTS

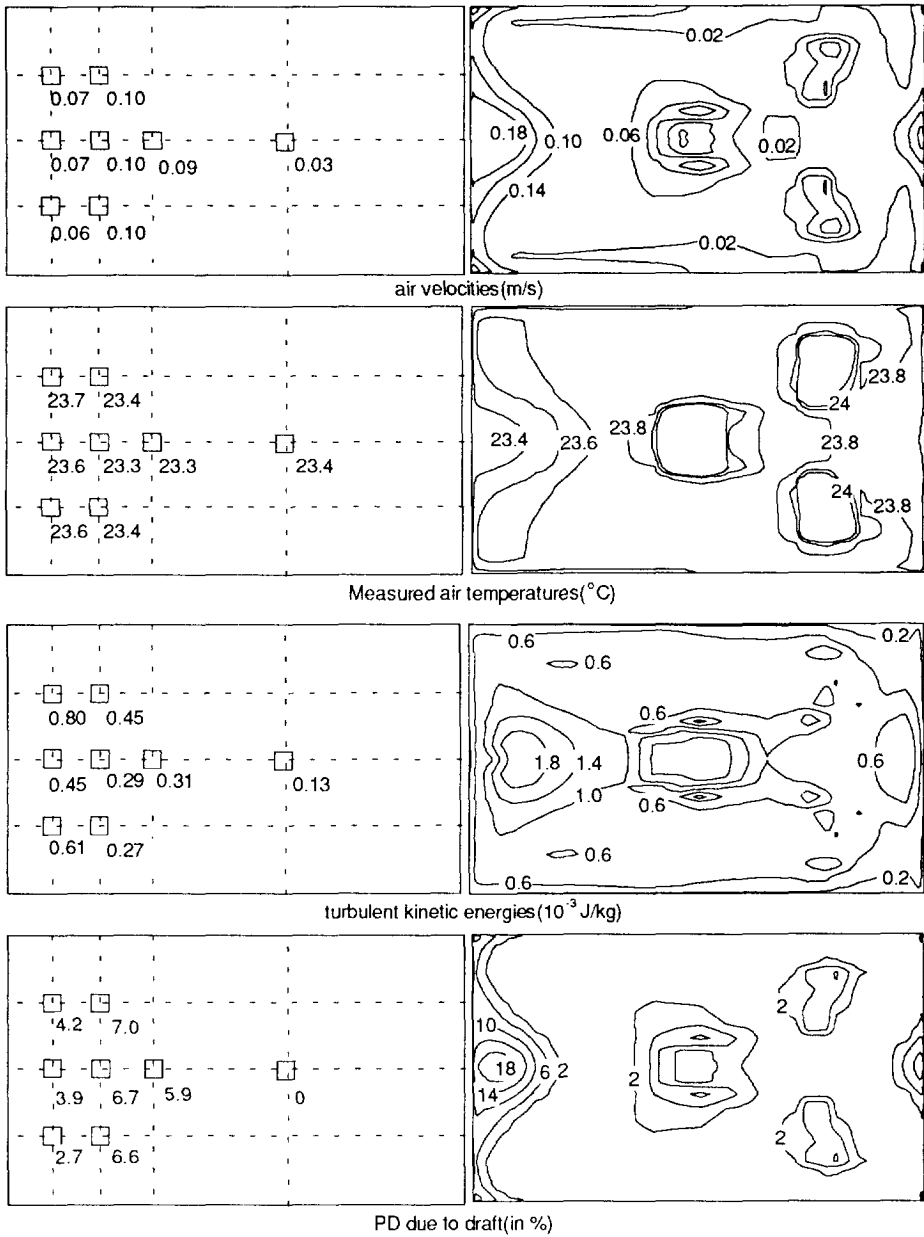
SIMULATION

Figure 6.3b Measured and simulated turbulence intensity distributions in the horizontal plane 10 cm above the floor

appears that the draft risks are very small in this test room, with the maximum PD of about 10% occurred below the diffuser near the floor. Subjective judgement by several people gave the same indications.

The tracer gas distribution is obtained from steady state measurements(Figure 6.5). A constant, known flow rate of tracer gas SF<sub>6</sub> (Sulphur Hex-Fluoride) is supplied continuously into the lamp-box and subsequently convected into the room air at the height about 1 meter above the floor. This tracer gas is supposed to simulate the odorous substances from human breathing although exact similarities are difficult to achieve. The measurements indicate a rather uniform vertical distribution, which may be attributed to the entrainment of the downward air supply. In terms of ventilation effectiveness, a value of higher than one is expected, which indicates that no short circuit of the air flow occurs in the room with the ceiling supply and ceiling extract configuration.

In summary, the air at a normal ventilation rate can be supplied at low temperature, 14.7°C in this test, and subsequently heated via the special ceiling panels to 1°C within the room average temperature. The supplied air then enters the room space through the ceiling low velocity diffuser and is accelerated and goes down to the floor and causes little draft near the floor. In this process, it appears that entrainment already occurs so that this air reaching the floor is already mixed with some old air in the room so that no clear concentration stratification is detected in the room. In this measurement, the cooling load is about 20 Watts/m<sup>2</sup>. For higher load situations, the comfort will be investigated by simulation technique.



MEASUREMENTS

SIMULATION

Figure 6.4a Measured and simulated air flow distribution and draft risks(PD) in the horizontal plane of **1 meter** above the floor



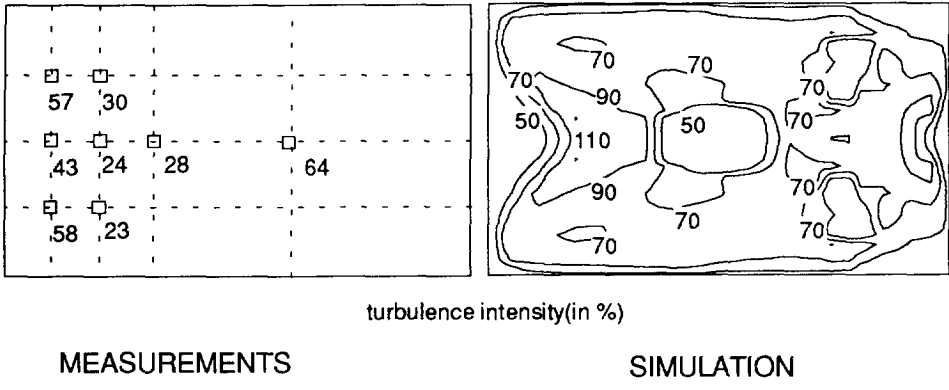


Figure 6.4b Measured and simulated turbulence intensities in the horizontal plane of 1 meter above the floor

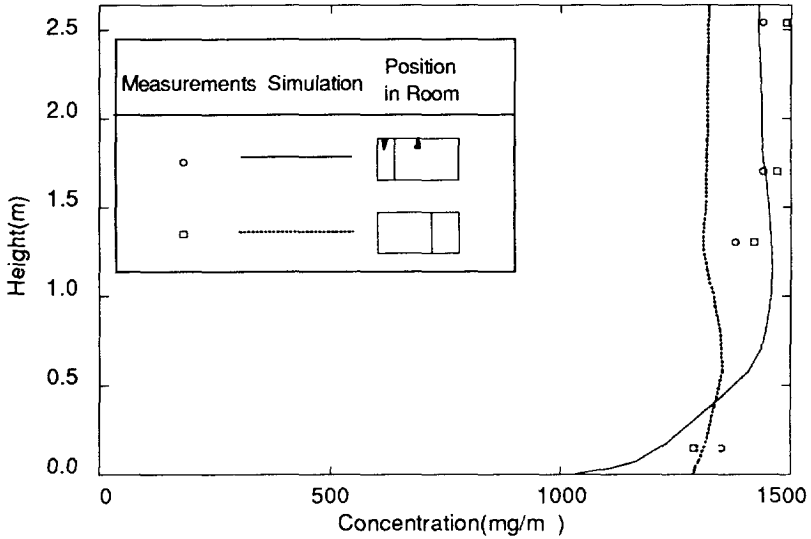


Figure 6.5 Measured and simulated tracer-gas concentration variations

## 6.5 EVALUATION OF CFD SIMULATION FOR AIR-CEILING SYSTEMS

To investigate higher load situations, CFD simulation in combination with ACCURACY simulation will be used. For an evaluation of the reliability and accuracy of the CFD simulation of the air flow parameters, a test case is first performed, which comprises using the measured supplied air temperature and wall temperatures and ceiling panel heat extraction as the input to calculate the distributions of the air flow, air temperature, turbulence intensity. The simulation results are to be compared with the field measurements mentioned above. The re-evaluation of the CFD simulation is necessary with following considerations:

1. As the present-state-of-the-art indicates, there are no general rules to control the errors caused by the empirical parameters contained in the  $k$ - $\epsilon$  turbulence model, as well as the numerical errors introduced in the discretisation procedure, such as the truncation errors, and the false-diffusions, etc.. These errors mix together in the simulation results, and the eventual magnitude varies from case to case.
2. The simulation is done with the standard  $k$ - $\epsilon$  turbulence model, using the optimized grid distance described in Chapter 3. However, the flow in the present situations will be characterised by mixed convection, the grid-optimization approach may still have some prediction errors.

Furthermore, some approximations in the numerical simulation have to be made to represent the complexities in rooms with cooled ceiling systems. The main approximations are:

1. The ceiling mounted air diffuser has a perforated-plate outlet, with a perforated area of about 50%. It will require too much storage and CPU time if we use fine finite-difference grids to approach the real geometry of the small holes. Therefore, an equivalent amount of momentum flux will be specified to model the inlet flow conditions. This allows us to use relatively coarse grids and avoids specification of the local outlet velocities and temperatures, as well as the turbulent quantities at each openings. This approach, reported by Chen and Jiang(1992), introduces some acceptable errors. The magnitude of this acceptable error for the low velocity diffuser needs evaluation.
2. Details about the turbulence quantities from the diffuser are not known. Practically, the correlations for calculating the turbulent kinetic energies  $k$  and its dissipation rate  $\epsilon$  from a fully-developed turbulent pipe-flow are used to approximate the average  $k$  and  $\epsilon$  from such an diffuser. Again, the errors that this approach may introduce needs evaluation.
3. As already described in the last chapter, air exchanges between the room air and cavity air occur through the between-panel gaps. It is necessary to take into account this convection when the comfort and contaminant distribution in the room space is investigated. As already shown in the last Chapter, this is possible by detailed modelling of the small gaps, but will require more computing CPU time. In the present simulation, this convection will be modelled by an equivalent convective heat sink or heat source attached to the ceiling panels. That is to say, the mass inflow and outflow through the gaps are

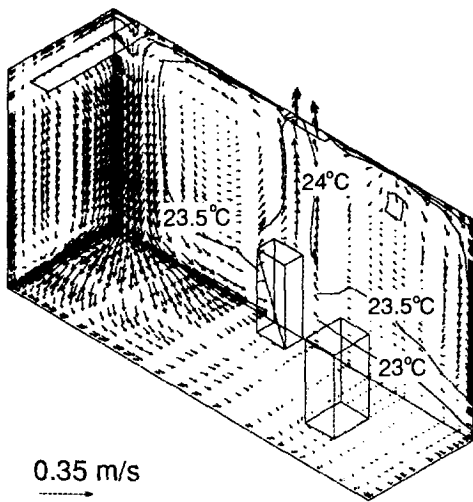
not calculated directly, while its convective effect on thermal balance is taken into account. For the situations where the exhaust duct is connected to the light-fittings, there is no net mass loss in the cavity. Therefore, this should be an reasonable approximation.

4. Taking advantage of the symmetry in geometry and thermal boundary conditions, simulation is performed only in the half of the room space.

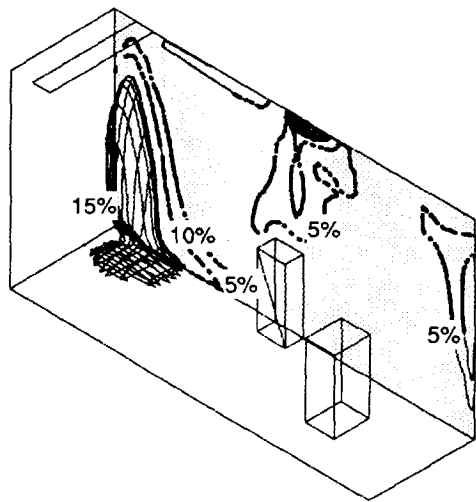
The simulated results are presented in 3-dimensional graphical form in Figure 6.6.a to 6.6.d. These figures give an overall perspective view of the flow patterns, temperature and tracer-gas distributions, as well as draft risks. Looking at Figure 6.6.a, the flow pattern indicated by the velocity vectors show good correspondence with the visualised flow pattern(Figure 6.2) in general. Some local recirculations below the ceiling diffuser calculated by the simulation were not exactly the same as observed in the experiment. The contours of temperature in the middle vertical plane(Figure 6.6.a) indicate little vertical temperature stratification, when the temperatures vs height are plotted in the same chart (Figure 6.1), the agreement between simulation and measurements is reasonable. Close to the ceiling, it appears that larger discrepancies exist. This may be attributed to the fact that, in the test room, the part of the ceiling above the mid-plane (the temperature measurement plane) is made of normal fibre-board, whereas in the simulation, the ceiling is assumed uniformly cooled with the total heat extraction rate remaining the same. This comparison indicates that this approximation method is acceptable if the flow parameters in the occupied zone are of the main interest. The PD values are calculated according to Equation (6.1). Illustrated in Figure 6.6.b is the region in which the PD is greater than 15%. The region lies below the diffuser and is very small. This high draft region is not observed in the measurements. Therefore, discrepancies between simulation and measurements about the draft risks are about 10% in terms of PD.

Simulation results are also plotted in contours in the two horizontal planes(Figure 6.3a and b, and Figure 6.4a and b), in which the above anemometry measurements have been done. Detailed comparison between the measured and simulated values in the two horizontal planes show that the predicted velocities are about 30 to 50% higher. The simulated air velocities contours indicate the decay of the supplied air jet along the floor. The comparison with the measurements shows discrepancies at the local points, which may be due to errors both in measurements and in the simulation. In general, the values of the simulated PD are about 5 to 10% higher than those obtained from the measurements. From the engineering point of view, the prediction does show that the draft risks are rather small, which agrees with the subjective judgements in the room.

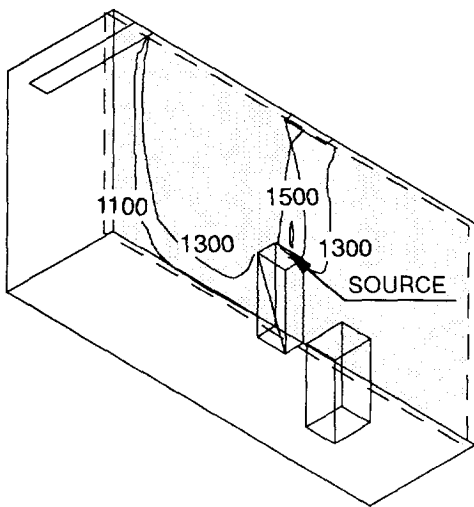
However, large discrepancies exist between measurements and simulations about the turbulence kinetic energy  $k$ (Figure 6.3a and Figure 6.4a). Especially in the region below the air diffuser near the floor(Figure 6.3a), the maximum difference is more than one order. In other regions, the agreements appear much better. This over-predicted  $k$  values are the main reasons of the over-predicted PD values. Although errors can be also expected in the measurements, these discrepancies may still indicate the  $k$ - $\epsilon$  model tends to over-predict the turbulence levels in room air flow situations.



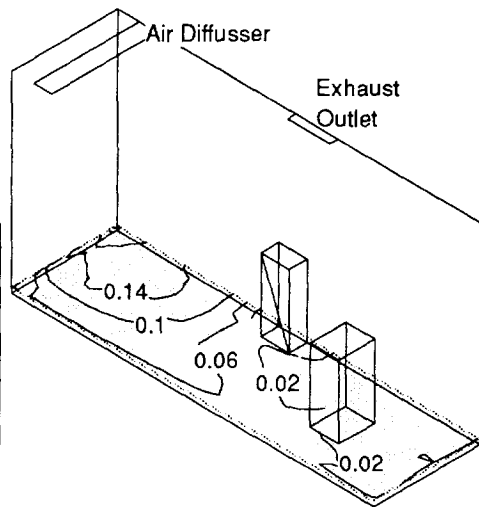
a. Velocity vectors, and isotherms in the vertical mid-plane



b. PD due to draft: Iso-surface of 15%, and contours(dotted lines) in the mid-plane



c. Contours of tracer-gas concentration ( $\text{mg}/\text{m}^3$ ) in the vertical plane



d. Contours of velocity magnitude(m/s) in the horizontal plane of 75 mm above the floor

Figure 6.6 Simulated field distributions of the test case: air supplied: 2.4 ach via air-type panels, other parameters are given in Table 6.1

As for the contaminant distribution simulation, the contours in the mid-plane indicate a uniform concentration distribution in the breathing zone(Figure 6.6c). When the vertical variations are plotted in the same chart(Figure 6.5) for the measurements, some discrepancies between simulation and measurements exist. In the measurements, the concentrations in the vertical line closer the air diffuser are generally lower than those in the vertical line in further away from the air diffuser. The measured data indicates a low but consistent vertical gradient, while the simulated results show a sharp gradient only near the floor closer to the ceiling diffuser. It appears that the emission source of the tracer-gas may not be well represented in the simulation. In the test room, the tracer-gas comes out from four openings on two sides of the lamp-box. In the simulation, it is assumed that the tracer-gas goes into the air uniformly from the box-side surfaces. Nevertheless, both simulation and measurement indicate that, with respect to the practical ventilation effectiveness, the vertical concentration stratification with this air-type cooled-ceiling system is insignificant. That is to say, the ventilation effectiveness can only be slightly higher than that of a mixed-ventilation system.

In summary, the overall comparisons between simulation and measurements indicate that the CFD simulation is reasonable as far as the practical values are concerned. However, some local discrepancies exist, especially about the turbulence quantities. The discrepancies have to be attributed to possible errors from both measurements and simulations. Bearing these discrepancies in mind, it may be concluded that when simulated values are used to interpret practical indications concerning thermal comfort and ventilation effectiveness, it should be used to investigate the relative influence tendencies of different system parameters, such as the supplied air velocity and temperature, and different configurations. It is based on this methodology that further investigations are performed by means of simulation(Niu and Kooi 1993, Niu and Kooi 1994).

## 6.6 NUMERICAL SIMULATION OF THREE COOLING SYSTEMS

Three typical air-conditioning systems are selected for investigations. They are a conventional displacement ventilation(DV) system, an air-type cooled-ceiling(ACC) system, and a water-type cooled ceiling system combined with displacement ventilation(CC + DV). The thermal load conditions for each case are chosen in such a way that they represent the practical situations to which they are expected to be applied. For example, a DV system is expected to be applied at thermal loads lower than  $40 \text{ W/m}^2$  floor area. Only for thermal loads higher than  $50 \text{ W/m}^2$  floor area, a cooled ceiling system will be applied.

The key point of indoor comfort study, whether it is experimental or numerical, is if the reality in terms of internal and external heat types(convective vs radiative) and their distributions are well represented in the model. As far as the ventilation effectiveness investigation is concerned, the location of the pollutant sources is rather important, e.g., it is important if the contaminants are from the occupants or other internal appliances, from the floor/carpet materials, or from the wall or even ceiling materials. It is these concerns that result in adopting the following seemingly-complicated investigation procedure, which is the combined simulation of building thermal dynamic behaviours and room air flows.

### 6.6.1 Dynamic Simulation of the Thermal Processes

We consider a room with a dimension of depth  $\times$  width  $\times$  height =  $5.1 \times 3.6 \times 2.64 \text{ m}^3$  and with 35% glazing area in the facade. Suppose that there are four occupants (each occupant generating a convective heat of 65 watts and radiant heat of 50 watts) (ASHRAE 1989). Heat gains also come from other internal heat sources in convective form. For the displacement ventilation, the convective heat is assumed to be 80 watts, generated by 4 small electrical appliances. For the cooled ceiling systems, this convective heat is assumed to be 340 watts, generated by 4 large electrical appliances. Heat gains will also come from the facade via radiation through the window and conduction through the walls. The question is how these heat gains will be distributed in a room with different cooling systems. This is also the question of how these heat gains will be converted into the cooling load, or the heat extractions from the room required for the cooling systems. This conversion process is different for the all-air system (e.g., the conventional mixed ventilation system or displacement ventilation system) and the cooled ceiling systems. For the all-air system, the heat is extracted from the room ultimately by the air, and therefore only those part of the heat gain that is convected into the room air directly constitutes the cooling load, while the radiant part undergoes a delay and attenuation. For the cooled ceiling system, part of the radiative heat gains will be directly absorbed by the cooled panels. To take into account these differences, the specially enhanced dynamic cooling load program ACCURACY is employed.

Table 6.2 Summary of the three cooling systems (Ventilation rate=4 ach)

Systems	Cooling Load					Vent. Air Temp. (°C)	Internal Heat Gains. (W)	External Heat gains - Heat Storage (W)
	Total (W)	W/m2 fl.	By Air (W)	By Panel (W)				
				Total	Convection			
DV	480	26	480	0	0	19	540	-60
CC + DV(*)	875	48	415	460	273	20	800	75
ACC(**)	864	47	217	647	433	13/23	800	64

(\*) 60% of the ceiling area are installed with water panels, supplied cold water temperature is about 19°C, with a temperature rise of about 1.5°C over the panels, the consequent panel surface temperature is about 20.2°C

(\*\*) 70% of the ceiling area are installed with air panels, the ventilation air temperature entering and leaving the panels are 13°C and 23°C respectively.

Using the program ACCURACY, thermal behaviour simulations are performed for a room with the three cooling systems respectively. As already mentioned, the

internal thermal loads are different for the three systems. In these simulations, the Dutch weather data in the year 1971 are used as external weather conditions. Also, thermal masses of the concrete floor and ceiling, and the external wall are included. The simulation period runs from July 1 to July 15, 1971. The simulations by the program ACCURACY give the convective and radiative heat extractions by the cooling panels, and also the radiant and convective heat from all the wall and window surfaces, together with the heat extractions by the ventilation air. Some of these results are given in Table 6.2, they are results for 15:00 pm, July 4, 1971. All the three systems maintain the operative temperature at 23°C in the room. While the average room air temperature is maintained at comfort level, local air velocity, turbulence level, and temperature gradients may be different significantly. These local differences are the focus of the following CFD simulation investigations.

### 6.6.2 CFD Simulation of Thermal Comfort and Contaminant Distributions

Using all the surface convective heat flows as given boundary conditions, the detailed air flow pattern, air temperature and the pollutants distribution in the room are simulated, corresponding to the situations given in Table 6.2, using the CFD program PHOENICS. Since the data in Table 2 are from the dynamic simulations, the CFD simulation may be considered as quasi-steady state simulation.

To quantify the pollutants in terms of perceived air quality, the perceived pollutant quantities *olf* and *decipol*, as well as the percentage dissatisfied (PD) people due to the odours are implemented into the program PHOENICS. Detailed description of these terms can be found in a series of publications by Fanger *et al.* (1988). These two units are based on human senses rather than on chemical analysis. The odorous and irritating compounds in indoor contaminants are perceived by human beings olfactory and chemical senses respectively. The pollutants emission rate from a standard person is defined as one *olf*, and if this amount of pollutants is diluted with a ventilation air at the rate of 10 l/s, the concentration is defined as one *decipol*. Obviously some chemicals, such as radon, carbon-monoxide, that are harmful to human's health and life but not perceived by human sense, are not included in these two units. They have to be considered separately. If the total odour sources in a room is  $G$  (olf), the perceived pollutants concentration in the room  $C_i$  can be determined from

$$C_i = C_o + 10 \frac{G}{Q} \quad (6.4)$$

where  $C_o$  is the perceived outdoor pollutant concentration (olf),  $Q$  is the ventilation rate (l/s). The percentage dissatisfied people in the room due to odours, PD, can be calculated by

$$PD = e^{5.98 - (112/C_i)^{0.25}} \quad (\%) \quad (6.5)$$

Equation (6.5) assumes that the air is well mixed in the whole room space. In practice, the  $C_i$  may vary from place to place in a room space. Therefore, the  $C_i$  should be

calculated locally, taking into account the convection and diffusion transport process occurring in a room.

In the present cases, it is assumed that the four occupants have a total emission rate of air pollutants (bio-effluent) of 6 olfs (with 2 people emitting 2 olfs each and the other two people emitting 1 olf each), emitted at the height of 1.1 m above the floor, and the pollutants emission rate is 1 olf from the floor and 1 olf from the wall and ceiling materials. If we assume the air is well mixed in the room, to maintain the average  $C_1$  at the level of 1.48 decipol, the outdoor ventilation air required will be 194  $m^3/h$  or 4 ach. Correspondingly, the PD due to odours will be about 20%[11]. Here it is assumed that 75% of the pollutants in the room are emitted from the nose positions, and contaminants from the floor levels is rather low. In the following calculations of the distributions of  $C_1$  in the room, the locations of these emission sources are rather important factors. To the author's opinion, investigations of the ventilation performances of any systems should address the influences of locations of the pollutant sources in the room.

The simulated velocity vectors, temperature distributions (isotherms), distribution of the pollutants concentration, as well as the percentage dissatisfied people (PD) due to draft and odours are presented in graphical forms in Figure 6.7 - Figure 6.9. At 2.3 meter from the inlet and 0.675 meter from the mid-plane, the vertical air temperature and pollutant concentration variations against the height of the room are plotted in Figure 6.10 a and Figure 6.10 b respectively. These results will be described in detail as below.

#### *System 1: Displacement Ventilation:*

The simulated flow pattern is typical of a displacement ventilation(Figure 6.7 a), and rather large vertical temperature difference exists in the room. From Figure 6.10 a it can be seen more clearly that the air temperature is about 25°C at the height of head(1.1 meter above the floor) and 22.5°C at the height of ankle(0.10 meter above the floor). This temperature difference  $\Delta T_{0.1-1.1} = 2.5$  K is smaller than the 3 K, the maximum value allowed for thermal comfort[12]. The risks of draft is greater near the air inlet. The region in which PD due to draft is higher than 15% is indicated in Figure 6.7b by plotting the iso-surface of 15% PD. Along the floor surface, this region accounts for 34% of the room depth. The pollutants concentration distributions (Figure 6.7 c and 6.7 d) indicate the vertical concentration stratification, which is desired for a better indoor air quality. The concentration at the breathing zone(1.1 meter above the floor) is about 1.0 decipol. It can be easily calculated through mass conservation that the pollutant concentration at the exhaust is about 1.48 decipols. Therefore, the ventilation effectiveness calculated according to Equation (6.3) is 1.48 in this case. Correspondingly, 15% PD due to odours can be achieved in the breathing zone(1.1 meter above the floor). The displacement ventilation system seems to be rather good at the cooling load of about 25  $W/m^2$  floor area and if 75% pollutant sources are from occupants' breathing. However another simulation indicates that when higher internal load is present, decreasing the supply air temperature gives much too large vertical temperature stratifications, and PD due to draft near floor is too high.



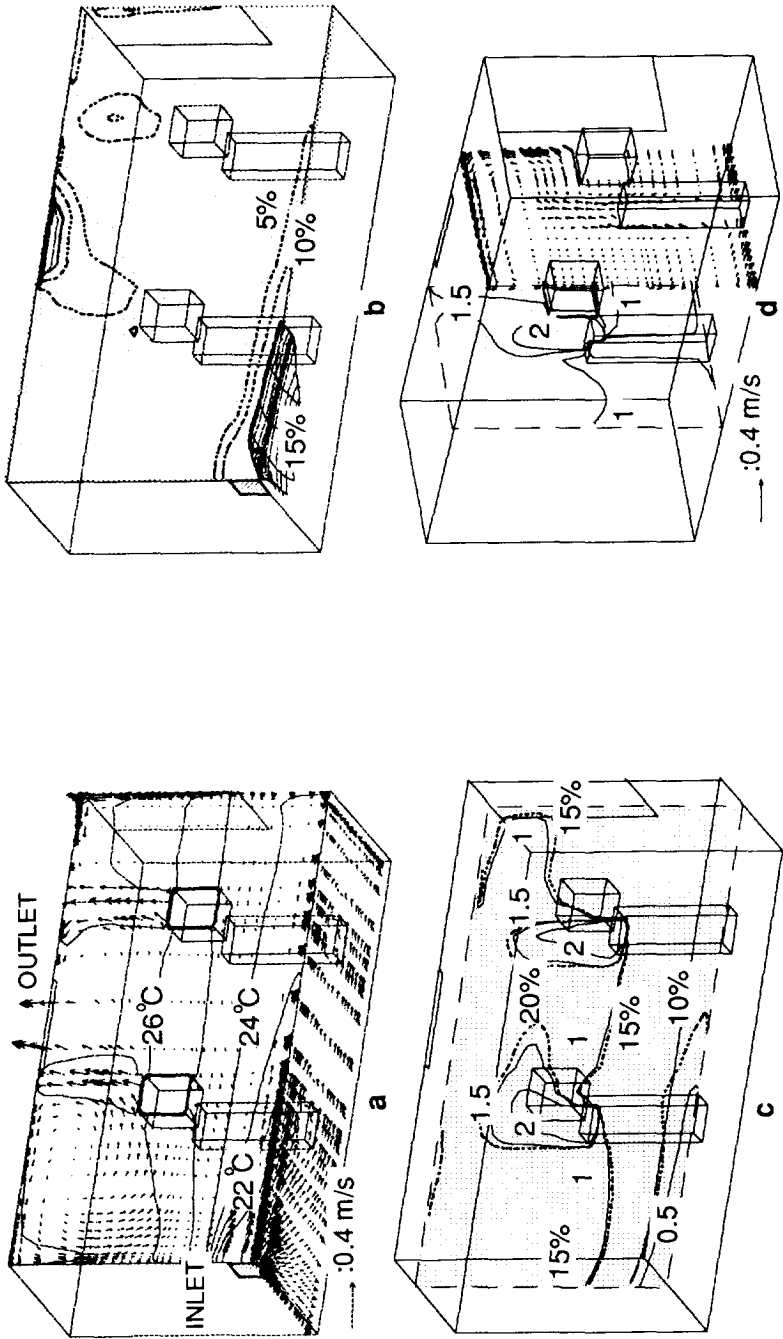


Figure 6.7 Simulated field distributions with displacement ventilation system: **a.** velocity vectors and isotherms; **b.** PD due to draft: the mesh indicates where PD > 15%, and the dotted lines are contours in the mid-plane; **c & d.** contours of odour concentration (represented by solid lines, key unit is *decipol*), and PD due to odours (represented by dotted lines), as well as velocity vectors

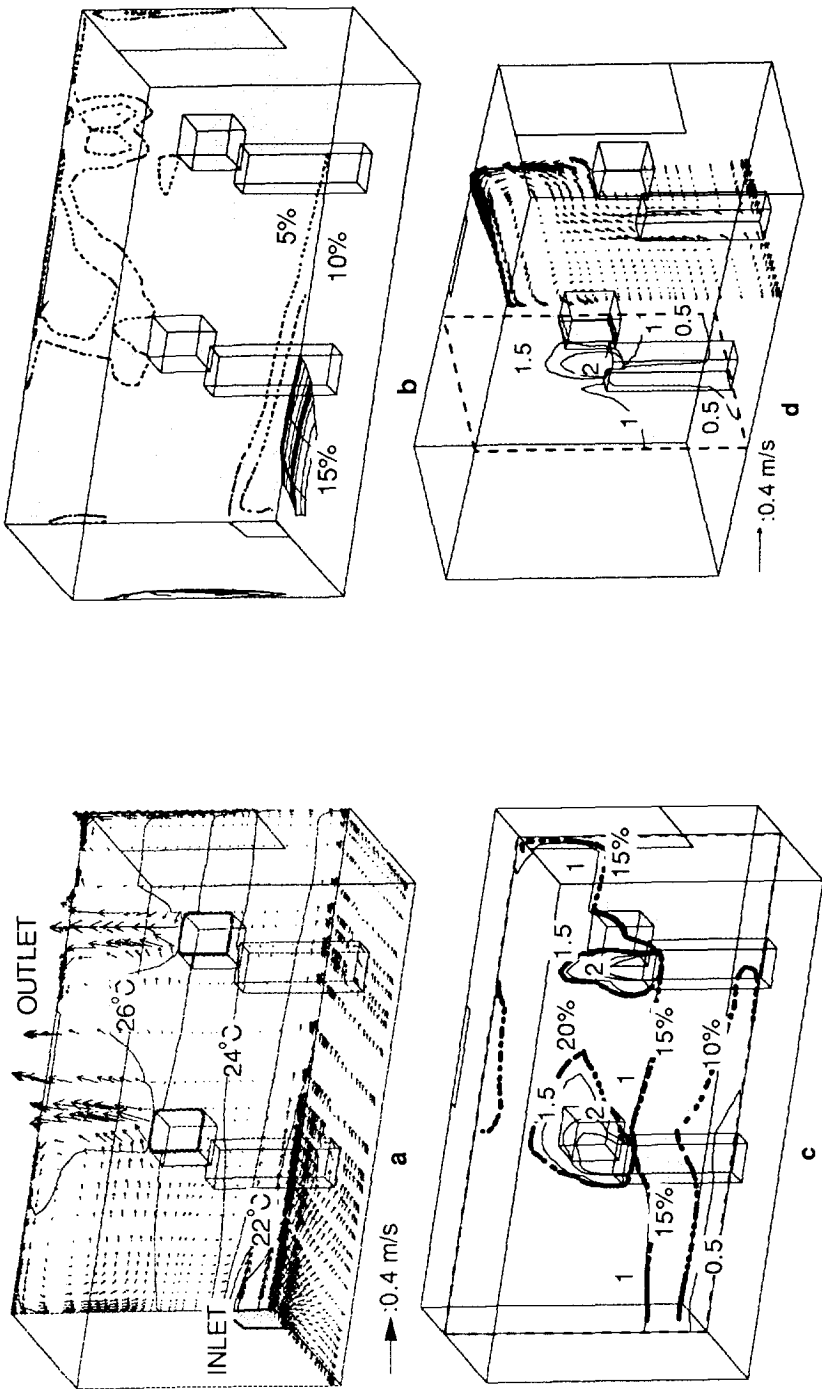


Figure 6.8 Simulated field distributions with displacement ventilation + cooled-ceiling system: a. velocity vectors and isotherms; b. PD due to draft: the mesh indicates where PD > 15%, and the dotted lines are contours in the mid-plane; c & d. contours of odour concentration (represented by solid lines, key unit is decipol) and PD due to odours (represented by dotted lines), as well as velocity vectors

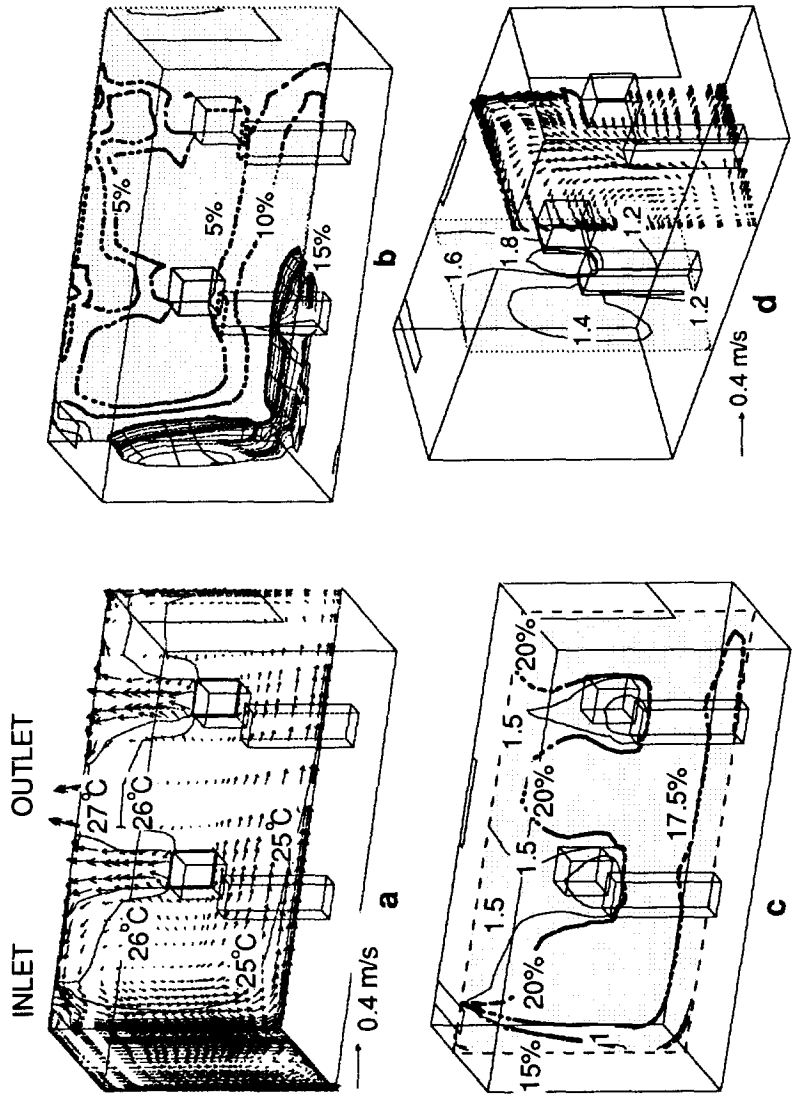


Figure 6.9 Simulated field distributions with cooled air ceiling + low velocity ceiling air supply: a. velocity vectors and isotherms; b. PD due to draft: the mesh indicates where PD > 15%, and the dotted lines are contours in the mid-plane; c & d. contours of odour concentration (represented by solid lines, contour key unit is *decipol*), and PD due to odours (represented by dotted lines), as well as velocity vectors

### System II: Displacement Ventilation + Cooled Ceiling System

In this case, 60% of the ceiling is installed with water panels insulated above and the ceiling is assumed to be closed. ACCURACY simulation shows that, with the average water panel surface temperature of 20.2°C, 460 watts of heat is absorbed by the water panels with 273 watts by convection, and the cooling load reaches 875 watts, together with the heat extraction by the ventilation air. The simulated flow pattern (Figure 6.8 a) is rather similar to the first case described above. The vertical temperature difference  $\Delta T_{0.1-1.1} = 2$  K (Figure 6.10a). The high draft region, where PD > 15%, accounts for 33% of the room depth (Figure 6.8 b). The vertical concentration stratification is maintained at certain extent (Figure 6.8 c and d). The ventilation effectiveness is 1.34 (Figure 6.10b), slightly lower than in the previous case. This achievement can probably be better understood from the point of view of displacement ventilation, by arguing that the cooled ceiling reduces its load by radiation and convection in the upper zone of the room, so that the displacement ventilation is working at a favourable condition.

### System III: Air Ceiling with Low Velocity Ceiling Supply

In the present simulation, the supplied air temperature is 13°C, the cooling capacity is 864 watts. With 70% of the ceiling installed with the air panels, 647 watts of the heat are absorbed by the cooling panels, and the air is heated to about 23°C before entering the room. The general flow pattern (Figure 6.9a) is rather different from the two cases

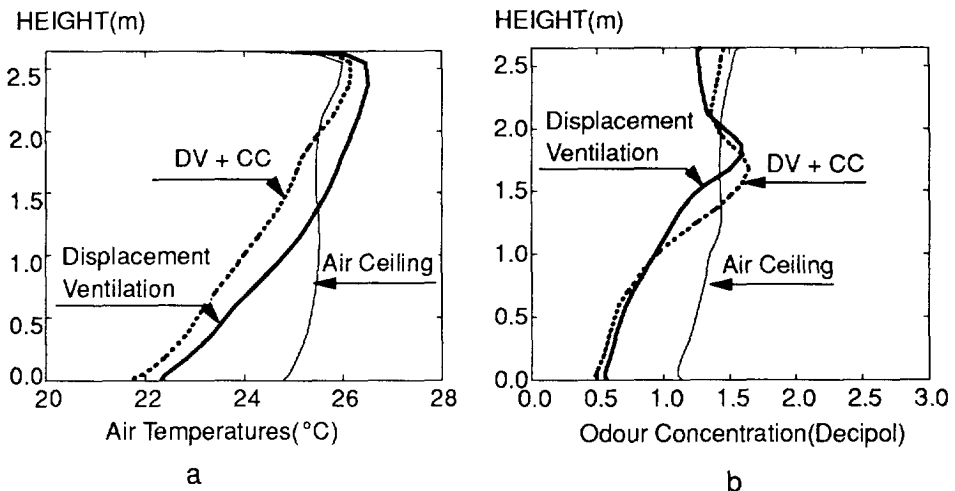


Figure 6.10 Vertical variations of air temperature (sub-figure a) and odour concentration (sub-figure b)

described above. Due to buoyancy effect, the supplied air undergoes a free-fall and therefore is accelerated before reaching the floor. Consequently, the draft risk is higher along the floor, though the exit velocity of the air is only 0.1 m/s. The high draft region

penetrates nearly half of the room depth(Figure 6.9 b). The pollutant concentration is mixed up in the room(Figure 6.9 c and d), due to the induction effect of the ventilation air and the convective flow of cool air from panel surfaces, and the ventilation effectiveness is reduced to 1.10 (Figure 6.10b). By looking at the pollutant concentration distribution and the velocity vectors in the two cross sections(Figure 6.9 d), it can be seen that the cool air convection from the ceiling panels play a major role in the pollutant recirculation. Nevertheless, using the criterion that  $PD < 15\%$ , and taking into consideration that PD index used in this calculation is for the draft sensation at head level and is about 5% higher than that for the ankle level[11], the thermal environment is acceptable. Therefore,  $13^{\circ}\text{C}$  seems to be the minimum supplied air temperature allowed due to comfort requirement for the configuration of air panels in combination with ceiling supply inlet. Correspondingly, the maximum cooling load would be about  $50 \text{ W/m}^2$ .

### **6.6.3 Discussions of the Simulation Results**

From these simulation results, it can be concluded that the cooled ceiling combination with a displacement ventilation gives a rather good performance in thermal comfort and ventilation effectiveness at the cooling load  $50 \text{ W/m}^2$  floor area. The thermal comfort and ventilation effectiveness is almost equivalent to those of a displacement ventilation system at the cooling load of  $25 \text{ W/m}^2$ .

The air-ceiling system creates a flow pattern more close to well mixed situations, with a ventilation effectiveness still higher than one at the cooling load of  $50 \text{ W/m}^2$  floor area. However, the free-falling ventilation air stream, enhanced by the downward convective flow from the cooling panels tends to create draft along the floor, although the PD due to draft is still acceptable in the simulation case. The entrainment effect of the downward supplied air jet also reduces the ventilation effectiveness. In fact, locating the air outlet in the ceiling is mainly for installation considerations. If this air diffuser is located near the floor, the draft risks near the floor will be reduced and ventilation effectiveness will be higher. This can be easily seen by comparing the field distributions of water-ceiling and the air ceiling, since the total heat extractions of the two cases are almost the same.

## **6.7 CONCLUSIONS**

1. The tests in the climate room indicates the possible cooling capacities of the water-panel and air-panel cooled ceiling systems. For the water-panel cooled ceilings, the cooling capacity is determined by the cooled panel areas in the ceiling and the supplied water temperatures. It can be expected that the cooling capacities can easily reach 100 watts per  $\text{m}^2$  of floor area, with the additional cooling capacities of cooled ventilation air.
2. For air-panel cooled ceiling systems, the test indicates that ventilation air supplied at low temperatures through the panels can be automatically heated to a temperature close to the room average air temperature in the room. This result has two practical indications. Firstly, reheating energy can be very much reduced. Secondly, a same amount of ventilation air may extract a larger amount of heat from the room.
3. Measurements using tracer gas and anemometer are also performed to investigate the

draft risks and contaminants distributions for the air-panel cooled ceiling systems with ceiling-located low velocity air diffuser. Also the supplied air jet are visualised using smoke. These measurements reveals the main characteristics of the air flow and contaminant distributions in such a configuration. There exists small vertical stratifications of air temperature and contaminant(tracer gas) concentration in the occupied zone. Although large errors are expected in the anemometry measurements, the results still indicate that the air jet is accelerated due to buoyancy effect when it reaches the floor. Nevertheless, subjective judgements by several people indicates the draft risks thus created are negligible.

4. The field distribution measurements are used to estimate the reliability of CFD simulations. Discrepancies are found in flow details, especially about the air flow velocities when the supplied air jet reaches the floor. The predicted turbulence kinetic energy and turbulent intensity are much higher in the region below the air-diffuser than those found in the measurements. The PD values predicted are higher by a value of 5~10% than the measured ones. Bearing these discrepancies in mind, the overall prediction of the flow pattern, temperature distribution, as well as the contaminant distributions can still be used to give some indications concerning thermal comfort and ventilation effectiveness from the point of view of practice.

5. Three representative simulations are performed to investigate the thermal comfort and ventilation effectiveness of three typical cooling/ventilation systems, namely, the conventional displacement ventilation system, the water-type cooled-ceiling system coupled with displacement ventilation, and air-type cooled-ceiling system. The simulation results indicate that water-panel cooling can very much increase the cooling capacities of the displacement ventilation system, without significantly reducing its higher ventilation effectiveness. The air-panel system can cool a room at a higher load of about 50 W per m<sup>2</sup> floor area, with a ventilation effectiveness slightly higher than 1 but much lower than that of the displacement ventilation system. The simulation results also indicate the possibilities of improving the performances of the air type cooled-ceiling system by locating the air diffuser in the near floor level.



## CHAPTER 7

# ANNUAL ENERGY ANALYSIS: COOLED-CEILING SYSTEM VERSUS ALL-AIR SYSTEMS

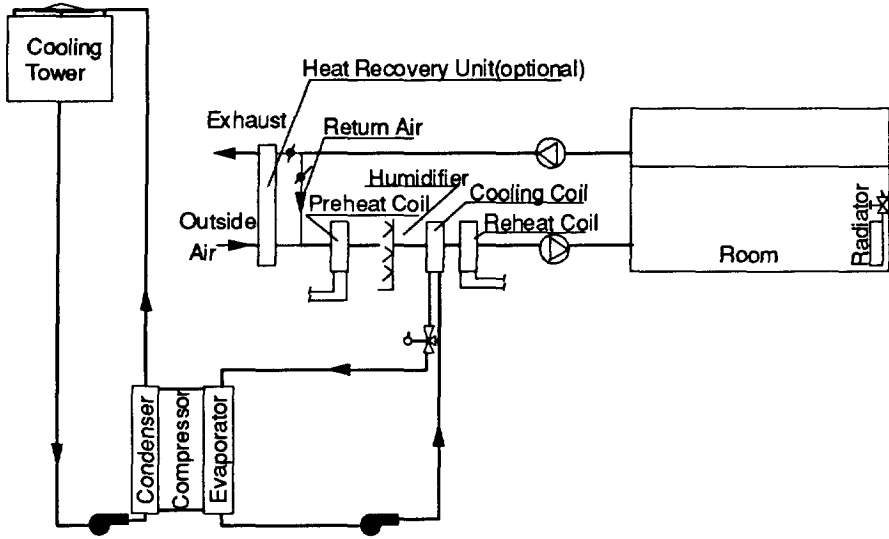
### 7.1 INTRODUCTION

People have devised various systems to maintain the thermal comfort in buildings. The previous chapter discusses the thermal comfort and indoor contaminant distribution in a room served with different systems. This chapter will focus on the other important aspect - the energy use of these systems.

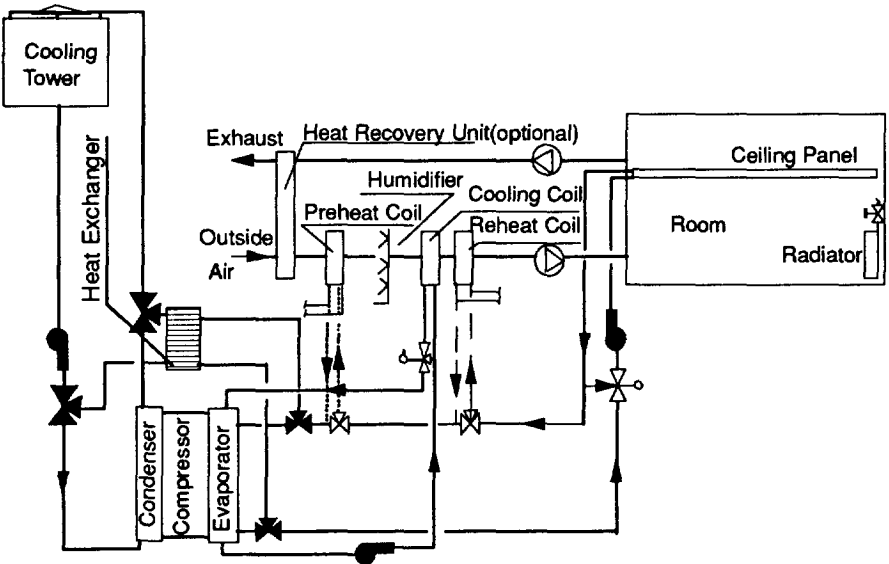
Let us have a look at the two basic systems: the all-air system and the air-water system. The water-panel type cooled-ceiling(CC) systems may be classified as the second type system. In this sense, the water-panel type cooled-ceiling systems are not completely new. Figure 7.1 shows the schematic for an all-air system and a cooled ceiling system. The main operational characteristics of three systems are summarized in Table 7.1. According to their operational differences, all-air systems are further classified as constant air volume(CAV) systems and variable air volume(VAV) systems. In a constant air volume system, the supplied air flow rate to a room remains constant throughout the year, the supplied air temperature is regulated according to the room requirement. A VAV system operates in another way, the air temperature supplied into a room is fixed, while the supplied air flow rate changes according to thermal load requirement. In comparison with a CAV system, a VAV system reduces energy consumption in two ways. In the first place, fan energy is very much reduced; secondly, the reheat energy required after dehumidification in air handling process, especially in the transit seasons, is also very much reduced.

A water-panel type cooled-ceiling system operates in another way. Only outside air will be supplied for humidity control and ventilation purposes. The task of thermal loads removal is mainly assigned to the water cooled ceiling panels. Therefore, a cooled ceiling system has a relatively small air handling unit(AHU), and reduced fan energy consumption. On the other hand, as already discussed in the previous chapters, the cooling load dynamics with respect to heat accumulation, change very much due to the existence of ceiling panels in a room space. In view of the increased interest in cooled ceiling technique, it is





a



b

Figure 7.1 Schematic for all-air systems(a) and CC systems(b)

Table 7.1 Operational Characteristics of Different Air Conditioning Systems

Systems	Air Volume(Flow Rate)	Air Supply Temperature	Unit Heating or Cooling
CAV	Fixed with Design Load Condition	Variable	Radiator (optional)
VAV	Variable	Fixed	Radiator(opt.)
CC	Fixed with Minimum Ventilation	Fixed	1.Radiator(opt.) 2.Ceiling Panels for Cooling
Ideal systems	All should be variable, coordinated by an optimization scheme		

significant to understand the system dynamics of CC systems, especially the consequent year energy consumptions. This topic forms the content of this chapter.

## 7.2 METHODOLOGY

We adopt the system modelling approach to make this investigation. This investigation will be based on the mathematical models described in Chapter 4. As a step further forward, the model will be coupled with models for air handling unit, as well as models for primary equipments, such as boilers, compressors and air fans. The detailed procedure goes as described below.

1. ACCURACY gives the year round, hour by hour data of cooling/heating loads, and room exhaust air temperatures. As has been indicated in Chapter 4, in rooms with cooled-ceiling, this cooling load is split into two parts: the heat extraction by the ventilation air and the heat extraction by the ceiling panels. Also, the exhaust air temperatures are calculated from the required operative temperatures;

2. Based on these data, another program called ENERK(Paassen 1986), the essential of which will be discussed in more detail in the following section, calculates the energy requirement of air handling unit, and subsequently the end energy use in terms of the required electricity for chillers and air fans, and consumed gas for boilers.

Therefore, the differences in energy use of different systems are counted in two steps: the cooling load calculation procedure and the air handling and transport and chilled water production and transport system modelling procedure. The newly developed cooling load calculation procedure is already fully described in Chapter 4, the following section will focus on the second step of the whole procedure.

## 7.3 MODELLING AIR HANDLING UNIT(AHU)

In an air-conditioning system, intensive energy transport occurs in the air handling unit. Full understanding of the processes have impact on two aspects of the HVAC system: the

initial sizing of the system components and the related selection of primary equipments, and the determination of the proper control strategies.

Paassen(1981, 1986) proposed a computerized method to analyze the energy impact of different control strategies for air handling units. In his method, the hour-by-hour cooling load and room extraction air temperature, are statistically treated in relation with the outdoor weather data. These data are represented in the psychrometric chart, in different sections with corresponding joint occurring probabilities(Figure 7.2). For each section, the air handling processes are analyzed, and consequently the energy consumptions are calculated. In such a way, the system annual energy consumption can be estimated.

Here, we can see that the link between the model for AHU and the dynamic simulation of the served room is the hour-by-hour cooling load data and the extracted room air temperature. In fact, the model for AHU can be alternatively based on more rigorous hour-by-hour calculations. Mierlo(1986) has compared the differences between this statistical method and the hour-by-hour calculations, and his conclusion is that the difference in terms of the gross year energy consumption is no more than 5%. Therefore, the following calculations are based on this statistical approach.

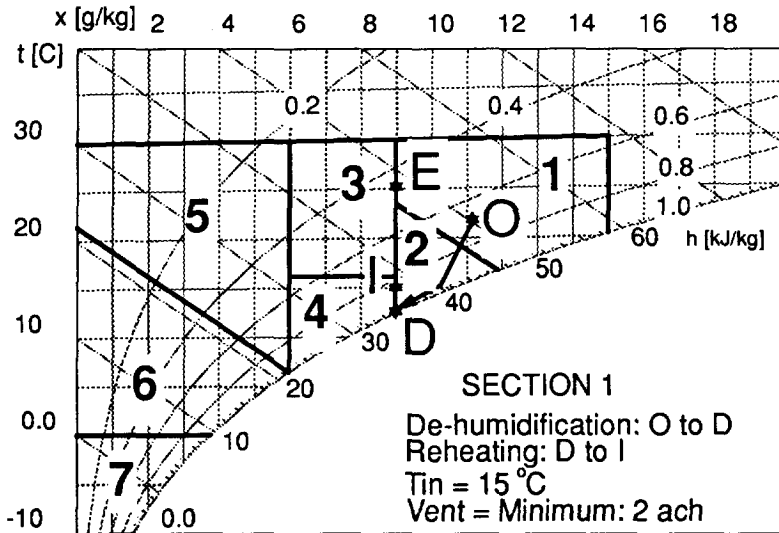


Figure 7.2 The division of a psychrometric chart and an example of representation of air-handling processes

#### 7.4 PRIMARY EQUIPMENTS MODELS

The equipment energy performances are required to estimate the end energy uses of the primary equipments such as the compressor, the boiler and the air fans. As suggested in ASHRAE publications (ASHRAE 1990), a kind of semi-empirical models will be suitable for building energy analysis calculations. Unlike the detailed thermal dynamics and heat

transfer analysis for building components, semi-empirical algorithms and models use a "black box" concept that is supported by physical laws. The equipment is treated as a single unit. No information is required about the interactions between the equipment components or about the physical dimensions and properties that characterize the equipment. In general, analysis of variance, regression analysis, and intuition, aided by a knowledge of general engineering principles, are used to select input variables that are important in representing equipment performance and to develop the form of the equations that correctly relate the input variables to the desired output variables. Specifically, regression analysis is used to fit the equations to discrete performance data obtained from the equipment manufacturer, from laboratory tests, or from more detailed models or simulations.

Models or algorithms obtained in this way can very well predict equipment performance within the range of available test data for the particular equipment. With hourly data of the required cooling or heating from the air handling unit, ceiling-panels or radiators available from the previous rigorous calculations, these simple and flexible models or algorithms can be easily coupled with, and be easily modified to account a wide range of equipments.

The energy performance of a water chiller is quantified by its COP(coefficients of performance), defined as the ratio of the cooling energy to the electricity input power. For a specific system, the COP is the function of the required chilled water temperature  $T_w$ , the ambient air temperature  $T_o$ , and humidity  $X_o$ , as well as the operation capacity  $Q$ , i.e.,

$$COP = f(T_o, X_o, Q, T_w) \quad (7.1)$$

In such a way, the performance of the cooling tower is already empirically taken into account. Subsequently, the required electric power input can be calculated according to

$$\text{Chiller power} = \frac{Q_c}{COP} \quad (7.2)$$

The performance of a boiler depends on boiler load, boiler characteristics, and to a lesser extent, on ambient air temperature. More discussions can be found in ASHRAE Handbook (ASHRAE 1993). As the boiler technology advances, some boilers with dampers or other means of maintaining an almost constant air/fuel ratio for varying loads may have an almost constant efficiency until very low loads are encountered.

Fan energy is an important factor in the annual energy consumption of a HVAC system. Fan performance can be characterized by its efficiency, which itself is dependent on operational air flow rate. Mostly, rated volumetric flow rate, pressure rise and efficiency are available from the manufacturer. Then rated power can be calculated as

$$\text{Fan power} = \frac{Q \Delta p}{3600 \eta} \quad (W) \quad (7.3)$$

where

- $Q$  = air volumetric flow rate,  $m^3/h$
- $\Delta p$  = fan total pressure rise, Pa

$\eta$  = fan efficiency

However, fan efficiency normally changes very much as the working air flow rate is modulated in operation, depending on the method of air volume control. Therefore, computation of real fan power should be based on a characteristic curve, which gives fraction of rated input power versus fraction of rated volume. These curves can be determined experimentally or obtained from the manufacturer. Also, general and accurate enough curves are available in ASHRAE Handbook(ASHRAE 1993), which show three characteristic curves respectively with discharge damper control, inlet vane control and variable-speed motor control method.

### 7.5 SIMULATION CONSIDERATIONS

The whole modelling procedure is applied for the chilled water ceiling system versus all-air systems. They are supposed to serve an office building. For the cooling load or heat extraction calculations, only one room is picked up for analysis. The room is assumed to be situated in the intermediate storey, with identical adjacent rooms, and above and below. The facade is south-facing with 35% double glazing area. The window is installed with venetian blinds. The external wall consists of three layers - 180 mm thick concrete slab inside, and 100 mm thick brick layer outside with 60 mm insulation in between. The floor (also the ceiling) has a 320 mm thick concrete slab base with another 70 mm thick cement layer. The storey height is 3.3 meters. The lowered ceiling or false ceiling is located at the height of 2.64 meters from the floor, and therefore there is an air space above the false ceiling. With cooled-ceiling systems, ceiling panels will replace 60% of the false ceiling. The false ceiling is supposed to have openings which allow air recirculation. The room has a width of 3.6 meters and a depth of 5.1 meters. The partition walls are made of 26 mm gypsum board.

The building is occupied only in the working hours: from 8:00 until 18:00. In the working hours, the total internal sensible load is 800 watts in the room, or about 40 W/m<sup>2</sup> floor area, with 37% radiant heat. In the calculation of cooling load, no air infiltration occurs. The Dutch short reference year weather data(Paassen 1981) are used as outside conditions.

The room operative temperature, as defined in Equation (4.45), is controlled at 25.6°C and 22°C respectively in cooling and heating period. With all-air system, 22°C is also the setting-point of the thermostat for radiator control. In fact, allowing temperature floating is not necessarily good for energy-saving with CAV systems in cooling season as implied by the simulation results from Chen *et. al*(1990) since more energy will be required for reheating of the supplied air. For VAV system, raised setting point means heat storage in building envelopes and reduced air volumes, both of which will be favourable for energy savings.

The minimum outdoor air is 100 m<sup>3</sup>/hour, which is about 2 ach in terms of the room volume. This will be the design air flow rate for CC systems, with corresponding constant supplied air temperature of 15°C. The real air flow rate for VAV systems will be changing according to cooling requirements of the room, and the air recirculation rate to the AHU will be governed by the general control strategies for VAV systems. This will be

seen more clearly in the simulation results in the following section. The three system components are those as shown in Figure 7.1a and Figure 7.1b. The supplied chilled water flow rate to the ceiling panel in the room is 0.119 kg/s, which means a heat extraction capacity of about 45 W/m<sup>2</sup> floor area with a temperature rise of about 1.6°C. The year round energy analysis will be done for both CAV and VAV all-air systems and for CC systems, first without and then with heat recovery unit. Also, by using system heat balance analysis method, the possible unique energy saving measures for CC system will be analyzed.

For the present simulation, the performances of the primary equipments are modelled with certain constant indices: the COP of the chiller system is 3.5; the boiler efficiency is 75%, and fan efficiency 60%; the fan pressure rise is 1400 Pa. The errors that may be introduced due to these simplifications will be discussed in the simulation result analysis.

## 7.6 SIMULATION RESULTS ANALYSIS

### 7.6.1 Required Heat Extraction Rates

The cooling load program actually calculates the required heat extraction rates from the room, together with the extracted air temperatures, and required chilled water temperatures for the ceiling panel with CC system. These informations are hourly data. A sample of one day is shown in Table 7.2 and Table 7.3. The differences between the CC system and all-air system can be already seen by comparing the different heat extraction rates (Figure 7.3). The required heat extraction rates are higher in the first half of the day, but lower in the second half of the day for the CC system in comparison with the all-air system. In total, the required heat extraction in the day is higher with CC system, as given at the bottoms of Table 7.2 and Table 7.3. The primary reason is the direct absorption of radiant heat by the ceiling panels and the consequent reduced heat accumulation in the wall, as illustrated in Figure 7.3. As generally known, reducing the heat storage capacity is not good for reducing the peak load of the air-conditioning system. However, on the other hand, the air temperature in the room is higher at the same operative temperature due to radiant effect, which means that the ventilation air is extracting an increased amount of heat. Taking into account this effect, the increased cooling requirement will be somewhat lower than that indicated in Figure 7.3. The ultimate effect on energy consumption will be calculated automatically in the second step.

After a statistical analysis, these informations are represented by an averaged heat extraction, averaged extracted air temperature, as well as the averaged outdoor temperature and humidity in each sections in the psychrometric chart, together with the joint occurring probabilities for the section. These data are summarized in Table 7.4 and Table 7.5 respectively. The sections in psychrometric chart are those represented in Figure 7.2. It should be noted that the data, except the required air supply air temperatures, in Table 7.2 apply for both CAV and VAV systems, if the influence of different air flow patterns on cooling load is neglected.

Table 7.2 Hourly heat extraction rates and temperatures calculated by dynamic simulation(all-air system)

Hour	Heat Extraction Rate (W)	Operative Temperature(°C)	Extracted Air Temperature(°C)	Supplied Air Temperature(°C) (°)
1	0.0	25.0	—	—
2	0.0	24.9	—	—
3	0.0	24.8	—	—
4	0.0	24.8	—	—
5	0.0	24.8	—	—
6	0.0	24.8	—	—
7	0.0	25.0	—	—
8	0.0	25.4	—	—
9	775.3	25.6	25.2	17.4
10	915.7	25.6	25	15.8
11	981.2	25.6	25	15.1
12	1003.7	25.6	24.9	14.8
13	989.4	25.6	24.9	15
14	949.1	25.6	25	15.4
15	883.6	25.6	25.1	16.2
16	823.9	25.6	25.2	16.8
17	813.5	25.6	25.2	17
18	799.1	25.6	25.2	17.1
19	0.0	25.9	—	—
20	0.0	25.7	—	—
21	0.0	25.6	—	—
22	0.0	25.4	—	—
23	0.0	25.3	—	—
24	0.0	25.4	—	—
<b>Total</b>	<b>8.9 kW.h</b>	—	—	—

(°) for CAV system

Table 7.3 Hourly heat extraction rates and temperatures calculated by dynamic simulation for CC system

Hours	Heat Extraction(W)		Operative Temperature (°C)	Extracted Air Temperature (°C)	Panel Inlet Water Temperature(°C)
	By Air	By Panel			
1	0	0	24.1	—	—
2	0	0	24.0	—	—
3	0	0	24.0	—	—
4	0	0	23.9	—	—
5	0	0	23.9	—	—
6	0	0	23.9	—	—
7	0	0	24.1	—	—
8	0	0	24.5	24.6	24.6
9	363.5	358.9	25.6	25.7	23.3
10	363.3	754.0	25.6	25.7	20.9
11	362.8	767.8	25.6	25.7	20.3
12	362.6	763.1	25.6	25.7	20.1
13	362.6	709.1	25.6	25.7	20.4
14	362.7	625.3	25.6	25.7	20.8
15	362.8	506.1	25.6	25.7	21.6
16	363.0	420.7	25.6	25.7	22.2
17	363.1	443.6	25.6	25.7	22.3
18	363.2	420.1	25.6	25.7	22.4
19	0	0	25.1	—	—
20	0	0	24.9	—	—
21	0	0	24.7	—	—
22	0	0	24.5	—	—
23	0	0	24.4	—	—
24	0	0	24.3	—	—
Total	9.4 kWh		—	—	—



Table 7.4 Probability analysis of the required heat extraction and extracted air temperature with all-air systems

Sections in Psychro. Chart	Cooling Period			Heating Period		
	Heat Ex- traction (W)	Extract Air T <sub>e</sub> (°C)	Joint Probab- ility (%)	Heat Ex- traction (W)	Extract Air T <sub>e</sub> (°C)	Joint Probab- ility(%)
1	879	25.1	4.3	_____	_____	0
2	698	25.2	12.3	_____	_____	0
3	821	25.1	11.1	_____	_____	0
4	420	25.3	22.1	_____	_____	0
5	414	25.4	13.6	_____	_____	0
6	137	24.9	27.8	-44	24.9	0.7
7	0	24.0	7.3	-57	24.1	0.9

Table 7.5 Probability analysis of the required heat extraction and extracted air temperature with CC systems

Sections in Psychro. Chart	Cooling Period			Heating Period		
	Heat Ex- traction (W)*	Extract Air T <sub>e</sub> (°C)	Joint Probab- ility (%)	Heat Ex- traction (W)	Extract Air T <sub>e</sub> (°C)	Joint Probab- ility(%)
1	976(612)	25.7	4.3	_____	_____	0
2	756(394)	25.6	12.3	_____	_____	0
3	898(533)	25.7	11.1	_____	_____	0
4	421(65)	25.4	22.1	_____	_____	0
5	417(55)	25.6	13.4	-10	26.2	0.2
6	123	24.9	27.8	-45	24.8	0.7
7	0	24.0	7.3	-58	24.1	0.9

\* Figures in the brackets are required heat extraction for ceiling-panels

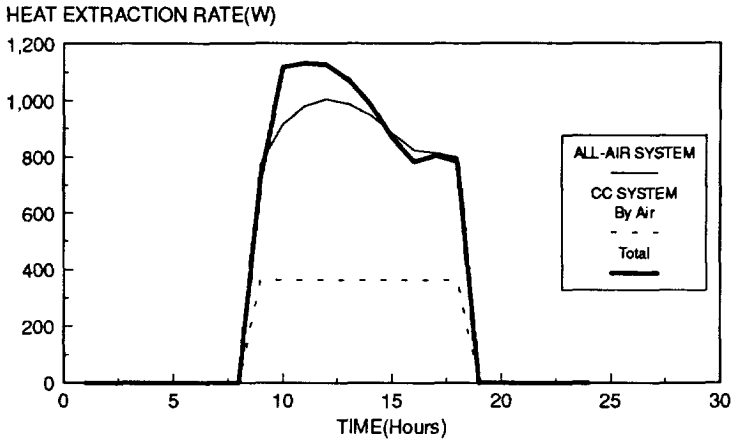


Figure 7.3 Required heat extraction rates: CC system vs all-air system

### 7.6.2 Annual Energy Cost

For each section, the energy requirement for the air handling can be calculated based on psychrometrics. These air handling processes are illustrated in Figure 7.4 a & b and Figure 7.5 a & b for CC systems and for VAV systems respectively in cooling seasons and heating seasons. Subsequently, the energy required for the primary equipments is calculated. These results are summarised in Table 7.6 and Table 7.7 for CC systems and VAV systems. Since the total energy expressed in gross terms does not reflect the real energy value, the electricity consumptions are converted into the equivalent primary energy by multiplying a factor of 3, and are presented in the last rows of Table 7.6 and 7.7. Also, the cost of the energy consumption is calculated based on the current prices in the Netherlands: 0.246 Dfl/kW.h for electricity and 0.505 Dfl/m<sup>3</sup> for gases (The heat value of gas is 9.72 kW.h/m<sup>3</sup>), and these costs are given in the last rows of Table 7.6 and Table 7.7. The annual primary energy consumption and cost are also illustrated in Figure 7.6. The first impression we can have is that the total energy costs are close with each other for CC systems and VAV systems. As already well-known, CAV systems consume more energy for reheating and require higher fan energy.

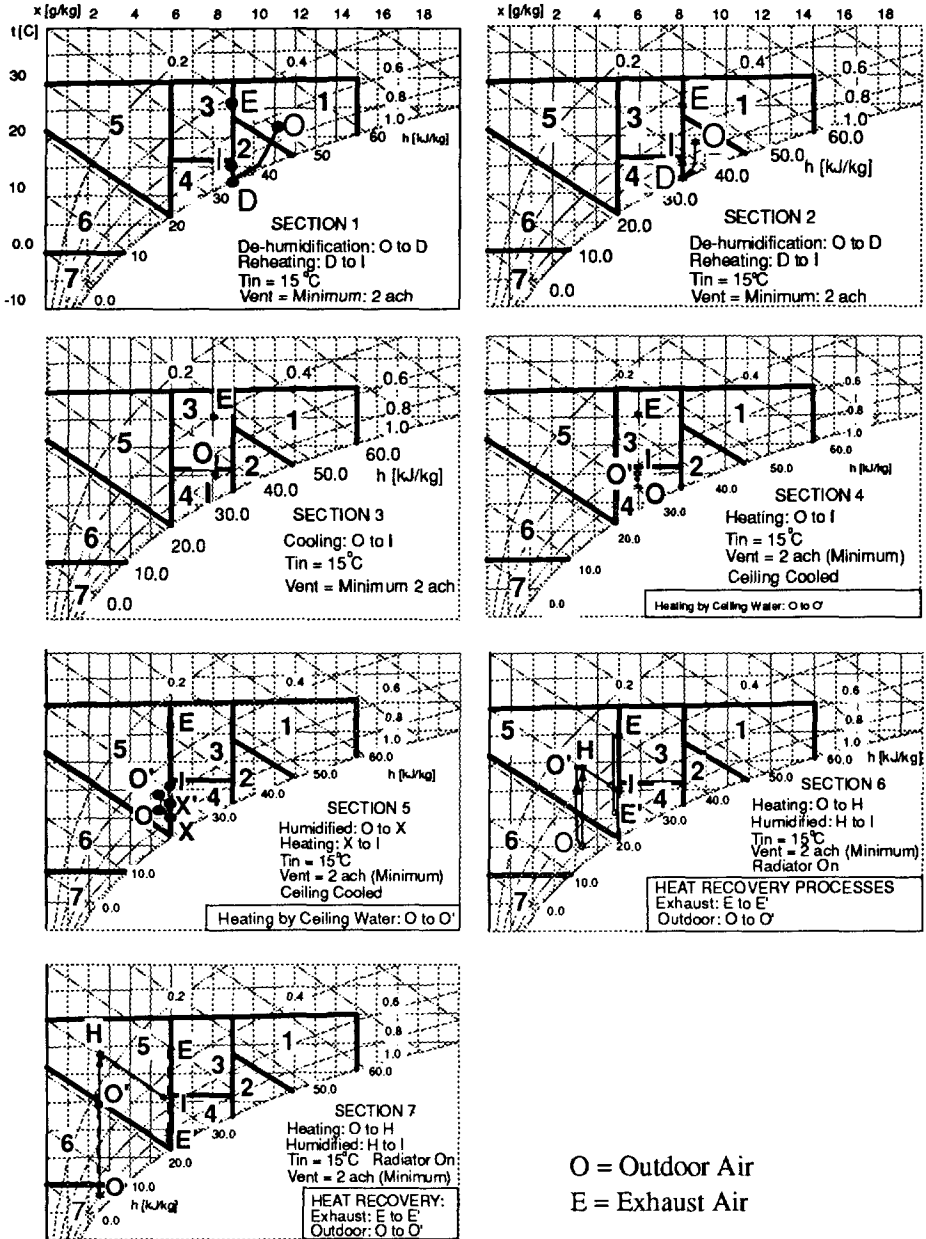


Figure 7.4a Air handling processes for cooling with CC system (optional heat recovery and possible free cooling using ceiling-water are illustrated)

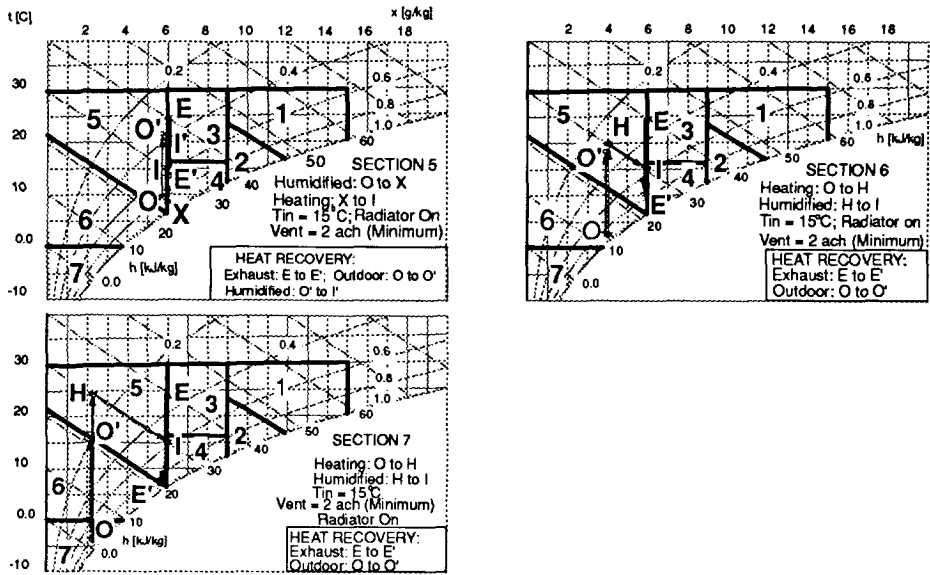


Figure 7.4b Air handling processes for heating with *CC system* (optional heat recovery processes are also illustrated)

Table 7.6 Energy consumption and cost in different seasons: *CC system* + minimum ventilation air

Sections in Psychr. Chart	Cooling Period				Heating Period		Cost in Dfl
	Chiller(kW.h)		Boiler (kW.h)	Fan (kW.h)	Boiler (kW.h)	Fan (kW.h)	
	Ceiling	AHU					
1	21.7	18.4	12.5	7.9	0	0	12.4
2	39.5	27.4	35.6	22.5	0	0	23.8
3	48.7	11.4	0.0	20.4	0	0	19.8
4	11.7	0.0	67.9	40.4	0	0	16.4
5	6.0	0.0	93.1	24.6	5.3	0.4	12.8
6	0.0	0.0	750.4	50.9	25.5	1.3	53.2
7	0.0	0.0	330.8	13.3	46.0	1.7	23.3
<b>TOTAL</b>	<b>127.6</b>	<b>57.2</b>	<b>1290</b>	<b>180.0</b>	<b>76.8</b>	<b>3.4</b>	<b>161.7</b>
Equivalent Primary Energy	383	172	1290	540	76.8	10.2	—

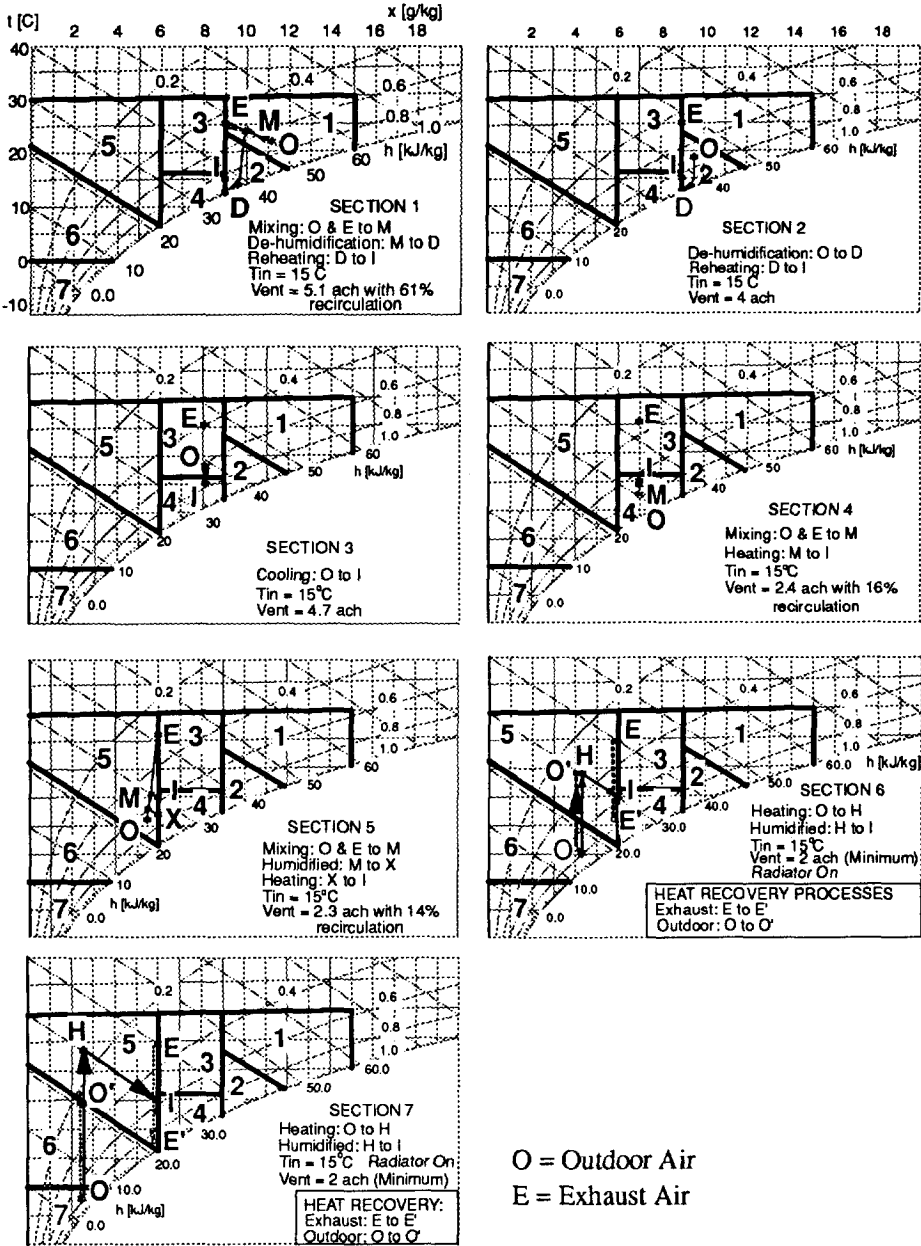


Figure 7.5a Air handling processes for cooling with VAV system (optional heat recovery processes are illustrated)

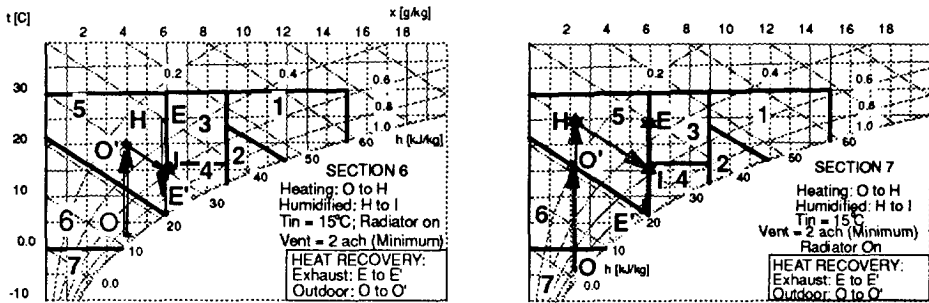
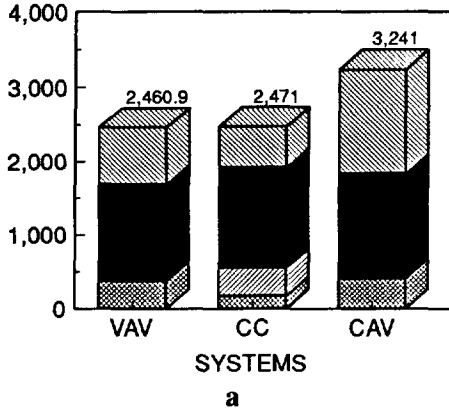


Figure 7.5b Air handling processes for heating with VAV system (optional heat recovery processes are also illustrated)

Table 7.7 Energy consumption and cost in different seasons: VAV system

Sections in Psychr. Chart	Cooling Period			Heating Period		Cost in Dfl
	Chiller (kW.h)	Boiler (kW.h)	Fan (kW.h)	Boiler (kW.h)	Fan (kW.h)	
1	41.8	32	20.3	0	0	16.9
2	54	71	45	0	0	28.1
3	27.1	0	48.5	0	0	18.6
4	0	9.8	48.2	0	0	12.4
5	0	65	29	0	0	10.5
6	0	736	51	25.5	1.3	52.5
7	0	331	13	46	1.7	23.2
Total	122.9	1245	255	71.5	3	162.2
Equivalent Primary Energy.	369	1245	765	71.5	9	—

Year Energy Consumption(kWh of P.E)



YEAR ENERGY COST (Dfl)

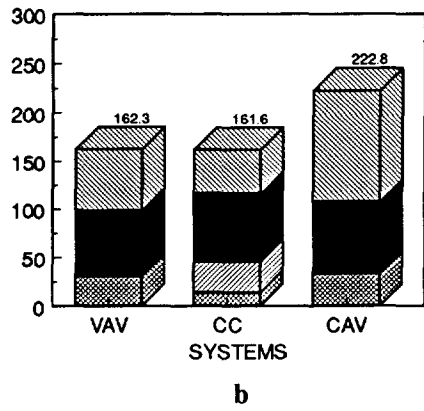
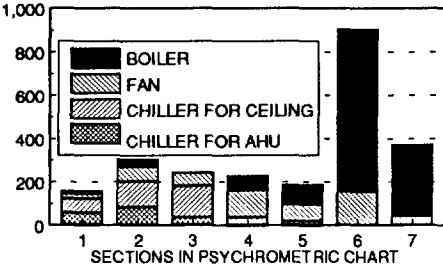
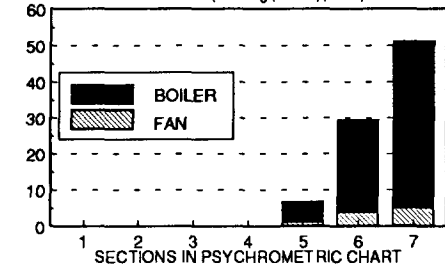


Figure 7.6 Comparison of: a. annual energy consumptions, and b. annual energy cost of CC system, VAV system and CAV system

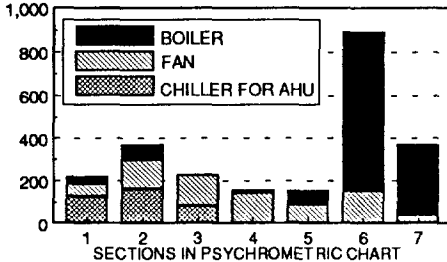
ENERGY CONSUMPTIONS(cooling period) (kWh)



ENERGY CONSUMPTIONS(heating period)(kWh)



ENERGY CONSUMPTIONS(cooling period) (kWh)



ENERGY CONSUMPTIONS(heating period)(kWh)

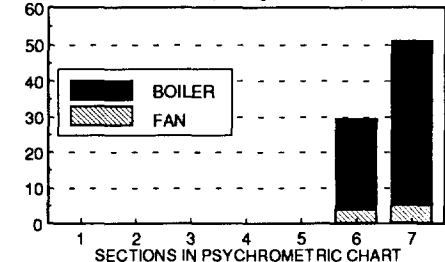


Figure 7.7 Primary energy consumption in different periods represented by the 7 sections in a psychrometric chart: with CC system(top) and VAV system(bottom)

The charts in Figure 7.6a indicates that the chiller consumes more energy in a CC system, while the fan energy is much lower. The reduced fan energy is obviously due to the fact that CC system always has a minimum air flow rate. But why does a CC system require more chiller energy? One reason is the increased cooling requirement in the room due to the radiant effect of the ceiling panels, as can be seen in Table 7.2 until Table 7.5. Moreover, there are other reasons associated with the system characteristics. Let us further analyze the energy consumption at different seasons represented by the 7 sections on the psychrometric chart. The primary energy consumptions in each section are shown in Figure 7.7. We can also compare the figures in Table 7.6 and Table 7.7. We can see that the chiller energy in section 1 is about the same for both systems. For sections 4 and 5, the VAV system does not require chilled water at all. This can be better understood by looking at the air-handling processes in the psychrometric chart(Figure 7.5a). The system tries to use the outdoor air as a free cooling source by changing the air volume, and also tries to use the recirculated air to reduce the heating energy required. In section 2, VAV system also consumes much less chiller energy for dehumidification purposes because of the relatively low outdoor temperature. In contrast, CC system only has a minimum air flow rate. When this amount of air is supplied at 15°C, the cooling capacity is not large enough to cool the room. Therefore, chilled water is required for the ceiling panels even in section 4 and section 5. At the same time, outdoor air is being heated up to 15°C. The eventual required chiller energy is higher in the CC system. It also should be noticed that the COP of the chiller is assumed to be constantly 3.5 in this calculation, irrespective of the varying outdoor temperatures and humidities. In the transient seasons, the COP might become higher due to lowered condenser water temperature, and therefore the required input electric power for the compressor would be lower than calculated here.

After these discussions, it can be generally concluded that the annual energy consumption of a CC system is not substantially different from that of a VAV all-air system. However, the inherent components are different, in terms of their association with equipments and seasons. A CC system consumes much less fan energy and reheating energy in section 1, which represents hot, humid weather conditions. Does this mean a CC system is a more energy-efficient system for hot, humid climate? The answer seems to be 'Yes'. Therefore, the differences in energy consumption between VAV system and CC system depends on their application climate. In fact, a report of the comparison of annual energy consumptions between CC systems and VAV all-air systems indicated that, in the Finnish climate, a CC system is less favourable for energy saving than a VAV system(Laine 1993).

### **7.6.3 Benefit of Heat Recovery**

Let us focus on the temperate climate conditions imposed in this simulation study. Looking at Figure 7.6, the energy required for heating constitutes a dominant part in terms of gross energy consumption, although the room considered predominantly requires cooling. In general, the heating energy consists of three parts. The first part is for air reheating, which is required after dehumidification. This happens in hot, humid outdoor conditions represented by sections 1 and 2 in the psychrometric chart. The second part is for the (pre)heating of the outdoor air to the required supply air temperature, and the subsequent heating required in the room to compensate the heat extraction by this amount of air. This



energy is mostly called ventilation energy losses. This energy happens in the cool seasons represented by section 4, 5, 6 and 7 in the psychrometric chart. The third part of heating required is to heat the room to compensate the conduction heat losses, which are the calculated heating loads as given in Table 7.3 and Table 7.4. This happens in section 6 and 7, but this amount is very small. Therefore, the main contributor is the ventilation energy loss. Since one advantage with a balanced ventilation system is the possible recovery of this heat, the possible benefits will be discussed here, based on the current simulation results.

Table 7.8 Benefit of Heat Recovery: VAV system

Sections in Psychr. chart	Saved Boiler Energy		Fan Energy Increase		Benefit
	kW.h	Dfl	kW.h	Dfl	Dfl
4	9.8	0.5	5.8	1.4	-0.9
5	65.0	3.4	3.5	0.9	2.5
6	517.0	26.9	6.3	1.5	25.3
7	195.0	10.1	1.8	0.4	9.7
Total	786.8	40.9	17.3	4.3	36.7

Table 7.9 Benefit of Heat Recovery: CC system

Sections in Psychr. chart	Saved Boiler Energy		Fan Energy Increase		Benefit
	kW.h	Dfl	kW.h	Dfl	Dfl
4	68.0	3.5	4.8	1.2	2.3
5	96.0	5.0	3.0	0.7	4.3
6	516.9	26.9	6.2	1.5	25.3
7	195.0	10.1	1.8	0.4	9.7
Total	875.9	45.5	15.9	3.9	41.6

Consider a fixed-plate exchanger as the exhaust/intake air heat exchanger. The arrangements in the systems are shown in Figure 7.1b. This is a sensible heat recovery device. The normal heat exchange effectiveness is about 70% at air face velocity of 3.6 m/s with air-pressure drop of 174 Pa (ASHRAE, 1988). With this effectiveness, the possible heat recovery processes are illustrated in Figure 7.4 and Figure 7.5, in sections 6 and 7 in both cooling and heating situations. Specifically, in section 5 with CC systems when the room needs heating, it is possible to heat-up the intake outdoor air up to a higher temperature than 15°C, so that less energy would be required for the radiator. This

accordingly needs change of the control strategy. In sections 4 and 5, it is obviously possible to completely avoid extra heating energy by modulating the heat recovery unit. With these analyses, a summary is given of the possible energy savings from the heat recovery unit (Table 7.8 and 7.9). In fact, the associated pressure rise requirement is also calculated. It can be seen that the annual energy saving is substantial. It should be mentioned that in the transient seasons, with VAV system, using heat recovery may substitute the return air, which will be favourable for improving indoor air qualities.

#### **7.6.4 Using Outdoor Air for Free-Cooling in CC System**

As mentioned in Section 7.6.2, in CC systems the free cooling capacity of outdoor air is limited in the seasons represented by sections 3, 4 and 5. However, a CC system has some unique characteristics, which can be employed to further reduce system energy consumptions. Some of the possibilities will be analyzed here.

In section 4 and 5, what is happening is that, while the outdoor air is heated-up to 15°C, ceiling panel is cooled with chilled water. This simultaneous heating and cooling is obviously not desired. The outdoor air temperature is respectively 12.7°C in section 4, and 11°C in section 5. The required chilled-water temperature is not lower than 20°C as indicated in Table 7.3. Therefore, from the point of view of heat transfer, the outdoor air is cool enough to provide the required water temperature for the ceiling panel, so that external cooling from the chiller can be eliminated. In fact, the average required cooling capacity is 65 W and 55 W (see Table 7.5) respectively in section 4 and 5. Using the water from the ceiling panels means that the same amount of energy can be used for the preheating of the outdoor air, and these heating processes are illustrated by the line O to O' in Figure 7.4a in the corresponding sections. The overall effect is that a better energy balance is achieved, avoiding running chiller system in sections 4 and 5 and at the same time reducing the heating energy required. This heat exchange processes can be realized by providing proper-piping between the ceiling panels and the pre-heat coil in the AHU (illustrated in Figure 7.1b by the dotted lines) and adopting proper control strategies.

Another possibility with a CC system is to use the water from the ceiling-panels for reheating of dehumidified air, which will reduce the chilled water requirement at the same time. As we can see from the psychrometric chart of section 1 and 2 in Figure 7.4a, the dehumidified air has to be reheated from 12.8 to 15°C after dehumidification. At the same, the outlet water temperature from the ceiling panel is higher than 20°C, and if it is used to heat-up the air, it will be cooled at the same time, so that the required cooling from the chiller will be by a certain amount less. This heat exchange process can be realised by providing proper-piping connecting the ceiling panels with the reheating coils in the AHU (represented by the dashed piping in Figure 7.1b).

With these two measures adopted, the possible energy savings are indicated in Table 7.10. The saving is substantial. Generally, these measures do not require much additional cost, rather they may benefit from proper arrangement of system components and proper piping between them, and adopting corresponding control strategies. Therefore, the associated technical feasibility and any increased cost deserve special investigations.

Although no detailed calculation is not done for air-panel type cooled-ceiling system, it is good to discuss some characteristics of the system in respect with energy consumptions. As indicated in the previous chapters, ventilation air can be supplied into

the ceiling panel at a relatively low temperature of around 13°C. This means reduced air volume and therefore reduced fan energy, and also reduced reheating energy.

Table 7.10 Possible energy savings in CC system by process integration

Sections in Psychr. Chart	CHILLER		BOILER		Total
	kW.h	Dfl	kW.h	Dfl	Dfl
1	2.7	0.7	12.5	0.6	1.3
2	7.6	1.9	35.6	1.8	3.7
4	11.8	2.9	55.0	2.9	5.8
5	6.1	1.5	28.0	1.5	3.0
Total	28.2	6.9	131.1	6.8	13.7

#### 7.6.6 Combination of Cooled-ceiling with Cooling Towers for Free Cooling

As indicated in Table 7.3, the required water temperature for ceiling-panels is relatively high, depending on the installed cooled-ceiling areas. This offers more opportunities for evaporative free cooling of using cooling tower. For rooms with an internal thermal load of 45 W/m<sup>2</sup> floor area, when ventilated by 2 ach of outside air cooled to 15°C, the required *minimum* water temperature is given in Table 7.11, corresponding to different ceiling areas. These data are obtained from three simulations performed with the short reference year weather data, and they are consistent with the design curves provided by the manufacturer. Small panel-area requires lower chilled-water temperature, which is not desired since condensation risks will become greater. 13°C may be the minimum chilled water-temperature allowed to the ceiling panels, depending on the fin-effectiveness of the panel. With larger ceiling panel area, higher water temperature will be allowed, which means reduced condensation risks and more opportunities for evaporative cooling. Of course, large area means higher initial cost. Ultimately, the designer is concerned both with the equipment cost for free cooling and with potential for energy savings. Each project demands these two contradictory directions. In addition, it is important to consider climate and load variations. Since the equipment costs are related to specific manufacturers, the present simulations are performed to estimate the possible energy savings in compressor running, addressing the climate and load conditions.

Table 7.11 Required minimum water temperatures for ceiling panels at different panel areas

Panel Area(%)	25	40	60
T <sub>w,i</sub> (°C)	13	15	>17

Table 7.12 Hourly temperature variations and heat extraction rates by mechanical cooling and evaporative free cooling

Time Hour	$Q_{air}$ (W)	$T_{op}$ (°C)	$Q_{chiller}$ (W)	$Q_{tower}$ (W)	$T_{d,b}$ (°C)	$T_{w,b}$ (°C)	$T_{w,i}$ (°C)
1	0	24.3	0		14.2	12.6	—
2	0	24.3	0	0	14.2	12.6	—
3	0	24.3	0	0	14.3	12.6	—
4	0	24.3	0	0	14.3	12.7	—
5	0	24.2	0	0	14.5	12.9	—
6	0	24.3	0	0	15.2	13.5	—
7	0	24.4	0	0	16.4	14.3	—
8	0	24.6	0	0	17.5	15	—
9	364	25.6	0	180	18.5	15.6	24.3
10	364	25.6	0	532	19.2	16	22.3
11	363	25.6	0	530	19.7	16.2	21.9
12	363	25.6	539	0	19.9	16.3	21.7
13	363	25.6	529	0	20	16.4	21.7
14	363	25.6	503	0	20.1	16.5	21.9
15	363	25.6	462	0	20.2	16.8	22.1
16	363	25.6	446	0	20.4	17	22.3
17	363	25.6	420	0	20.6	17.2	22.4
18	363	25.6	388	0	20.5	17.4	22.6
19	0	25.1	0	0	20.3	17.5	—
20	0	25.0	0	0	19.7	17.3	—
21	0	24.8	0	0	19	17	—
22	0	24.8	0	0	18.4	16.8	—
23	0	24.7	0	0	17.8	16.4	—
24	0	24.7	0	0	17.7	16.5	—

Consider the chiller systems illustrated in Figure 7.1 b. A heat exchanger is installed for indirect evaporative free cooling. Assume the size of the cooling tower is such that the *approach* is 4.5°C at the maximum design load. The additional heat exchanger can function properly with only a small temperature difference as low as 1.1°C. The cooled water temperature available for free cooling will be within 5.6°C above the wet-bulb temperature and lower in part load situations. In fact, with specific cooling tower, the cold water temperature available could be calculated rather precisely according to the specific tower performance curves. For the present simulation purposes, a constant approach of 5.6°C is assumed, i.e., the cooled water temperature directly available from the cooling tower (after heat exchange in the go-between heat exchanger) is calculated according to the formula

$$t_{w,i} = t_{w,b} + 5.6 \quad (^\circ\text{C})$$

At partial load, the water temperature can be lower than this temperature. Therefore, it should be noted that this assumption tends to under-estimate the free-cooling opportunity.

The operation strategy is that, whenever the required water temperature becomes lower than that directly-available from the cooling tower, the compressor will be switched off and the tower water will by-pass the condenser and goes through the special heat exchangers. Simultaneously, the panel water will by-pass the chiller and goes through the heat exchanger, too. By such an action, the running time of the compressor will be reduced. Table 7.12 presents a detailed simulation results of hourly variations on one day. The results indicate that in the first three working hours in the morning, the room can be cooled using water from the indirect cooling tower system. Comparison of the wet-bulb temperatures  $T_{w,b}$  in the night hours and the required water temperature  $T_{w,i}$  in the working hours indicates the great potentials of night cooling energy storage by using tower water.

Table 7.13 Energy savings using evaporative free cooling with different panel areas

Panel Area(%)		25	40	60
Energy Saved	kW.h	47	69	90
	Dfl.	12	17	22
	% of Annual Energy Cost	8	12	15
	% of Total Chiller Energy	25	37	49

Summary of the simulation results with different ceiling-panel areas is presented in Table 7.13. The results indicate the energy savings that can benefit from free-cooling with different ceiling panel areas. It is obvious that larger area offers some more energy savings. Even with 25% ceiling-panel area, the saving is still substantial. Such kind of data sets could be used for further life-cycle cost-effect analysis for a specific project.

### 7.6.7 CFC-free Evaporative Cooling

It is tempting to test if the compressor-driven chilled water system can be totally eliminated or substituted by a large size cooling tower in combination with large areas of ceiling panel installations. In view of the depletion effect of the chlorofluorocarbon type refrigerant CFC on the ozone layer, the totally-passive-cooling scheme will have significant benefit for global environment protection.

There are two possibilities for CFC-free evaporative cooling: 1. ceiling panel + evaporative air cooler system; 2. ceiling panel + open window ventilation. The cost of air cooler and the cost of ceiling panels have to be balanced to achieve an optimized or minimized life-cycle cost. As a demonstration, the present simulation will be done with the second scheme.

The simulated system is illustrated in Figure 7.8. The water is cooled to within 2.5 to 4°C of the wet-bulb temperature  $T_{wb}$  of the ambient air. The control schedule is: during the occupied period, the operative temperature of the room is maintained at 22°C; during the night(un-occupied), cooled water is supplied to maintain the room operative temperature in the room as low as 18°C, so that more night cooling energy can be stored in the thermal mass of the floor. Different from previous situations, the room is assumed ventilated with un-conditioned outside air, at a constant rate of 2 ach. The air enters the room through vent-openings integrated in the window and leaves the room through central exhausts. This air may provide night cooling and serve for ventilation purposes during the day. Since pump energy is minimal, the cool water flow rate through the panel is determined in such a way that the temperature rise over the ceiling panels is about 1°C at peak load.

As common with passive systems, what will happen is that the operative temperature tends to exceed the required comfort temperature at peak loads on the hot and humid days (as indicated in Figure 7.9). Also, excessive night cooling may impose a too low temperature in the room in the morning. Therefore, as a general rule for a passive system performance estimation, thermal comfort must be estimated together with energy saving analysis. To estimate these uncomfortable situations, the PMV (predicted mean vote) is calculated, according to which the so called PMV weighted number of temperature-exceeding hours (PWH) will be calculated if  $|PMV| \geq 0.5$ . For instance,  $PWH = 1.5$  if  $PMV = 0.7$  for each hour. A room is considered to be thermal-comfortably acceptable if the total PWH in a year are less than 150. Therefore, the total PWH in a year is used as an index to estimate the thermal performances of a cooling system.

A number of simulations have been performed, with different system parameters, such as, different cooled-panel areas, ceiling-panel constructions(open or closed), vertical air temperature stratifications in the room, internal cooling load, outdoor climate, as well as tower approaches(Niu & v.d. Kooi 1993, Subagyo 1993). These results are summarized in Table 7.14.

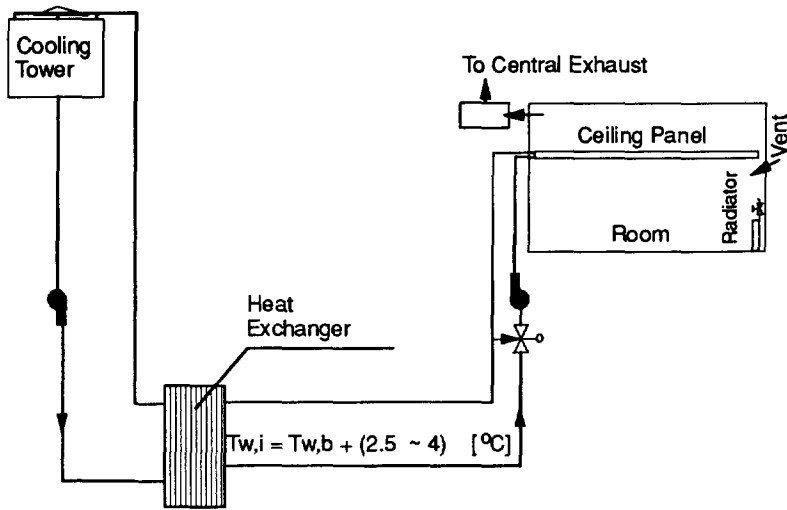


Figure 7.8 Schematic for CFC-free evaporative cooling system using cooled-ceiling technique

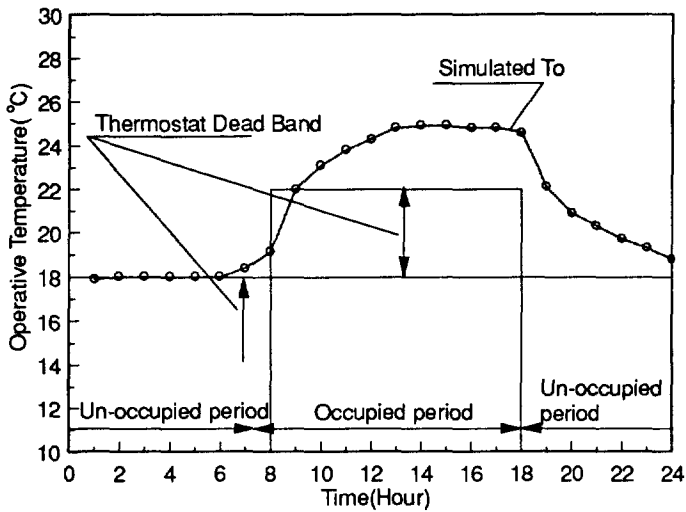


Figure 7.9 Thermostat setting and 'actual' simulated operative temperature variations on a hot day

It can be seen that the internal load is rather high in the cases investigated. It can be expected that, for a room with lower internal load, e.g., 30 or 40 W/m<sup>2</sup> floor area, a low percentage of cooled ceiling panels will be required. Therefore, it may be concluded that evaporative cooling in combination with cooled ceiling system is able to provide good thermal comfort for office buildings in the Dutch climate. The assumption that water can be cooled to within 2.5 to 4 °C of the wet-bulb temperature can be realized with a reasonable size of cooling towers available in the market. The energy saving in general will be substantial - all the chiller energy illustrated in Figure 7.5 will be saved with a small amount of additional fan and pump energies required for the tower operation. Of course, this will not be achieved without sacrifices of comfort standard. In this case, the lowered comfort is acceptable. This is extremely important when comparing the energy consumptions of a full-capacity, and mostly oversized mechanical system with a limited-capacity passive system. Therefore, the remaining question is if the associated equipment costs, especially the ceiling-panel costs, will impose a higher initial cost burden. A designer will face the task of balancing these two opposing forces. As mentioned in the beginning in this section, a combined evaporative air cooler system may reduce the panel area requirement. This combination deserves further investigations.

Table 7.14 Simulated room thermal comfort using evaporative cooling at different conditions<sup>(†)</sup>

Internal Load (W/m <sup>2</sup> )	Per- formance of Tower: Approach	Year 1964		Year 1971	
		PWH <sup>-</sup>	PWH <sup>+</sup>	PWH <sup>-</sup>	PWH <sup>+</sup>
60	2.5°C	265(416)	149(49)	173(354)	100(18)
60	4°C	264(409)	317(123)	167(350)	267(73)
50	4°C	108(738)	188(69)	91(780)	134(27)

PWH<sup>-</sup> counts when PMV ≤ -0.5;  
PWH<sup>+</sup> counts when PMV ≥ 0.5;  
<sup>(†)</sup> 70% ceiling area is installed with cooling panels; the two set figures of PWH correspond to the *assumption* that air temperatures near the ceiling are respectively 1.5 or 3°C above the average room air temperatures

Armed with a simulation program, the designer's analysis then depends on performances provided by the various equipment suppliers involved and on the suppliers' ability to assist the designer. As with any non-traditional application, the successful designer should work closely with the manufacturers of the major equipment (particularly the chiller, the heat exchanger and the cooling tower) to assure total system compatibility in terms of system performance and life-cycle cost.



## 7.7 CONCLUSIONS

This chapter demonstrates the possibilities using dynamic building simulation data for further annual energy analysis. The methodology, applied to all-air systems and CC systems, reveals some inherent characteristics of the two systems. The simulation results give following practical indications:

1. The radiant effect of horizontal ceiling panels will limit the heat storage capacity of the building envelope, and therefore tends to increase the required heat extraction rates in a room served by cooled-ceiling systems on one hand, and have an raised air temperature, and therefore increases the heat removal capacity of the supplied air on the other hand;
2. The overall effect is that the CC system has a compatible energy performances with the VAV all-air systems in the temperate Dutch climate;
3. CC system would have a better energy performances in hot, humid climate;
4. In the Dutch climate, with well-insulated building, application of heat recovery exchangers can be great beneficial for energy saving and improvement of indoor air qualities;
5. Through proper system-component arrangements and piping and the use of corresponding control strategy, a CC system can offer a better energy performance;
6. The numerical simulation of evaporative cooling for office buildings in combination with cooled ceiling system shows a promising potential of this passive cooling scheme for office-building cooling in the Dutch climate.
7. The present chapter by no means explores all the possibilities of using CC technique for free cooling, rather it mainly demonstrates the capabilities of the enhanced dynamic simulation program ACCURACY in assisting us to do this.

## CHAPTER 8

# CONCLUDING REMARKS AND RECOMMENDATIONS

Since conclusions have been given at the end of each chapter, here only some of the main points will be highlighted.

### 8.1 Turbulence Modelling and Its Applications

The present state-of-the-art turbulence modelling technique still contains a large number of empirical assumptions. The discretization-scheme and iteration solution procedure also introduce some errors. The success of the application still very much depends upon the users expertise and experience in this special field. Being aware of this fact, the current work given in this book presents some empirical 'tips' for the proper application of this technique, based on detailed experimental validations. The main 'tips' are:

1. Using the standard  $k$ - $\epsilon$  turbulence model, the predicted surface convective heat transfer has some unique dependence on the so-called first-grid distance. For convective boundary layers, much finer grid-spacing should be used so that the dimensionless distance  $y^+$  lies in the range around 9.2;
2. Alternatively, some experimentally obtained correlations about the surface convective heat transfer coefficients can be combined to set a fix-flux thermal boundary condition; the simulated results will become less grid-dependent in the near-wall region;
3. Using the Lam and Bremhorst low Reynolds number  $k$ - $\epsilon$  turbulence model, extremely fine grids will be required in the near-wall region to achieve solution convergence and good prediction correspondence. This imposes computing-time burden for practical purposes, especially when the simulated flow field domain has a large size. It is suggested that for small-size flow fields such a model be used;
4. Due to the iteration nature of the numerical solution algorithm, excessive iteration cycles will be required when dealing with buoyancy-driven flows; also, the convergence tends to be sensitive to the under-relaxation devices used. Therefore, it is essential that interpretation of the simulation results be based on good convergence;

5. For room air flow simulation, it is interesting to notice the influences of sizes of the exhaust air outlet on numerical convergence. Consider a room that has one air inlet and one air outlet. It is possible that some local small scale recirculation exists in the air exhaust outlet. In other words, there are some inflows at parts of the outlet surface. In such cases, assuming an constant external pressure as a kind of boundary condition for the exhaust will produce unexpected erroneous results or cause oscillation in the consequent iteration procedure, since the inflow parameters are not definitely specified. There are three possibilities to solve this problem. One is to extend the computation domain until inside of the exhaust duct where the flow is in one direction. This method requires extra computation, and therefore is recommended only when the flow details around the outlet are of interest. The second method is to give a fixed reference pressure at another location rather than at the outlet, and specify a fixed flux boundary condition at the outlet. The third possibility is to make the outlet in the simulation smaller than that in reality. The last approach is recommended if the flow details around the exhaust outlet are out of interest.

### **8.2 Building Thermal Dynamic Simulation Coupled with Cooled-ceiling Modelling**

It is found that such a rigorous simulation procedure that combines the ceiling-panel details with building component modelling is feasible. The radiant heat exchange effects on both the heat storage and thermal comfort can be taken into account. The convective parameters such as the panel surface convective heat transfer coefficients and air exchange rate through ceiling-openings are experimentally validated. Also, the enhanced dynamic simulation program ACCURACY allows some more complicated processes to be modelled such as the different air flow regimes through ceiling openings. The detailed information about the required ceiling-panel areas and chilled water temperatures calculated by the program provides the possibility to directly couple the primary HVAC equipment models for system energy and thermal performance analysis.

Some recent developments in quantifying human-beings' perception of thermal comfort are integrated in the whole simulation procedure. Therefore, thermal performance of any passive system can be estimated by the so-called PMV(Predicted Mean Vote) weighted temperature exceeding hours(PWH).

Detailed measurements of dynamic responses of a room to the cool-ceiling systems are compared with the simulation results. Comparison of the response curves validate the acceptable prediction accuracy of the program.

### **8.3 Combination of CFD and Building Dynamic Simulation**

Two possibilities are tested in the present research. One is to use CFD simulation to generate some correlations about the air exchange rate through ceiling-panels that can be used for the thermal dynamic simulation. It is found that extremely fine-grids around the ceiling panels will be required, and 3-dimensional simulation has to be performed to obtain good accuracy. Since discrepancies exists, it is suggested that, for practical purposes, this use should be supported by some kind of 'calibration' measurements.

The combined use of the two for indoor thermal comfort and contaminant distribution investigation is tested. It is found that large discrepancies of turbulent kinetic energies between simulation and measurements exists, and somewhat smaller discrepancies exist for the mean air flow parameters. As a result, draft risks tend to be over-predicted by

about 10%. Despite all these discrepancies, the results about high draft-risk regions, vertical temperature stratification in the occupied zone, as well as the contaminant concentration distribution are still reasonably indicated. Therefore, CFD simulation result analysis should take into account these discrepancies.

## 8.4 Some Practical Conclusions

### 1. Comfort and Ventilation Effectiveness

Based upon experimental and simulation comparisons of a base case, air flows in rooms respectively with three typical systems are analyzed using simulation. In agreement with previous experimental studies, a conventional displacement ventilation(DV) system tends to create a too high vertical temperature gradient in the occupied zone when cooling loads are higher than  $30 \text{ W/m}^2$  floor area. In comparison, the water-panel type cooled-ceiling(CC) combined with displacement ventilation system gives better thermal comfort in terms of draft risks and vertical temperature gradients in the occupied zone at cooling loads of up to  $50 \text{ W/m}^2$  floor area. The ventilation effectiveness  $\epsilon_v$  can be still much higher than one. The air-panel type cooled-ceiling(ACC) system presents a performance close to a mixed ventilation system, with the ventilation effectiveness  $\epsilon_v$  slightly higher than one. The high draft-risk region below the low-velocity air diffuser is small, and if the simulation discrepancy is taken into account, the draft risks are negligible at the cooling load up to  $50 \text{ W/m}^2$  floor area. The simulation results also indicate that performances of the ACC system can be much improved if the supply air diffuser is connected to the near floor level.

### 2. Energy Consumption

By coupling the building dynamic simulation with models for air-handling-unit and primary energy equipments, the annual energy consumptions of three types of air-conditioning systems are analyzed. Simulation results show that, in the Dutch climate, the water-panel type cooled-ceiling system fixed with a minimum volume of outdoor air has a comparable annual energy consumption as a variable-air-volume all-air system. The main difference is that a CC system consumes more energy for the chiller, and VAV consumes more energy for the air fan.

### 3. Energy Saving and Free-cooling

Based on the simulation results, some energy saving measures are estimated. It is indicated that, in the Dutch climate, much heating energy can be saved by applying the sensible heat recovery devices in ventilation systems in well-insulated office buildings.

Some unique energy saving possibilities associated with a CC system that are estimated in this research include: 1). using internal room heat via water-flow from ceiling-panels to heat up the ventilation air or to reheat dehumidified air in AHU; 2). using evaporative cooling to reduce chiller running hours; 3). eliminating chiller by using large size of cooling tower and large area of ceiling-panel. All these possibilities have application potentials. The first two measures may benefit from good-arrangement of system components and proper control strategy without necessarily increase additional installation cost. The third possibility require more rigorous estimation of the increased initial cost.

## 8.5 Remarks about CC Systems and Recommendations for Future Research

### 1. Condensation

Obviously, avoiding condensation should be considered with cooled-ceiling systems. Therefore, the effective control of the dew-point of the ventilation air in the coupled air-handling-unit is crucial, especially if the system is applied in hot, humid climates. In addition, a safeguard in the water-loop control to ensure that the minimum temperature that is admitted to the ceiling-panel is higher than the dew-point in the room will avoid condensation on the cooled-panel surface.

### 2. Air-panel type cooled-ceiling(ACC) system

In the present study, mainly thermal comfort performance and ventilation effectiveness are investigated for the ACC system. However, some impacts on annual energy consumption should not be overlooked. For instance, the required supply temperature can be generally lower than other all-air systems, because the air is *preheated in the ceiling panel by internal room heat*. Remembering that, in the ordinary air-handling-unit, the reheating of dehumidified air always consumes energy, this reheating by ceiling panels will reduce the heating energy required. The annual energy impact may be further investigated, using the present approach.

### 3. Simultaneous Heat and Moisture Transport Modelling

The present research has shown the application potentials of the evaporative free-cooling for office building cooling in the temperate Dutch climate, coupled with natural ventilation. There are two questions concerning humidity. The cooled-panel surface temperature will be mostly several degrees higher than the wet-bulb temperature of the outdoor air. However, due to the presence from any internal water-vapour sources, such as human body, the indoor air absolute humidity may be higher than the outdoor's. Therefore, the condensation risks should be estimated. Since the eventual indoor humidity will fluctuate very much, in comparison with conditioned-air supplies, any discomfort associated with excessive humidity should also be estimated. For these purposes, the combined heat and moisture storage and transport modelling will be very useful.

### 4. Using real performance curve and real physical size

In the present simulation, some general purpose performance indices are used to model the end energy use of the primary equipments, i.e. the air fans, chiller system, and the boilers, as well as the evaporative cooling tower. To estimate any temperature exceeding possibilities associated with the capacity limit of a specific equipment, models should take into account the physical size of the equipment. For instance, at present, the ceiling panel areas are counted in very detail. The same can be done in future to model a cooling tower, using the specific dynamic performance curve from a specific manufacturer.

### 5. Adopting Appropriate Control Strategy

In the present simulation study, control strategies are rather simplified. For instance, with the evaporative cooling, the night and day dual setting is assumed for the indoor thermostat. As a result, excessive cooling may be encountered in the morning. More

sophisticated control strategies such as predictive control may be integrated into the whole system to optimize the system performance.



## REFERENCES

Aiulfi, D., K. Fort, and T. Ottin, Modelization of floor heating and oil furnaces for the utilization of microprocessors in DDC, *Proceeding of CLIMA-2000: Vol.6: Heating, ventilating and air-conditioning systems*, Copenhagen 1985, pp.743-748

Alamdari, F. and G.P. Hammond, Improved data correlation for buoyancy-driven convection in rooms, *Rep.SME/IJ83/01*, Cranfield Institute of Technology, Cranfield, U.K., 1983

Allard, F. and Y. Utsumi, Airflow through large openings, *Energy and Buildings*, Vol.18, No.2, 1992, pp.133-145

Altmayer, E.F., A.J. Gadgil, F.S. Bauman, and R.C. Kammerud, Correlations for Convective Heat Transfer from Room Surfaces, *ASHRAE Transactions*, Vol.89, 1983, Part 2A, pp.61-77

*ASHRAE Handbook - 1985 Fundamentals*, Chapter 11 Air Contaminants, p.11.9

*ASHRAE Handbook-1987, HVAC Systems and Applications*, Chapter 2 All-air systems, pp.2.1-2.18

ibid. Chapter 3 Air-and-Water systems, pp.3.1-3.12

*ASHRAE Handbook-1988, Equipment*, Chapter 34 Air-to-air energy recovery equipment, pp.34.1-34.16

*ASHRAE Handbook - 1989 Fundamentals*, Chapter 8. Physiological Principles, Comfort, and Health, pp.8.20-8.22

*ASHRAE Handbook - Fundamentals*, 1989, Chapter 3 Heat Transfer, p.3.12

ASRHAE, *An anotated guide to models and algorithms for energy calculations relating to HVAC equipment*, 1990

*ASHRAE Handbook - 1993, Fundamentals*, Chapter 28 Energy Estimating Methods, p.28.20

Awbi, H. B. and M.M. Nemri, Scale effect in room air movement modelling, *Proceedings CLIMA 2000*, Aug. 27 - Sept. 1, 1989, Yugoslavia



Baker, A.J. and R.M. Kelso On Validation of Computational Fluid Dynamics: Procedures for room air motion prediction, *ASHRAE Transactions*, Vol.96, part. 1990, pp.760-771

Basset, M., *Infiltration and leakage paths in single family houses - A multizone infiltration case study*, AIVC technical notes TN 27, 1990

Boussinesq, J., 'Essai sui la theorie des eaux courantes', *Mem. Presentes Acad. Sci.*, 1877, vol. 23, p.46, Paris

Brouwers, G.F.M. and A.C. van der Linden, Beoordeling van het thermische binnenklimaat, *Klimaatbeheersing*, 18, 1989, nr.7, pp.257-264

Brown, W. G., Natural convection through rectangular openings in partitions. 2 - horizontal partitions, *Int. J. Heat Mass Transf.*, 5(1962), pp.869-878

Broyd, T. W., R.B. Dean, and S.G. Oldfield *et al.*, The use of a computational method to assess the safety and quality of ventilation in industrial buildings, *Int. Mech. Eng. Conference on Heat and Fluid Flow in Nuclear and Process Plant Safety*, London, 1983, C97/83, pp.65-74

Broyd, T.W., Deaves, D.M., and Oldfield S.G. The use of computational modelling techniques for cleanroom design, *Semicon/Europa 1983 Semiconductor Processing and Equipment Symposium*, Zurich, Switzerland, March 1983, pp.324-347

Charlesworth, P.S., *Air exchange rate and airtightness measurement techniques - An application guide*, AIVC application guide 2, 1988

Chen, Q., *The fundamentals of the computer code accuracy*, Promotion Report no.8, Laboratory for Refrigeration and Indoor Climate Technology, Delft University of Technology, Report No.126, 1987, The Netherlands

Chen, Q., J. van der Kooi, and A. Meyers, Measurements and Computations of Ventilation Efficiency and Temperature Efficiency in a Ventilated Room, *Energy and Buildings*, Vol.12, No.2, 1988, pp.85-99

Chen, Q., *Indoor Air Flow, Air Quality and Energy Consumption of Buildings*, Ph. D. Thesis, 1988, TU Delft

Chen, Q. and J. van der Kooi, ACCURACY: A computer program for combined problems of energy analysis, indoor air flow and air quality, *ASHRAE Transactions*, vol.94, part 2, 1988, pp.196-208

Chen, Q., C.A. Meyers, and J. van der Kooi, Convective Heat Transfer in Rooms with mixed Convection, *International Seminar on Indoor Air Flow Patterns*, Laboratory of Thermodynamics, university of Liege, Belgium, February 9, 1989

Chen, Q., T.G. Hoornstra, and J. van der Kooi, Energy Analysis of Buildings with Different Air Supply and Exhaust Systems, *ASHRAE Transactions*, vol.96, part 1, 1990, pp.344-356

Chen, Q. and J. van der Kooi, A Methodology for Indoor Air Flow Computations and Energy Analysis for a Displacement Ventilation System, *Energy and Buildings*, Vol.14, 1990, pp.259-271

Chen, Q., A. Moser, and A. Huber, Prediction of Buoyant, Turbulent Flow by a Low-Reynolds-Number  $k-\epsilon$  Model, *ASHRAE Transactions 1990*, V.96, Pt.1, pp.564-573

Chen, Q., P. Suter, and A. Moser, Evaluation of Indoor Air Quality by a Perceived Comfort Equation, *Proc. of Conference on Indoor Air Quality and Climate: Indoor Air90*, July 29 - August 3, 1990, Toronto, Canada

Chou, P.Y., On the velocity corrections and the solution of the equations of turbulent fluctuations, *Quart. Appl. Math.*, 1945, vol.3, pp.38-54.

Davis, M., Concluding Remarks at *International Seminar, Energy Savings in Buildings, The Hague, The Netherlands, 14 - 16 November 1983*, Commission of the European Communities, pp.799-801

Davidson, L., Second-order corrections of the  $k-\epsilon$  model to account for non-isotropic effects due to buoyancy, *Int. J. Heat Mass Transfer*, Vol.33, No.12, pp.2599-2608, 1990

Deardorf, J.W., A Numerical Study of Three Dimensional Turbulent Channel Flow at Large Reynolds numbers, *J. of Fluid Mechanics*, vol. 41, part 2, pp.453-480, 1969

Deardorf, J.W., The use of subgrid transport equations in a three dimensional model of atmospheric turbulence, *Trans. ASME, J. Fluid Eng.*, pp.429-438, Sept. 1973

Epstein, M., Buoyancy-driven exchange flow through small openings in horizontal partitions, *J. Heat Transfer*, 110, Nov. 1988, pp.865-893  
Fanger, P.O. and N. Christensen. Perception of draught in ventilated spaces, *Ergonomics*, 1986, Vol.29, No.2, pp.215-235

European Concerted Action Indoor Air Quality & Its Impact on Man. Report No. 11, *Guidelines for Ventilation Requirements in Buildings*. Office for Publications of the European Communities, Luxembourg, 1992

Fanger, P.O., *Thermal Comfort Analysis and Applications in Environmental engineering*. McGraw-Hill, New York, 1970

Fanger, P.O., *Thermal Comfort*, Robert E. Krieger Publishing Company, Malabar, FL., 1982

Fanger, P.O., and N. Christensen. Perception of draught in ventilated spaces, *Ergonomics*,

1986, Vol.29, No.2, pp.215-235

Fanger, P.O., A. Melikov, H. Hanzawa, and J. Ring Air Turbulence and Sensation of Draught, *Energy and Buildings*, 1988, No.1, pp.21-39

Fanger P.O., Introduction of the olf and the decipol units to quantify air pollution perceived by humans indoors and outdoors, *Energy and buildings*, 12;1988;1-6

Fanger, P. O. The new equation for indoor air quality, The Human Equation: Health and Comfort. *Proceedings of IAQ 89*, San Diego: American Society of Heating, Refrigerating, and Air Conditioning Engineers, Inc., pp.1-9.

Haghighat, F., Z. Jiang, and J.C.Y. Wang, Natural Convection and Air Flow Pattern in a Partitioned Room with Turbulent Flow, *ASHRAE Transactions*, vol.95, part 2, 1989, pp.600-610

Hammond, G.P. Profile analysis of heat/mass transfer across the plane wall-jet, *Proceedings of the 7th international Heat Transfer Conference*, Munich, Vol.3, pp.349-355, 1982

Hanzawa, H., A. Melikov and P.O. Fanger, Air flow characteristics in the occupied zone of ventilated spaces, *ASHRAE Transc.*, V.93, 1987, pp.524-539

Henkes, R.A.W.M. and C. J. Hoogendoorn, Comparison of turbulence models for the natural convection boundary layer along a heated vertical plate, *Int. J. Heat Mass Transfer*, Vol.32, No.1, pp.157-169, 1989

Henkes, R.A.W.M., *Natural convection boundary layers*, Ph.D. Thesis, Chapter 5, Delft University of Technology, The Netherlands, 1990

Holmes, M.J., J.K.M. Lam, K.G. Ruddick, and G.E. Whittle, Computation of conduction, convection and radiation in the perimeter zone of an office space, *Proceedings ROOMVENT'90 - Engineering Aero- and Thermodynamics of Ventilated Room, Second International Conference - Oslo, Norway*, June 13 -15, 1990

International Standard ISO 7730, *Moderate thermal environments - Determination of PMV and PPD indices and specification of the conditions for thermal comfort*, Ref. No. 7730-1984(E), August, 1984

Ito, N., K. Kimura, and J. Oka, A field experiment study on the convective heat transfer coefficient on exterior surface of a building, *ASHRAE Transactions*, Vol. 78, part 1, 1972

Jacob, M., *Heat Transfer*, Wiley, New York, 1949

Jones, B.W., K. Hsieh, and M. Hashinaga, The effect of air velocity on the thermal comfort at moderate activity levels. *ASHRAE Transactions*, Vol.92:2, Part 2B, 1986, pp.761-769

Jørgensen, F.E., Instrument for measurement of low air velocity in spaces, *Proc. CLIMA-2000*, Vol.6, Copenhagen, pp.587 - 592

Kerestecioglu H, M. Swami, P. Fairey, G. Lixing and S. Chandra, Modelling Heat, Moisture and Contaminant Transport in Buildings: toward a new generation software, USA, *Florida Solar Energy Center, FSECPF16589*, 1989

Khalifa, A.J.N. and R.H. Marshall, Validation of heat transfer coefficients on interior building surfaces using a real-sized indoor test cell, *J. Heat Mass Transfer*, Vol.33, No.10, pp.2219-2236, 1990

Kimura K., *Scientific Basis of Air Conditioning*, Applied Science Publishers Ltd., London, 1977, Chapter 3. Radiative and Convective Heat Transfer in Buildings, p.77

Knol K., New low pressure controlled air inlet, *Air infiltration review*, Vol.14, No.4, 1993, pp.9-11

Kooi J. van der and Chen Q. Numerical Simulation of Air Movement and Temperature Field in a Room with cold and Hot Window surface, *Proceedings of Euromech Colloquium 207 in Natural Convection*, April 7 - 9, 1986, Delft, the Netherlands

Kooi J. van der and Chen Q., Thermal Performance of a Room with Air Displacement Ventilation System, *Proceedings of the Second world Congress of Heating, Ventilating, Refrigerating and Air conditioning, CLIMA-2000*, Sarajevo, August 27 - September 1, 1989

Lafeber, M. 1987 *Numerical and Physical Aspects of Large Eddy Simulation of Turbulent Flows*, Ph. D. Thesis, Delft University of Technology, Delft, the Netherlands

Laine, T., *Cool ceiling system: for better control of office building indoor climate*, Proc. Indoor Air'93, Vol. 5, pp425-430)

Lam, C.K.G. and K. Bremhorst, A Modified Form of k- $\epsilon$  Model for Predicting Wall Turbulence, *Journal of Fluids Engineering, ASME Transactions*, 1981, Vol.103, pp.456-460

Lauder B.E. and D.B. Spalding, The Numerical Computation of Turbulent Flow, *Comp. Methods Appl. Mech. Eng.*, 1974, Vol. 3, p.269.

Liddament M.W. and A. Carolyn, *The validation and comparison of mathematical models of air infiltration*, AIVC Document AIC-TN-11-83, 1983

Liddament M.W., *Air-infiltration calculation techniques - An application guide*, AIVC application guide 1, 1986

Lonsdale R.D., The ASTEC code: *an algorithm for solving thermal hydrolic equations in complex geometries*, UK, AEA, Dounreay Nuclear Power Development Establishment,

1988

Lute, P.J., and A.H.C. van Paassen, Integrated control system for low energy buildings, *Proc. ASHRAE symposium Building Operation Dynamics*, Louis, Missouri, June 9-13, 1990

Lute, P.J., and A.H.C. van Paassen, Optimal predictive control of passive climate systems, paper presented at *The third international congress CLIMA-2000: Engineering the built environment*, London, November 1 -3, 1993

Markatos, N.C., Computer analysis of building ventilation and heating problems, *2nd International PLEA Conference, Crete, June 28 - July 1, 1983*. In *Passive and Low Energy Architecture*, Edited by Simos Yannas, Oxford: Pergamon, 1983, pp.667-675

Matsumoto H., F. Hasegawa, and Y. Utsumi, Numerical Analysis of room Air Distribution by the finite Element Method, *Journal of Architecture, Planning and Environmental Engineering(Transactions of AIJ)(in Japanese)*, No.352, 1985, pp.31-39

Matsumoto H, F. Hasegawa, and Y. Utsumi, Numerical Analysis of Air Flow and Pollution in Buildings, *Third International congress on Building Energy Management, III. Ventilation, air movement and air quality: field measurement and energy auditing*, Lausanne, Switzerland, September 28 - October 2, 1987

McIntyre, D.A., The effect of air movement on thermal comfort and sensation, In *Indoor Climate*, P.O. Fanger and O. Valbjorn, eds., Danish Building Research Institute, Copenhagen, 1979, pp.541-560

Mertz G., Chilled ceilings and ventilating systems - Thermal comfort and energy saving, *Air Infiltration Review*, 13.3;June 1992;7-10

Mierlo, W.J.M. van, *Onderzoek naar de nauwkeurigheid van het programma ENERK*, Rapport Nr. ST-255, Lab. Refrigeration and Indoor-Climat, Delft University of Technology, September 1986

Morant, M. A. and M. Strengnart, Simulation of a hydronic heating system: radiator modelling, *Proceeding of CLIMA-2000: Vol.6: Heating, ventilating and air-conditioning systems*, Copenhagen 1985, pp.725-730

Murakami S., S. Kato, and Y. Suyama, Three Dimensional Numerical simulation of Turbulent Air Flow in a ventilated Room by Means of Two Equation Model, *ASHRAE Trans.*, vol.93, part 2, 1987, pp.621-642

Murakami S., S. Kato, and Y. Suyama, Numerical and Experimental Study on Turbulence Diffusion Fields in Conventional flow type Clean Rooms, *ASHRAE Trans.*, vol.94, part 2, 1988, pp.469-493

Murakami, S., S. Kato, and Y. Suyama, Numerical Study on Diffusion field as affected by arrangement of supply and exhaust openings in convectional flow type clean room, *ASHRAE Trans.*, vol.95, part 2, 1989, pp.113-127

Murakami S. and S. Kato, Numerical and Experimental Study on Room air flow: 3-D predictions using the k- $\epsilon$  turbulence model, *Building and Environment*, vol. 24, No 1, 1989, pp.85-97

Murakami, S. and A. Mochida, Three dimensional numerical simulation of turbulent flow around buildings using the k- $\epsilon$  turbulence model, *Building and Environment*, vol.24, No 1, 1989, pp.51-64

Nielson, P.V., Progress and Trends in Air Infiltration and Ventilation Research. *Proc. 10th AIVC conf.*, Convetry: Air Infiltration and Ventilation Centre, 1989

Nieuwstadt, F.T.M. and Brost, R.A., The Decay of Convective Turbulence, *J. Atm. Sci.*, 1986, Vol.43.6, pp.532-546

Niu, J. *Experimental Validation of Numerical Simulation of Natural Convection and Heat Transfer in an Enclosed Room*, Internal Report nr. K -170: Lab. Koudetechniek en Klimatregeling, Delft University of Technology, Delft, The Netherlands, August, 1991

Niu, J. and A.H. Visser, Numerical Simulation and Experimental Investigation of Natural Convection in an Enclosed Room, *PHOENICS UK Users Meeting, London, 1991*, CHAM Ltd., p.35

Niu, J. and J. van der Kooi, 2-dimensional simulation of air flow and thermal comfort in a room with open-window and indoor cooling systems, *Energy and Buildings*, vol.18, No.1, 1992, pp.65-75

Niu, J. and J. van der Kooi, Grid Optimization of k- $\epsilon$  Turbulence Modelling of the Natural Convection in Rooms, *Proceedings ROOMVENT-92 Air Distribution in Rooms - Third International Conference*, Vol.1, pp.207-pp.223, Aalborg, Denmark, Sept. 4-6, 1992

Niu, J. and J. van der Kooi, Numerical Investigations of Thermal Comfort and Indoor Contaminant Distributions In a Room with Cooled Ceiling Systems, *Proceedings of INDOOR AIR 93 - the 6th International Conference on Indoor Air Quality and Climate*, Vol.5, pp.331-336, Helsinki, Finland, July 4-8, 1993

Niu, J. and J.V.D. Kooi, Dynamic Simulation of Combination of Evaporative Cooling with Cooled Ceiling Systems for Office Room Cooling, *Proceedings Building Simulation 93 - Third International Conference*, Adelaide, Australia, 16-18, August 1993, pp.407-412

Niu, J. and J. van der Kooi, A dynamic cooling load program for cooled ceiling systems and its validation in a climate room, paper presented at *The third international congress*

*CLIMA-2000: Engineering the built environment*, London, November 1 -3, 1993

Niu, J. and J. van der Kooi, Thermal Climate in Rooms with Cool Ceiling Systems, *Building and Environment*, 1994, No.29.3

Nobile E., T. Russo, and G.S. Barozzi, An efficient parallel algorithm for the numerical solution of Navier-Stokes equations using FORTRAN structured multiprogramming, In *Applications of supercomputers in engineering: Fluid flow and stress analysis applications - Proceedings of the first international conference*, Southampton, UK, September 1989, C.A. Brebbia and A. Peters, eds., Elsevier and Computational Mechanics Publications, 1989

Oegema, S.W.T.M., *De berekening van het binnenklimaat in gebouwn met behulp van een digital rekenautomaat*, Applied Physics Department, Delft university of Technology, Delft, The Netherlands, 1970

Olesen, B.W., M. Scholer, and P.O. Fanger, Vertical air temperature differences and comfort, In *Indoor Climate*, P.O. Fanger and O. Valbjorn, eds., Danish Building Research Institute, Copenhagen, 1979, pp.561-579

Ozoe, H, A. Mouri, M. Ohmuro, S. W. Churchill and N. Lior, Numerical calculations of laminar and turbulent natural convection in water in rectangular channels heated and cooled isothermally on the opposing vertical walls. *Int. J. Heat Mass Transfer* 28, pp.125-138, 1985

Paassen, A.H.C. van, Control aspects of indoor climate technology, *Journal A*, Vol.22, No.3, 1981

Paassen, A.H.C. van, *Indoor climate, outdoor climate and energy consumption*, Ph.D. Thesis, WTHD-137, Delft University of Technology, 1981

Paassen, A.H.C. van, Design of low energy HVAC-systems with a computerized psychrometric chart - A designer-friendly method for energy calculations, *Proc. the international conference on system simulation in buildings*, Liege, Belgium, December 1-3, 1986

Paassen, A.H.C. van, Passive solar energy in intelligent buildings, *ASHRAE Trans.*, V.94, part 1, 1988, pp.1289-1297

Paassen, A.H.C. van and P.J. Lute, Performance and feasibility of passive climate systems, paper presented at *The third international congress CLIMA-2000: Engineering the built environment*, London, November 1 -3, 1993

Patankar, S.V., *Numerical Heat Transfer and Fluid Flow*, Chapter 7, pp.139 - 143., Hemisphere Publishing Corporation, 1980.

Patankar, S.V., Recent Developments in Computational Heat Transfer, *Transactions of the ASME - J. Heat Transfer*, Nov. 1988, Vol. 110, pp.1037-1045

Patel V.C., W. Rodi, and G. Scheuerer, Turbulence models for near wall and low Reynolds number flows: a review, *AIAA Journal*, Vol.23, No.9, pp.1308-1319, 1985

Peutz & Associés Adviesbureau, *Onderzoek naar bouwfysische eigenschappen van thermisch open plafonds*, Rapport nr. E 131-3, Nijmegen, December 1986

Peutz & Associés Adviesbureau, *Onderzoek naar bouwfysische eigenschappen van thermisch open plafonds in een mechanisch geventileerde ruimte, meet-programma en computersimulatie*, September 1988

Renz, U. and U. Terhaag, Predictions of air flow pattern in a room ventilated by an air jet - the effect of turbulence model and wall function formulation, *Proc. of ROOMVENT-90: Engineering Aero- and Thermodynamics of Ventilated Room, Second International Conference*, Oslo, Norway, June 13-15,1989

Rosten, H. I. and D. B. Spalding, *The PHOENICS Reference Manual*, Chapter 6, CHAM TR/200, Oct. 1987, pp.6.91-6.92

Sandberg, M., Definition of ventilation efficiency and the efficiency of Mechanical ventilation systems. *3rd AIC Conference Energy Efficient Domestic Ventilation Systems for Achieving Acceptable Indoor Air Quality*, September 20-23, 1982, U.K., PP.13.1-13.22

Sandberg M and C. Blomqvist, Displacement ventilation in office rooms. *ASHRAE Trans.* 95;1989;1041-9

Siegel, R. and J.R. Howell, *Thermal Radiation Heat Transfer*, McGraw-Hill Book Co., Inc., New York, 1981, pp.798-799

Skaret, E. and H. Mathisen, Ventilation Efficiency. *International Symposium on Indoor Pollution, health and Energy Conservation*, Massachusetts 13-16 October 1981

Skarret E., Displacement ventilation, *Room Vent 87, International conference on air distribution in ventilated spaces*, Stockholm, 1987

Steimle, F., Development of Modern Heating Technology, *International Seminar, Energy Savings in Buildings, The Hague, The Netherlands, 14 -16 November 1983*, Commission of the European Communities, pp.30-40

Strub, A., Opening Address at *International Seminar, Energy Savings in Buildings, The Hague, The Netherlands, 14 -16 November 1983*, Commission of the European Communities, pp.6-9



Subagyo, D.A., *Metingen en Berekeningen aan een Koelplafond*, Rapport Nr. KK 1059, Lab. Refrigeration and Indoor-Climat, Delft University of Technology, December 1993

Sun, T.Y., Shadow area equations for window overhangs and side fins and their application in computer calculation, *ASHRAE Semi-annual Meeting*, Ohio, Paper no. 2059, 1968

Tennekes, H. and J.L. Lumley, *A First Course in Turbulence*, The MIT Press, 1978, Chapter 3. The Dynamics of Turbulence, p.97

Thompson, C.P., Leak G. K., and Vanka S. P. *Application of a Multigrid method to a buoyancy -induced flow problem*, Argonne National Laboratory, USA, 1988

Thorshauge, J., Air velocity fluctuations in the occupied zone of ventilated spaces, *ASHRAE Trans.*, 1982, v.88

Tsutsumi, J., Numerical Simulation of Thermal Convection in a Room with Natural Ventilation Caused by Buoyancy, *International CIB W67 Symposium on Energy Moisture and Climate in Buildings*, Sept. 1990, Rotterdam, The Netherlands

Vanka, S.P. and K.P. Misegades, Vectorized multigrid flow calculations on a Cray XMP/48, *International Journal for Numerical Methods in Fluids*, vol.7, 1987, pp.635-648

Wang, H. W., *Modelling of a Refrigerating System Coupled with a Refrigerated Room*, Ph. D. Thesis, Delft University of Technology, The Netherlands, 1991, Chapter 7, pp.178-180

Wilkins C.K. and R. Kosonen, Cool ceiling system: A European air-conditioning alternative, *ASHRAE Journal*, August 1992;41-45

Wilson, D and I. Walker, *Infiltration data from the Alberta home heating research facility*, AIVC technical note TN 41, 1993

Wong, H.Y., *Heat Transfer for Engineers*, Longman, London, 1977

Zhang, J.S., L.L. Christianson, and G.L. Riskowski, Regional airflow characteristics in a mechanically ventilated room under non-isothermal conditions, *ASHRAE Transactions*, Vol.95, Part 2, 1989

## APPENDIX A

### Principles of Determination of Air Exchange by Tracer-gas Techniques

The idea of using tracer gas technique to measure air change rate is not new. However, for the interpretation of the measurements of air exchange through the ceiling openings, some specific mathematical formulation will be required. The present contents are the deduction of these formulas.

Consider a room with two air spaces - the cavity above the ceiling and the room below the ceiling. Due to buoyancy effect, natural convection will occur, which causes convective air exchanges between the cavity above the ceiling and the room. To investigate this buoyancy effect, no external air is supplied. Imagine that a tracer gas is supplied uniformly into the room and quickly mixed in the room (Figure A.1 a). Then we have a concentration of  $C_{R,0}$  in the room and a  $C_{C,0}$  in the cavity. After the tracer gas is switched off, the concentration in the room will decay while the concentration in the cavity will increase, as indicated in Figure A.1 c. Ultimately, the concentration will reach the equilibrium state, with a uniform concentration  $C_b$  through out the room (Figure A.1 b). This decay/increase process can be described by the following mathematical method. Consider the cavity and the room as two well-mixed chambers. Then we have balance equation of the tracer gas in the room volume:

$$v (C_R - C_C) = -V_R \frac{dC_R}{d\tau} \quad (A.1)$$

,  
balance equation of the tracer gas in the cavity space:

$$v (C_R - C_C) = V_C \frac{dC_C}{d\tau} \quad (A.2)$$

,

and mass conservation of the tracer gas in the whole space:

$$V_c C_c + V_R C_R = (V_c + V_R) C_b \quad (\text{A.3})$$

From Equation (A.3), we get

$$C_R = \left(1 + \frac{V_c}{V_R}\right) C_b - \frac{V_c}{V_R} C_c \quad (\text{A.4})$$

Substitute  $C_R$  in Eq.(A.2) with Eq.(A.4), we get

$$v \left(1 + \frac{V_c}{V_R}\right) (C_b - C_c) = V_c \frac{dC_c}{d\tau} \quad (\text{A.5})$$

Let  $C_{b-c} = C_b - C_c$ , and, since  $C_b$  is a constant, Equation (A.5) can be changed into

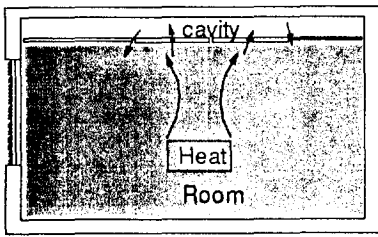
$$- \frac{dC_{b-c}}{C_{b-c}} = \frac{v}{V_c} \left(1 + \frac{V_c}{V_R}\right) d\tau \quad (\text{A.6})$$

Integration of Equation (A.6) yields

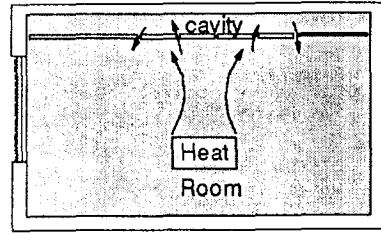
$$\ln \frac{C_{b-c,0}}{C_{b-c}} = \frac{v}{V_c} \left(1 + \frac{V_c}{V_R}\right) (t - t_0) \quad (\text{A.7})$$

where,  $C_{b-c,0} = C_b - C_c(t_0)$ . That is to say, the logarithm of the dimensionless concentration is directly proportional to the time. Therefore, if the concentration increase in the cavity is measured, and results are plotted according to Equation(A.7), then the air exchange rate is related to the slope  $k$  of the curve(Figure A.1 d) according to the equation

$$v = k \frac{V_c}{1 + V_c / V_R} \quad (\text{A.8})$$



a



b

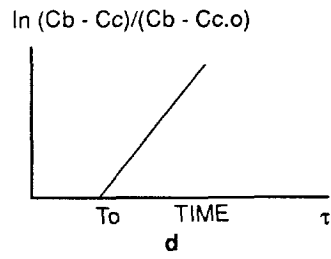
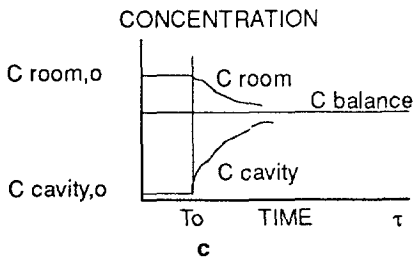


Figure A.1 The respective decay and increase of tracer gas concentration in the room and cavity



## NOMENCLATURE

A:	Area of a surface	$m^2$
$A_i$ :	Area of surface i	$m^2$
Ar:	Archimedes number(= $\beta g d \Delta T_o / u_o$ )	[-]
$\alpha$ :	Thermal diffusivity( = $\lambda / (\rho C_p)$ )	$m^2/s$
$a_c$ :	Cloud cover ratio	[-]
$a_s$ :	Weighting factor for calculation of operative temperature	[-]
$a_i$ :	Weighting factor for calculation of mean water temperature in the panel	[-]
$a_{od}, a_{oi}$ :	Absorptivities of an outside wall surface to direct and diffuse solar radiation	[-]
Br:	Emissivity of the atmosphere	[-]
$C_b$ :	Equilibrium tracer gas concentration in the room	$mg/m^3$
$C_c$ :	Tracer-gas concentration in the cavity	$mg/m^3$
$C_e$ :	Pollutant concentration in the exhaust air	decipol
$C_i$ :	Pollutant concentration in the occupied zone	decipol
$C_p$ :	Specific heat of air	J/(kg K)
$C_{p,w}$ :	Specific heat of water	J/(kg K)
$C_R$ :	Tracer-gas concentration in the room	$mg/m^3$
$C_1, C_2,$ $C_3, C_\mu$ :	Empirical coefficients in the k- $\epsilon$ turbulence model	[-]
D:	Modified term in k equation in low Reynolds number k- $\epsilon$ models or the width of a horizontal opening or the hydraulic diameter of air duct	W/kg m m
E:	Modified term in $\epsilon$ equation in low Reynolds number k- $\epsilon$ models	W/kg
$F_{i,j}$ :	View factor from surface i to surface j	[-]
$f_d$ :	Surface area ratio of clothed-man to nude-man	[-]
$f_\mu, f_1, f_2$ :	Functions in low Reynolds number k- $\epsilon$ models	[-]
G:	Irradiation of a surface or Supplied water flowrate in the ceiling panel	$W/m^2$ kg/s
$G_B$ :	Buoyancy production term in k equation	W/kg
Gr:	Grashof number( = $L^3 \rho^2 \beta g (\Delta t) / \mu$ )	[-]
g:	Gravitational acceleration	$m/s^2$
$g_i$ :	The ith direction component of gravity	$gm/s^2$
H:	Enthalpy	J/kg
$H_0$ :	Reference enthalpy	J/kg
h:	Convective heat transfer coefficient	$W/(m^2 K)$
$h_o$ :	Convective heat transfer coefficient of ceiling-panel surface	$W/(m^2 K)$

I:	Turbulence intensity	[-]
$I_d$ :	Thermal resistance of clothing	$m^2C/W$
$I_{De}$ :	Direct solar radiation on a tilted surface under a cloudy sky	$W/m^2$
$I_{dca}, I_{dca}$ :	Diffuse and reflect solar radiation on a vertical surface	$W/m^2$
J:	Radiosity of a surface	$W/m^2$
$K_c$ :	Cloud reduction factor	[-]
k:	Turbulence kinetic energy	$J/kg$
L:	Characteristic length	m
L/D:	Aspect ratio of horizontal opening	[-]
l:	Mixing length	m
M:	Metabolic rate	$W/m^2$
$m'$ :	Air flow rate through a horizontal opening	$m^3/s$
N:	Number of sampling points	[-]
Nu:	Nusselt number( = $\alpha L / \lambda$ )	[-]
n:	Total number of enclosure surfaces	[-]
$P_a$ :	partial water vapour pressure	Pa
$P_k$ :	Production term in k equation	$W/kg$
PD:	Percentage dissatisfied due to draft	%
PMV:	Predicted Mean Vote	[-]
PWH:	PMV weighted temperature-exceeding hours	hour
Pr:	Prandtl number( = $\mu c_p / \lambda$ )	[-]
p:	Modified static pressure	$N/m^2$
$p_{new}$ :	Pressure value of the present iteration	$N/m^2$
$p_{old}$ :	Pressure value of the previous iteration	$N/m^2$
$p_s$ :	Static pressure	$N/m^2$
$Q_s$ :	Total transmitted solar radiation through fenestration	W
$Q_{ext}$ :	Heat extraction by mechanical ventilation	W
$Q_{c,i}$ :	Convective heat from wall surface i	W
$Q_{ic}$ :	Internal convective heat	W
$Q_{inf}$ :	Heat of air infiltration	W
$q_{c,i}$ :	Convective heat exchange of surface i to room air	$W/m^2$
$q_o, q_M$ :	Heat fluxes through outside and inside wall surfaces	$W/m^2$
$q_{o,ex}$ :	Extra heat radiation absorbed by an outside wall surface	$W/m^2$
$q_{o,rc}$ :	Combined radiative and convective heat loss of outside wall surface	$W/m^2$
$q_{ir,i}$ :	Internal radiation apportioned to surface i	$W/m^2$
$q_{r,i-k}$ :	Radiant heat exchange between surface i and k	$W/m^2$
$q_s$ :	Absorbed solar radiation of outside wall surface	$W/m^2$
$q_{s,i}$ :	Solar radiation apportioned to surface i	$W/m^2$
$q_{ti}$ :	Wall heat conduction flux through inside surface	$W/m^2$
$q_z$ :	Modified sky radiation of a outside wall surface	$W/m^2$
Re:	Reynolds number ( = $ud/v$ )	[-]
$Re_k$ :	Local turbulence Reynolds number( = $k^{1/2} y/v_1$ )	[-]
$Re_p$ :	Local turbulence Reynolds number( = $k^2/v_1 \epsilon$ )	[-]
S:	Skin friction factor	[-]
$S_D$ :	Shading factor for direct solar radiation	[-]

$S_{dcs}$ :	Shading factor for sky diffuse solar radiation	[-]
$S_{dcf}$ :	Shading factor for ground reflective solar radiation	[-]
$S_{\Phi}$ :	Source term of $\Phi$ transport equation	
$T$ :	Temperature	K
$T_a$ :	Ambient air temperature or Mean room air temperature	K
$T_{d,b}$ :	Dry-bulb temperature of the ambient air	°C
$T_e$ :	Ground surface temperature	K
$T_{sup}$ ,		
$T_{ext}$ :	Supplied and extracted air temperatures	°C
$T^{\circ}$ :	Overall transmission coefficient to direct solar radiation	[-]
$T_c$ :	Cavity air temperature	K
$T_m$ :	Temperature of the middle-layer of a multi-layer window	K
$T_{m0}$ :	Temperature of the air-layer between the middle- and outside- layer of a multi-layer window	K
$T_{mi}$ :	Temperature of the air-layer between the middle- and inside- layer of a multi-layer window	K
$T_{mr}$ :	Mean radiant temperature	K
$T_{p,i}$ ,	Temperature of ceiling-panel surface facing the room	K
$T_{p,c}$ :	Temperature of ceiling-panel surface facing the cavity	K
$T_r$ :	Room air temperature	K
$T_{r,i}$ :	Local air temperature	K
$T_{s,i}$ :	Supplied air temperature to the air-panel	K
$T_{s,o}$ :	Air temperature leaving the air-panel	K
$T_w$ :	Mean water temperature in the ceiling-panel	K
$T_{w,b}$ :	Wet-bulb temperature of the ambient air	°C
$T_{w,i}$ :	Inlet water temperature of the ceiling-panel	K
$T_{w,o}$ :	Outlet water temperature of the ceiling-panel	K
$T^+$ :	Dimensionless temperature( = $(T_w - T) / T_{\tau}$ )	[-]
$T_{\tau}$ :	$T_{\tau} = -v / (Pr u_{\tau}) (\partial T / \partial y)_w$	K
$T_0$ :	Reference temperature	K
$t_a$ :	Air temperature	°C
$t_{cl}$ :	Surface temperature of clothing	°C
$t_{mr}$ :	Mean radiant temperature	°C
$t_o$ :	Operative temperature	°C
$t_f^{\circ}$ :	Overall transmission to ground reflections	[-]
$t_s^{\circ}$ :	Overall transmission to diffuse solar radiation	[-]
$U$ :	Overall heat transmission coefficient	W/(m <sup>2</sup> K)
	or Wind velocity	m/s
$u$ :	Air velocity near building surface	m/s
$u_i$ :	Velocity component in $x_i$ direction	m/s
$u_i'$ :	Instantaneous air velocity fluctuation	m/s
$u_{i,max}$ :	Maximum velocity in the $i$ th direction	m/s
$u_{\tau}$ :	Friction velocity	m/s
$u^+$ :	Dimensionless velocity( = $u / u_{\tau}$ )	[-]



$V_a$ :	Magnitude of air velocity	m/s
$V_C$ :	Cavity space volume	$m^3$
$V_o$		
$V_{m-o}$ :	Infiltration and exfiltration rates per unit area through the outside layer of a multi-layer window	m/s
$V_{m-o-i}$		
$V_{m-i-o}$ :	Infiltration and exfiltration rates per unit area through the middle layer of a multi-layer window	m/s
$V_{m-i-i}$		
$V_i$ :	Infiltration and exfiltration rates per unit area through the inside layer of a multi-layer window	m/s
$V_R$ :	Room space volume	$m^3$
$v$ :	Air volume of ventilation	$m^3/s$
	or Air exchange rate through ceiling openings	$m^3/s$
$W$ :	External work	$W/m^2$
$W_b$ :	Emissivity of a black body	$W/m^2$
$WF$ :	Weighting factor	[-]
$x, y, z$	Cartesian coordinates	m
$y$ :	Distance of the first grid from the wall	m
$y^+$ :	Dimensionless first grid distance from the wall( = $y u_f/\nu$ )	[-]
$x_i$	tensor notation of Cartesian coordinates	m

**Greek Symbols:**

$\alpha$ :	Relaxation factor	[-]
$\alpha_{c,i}$ :	Inside wall surface convective heat transfer coefficient	$W/(m^2 K)$
$\alpha_{i,o}$ :	Outside surface convective heat transfer coefficient of the inside layer of a multi-layer window	$W/(m^2 K)$
$\alpha_{m,i}$		
$\alpha_{m-o}$ :	Inside and outside surface convective heat transfer coefficients of the middle layer of a multi-layer window	$W/(m^2 K)$
$\alpha_{o,i}$ :	Inside surface convective heat transfer coefficient of the outside layer of a multi-layer window	$W/(m^2 K)$
$\alpha_o$ :	Convective heat transfer coefficients of ceiling-panel or combined heat transfer coefficient of an outside wall surface	$W/(m^2 K)$
$\alpha_{o,c}$ :	Convective heat transfer coefficient of an outside wall surface	$W/(m^2 K)$
$\alpha_{o,r}$ :	Radiative heat exchange coefficient between an outside wall surface and the sky	$W/(m^2 K)$
$\alpha_{p,c}$ :	Convective heat transfer coefficient of panel surface facing the cavity	$W/(m^2 K)$
$\alpha_{p,r}$ :	Convective heat transfer coefficient of panel surface facing the room	$W/(m^2 K)$
$\alpha_{r,j,k}$ :	Radiative heat exchange coefficient between surfaces j and k	$W/(m^2 K)$
$\alpha_{r,m-i}$ :	Radiative heat exchange coefficient between the middle-layer and inside layer of a multi-layer window	$W/(m^2 K)$
$\alpha_{r,m-o}$ :	Radiative heat exchange coefficient between the middle-layer and outside	$W/(m^2 K)$

	layer of a multi-layer window	$W/(m^2 K)$
$\alpha_w$ :	Convective heat transfer coefficient inside ceiling panel	$W/(m^2 K)$
$\beta$ :	Coefficient of gas thermal expansion	$K^{-1}$
$\Gamma$ :	Turbulent diffusivity	$m^2/s$
$\Delta T, \Delta T$	Convective heat transfer temperature difference	$K$
$\Delta t_f$ :	False-time-step	$s$
$\Delta t_{f,i}$ :	False-time-step for $u_i$ equations	$s$
$\Delta T_{r,j}$ :	Local temperature difference	$K$
$\Delta x_i$ :	Grid-spacing in the $i$ th direction	$m$
$\Delta \rho$ :	Air density difference	$kg/m^3$
$(\delta \rho C)_m$ :	Heat capacity of unit surface area of panel shell	$J/m^2 K$
$(\delta \rho C)_w$ :	Heat capacity of water layer per unit area of panel	$J/m^2 K$
$\delta_{ij}$ :	Kronecker delta( $\delta_{ij} = 1$ for $i = j$ and $\delta_{ij} = 0$ for $i \neq j$ )	$[-]$
$\varepsilon$ :	Dissipation rate of turbulence energy or emittance of an surface	$W/kg$ $[-]$
$\varepsilon_e$ :	Ground emissivity	$[-]$
$\varepsilon_p$ :	Value of $\varepsilon$ at the first grid from the wall	$W/kg$
$\varepsilon_v$ :	Ventilation effectiveness( = $C_v/C_i$ )	$[-]$
$\theta$ :	Modified enthalpy( = $H - H_0$ )	$joule/kg$
$\lambda$ :	Heat conduction coefficient	$Wm^{-1}K^{-1}$
$\nu$ :	kinetic viscosity of air	$m^2/s$
$\nu_\tau$ :	Turbulence(eddy) viscosity	$m^2/s$
$\rho$ :	Air density	$kg/m^3$
$\rho_0$ :	Reference air density	$kg/m^3$
$\sigma$ :	Boltzman constant( = $5.67 \times 10^{-8}$ )	$W/(m^2 K^4)$
$\sigma_k, \sigma_c$ ,		
$\sigma_H, \sigma_\varepsilon$ :	Turbulent Prandtl number and Schmidt number	$[-]$
$\tau$ :	Time	$s$
$\tau_s$ :	Skin shear stress( = $\mu (\partial u / \partial y)_w$ )	$N/m^2$
$\Phi$ :	Universal transport variables	
$\phi_a$ :	View factor of an outside wall surface to the sky	$[-]$
$\phi_e$ :	View factor from an outside wall to ground	$[-]$
$\psi_{jk}$ :	Fraction of heat emission by surface $j$ absorbed by surface $k$	$[-]$



## ACKNOWLEDGEMENTS

This thesis describes the research work I have done during my appointment as an Assistant in Education at the Laboratory of Refrigeration Engineering and Indoor Climate Technology, Delft University of Technology, The Netherlands. During these four and a half years, I am greatly indebted to my family, colleagues and friends. Without their support and friendship, this thesis would not have been possible. I am especially grateful to my supervisor Prof. ir. H. van der Ree for his indispensable guidance and constant encouragement for the accomplishment of this thesis. I am especially grateful to my advisor Dr. ir. Jan van der Kooi for creating the possibility of this research program, guiding the research and offering support in any case in the Laboratory for Refrigeration and Indoor Climate Technology, and also for his effort to help me in making wide range contacts with the HVAC industry in The Netherlands.

I wish to express my gratitude to all of my colleagues at the Laboratory for Refrigeration Engineering and Indoor Climate Technology, for their full support and their friendship. Particularly, I am grateful to Mr Martin Verwaal for his home-made PC, which helped in speeding up the accomplishment of this thesis. Special thanks are given to Mr. H. Liem for providing the well-formatted Dutch weather data. Special thanks are given to Dr. A.H.C. van Paassen and Mr H. de Niet for their help in using the computer code ENERK, and to Dr. ir. P.J. Lute for providing his computerised psychrometric chart. Mr. J. Keuvelaar has done a lot for the final layout of this thesis.

I wish to extend my gratitude to all other people who have helped me in this research work. Among them, special thanks are given to Dr. Q. Chen of the Laboratory of Aero- and Hydro-Dynamics, for his help in using the computer code PHOENICS, and for his permission of my full access to the on-going IEA(International Energy Agency) Annex-20 research project carried-out at the Laboratory for Energy systems, ETH, Switzerland in March 1990 when I was there as an exchange student. Special thanks are also given to Mr C. Gerritsen of the Laboratory of Aero- and Hydro-Dynamics for providing the DISA anemometer apparatus. Particularly, several students have also contributed to the work in this thesis: Mr. Tomer Peled, a guest student from Israel, did excellent measurements in our test room, and Mr. ir. Dwi Subagyo have performed both measurements and simulations concerning cooled-ceiling systems. Discussions with Mr C.J. Bal of Modern Office Climate B.V. concerning the evaporative cooling schemes proved to be very much rewarded.

To my wife Xiuhong I am very grateful for abandoning her nice job in China to join me and for her patience and understanding when I spent most of my time in books and in front of computers during this period. Also to my baby daughter Shuang-yuan, who has provided the inspiration for a book partly on thermal comfort.



## Curriculum Vitae

Jianlei Niu was born on April 21, 1962 in Henan province of China. He received his primary and secondary educations at his home town from 1969 until 1978. Upon graduation from senior high school in 1978, he entered Tsinghua University, Beijing, China. There he studied at the Department of Thermal Engineering for five years, and he was granted a bachelor degree in engineering in July 1983, with his major field in air-conditioning engineering. In July 1986, he received his MSc in Mechanical Engineering from Tsinghua University, with his major field in thermal engineering and his thesis titled *Aero-Dynamic Flow and Mixing Processes in a Swirled-type Pre-combustion Chamber for Pulverized-coals*. From July 1986 until December 1989, he was employed, first as an associate-lecturer and then as a lecturer, at the Department of Thermal Engineering of Tsinghua University, engaged in various research and application, as well as teaching activities concerning coal conversion and flue-gas cleaning technologies. In between, he was with NEI(Northern Engineering Industry) International Combustion Ltd, Derby, England for six months as a CBI(Confederation of British Industries) Overseas Scholarships exchange engineer, involved in the development of low NO<sub>x</sub> emission coal burner technologies..

Since January 1990, he has been employed as an AIO(*Assistent-in-Opleiding*) at the Laboratory for Refrigeration and Indoor-Climat Technology, Division of Process and Energy, Faculty of Mechanical Engineering, Delft University of Technology, The Netherlands. The contents of this thesis are the research work he has been doing in this Laboratory under the supervision of Prof. H. van der Ree and Dr. Ir. J. van der Kooi.

His major interest will continue in the area of clean fossil fuel conversion technologies, energy conservation in industrial processes, and of course, also in the area of thermal comfort, indoor air quality and energy conservation in buildings.